

FOREWORD

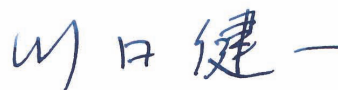
The earth is the third planet in the solar system. Everything that happens around us is a physical phenomenon on this planet. Physical phenomena may occur in any scale. Their scales have nothing to do with the scales of human beings. They, of course, occur without paying any attention to the existence of the human being.

The great Sichuan earthquake, occurred last year in China, has reminded us the hugeness of the natural phenomena. The tsunamis brought by the great Sumatra-Andaman earthquake, the hurricane Katrina and the great Hanshin earthquake, they also had occurred in the scale far above our preparation. Natural power may change the lay of mountains, coastlines and create new lakes in minutes.

Recent high public eco-consciousness often leads us to an exaggerate expression, “Save the earth”, giving intimation that as if we were destructing the earth. However the most enormous power on the earth is coming from the earth itself and the physical phenomena generated by solar energy around the earth. They bring us wonderful seasons and devastating disasters.

I am writing these words on 6th of April. Cherry blossoms are fully blooming. It is the most beautiful season in Japan. On the other hand, I have just received the news about the serious damage to the city, L'Aquila, Italy, hit by a heavy earthquake.

We should never forget that human being is the most delicate creature on the earth. We can never stop the preparation in order to protect our existence from such threats of natural phenomena that may occur in any scale.



Ken'ichi Kawaguchi,
Professor, Ph.D.
Institute of Industrial Science
The University of Tokyo



A QUANTITATIVE APPROACH TO ASSESS LANDFORM CHANGES OF HATTIAN BALLAH LANDSLIDE DAM FORMED BY 2005 KASHMIR EARTHQUAKE

Ahsan SATTAR¹, Kazuo KONAGAI², Takaaki IKEDA³, Takashi KIYOTA⁴,
Zaheer Abbas KAZMI¹, Masahiro KOIKE⁵

ABSTRACT:

A huge landslide triggered by Kashmir 2005 earthquake blocked the Karli and Tang branches of Jhelum River and formed two land slide-dammed lakes with larger being of volume 62 million m³. The location of landslide dam is region of active landslides which predates the 2005 earthquake. An outburst flood now threatens the downstream areas and Muzaffarabad city. A quantitative approach of GPS measurements of landslide mass body indicates excessively large settlements and northwestward in-plane movement of whole dam body. Slaking, the resulting consolidation and washout process at surface are also components of resulting deformations. Isotopes study indicates seepage still from shallower coarser part of debris mass as initially assessed from seepage and water level measurements of lakes. Continual monitoring of landmass and potential landslide masses at critical stability on banks of large lake is essential for hazard assessment, risk awareness and preparedness in case of flood outburst.

Key Words:

Hattian-Ballah; Rock Avalanche; Landslide dam, GPS measurements; Quantitative approach, Kashmir Earthquake, Isotopes, Landform changes

INTRODUCTION

The October 8, 2005 earthquake of magnitude 7.6 (Mw) (US Geological Survey) with epicenter (34°29'35"N, 73°37'44"E at focal depth 10km) some 95 km from Islamabad caused widespread destruction in Kashmir and other northern areas of Pakistan. Landslide dams usually form in mountainous areas of high terrain (Costa and Schuster, 1988), where there are proper conditions for preparation (high hills-slope gradients and discontinuities such as bedding, faults, joints) and triggering factors of slope failure (Korup, 2002). In addition to widespread destruction to cities another major event during earthquake, was the formation of a huge landslide dam comprising 85 million m³ which buried the Parhore valley (Owen, 2008) and blocking the waterways of the Karli and Tung tributaries of the Jhelum River. The landslide alone killed more than 1000 people equivalent to 1.1% of total earthquake fatalities, and 3.7% of the deaths caused by landslides; making it one of the most devastating recorded historical landslide events (Dunning, 2007). Failure of landslide dams usually results in catastrophic downstream flooding causing loss of life, housing and infrastructures. The Raikhot landslide dam of some 200–300 m in height which impounded a 65-km-long lake on the Indus River, Pakistan collapsed in 1841, which was the largest damming by landslide and resulting catastrophic flood that has been documented in the world (Duman, 2008). Some 200 km south of Raikhot is the huge Hattian-Ballah landslide mass posing a similar flood hazard to the downstream

¹ Graduate Student, Institute of Industrial Science, University of Tokyo

² Professor, Institute of Industrial Science, University of Tokyo

³ Senior Research Engineer, RTI, Tobishima Corp.

⁴ Assistant Professor, Tokyo University of Science

⁵ Technical Associate, Institute of Industrial Science, University of Tokyo

area including Hattian village and Muzaffarabad city. The major concerns are the stability of landslide mass itself and the evaluation of the surrounding unstable slopes which are threat to impounding large lake of volume 62 million m³ (Schneider , 2008) which can eventually breach the landslide mass. However, literature regarding landslide dams is mostly of qualitative nature because of lack of observations during formation and failure events of these landslide dams, therefore making the evaluations difficult. The authors have been observing the landslide mass from time to time since its formation. Our research team initiated one of very few of its kinds, the quantitative approach for Hattian-Ballah landslide dam. Two surveys were conducted one in June 2008 and other one in November 2008 for GPS measurements over the landslide mass and collection of water samples for isotopes measurements of waters in impounding lakes and overflowing spillways. This report presents the data and results of GPS surveys, isotopes measurements, and there relation to landform changes scenarios of landslide mass till November 2008.

GEOLOGICAL SETTING OF 2005 KASHMIR EARTHQUAKE

The 2005 earthquake was a result of subduction of Indian Plate under the Eurasian plate. Fault solution shows that the earthquake was due to trusting causing a slip of maximum 9m and maximum uplift of 6m of area north of Muzaffarabad, (GSJ, 2006). It was the largest historical earthquake on the Indus-Kohistan Seismic Zone (IKSZ) and the first Himalayan earthquake to be accompanied by surface rupture, reactivating the Tanda reverse fault and locally offsetting the Main Boundary thrust (MBT) (Ahmad, 2008). The cities of Muzaffarabad, Bagh and Balakot were extremely damaged which lie along the Jhelum fault (Fig. 1). A total of 1778 after shocks were recorded northwest (continental convergent zone) of Muzaffarabad at the end of 2005 (Pakistan Metrological Department, 2006). Hattian-Ballah landslide dam lies at the southern end of the Tanda fault some 33km south east of Muzaffarabad and 3.4 km from Tanda fault. The source area of landslide is formed of Miocene aged Murree formation mudstones and sandstones (Fig. 2) with minor amount of limestone on hanging wall of Tanda fault (Dunning, 2007).

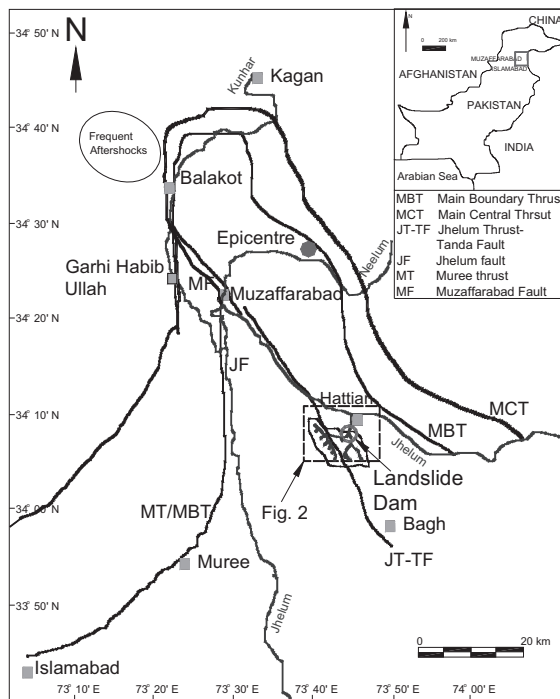


Fig. 1. Broad scale regional tectonics of Northern area of Pakistan. The Hattian Landslide is marked with a red circle with catchment area of streams. The epicenter of the 8-10-2005 earthquake is marked; the main cluster of aftershocks is located north west of it. The landslide dam is located near the SE-end of the Tanda Fault.

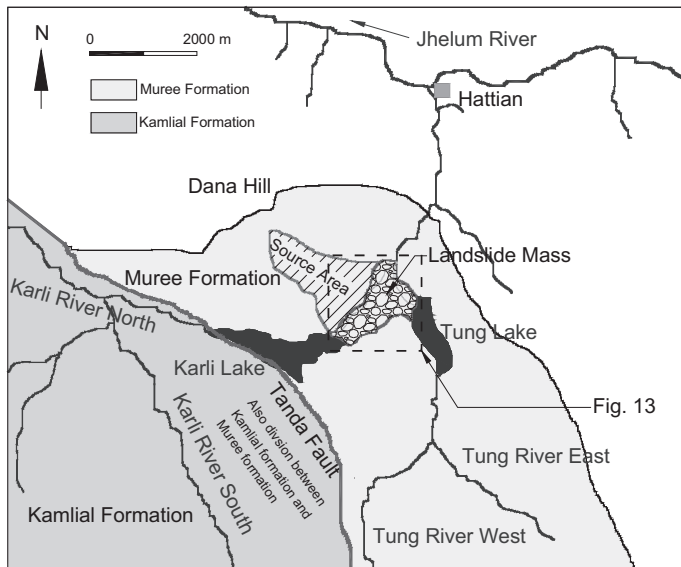


Fig. 2. Schematic map of Hattian Ballah landslide area showing the Tanda fault at south and landslide source scar parallel to the fault. Tanda fault lays the boundary between Kamliyal formation and Muree formation. (Compiled from different sources).

Waters from Hattian-ballah joins Jhelum River and Jhelum River initially flows north-west along the Tanda fault before an abrupt turn southward to flow along Murree fault after its junction with already southwardly flowing Neelum River. The location of debris mass is a region of landslide activities which predates the 2005 earthquake.

HATTIAN-BALLAH ROCK AVALANCHE AND LANDSLIDE DAM

Source failure and Formation process

At 3.5 km south of Hattain village a huge landslide mass of volume 85×10^6 million m^3 was triggered during the earthquake. The collapse of source Dana hill happened in three distinct phases (Dunning, 2007) during its failure parallel to the Tanda fault at south as shown in Fig.2. Initially the landslide mass travelled a maximum drop height of 800m from Dana hill. Then the debris mass raised on the opposite side of the valley while travelling towards the valley. Finally the debris material spread in both northeast and south west direction. After mass impact on the opposite side of the valley, a super elevation is created with a minor valley between the debris mass and opposite side of valley. The resulting debris deposit with length-to-width ratio of 2.5, created a natural dam blocking the waterways of Karli and Tang tributaries of Jhelum River.

A summary of information about the Hattian-Ballah landslide dam and lakes from the assessed and inferred data from various authors is given in (Table 1). Hattian Ballah lies among the huge landslide dams of the world as shown in Fig. 3. Using the data of (Table 1) various geomorphic indicators for Hattian Ballah landslide mass are shown in (Table 2) based on available data of landslide-dammed lakes from Northern Apennine (Casagli and Ermini, 1999), New Zealand (Korup 2004) and selected worldwide (Ermini and Casagli, 2002). The landslide mass is indicated as stable for most of the indicators, apart from few showing it to be unstable.

Characteristics of final deposit and changes

Tanda fault separates the Murree formation from Kamliyal formation as shown in Fig 2. It is the red sandstone, siltstone and clay stone formation called Murree formation where the landslide originated. Deposited debris mass is composed of coarser bouldery surface which is relatively shallower part of dam body; a term called Carapace facies (Dunning, 2006). The transportation process produced highly fragmented and angular particles over the surface. Boulder sized Mudstones are expected to be disintegrated at interior of land mass because of their weak and weather able structure.

Flood / Debris Flow Hazard

The huge landslide mass is a possible flood and debris flow hazard for the downstream areas including Muzaffarabad city. As shown in Fig. 1 Jhelum river takes a sharp turn southwards at Muzaffarabad city

Table 1:- Summary of information about the Hattian-Ballah landslide dam and lakes.*

Characteristics of landslide dam and lake	Data (assessed and inferred)
1. Location and date of dam formation	Hattian-Ballah, 8 Oct 2005 (34°08'N, 73°43'E)
2. Trigger or cause of landslide	8 th Oct. 2005 M=7.6, 44 km from epicenter
3. Type and characteristics of landslide forming dam	Rock and debris avalanche
a) Landslide volume	85 million m ³
b) Landslide scar altitude	2038-1290 m
c) Length of debris runout (max.)	2609 m
d) Debris above valley bottom	130 m
e) Landslide surface area	1.33 km ²
f) Source maximum length up to deposited surface	1720 m
g) Source maximum width	520 m
h) Source average depth	60m
i) Morphology (Costa and Schuster, 1988)	Type III
4. Rock type	Miocene Murree formation Mudstones
5. Underlying causes of landslide	Seismically Reactivated landslide
6. Landslide dam	
a) Height of landslide dam	130 m
b) Width of landslide dam	1587m
c) Base length of landslide dam	618m
d) Volume of landslide dam	85 million m ³
e) Slope of dam faces	Downstream 20-30° / Flat near crest
f) Status	Overflowing through spillway as on November 2008. Stable with seepage
7. Physical characteristics of material forming landslide dam	Boulders up to 8m covering the surface at middle part (Murree formation and Mudstones). Surface boulder layer is relatively shallow.
8. Karli Lake (Large lake)	
a) Volume	62 million m ³
b) Catchment area	44.17 km ²
c) Maximum altitude	2497 m
d) Minimum altitude	1237 m
e) Relief	1260 m
f) Relief ratio	53.7
g) Mean slope	20°
9. Tang Lake (Small lake)	
a) Volume	3.6 million m ³
b) Catchment area	30.10 km ²
c) Maximum altitude	2884 m
d) Minimum altitude	1149 m
e) Relief	1735 m
f) Relief ratio	120.7
g) Mean slope	25°

* Greater part of Data from Dunning 2007 and Schneider, 2008

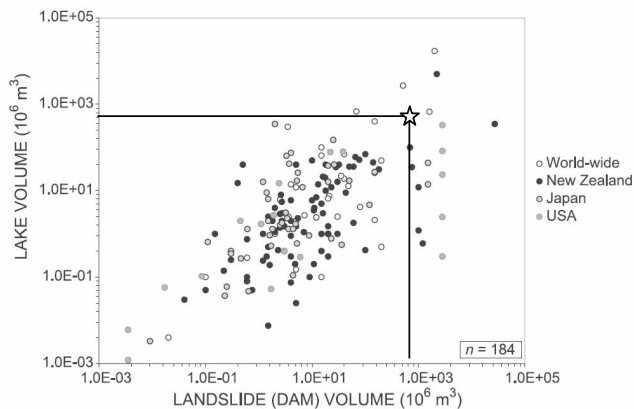


Fig. 3 Bivariate plot of landslide-dammed lake volumes versus landslide dam volume derived from a worldwide data set (n = 184), highlighting occurrences in New Zealand, Japan, and the USA according to Korup (2004) and data from Hattian-Ballah landslide dam and lakes.

while joining the Neelum River. Breach analysis results published in WAPDA, 2006 report indicates a flood wave approaching 30 m for an extreme scenario of 30 minutes breach time along with 1000 year return period storm. Village of Hattain located at the junction of southern branch of Jhelum from landslide mass and west ward flowing Jhelum River. Dammed lakes and debris mass therefore pose flood hazard for downstream areas.

Table 2 :- Geomorphometric indices distinction of discrete domains of landslide dam stability results based on available data of landslide-dammed lakes from Northern Apennine (Casagli and Ermini, 1999), New Zealand (Korup 2004) and selected worldwide (Ermini and Casagli, 2002) and indices values for the Hattian-Ballah landslide dam and landslide-dammed lakes.

Index	Landslide dam stability	Index values for Hattian-ballah
Blockage Index for Northern Apennine landslide-dammed lakes data, Casagli and Ermini (1999)	$I_b = 3$ threshold ratio for formation of lakes $4 > I_b > 3$ unstable dams $5 > I_b > 4$ uncertainties $I_b = \log(V_D A_C^{-1})$	$I_b = 6.28$ Stable
Impoundment Index for Northern Apennine landslide-dammed lakes data, Casagli and Ermini (1999)	$I_i = 0$ threshold ratio for stable / unstable $I_i = \log(V_D V_L^{-1})$	$I_i = 0.137$ Stable
Blockage Index for New Zealand landslide dammed lakes data, Korup (2004)	$I_b > 2$ threshold ratio for formation of lakes $I_b < 4$ threshold ratio for unstable lakes $I_b > 7$ threshold ratio for stable existing lakes $I_b = \log(V_D A_C^{-1})$	$I_b = 6.06$ Stable
Dimensionless Blockage Index for Selected world wide data, Casagli and Ermini (2002)	$I_b' = 2.92$ is lower threshold ratio for stable, $I_b' = 3.25$ is upper threshold ratio for unstable, $I_b' = \log(H_D A_C V_D^{-1})$	$I_b' = 1.85$ Stable
Dimensionless Blockage Index for New Zealand landslide dammed lakes data, Korup (2004)	$I_b' = 3$ is lower threshold ratio for stable, $I_b' = 5$ is upper threshold ratio for unstable, $I_b' = \log(H_D A_C V_D^{-1})$	$I_b' = 1.85$ Stable
Impoundment Index for Northern Apennine landslide-dammed lakes data, Korup (2004)	$I_i = 1$ threshold ratio for stable / unstable $I_i = \log(V_D V_L^{-1})$	$I_i = 0.137$ Unstable
Backstow Index for New Zealand landslide dammed lakes data, Korup (2004)	$I_s < -3$ upper threshold ratio for unstable $I_s > 0$ lower threshold ratio for stable Data between these threshold remain inconclusive $I_s = \log(H_D^3 V_L^{-1})$	$I_s = -1.45$ Inconclusive
Basin index for New Zealand landslide dammed lakes data, Korup (2004)	$I_a > 3$ threshold for stable $I_a = \log(H_D^2 A_C^{-1})$	$I_a = 2.35$ Unstable
Relief Index for New Zealand landslide dammed lakes data, Korup (2004)	$I_r > -1$ threshold ratio for stable / unstable dam $I_r = \log(H_D H_R^{-1})$	$I_r = -0.98$ Marginally unstable

where V_D is volume of landslide dam and impoundment [in m^3], V_L is volume of landslide dam and impoundment [in m^3], A_C is catchment area upstream of the blockage [in km^2], H_D maximum crest height of landslide dam [in m], H_R is the relief upstream of the point of blockage [in m].

WAPDA Report

Soon after formation Water and power Development Authority of Pakistan have been monitoring the landslide mass. Fig. 4 shows inflow into the large lake, small lake and seepage through landslide mass along with the water levels in the small and the large lakes. The seepage through landslide dam increased all of a sudden on 11th January 2006. Water level in large lake was 1276m and projecting back (due to unavailability of data) level in small lake is estimated as 1212m. Seepage is either through the portion of landslide mass above 1276m in front of large lake or above 1212m in front of small lake. Seepage increased and on 23rd January it was again close to discharge into small or large lake. After 30th April the seepage came very close to discharge into small lake. Water level in small lake is decreasing on 30th April. This decrease in water level in small lake started gradually after 21st April. After 21st April till 5th June the seepage, discharge into large lake and small lake are all constant, but the water level of small lake is gradually reducing. So the stored water from small lake is also seeping. It is concluded that piping or seepage channels are formed after 21st April. This seepage initiation time of 21st April 2006 can also be confirmed from the sediment outflow curve (Fig. 5) which shows a final peak on 21st April.

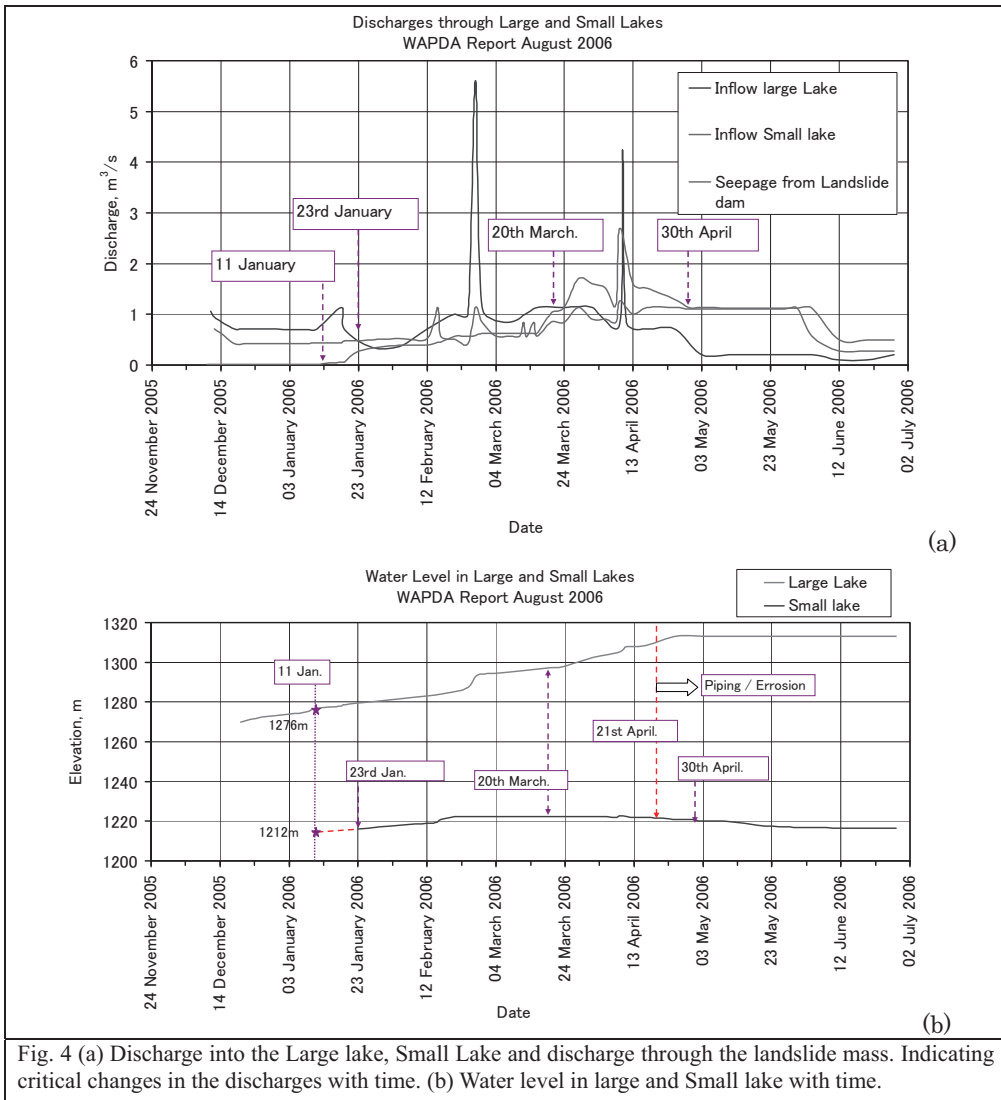


Fig. 4 (a) Discharge into the Large lake, Small Lake and discharge through the landslide mass. Indicating critical changes in the discharges with time. (b) Water level in large and Small lake with time.

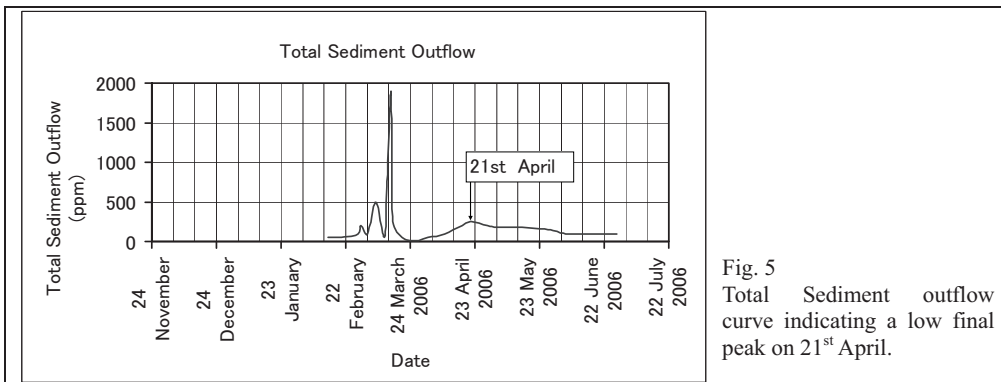


Fig. 5 Total Sediment outflow curve indicating a low final peak on 21st April.

Slaking and Washout process

Rocks from Murree formation are going through the slaking process over the landmass body. The clayey and silty reddish material is crumbled apart due to moisture contact (Fig. 6a). Resulting soil is relatively impermeable and in fact consolidating the land mass. Boulders of Murree formation are disintegrated to form soil dunes around the middle portion of mass body (Fig. 6b).

Apart from the consolidation process occurring on the landmass due to the slaking of mudstones and shale, portion of the slaked material is being washed by the overflowing water from spillway and along water path during monsoon season (Fig. 6c).



Fig. 6a



Fig. 6b



Fig. 6c

Fig. 6(a) Shale of Murree formation crumbled apart due to slaking process. The resulting material is relatively impermeable which is also filling the pours between bigger boulders on the surface. (b) Boulders of Murree formation weathered to form soil dunes around the middle portion of landslide mass. (c) Washout process of weathered material. Dried up path of water during monsoon season show clear reddish sediments deposited on grey sand stones.

GPS OBSERVATIONS

Literature regarding landslide dams is mostly of qualitative nature. Our research team initiated a quantitative approach of GPS measurements for Hattian-ballah landslide mass. The GPS instrument used is Leica GPS1200. Authors conducted GPS survey of the landslide mass twice, once in June 2008 and once in November 2008.

GPS Survey Lines

Two GPS traverse lines were laid. One line along the spillway because maximum settlement was expected along spillway (Longitudinal Line) and one line across longitudinal line (Transverse line). GPS points along with UTM coordinate for June 2008 survey are shown in Fig. 9. In November 2008 survey few points very missed due to unavailability of satellite signals at those points. Total of five points were lost, four along longitudinal line and one along transverse traverse line.

Accuracy of GPS Measurements

Geometric dilution of precision (GDOP) for both surveys was generally observed to be below 5, which is generally accepted threshold for precise measurements. Therefore the accuracy of measurements for

both surveys was good. GDOP for GPS points along longitudinal and transverse GPS points are given in Fig. 10. Tripod was used for better accuracy in November 2008 survey.

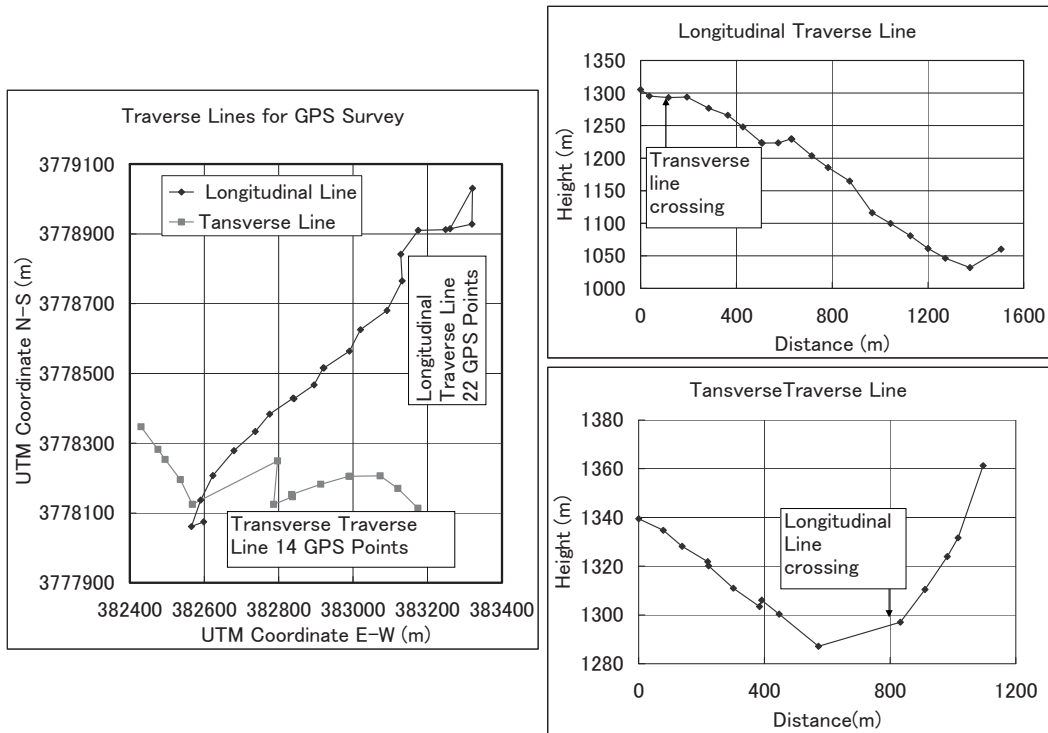


Fig. 9 UTM Coordinates of GPS points. Elevations for Longitudinal and Transverse Traverse lines. (June 2008 Survey Data)

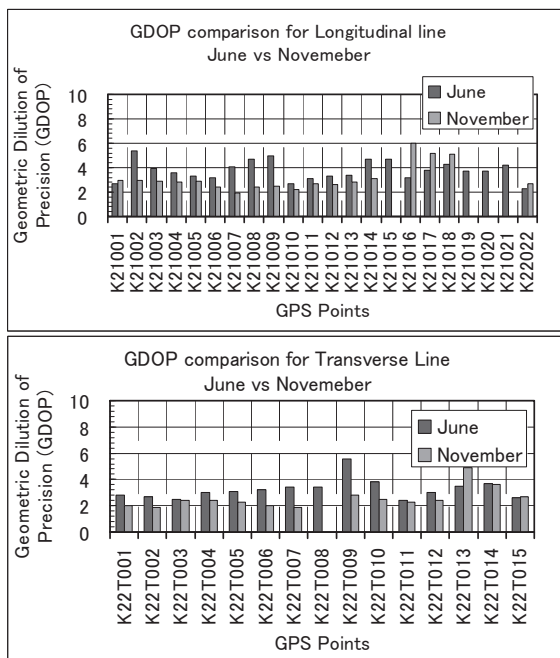


Fig. 10 Geometric dilution of precision for June 2008 and November 2008 surveys. Average of 3.7 and 3.1 for June and November survey respectively for longitudinal lines. Average of 3.0 and 2.5 for June and November survey respectively for transverse traverse line.

GPS Survey results

Results of comparison of GPS data for June 2008 and November 2008 surveys are presented in Fig. 11. Result shows an average settlement of 1.34 m for the longitudinal line with average of 1.72 m for the middle portion of landmass. The transverse line shows an average settlement of 1.46 m. Longitudinal line showed a northwestward movement for region from crest up to half of its length. Transverse line showed a similar trend of westward movement for its eastern half length and no clear trend for the western five GPS points lying on source area of landslide. Generally the GPS data shows a northwestward trend of landmass movement.

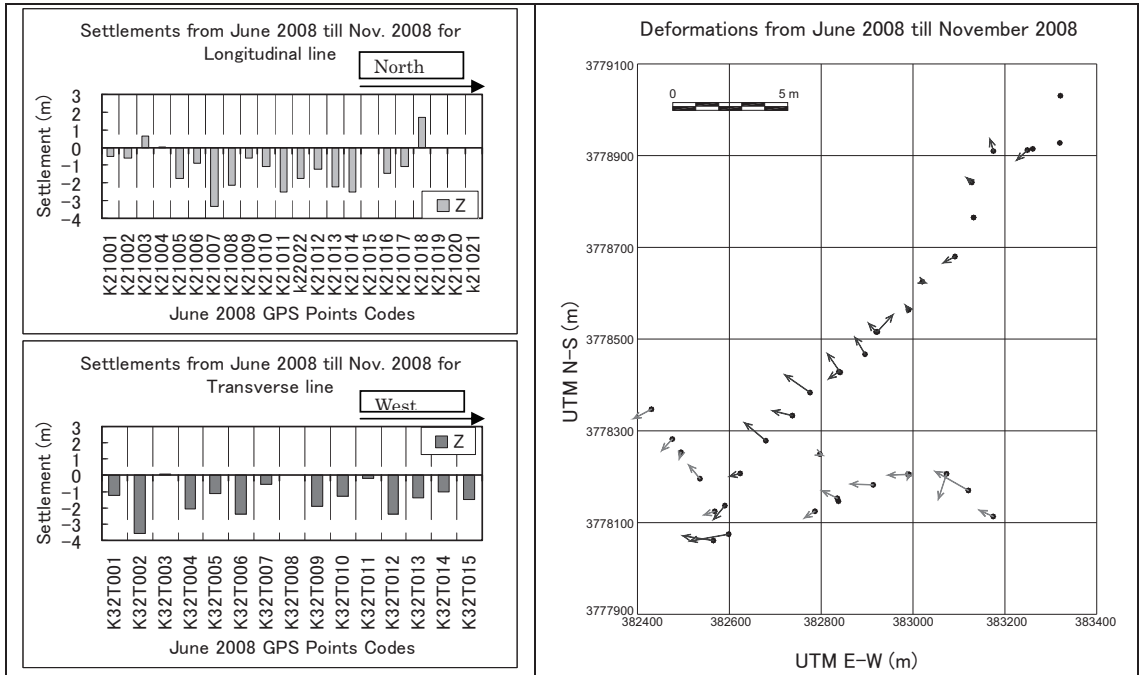


Fig. 11 Results of GPS Data comparison of June 2008 and November 2008. Settlements for Longitudinal and Transverse lines shown on left. Deformation vectors in N-S and E-W UTM coordinate plan shown for each GPS point shown on right.

ISOTOPES STUDY

Water samples from the water in lakes, spillways and downstream were taken during the surveys in order to determine the $\delta^{18}\text{O}$ ratios. The $\delta^{18}\text{O}$ ratio shows the percentage of stable isotopes of ^{18}O relative to ^{16}O isotopes of water. Measurements are made relative to internationally accepted standard VSMOW¹.

$$\delta = \frac{R_{\text{sample}} - R_{\text{VSMOW}}}{R_{\text{VSMOW}}} \times 1000$$

A positive ‘ δ ’ value indicates that sample is “enriched” and a negative sample is “depleted” relative to the VSMOW¹. Under specific conditions, there is a separation of heavier and lighter isotopes, the process called “fractionation”. When water evaporates the lighter isotopes of water (^{16}O) evaporates first while heavy isotopes (^{18}O) remain, due to stronger molecular bond. As the theory of isotope enrichment accompanying the evaporation process is now fairly well advanced, there have been attempts to quantify the water balance of lakes, based on degree of enrichment of stable isotopic

¹ VSMOW “Vienna Standard Mean Ocean Water”

species in them (IAEA, 1981).

Fig. 12 shows the determined $\delta^{18}\text{O}$ ratios for water samples from August 2007, June 2008 and November 2008 surveys. It was inferred from $\delta^{18}\text{O}$ ratios of water samples from August 2007 and June 2008 that water from deeper layers may be joining the downstream because of the fact that downstream isotopes values were greatly depleted then values of lakes or there spillway. $\delta^{18}\text{O}$ ratios of small lake for November 2008 water samples are again closer to value determined in August 2007. Therefore the scenario thought may not be correct because the small lake water is going through large seasonal changes in its isotopic composition as compare to gradual changes for large lake with season. The seasonal fluctuations in isotopic composition are largest in small lakes with short residence time and are dampened in larger systems (IAEA, 1981). On the other hand inhomogeneity occur in the vertical dimension as a result of seasonal stratification (meromixis), thus isolating the deeper water masses (hypolimnion) from surface waters. This stratification in the large lake is thought to be present within the shallower parts of both lakes. Therefore it is inferred that the water from the lakes is still seeping only from the surface couser part of landslide mass. Apparent variation in small lake isotopes values can also be due to the seepage of water from large lake to the small lake as the $\delta^{18}\text{O}$ ratios at the large lake is higher and can be an easier source of isotopes variation because of elevation difference of two lakes.

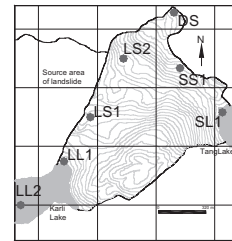
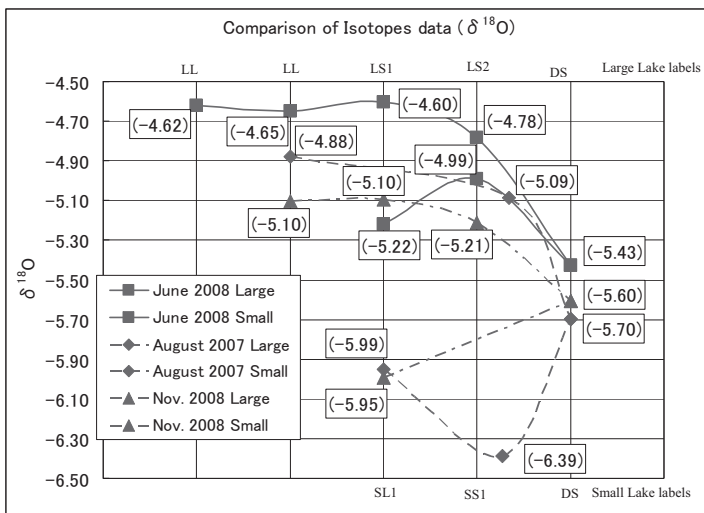


Fig. 12 $\delta^{18}\text{O}$ ratios for water samples from August 2007, June 2008 and November 2008 surveys.



November 2006



June 2008

Fig. 13 Toe part of landslide dam. Gradual erosion at parts indicated by arrows.

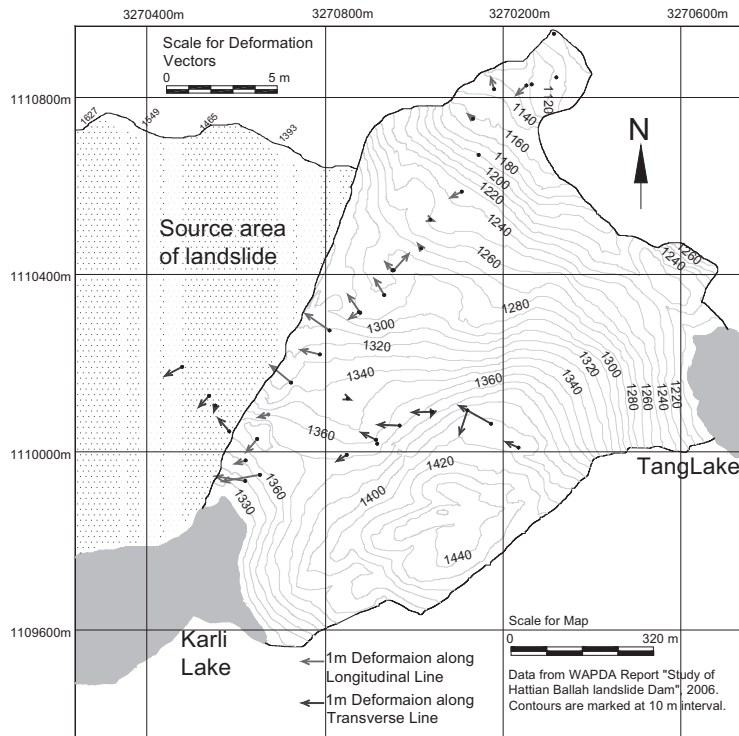


Fig. 14 Deformation Vectors superimposed on contour map. Map reproduced from WAPDA Report “Study of Hattian-Ballah landslide dam, 2006”. Northwestward trend of GPS points for southern half length of longitudinal line and Eastern half length of transverse line.

DISCUSSION

Natural landslide dams usually break within few years or otherwise consolidate with time. The water level from Large Lake reached the excavated spillway level at the end of March 2007 and overflowed from spillway then after (Dunning, 2007). According to NESPAK the spillway is performing well and the lakes are now handed over to Government of Azad Jammu and Kashmir. The authorities are now less concerned of the possibility of failure of landslide dam. However since the formation of landslide dam, there has been no major landslide into the Karli Lake (which is of major concern).

GPS Data showed a northwestward movement trend of the landslide mass (Fig. 14). During the formation process super elevation was created on the opposite side of valley and at the toe of landslide source area a gorge was created through which the spillway was latter excavated. GPS data indicates that the landslide mass is moving towards the lower portion. The settlement results are surprisingly large with average settlement of 1.34m and 1.46m for longitudinal and transverse GPS points respectively.

Deformations vectors and settlements of GPS points are composed of three main factors. Mass movement of dam body, the slaking process and subsequent washing and consolidation processes are components of resulting deformations. Last two factors are prominent near the toe part where the mass movement is less prominent because of lesser thickness of debris mass. Fig. 13 shows changes in the toe part from November 2006 till June 2008.

$\delta^{18}\text{O}$ ratios indicates the seepage from top coarser layer of debris mass. More water samples are required, especially at different depths of lakes along with some samples of rain water, in order to determine the depth variation and inflow values respectively of the lakes. The likely scenario of seepage of water from Large Lake to Small Lake has to be checked (using a 3 dimensional seepage model under processing). Using all information of isotopes values the depth of seepage zone through the landmass can be assessed.

Concentrating on the debris mass alone will rather be an unsafe approach for stability analysis. On the

left bank of Karli Lake there are a number of active slides hanging in equilibrium. These masses at stage of their critical stability can fall into the large lake and eventually they can cause overtopping and therefore breaching of dam body.

The mitigation measures done so far are valuable (excavation of spillway and preparation of hazard zonation map); however there is still certain amount of remaining risk, particularly towards the banks of large lake. Landslide mass seems to be stable for now, but there is a need of further detailed investigation and monitoring of land mass itself and active landslides on the banks of lakes. Knowing the hazards, risk awareness and preparedness on all levels can help save lives and property loss. This study is a part of ongoing research investigating the long term post earthquake issues of Kashmir and mitigating the problems the people are facing after 2005 Kashmir earthquake, which could eventually help ascertain the future evolution of landform of Kashmir.

ACKNOWLEDGMENT

Authors are grateful to Mr. Koike and Oki laboratory at IIS for helping us in isotopes determination of water samples and giving us helpful advices regarding isotopes hydrology. We are also thankful for great cooperation of ERRA (Earthquake Reconstruction and Rehabilitation Authority), DAM (Development authority of Muzaffarabad) and GSP (Geological Survey of Pakistan) with special thanks to Mr. Zahid Ameen Chairman DAM, AJK for his kind support for surveys in Muzaffarabad and Hattian Ballah.

REFERENCES

- [1] Ahmad H. et al. Geological setting of the 8 October 2005 Kashmir earthquake, *J Seismol*, (2008) Springer Science.
- [2] Casagli, N., Ermini, L., 1999. Geomorphic analysis of landslide dams in the Northern Apennine. *Transactions-Japanese Geomorphological Union* 20, 219–249.
- [3] Costa, J.E., Schuster, R.L., 1988. The formation and failure of natural dams. *Geological Society of America Bulletin* 100, 1054–1068.
- [4] Duman T. Y., 2008 The largest landslide dam in Turkey —Tortum landslide. *Physical Geography*.
- [5] Dunning, S.A., 2006. The grain-size distribution of rock-avalanche deposits in valley confined settings. *The Italian Journal of Engineering Geology and Environment* 1, 117–121.
- [6] Dunning SA, Mitchell WA, Rosser NJ, Petley DN (2007) The Hattian Bala rock avalanche and associated landslides triggered by the Kashmir Earthquake of 8th October 2005. *Eng Geol* 93(3–4):130–144
- [7] Ermini, L., Casagli, N., 2002. Criteria for a preliminary assessment of landslide dam evolution. In: Rybar, J., Stemberk, J., Wagner, P. (Eds.), *Landslides. Proceedings 1st European Conference on Landslides 24–26 June 2002, Prague, Balkema*, pp. 157–162.
- [8] Geographical Survey Institute of Japan (GSJ), Detection of crustal deformation of the northern Pakistan earthquake by satellite data, Seventeenth United Nations Regional Cartographic Conference for Asia and the Pacific Bangkok, 18-22 September 2006 Item 6 (b) of the provisional agenda E/CONF.97/1.
- [9] International Atomic Energy Agency (IAEA), Vienna, 1981, Stable Isotope Hydrology, Deuterium and Oxygen - 18 in the Water Cycle. Technical Report Series No. 210.
- [10] Korup, O., 2002. Recent research on landslide dams — a literature review with special attention to New Zealand. *Progress in Physical Geography* 26, 206–235.
- [11] Korup, O., 2004. Geomorphometric characteristics of New Zealand landslide dams. *Engineering Geology* 73, 13–35.
- [12] Pakistan Meteorological Department (2006) Earthquake / aftershocks report. <http://www.pakmet.com.pk/EQ-Report.html>.
- [13] Owen, L. et al: Landslides triggered by the 8 October 2005 Kashmir earthquake, *Geomorphology* 94 (2008) 1–9, ScienceDirect.
- [14] Schneider J. F, 2008 Seismically reactivated Hattian slide in Kashmir, Northern Pakistan. Springer Science.

- [15] Schuster, R.L., 1993. Landslide dams — a worldwide phenomenon. Proceedings Annual Symposium of The Japanese Landslide Society, Kansai Branch, 27 April, Osaka, pp.1–23.
- [16] WAPDA Report (2006), Study of Hattian Ballah landslide, Potential hazards of land sliding and mitigation measures at Hattian Ballah and other earthquake hit areas, National Engineering Services Pakistan limited (NESPAK) and Geological Survey of Pakistan (GSP), Water and Power Development authority, Government of Pakistan (WAPDA).



SLOPE FAILURE INDUCED DEBRIS FLOW HAZARDS IN THE OCTOBER 8, 2005, KASHMIR EARTHQUAKE

Zaheer Abbas KAZMI¹, Kazuo KONAGAI², Takaaki IKEDA³, Takashi KIYOTA⁴,
Koichi KONDO⁵, Ahsan SATTAR⁶

ABSTRACT: A devastating earthquake occurred in Kashmir, Pakistan on October 8, 2005. This earthquake is resulted from reactivation of known active fault later defined as Balakot-Garhi fault which caused widespread slope failure throughout its stretch, particularly around Muzaffarabad. This slope failure resulted in a huge amount of debris material which flows in incised nallahs (channels) during monsoon and hits the inhabitants in the valley along Muzaffarabad. Two GPS surveys, June 2008 and November 2008, have been carried out to investigate the effect of debris flows along these nallahs. During second survey, morphometric parameters of channels and some physical characteristics of the flowing material were also measured. Using the GPS measurements as elevation data for the study area, the actual debris flow is simulated using numerical code based on DAMPM (Depth Average Material Point Method). This paper briefly highlights the findings obtained from repeated field measurements and from the simulation of the actual flow.

Key Words: Kashmir earthquake, Balakot-Garhi fault, debris flow, nallahs, Depth Average Material Point Method

INTRODUCTION

The October 8, 2005 Kashmir earthquake occurred at 08:50 (03:50UTC) local time of Pakistan at 34.493°N, 73.629°E, about 10km NE of Muzaffarabad and 105km NNE of Islamabad (USGS). The earthquake was of moment magnitude 7.6 (Mw) and focal depth is fixed at 26km (USGS). This was the deadliest earthquake in South Asia's recent history, with >86000 fatalities, > 69000 people injured, >32000 buildings destroyed and 4 million people left homeless. The largest city affected by the earthquake was Muzaffarabad which is the capital of Azad Kashmir, a self governing state administrated by Pakistan.

The earthquake occurred as a result of reactivation of known thrust faults stretching from Balakot to Bagh with surface rupture observed at very few locations (e.g. at Bagh reported by Geological Survey of Pakistan). Using satellite data and fault modeling, various researchers [e.g. Hiroshi P. Sato et al., Geographical Survey Institute (GSI), Japan] found that high crustal deformation has occurred along the known active faults stretching northwest and southeast from epicenter [Nakata et al. 1991], with northeastern part moved upward. These known active faults are divided into two groups, the

¹ Graduate student, Institute of Industrial Science, University of Tokyo

² Professor, Institute of Industrial Science, University of Tokyo

³ Senior Research Engineer, RTI, Tobishima Corp.

⁴ Assistant Professor, Tokyo University of Science

⁵ Executive Director, SABO Technical Center

⁶ Graduate student, Institute of Industrial Science, University of Tokyo

Muzaffarabad fault (northwest of Muzaffarabad) and Tanda fault (southeast of Muzaffarabad) [Nakata et al. 1991]. Recently, Kumahara and Nakata (2006) gave a redefinition of Tanda fault and Muzaffarabad fault, and they comprehensively renamed them as Balakot-Garhi fault.

This earthquake triggered thousands of landslides and slope failures including debris slides and debris flow throughout the region, causing about one third of total fatalities, destroying roads and disrupting communications. Most failures were shallow, typically involving the top few meters of the weathered rock, regolith, and soil. Many of these failures are still active and loose fractured material is moving down the steep slopes even under the gravity. This failure is present all along the active fault but most serious around Muzaffarabad city for its extent and long lasting problems (Fig.1). The failure

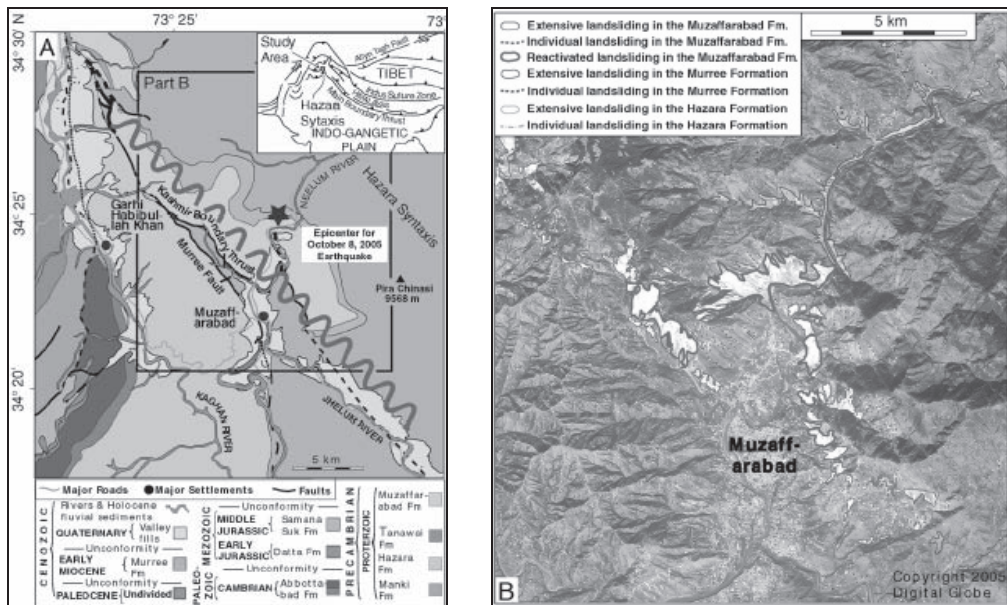


Fig.1 A) Simplified geological map of the area around Muzaffarabad and **B)** Quickbird image showing region of most extensive slope failure: Red wave indicates area of maximum crustal deformation (after Geological Survey Institute, 2006; Avouac et al., 2006).

occurred in Muzaffarabad Formation, which forms steep valley slopes, many $>50^\circ$ above the main rivers of the alluvial and valley fills. The Muzaffarabad Formation comprises thinly bedded and highly fractured dolomite constituting the lower beds in the hanging wall of Balakot-Garhi fault. This fractured loose material is a big source of debris flow with favorable conditions for the phenomena to occur. Fig.2 shows average rainfall data at Muzaffarabad from 2005 to 2008.

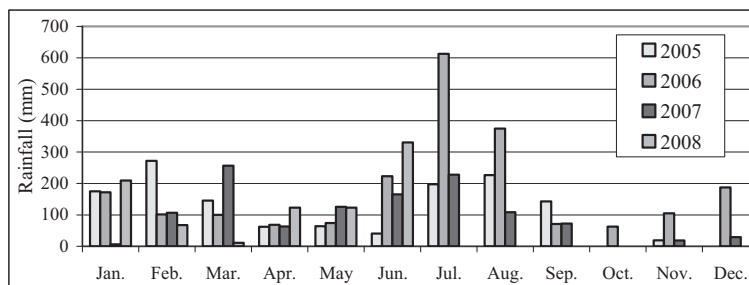


Fig.2 Monthly average rainfall at Muzaffarabad (data from Pakistan meteorological department)

The available data and district census report, 1998 suggests monsoonal climate with an average annual precipitation of about 1510 mm, with a major portion falling as rain during the monsoon season (June-August). At higher altitudes (above 1500m asl), precipitation falls as snow during the winter (December to March). The mean maximum and minimum temperature at Muzaffarabad are 16°C and 3°C during winter (January) and 38°C and 22°C during summer (June), respectively (District Census Report, 1998).

STUDY AREA

The causative Balakot-Garhi fault passing just behind the Muzaffarabad city, with city on its footwall, caused a widespread linear slope failure, with a huge amount of highly sheared and fractured loose material exposed (Fig.3a). During heavy rains of monsoon, this loose material combined with water moves as debris flows in the deeply incised nallahs (Urdu word used for channel) and hits the inhabitants. These nallahs directly pass through the Muzaffarabad city and feed the Neelum river flowing southward immediately at the western end of the city. People living in the valley along these nallahs are seriously effected by the debris flow with there houses half or full buried (Fig.3b). We selected two most damaging, Gulshan and Tariqabad nallahs (Fig.3a) passing through highly populated valley of Muzaffarabad city and carried out GPS measurements at two different times, June 2008 and November 2008, measured channel morphometric parameters and observed the changes. Processing the GPS data to formulate digital elevation data of the target area, flow is simulated for Gulshan nallah to understand actual flow behavior and damage distribution.

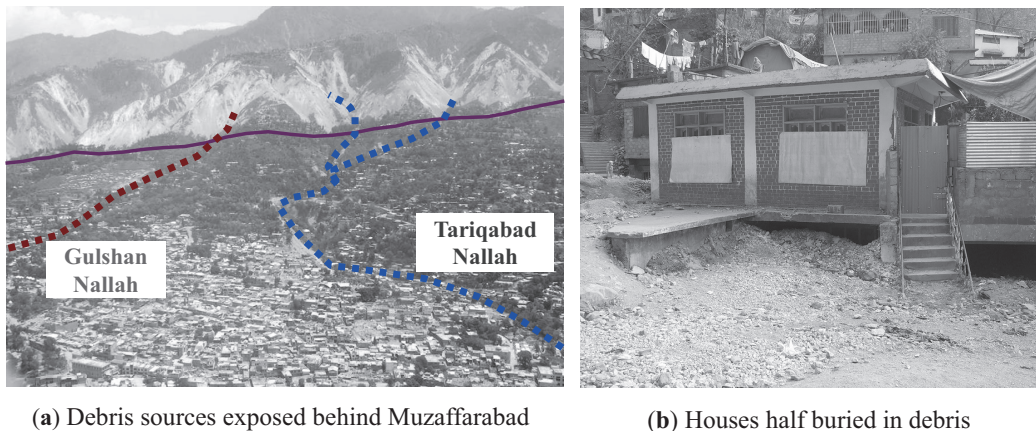


Fig. 3: Debris deposit from activated fault in Kashmir (Muzaffarabad): Purple line show the causative fault (Balakot-Garhi fault) of Kashmir Earthquake

GPS MEASUREMENTS

Two GPS measurements were taken enclosing the monsoon season to investigate the behavior and effects of debris flows in Gulshan and Tariqabad nallahs. The differential GPS system is used with one system installed at the fixed reference point (at the roof of DAM office), while the others worked as kinematic station taking measurements at a number of points marked along the selected nallahs (Fig.4a and 4b). The system also marks the points automatically at an interval of one second but the accuracy is not as high as that of marked points due to non-verticality of antenna pole and very short acquisition time. Two types of measurements are taken, one along the lowest point in the nallah to investigate the nallah bed erosion and deposition and the other at three different points to define the flow cross sections (Fig. 4b). The outer flow boundaries are found from available traces of debris material or mud marks. This also gives an idea about the erosion and deposition along the banks of

nallah and change in flow width.

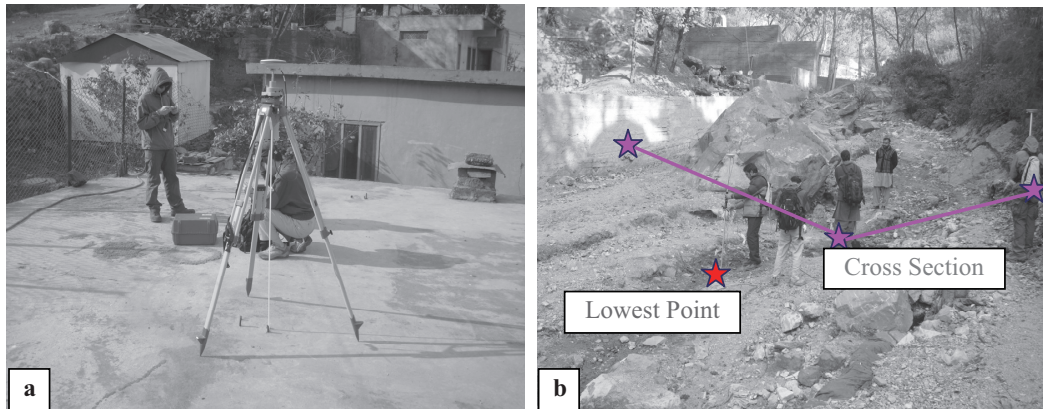


Fig. 4: GPS measurements along Gulshan and Tariqabad nallahs **a)** fixed reference station at roof of DAM office **b)** measurement for lowest point and cross section

The points marked along both the nallahs during two surveys do not lie exactly above each other. Therefore, all the measured points are transferred to a common projection plane for the comparison and investigation of nallahs bed erosion and deposition. The common projection plane is actually a combination of least square lines, each for certain group of points following certain trend. **Fig.5** shows the plan profile of both the nallahs, showing all the marked points along with the common projection plane. The detail erosion deposition analysis and other observations are explained in the following sub-sections separately for each nallah.

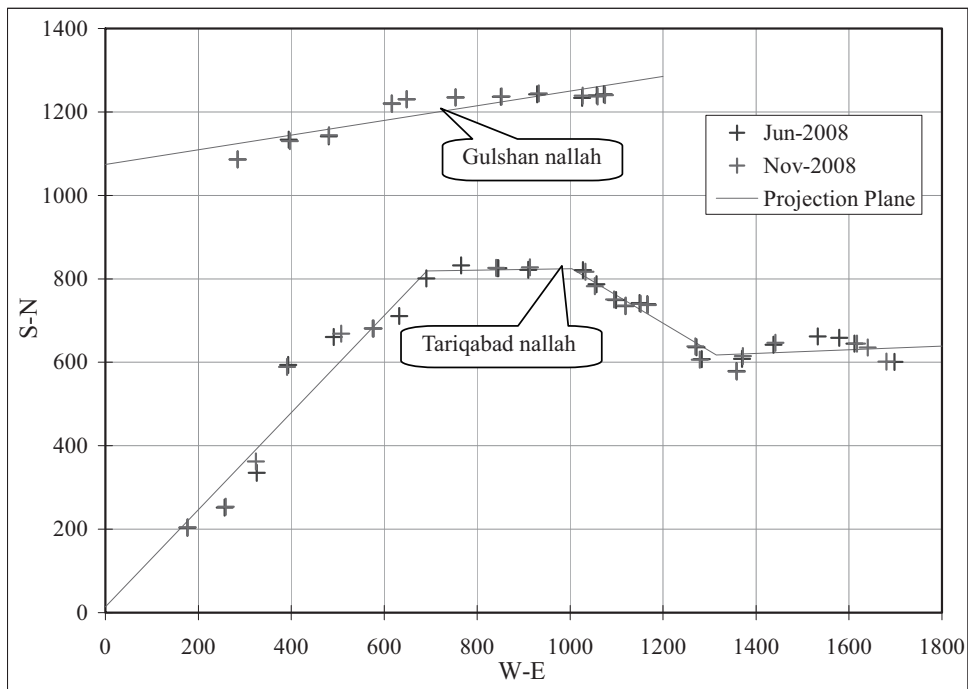


Fig. 5: Profiles of Gulshan and Tariqabad Nallahs along with a common projection plane

Gulshan Nallah

Gulshan nallah has a total length of about 900m with quite straight configuration. Since June and November measured points do not match exactly by location in the elevation plot (**Fig.6**), therefore curves are fitted to the marked data points by curve fitting technique using *spline* cubic function (**Fig.6**). The measured data points were divided into a number of groups following certain trend for smooth curve fitting. Even then this curve fitting may involve some error and gives an assumed profile between two measured points, but is a way to quantitatively evaluate erosion and deposition. By taking June measured points with fitted curve as reference, due to higher accuracy of June measurements, erosion and deposition analysis is carried out along the entire length of nallah.

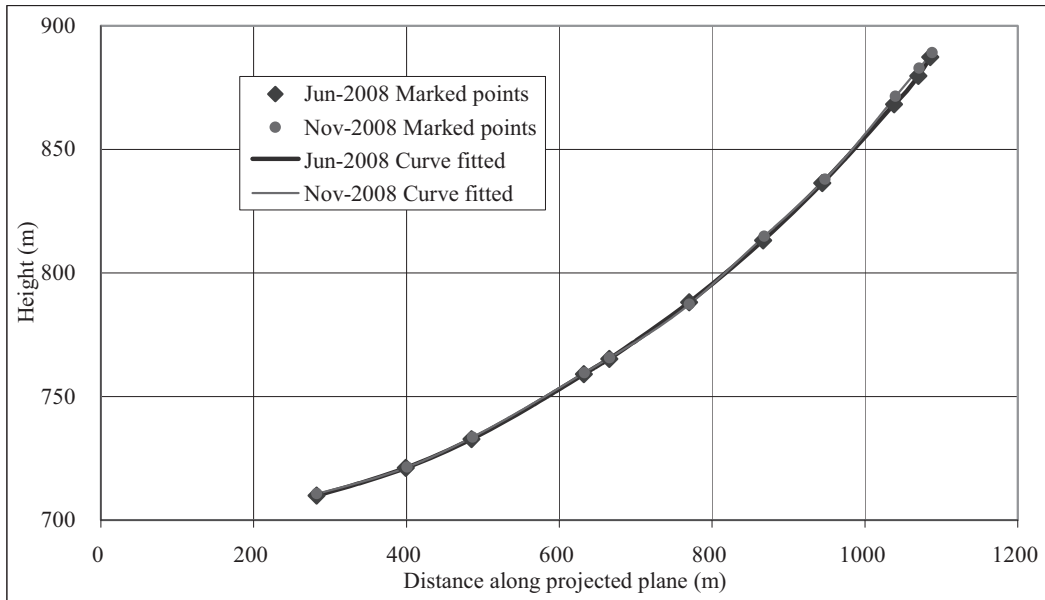


Fig. 6: Plot of June 2008 and November 2008 measured data points with curves fitted using cubic *spline* function

Fig. 7(a) shows the elevation changes of November measured points with reference to curve fitted to June measured data while **Fig.7(b)** shows the comparison of curves fitted to the both measured data indicating erosion and deposition along the total length of nallah with reference to the curve fitted to June measured data. In both of these figures, 7(a) and (b), negative values indicate erosion while positive values indicate deposition. **Fig.7(c)** shows the nallah bed gradient computed both from detail curve fitted data and measured points. The length above the point of 1000m along projected plane is the initiation zone with a bed gradient of $\geq 20^\circ$, verified by repeated field surveys. Very high depositional depth of about 3m shown in this zone is the accumulation of loose fractured material from the steep catchment of nallah which is then mobilized by rain water. Downstream of the point of 670m along the projected plane, data shows deposition along the channel with a gradient of $\leq 10^\circ$ defining the deposition zone. Data shows a depositional depth upto 0.9m with less depth at some places where material has been removed by local people for their use. Between these two points, both erosion and deposition have occurred defining the flow and transportation zone with the bed gradient between 10° - 20° . Erosion and deposition in this reach well agrees with the bed gradient variation with steep gradient responsible for erosion. This closely agrees with literature based on past observations in different areas of the world. Inhabitants are mostly populated in the depositional zone suffering from repeated debris flow events during monsoon.

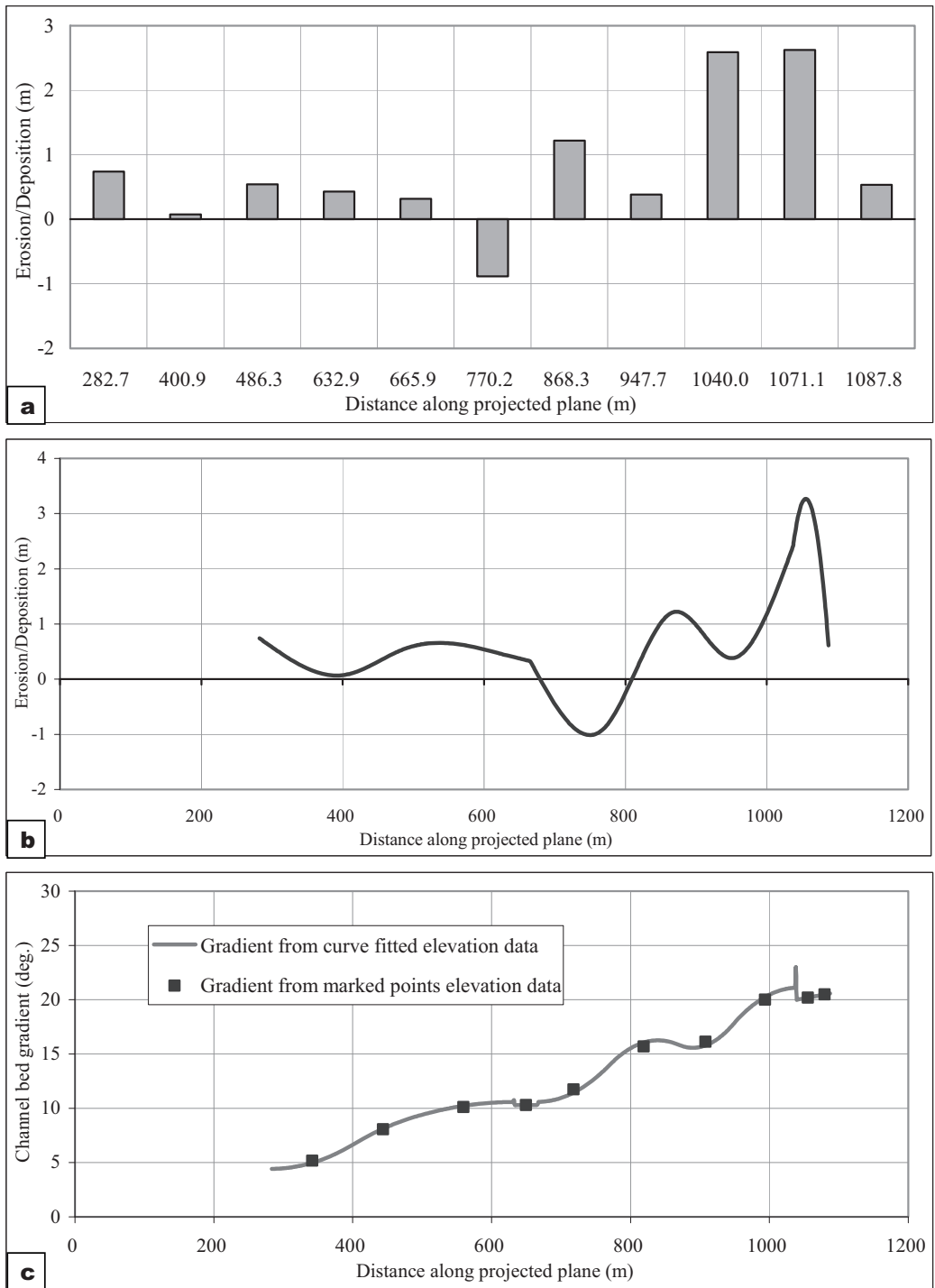


Fig. 7: a) Elevation changes of November measured points with reference to curve fitted to June measurement **b)** elevation changes along total length of nallah from curve fitted data **c)** nallah bed gradient

Tariqabad Nallah

Tariqabad nallah has a total length of about 1900m with an irregular configuration. Due to mismatching location of June and November measurements (**Fig.8**), curves were fitted using cubic *spline* function to the measured data points (**Fig.8**). Due to complex configuration of Tariqabad nallah, measured data points were divided into about 10 groups each following certain trend for smooth curve fitting. This curve fitting gives assumed profile of elevation between two measured points and may involve some error but makes quantitative evaluation possible. By taking June data as reference, erosion and deposition analysis is carried out along the nallah bed. **Fig.9(a)** shows the elevation changes of November measured points from curve fitted to June measured data while **Fig.9(b)** shows detail erosion and deposition comparing the curves fitted to measured data (negative values indicate erosion) with nallah bed gradient shown in **Fig.9(c)**. The length of nallah above point of 2000m along the projected plane is responsible for the initiation of the debris flow with a bed gradient of $\geq 18^\circ$. This reach has very steep channel banks with highly fractured loose debris material. This material flows down the steep slopes and is accumulated in nallah from where it is transported by already mobilized debris mass little upstream of it. GPS data indicates erosion in this reach which is the transportation of accumulated material and takes time to accumulate again. Downstream of point of 875m along projected plane, data shows deposition along the channel with a gradient of $<10^\circ$ defining the deposition zone. Depositional reach is relatively long with more depositional depth as compared to Gulshan nallah. This may be attributed to long length, irregular configuration and tributaries feeding at lower reach of nallah. Some points in this depositional zone indicate erosion which is resulted by man made changes and excavation of deposited material, observed during survey. Between both of the above mentioned points is flow and transportation zone where both erosion and deposition are indicated depending on the channel configuration and bed gradient. This flow and transportation zone has the bed gradient between 10° - 18° with some local high values.

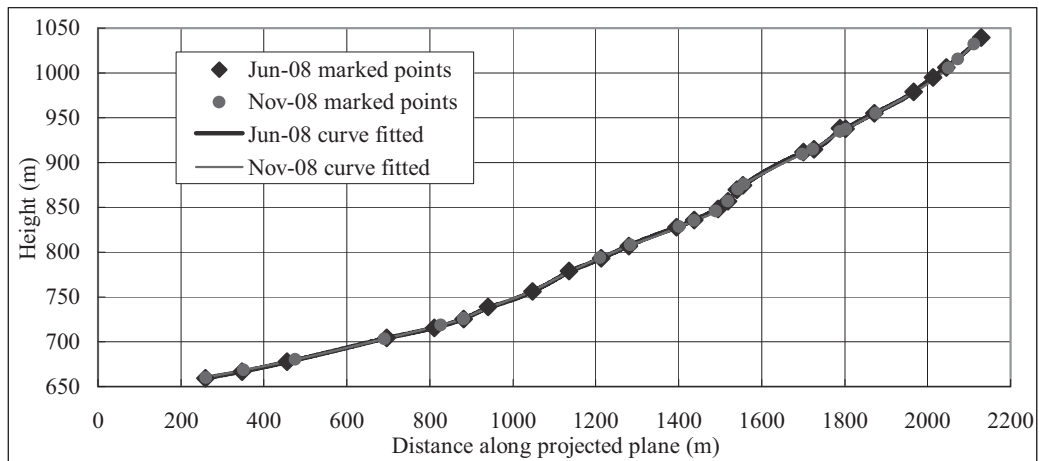


Fig. 8: Plot of June 2008 and November 2008 measured data points with curves fitted using cubic *spline* function

Inhabitants are mostly populated in the depositional reach with some living along the lower portion of flow and transportation zone. Due to irregular configuration of nallah, flow concentrates to outer sides of bend sections resulting in under cutting of outer bank. This undercutting causes landslides along the steep banks which is vital for inhabitants and some communication structures to considerable range. Such landslides inside the nallah are another source of debris material and are much dangerous due to bursting phenomena of temporary dams which they create.

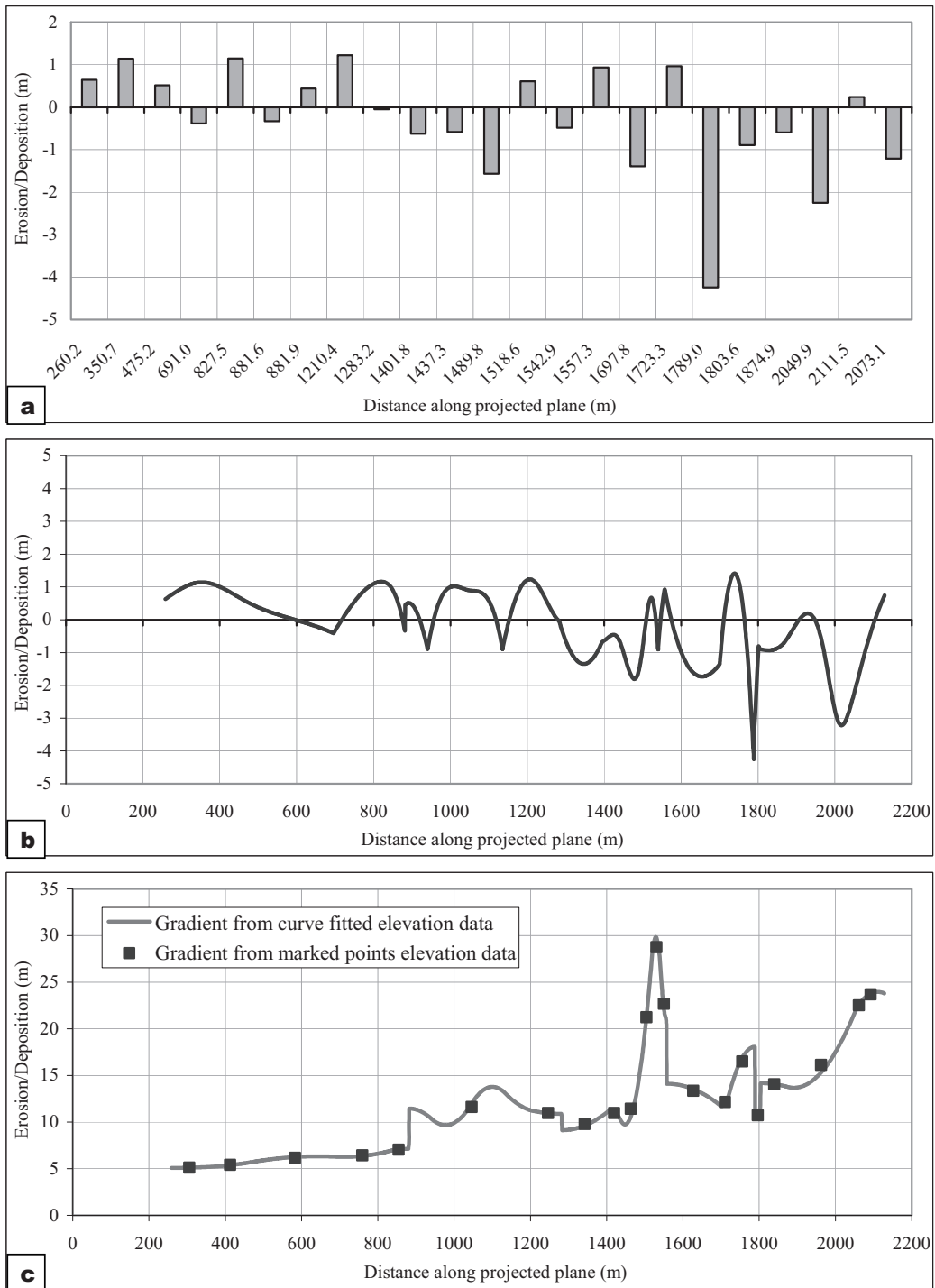


Fig. 9: a) Elevation changes of November measured points with reference to curve fitted to June measurement **b)** elevation changes along total length of nallah from curve fitted data **c)** nallah bed gradient

Fig.10 shows the change of flow width obtained from the measurements taken at the outer flow boundaries defined by traces of debris material or mud marks. Due to mismatching of marked points during two surveys, the detail comparison is quite difficult but the increased flow width in initial zone is evidences transportation of material accumulated in the nallah from steep banks. Decrease in flow width is possible with the disturbance of flow boundaries by nature or human activities. Depositional reaches of nallahs are usually disturbed by local people by removal of material for their use or by construction of some structure. This is quite clear that downstream of point *A* in figure 10, which is the populated zone, flow depth has more disturbances as compared to upstream of that

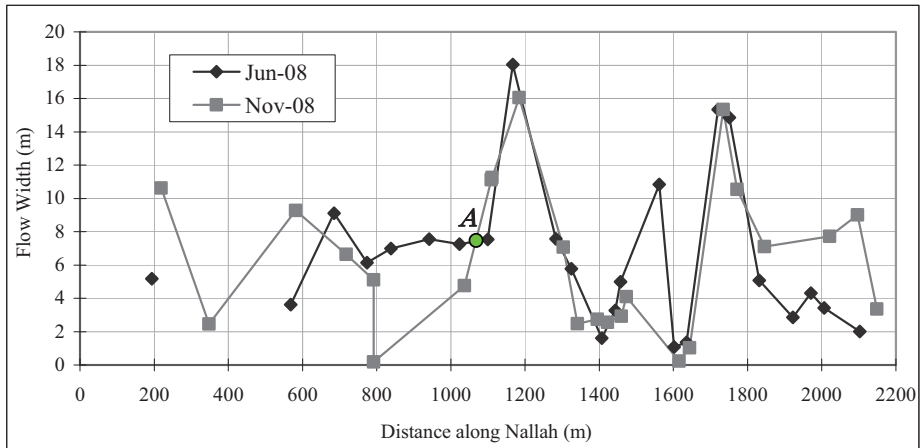


Fig.10 Channel flow width

CHANNEL MORPHOMETRIC PARAMETERS

During the second survey, 11 cross sections of both the nallahs were measured at bends (**Fig.11** and **Table1**). At these sections with channel slope less than 15° , the velocity of debris flow was estimated from superelevation of lateral deposits or mud lines left by the peak discharge according to Johnson (1984) as;

$$v^2 = g \times \psi \times \Delta h / W$$

Where g is the acceleration due to gravity, ψ is the radius of curvature of centre line of channel bend, Δh is the superelevation of flow and W is the flow width.

Due to quite straight configuration of Gulshan nallah, available numbers of sections for measurement were less compared to Tariqabad nallah. In the field superelevation angle of lateral deposit was measured by clinometer, cross section was measured with tape and radius of curvature was determined from the automatically marked points by GPS at an interval of one second. Velocity and peak discharge values, estimated as the product of average velocity and the flow cross section area, are reported in Table 1.

Velocities ranged from 4.8 to 10 m/s in the initiation and flow zones of Tariqabad nallah and about less than 4.0 m/s in the depositional reach. Debris flow peak discharge varied between 21 and 90 m^3/sec . The velocity range for main flow reach of Gulshan nallah is 5.3 to 6.9 m/sec while discharge lies between 37 to 76 m^3/sec . The depositional reaches of both the nallah are usually disturbed by removal of deposited material for local use. It is clear from the results that Gulshan nallah has more velocity and discharge compared to Tariqabad nallah. The first and 7th sections in Tariqabad nallah show high values of velocity and discharge which are local effects of feeding channels while Gulshan nallah has no tributary.

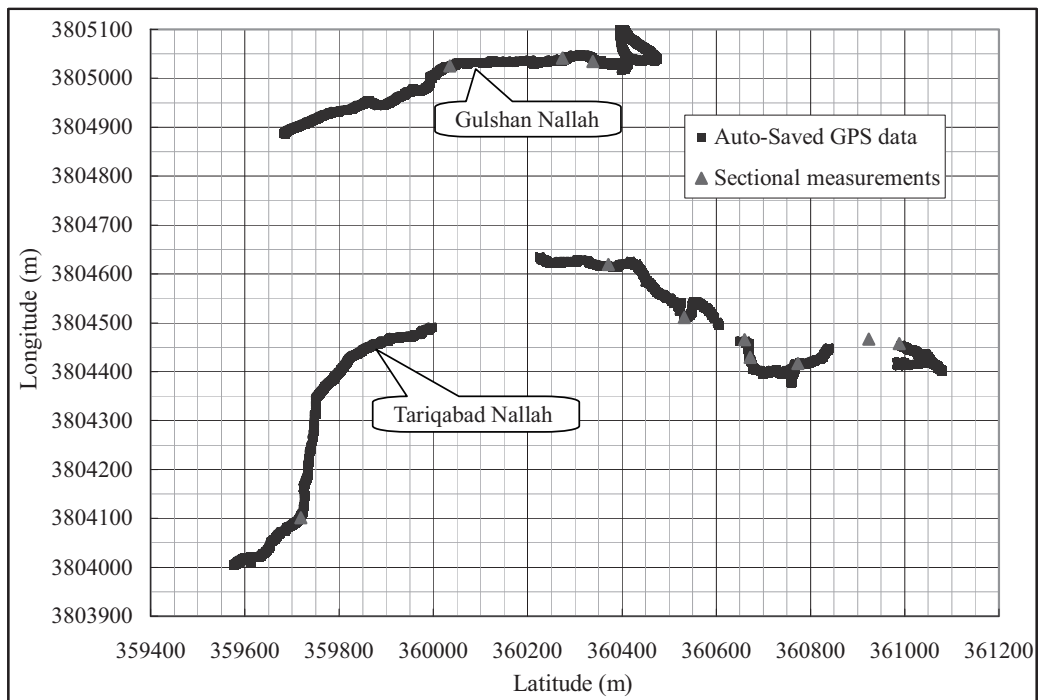


Fig.11 Auto marked GPS data showing profiles of nallahs along with sections of velocity and discharge measurement

Table 1 Morphometric measurements along Gulshan and Tariqabad nallahs

Nallah	Section #	Depth D (m)	Width W (m)	β ($^{\circ}$)	Ψ (m)	v (m/sec.)	Q (m^3 /sec.)
Tariqabad	1	1.20	3.30	11	52.38	9.99	39.58
	2	1.25	3.10	7	N/A	N/A	N.A
	3	0.63	8.50	4	53.57	6.06	32.20
	4	1.15	5.60	6	40.48	6.46	41.60
	5	1.65	4.30	8	16.67	4.79	34.01
	6	1.05	5.10	6	15.48	3.99	21.39
	7	1.20	10.00	5	65.48	7.50	89.96
	8	N/A	12.00	3	45.24	4.82	N/A
Gulshan	1	1.30	9.10	7	37.52	6.72	79.53
	2	1.15	9.60	8	34.72	6.92	76.39
	3	1.20	5.80	4	41.67	5.35	37.21

Inversion et al. (1994) analyzed the error involved in the superelevation method and found estimates to be within 30% of measured velocity values, with error mainly due to the passage of frontal bore in which conditions of steady and uniform flow are violated, particularly at sharp bends. Moreover splashing at the bends could exaggerate mud marks, and assumption of linear surface profile may overestimate the flow cross section (Jakob et al., 1997).

MATERIAL PHYSICAL CHARACTERISTICS

Grain size distribution has been performed on material sampled in deposition and source area. The grain size distribution, obtained on the fraction passing 20mm sieve, shows a difference between two areas (**Fig.12**). While flowing from initiation to deposition area percentage of fines (less than about 1 mm) is decreased but the fraction ranging from 1-20mm has significantly increased in both the nallahs. High shearing effect at the initiation area due to the fault may have caused extremely fine particles which may have washed during flow or flowed down the depositional reach as hyperconcentrated flow. But the sand size particles are increased due to the rolling and collision effect as well due to entrapping the bank material which consists of Murree formation having a good fraction of sand size particles.

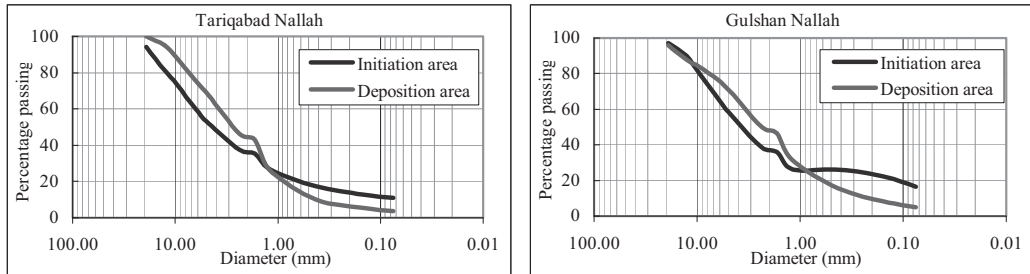


Fig.12 Grain size distribution of source and deposited material in Gulshan and Tariqabad nallahs

NUMERICAL SIMULATION

Though many erosion protection and mass flow control structures are being used to reduce the devastating effects of debris flow but still the hazard is there because the complete control of flowing masses is not possible. Thus it is important to evaluate the debris flow risk and perform hazard zoning with the help of run-out analysis and the contribution of any control structure in hazard reduction to its downstream. Also it is very important to understand the actual flow behavior for certain material and topographical settings.

To achieve the above mentioned goals, run-out analysis tool should be practical and should give satisfying results with limited input data from site investigations. For the subject study DAMPM (Depth Average Material Point Method) numerical tool is used. MPM (Material Point Method) is method proposed by Sulsky et al. (1995) to deal with large deformations, eliminating the mesh entanglement. In this method, the Material Points carry all the lagrangian parameters which are updated at each time step and more realistic constitutive models (Drucker-Prager Model) can be implemented. In DAMPM, modeling a debris flow mass as a group of material columns, following a simpler semi-empirical approach based on the concept of equivalent fluid, defined by Hungr (1995), is implemented in MPM for run-out analysis across three dimensional terrains. The practicality of the tool is proved by Abe et al. comparing the computational results with that of experimental results of open flume experiment performed by Denlinger et al.

Modeling

GPS detail measured data along Gulshan nallah is processed to formulate the digital elevation data of the target area defining the topographical setting. The domain outside the flow extent is just modeled as level area. The debris flow mass is modeled as a cluster of material columns. Some of the input parameters are tried to be adjusted to reproduce the close approximation of actual flow, observed during survey, while other taken as Abe et al. used in comparison of computational and experimental results.

The simulation results showing the flow depth and velocity distributions along the entire nallah are shown in **Fig.13** and **14** respectively. Color bars show the magnitude of the flow depth and flow velocity while solid lines in the figure are elevation contours showing three dimensional terrain in two dimensional setting (Pseudo 3D). Flow behavior (e.g. concentration of flow at outer edges of bend sections and front bore having high velocity) can also be observed from these animations. Computational parameters used as input for these animations are summarized in **Table2**.

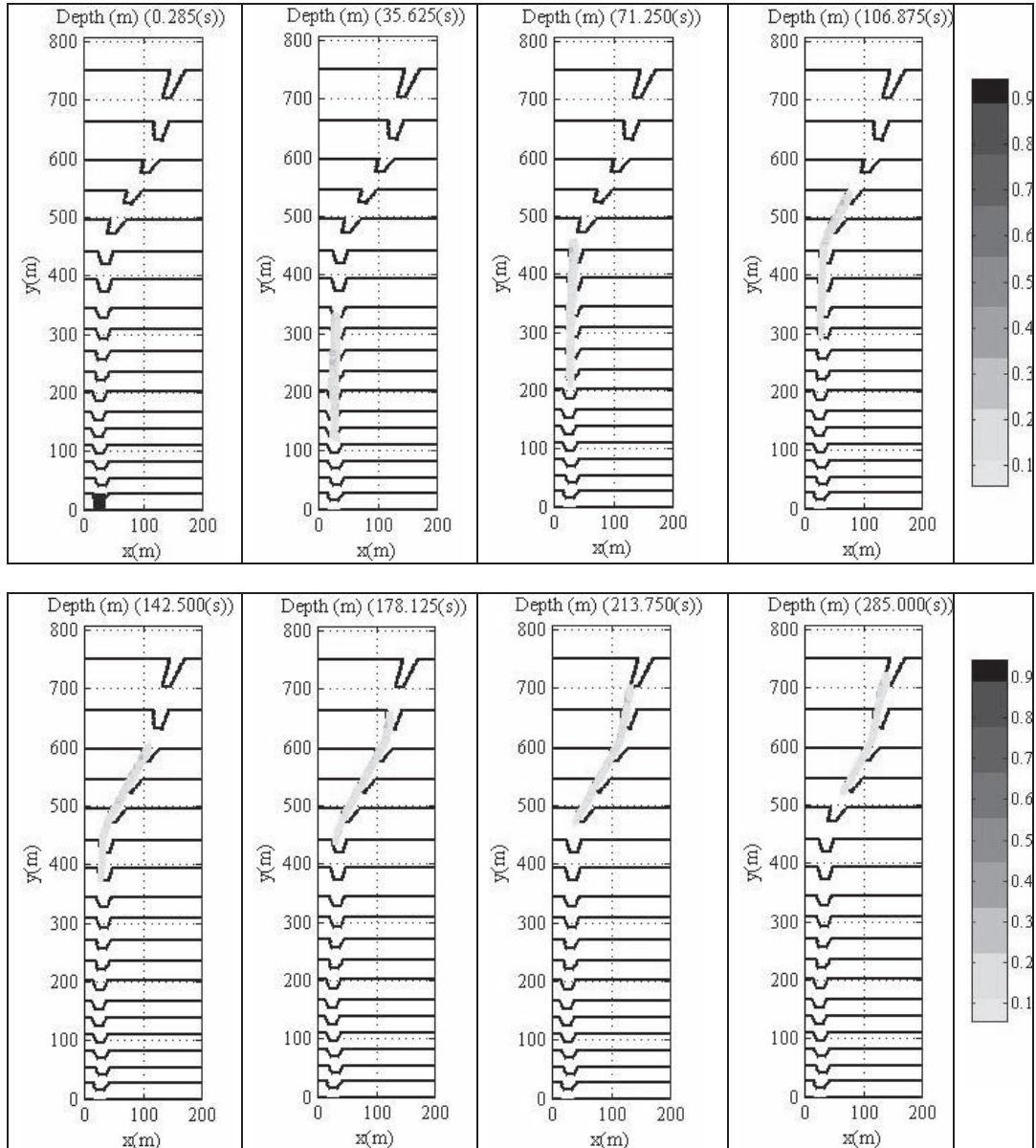


Fig.13 Flow depth distribution and flow behavior along the entire reach of Gulshan Nallah

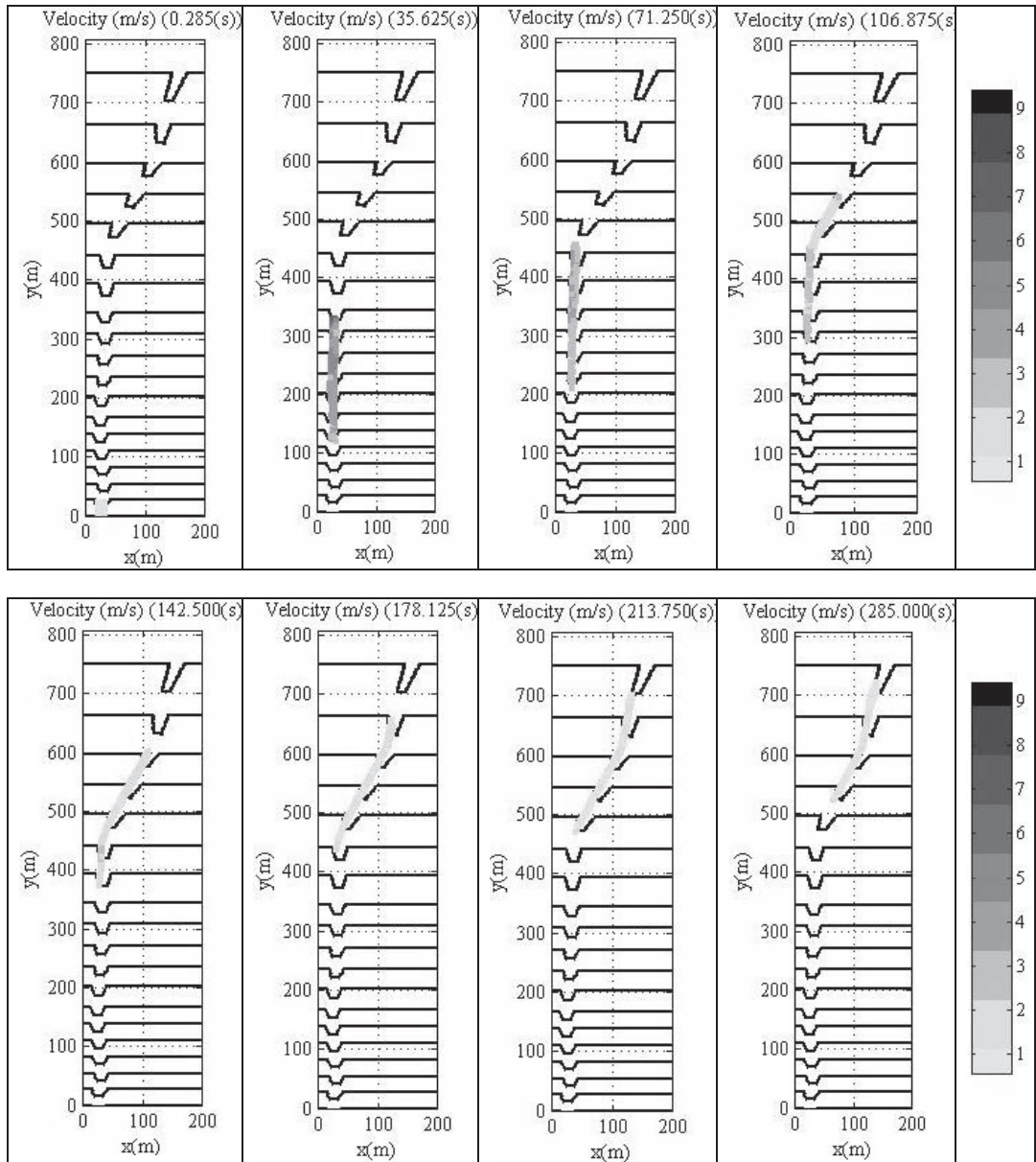


Fig.14 Velocity (in the direction of flow) distribution along the entire reach of Gulshan Nallah

Table 2. Input parameters used for Gulshan Nallah

Basal friction angle	5.7 (deg)	Angle of dilatancy	0.0 (deg)
Internal friction angle	30 (deg)	Number of material points/cell	9.0
Density	1590 (kg/m ³)	Length of mesh	2.0 m
Young's modulus	2.10×10^6 (Pa)	Turbulence coefficient	700 (m/sec ²)
Poisson's ratio	0.30		

Fig.15 shows the distribution of flow depth and flow velocity along the nallah along with the measured values by superlevation method. Both measured and simulation flow depth values are normalized with the flow depth at initiation section. The average flow velocity and normalized flow depth values by simulation are comparable to measured values except at section 3 where excavation of deposited material may have resulted in increased flow depth during measurement. For further calibration one should concentrate on these input parameters but should notice that measured values also involve an error upto 30% due to passage of front bore (Inversion at el., 1994). During the field investigation, authors found that downstream point *A* population has almost converged inside the nallah and it is very important to control debris upstream of this point by providing control structure/s. Upstream from point *A*, point *B* gives the least envelop with respect to maximum flow depth and maximum velocity suggesting an optimized location for any control structure.

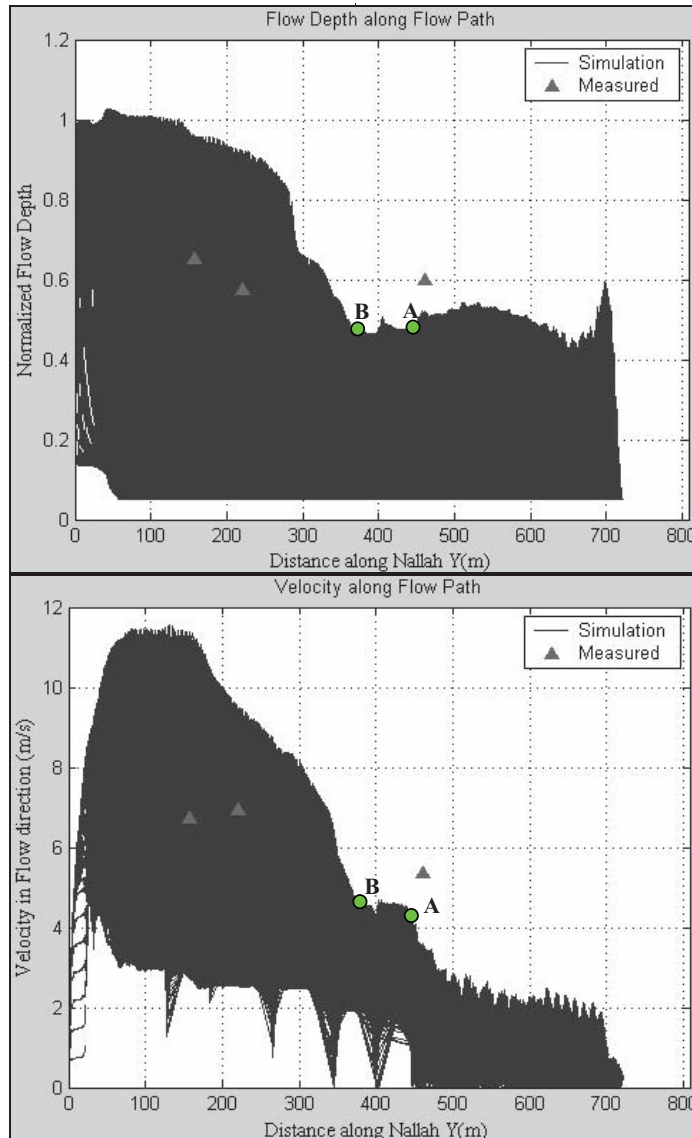


Fig.15 Flow depth and velocity distribution showing maximum and minimum envelopes along with measured values

CONCLUSIONS AND COMMENTS

1. A massive earthquake often causes long-lasting geological issues, and the October 8, 2008 Kashmir Earthquake was no exception. To quickly cope with these problems, a detail study is quite necessary.
2. The debris flows along both the studied nallahs follow the past experience for initiation, transportation and deposition and bed gradient. The debris flow effect along both the nallahs to inhabitants is rather depositional than impact.
3. Repeated and detail field measurements help in understanding the true behavior of debris flow and allow the estimation of hazard for different areas.
4. Although the structural and erosion control measures are used for debris flow control but it is almost impossible to completely stop the phenomena and totally trap the debris. Therefore, it is quite realistic to know the extent of debris flow target and prepare the hazard zoning. This can be done by simulating the debris flow for maximum possible discharge using some numerical tool. But this is very important that numerical tool should give realistic behavior and should be much practical requiring least possible input.
5. Instead of providing the control structures blindly, it will be more efficient and economical if the control structure is decided at the optimized location which is the location at which the flow as minimum energy.
6. DAMPM gives close approximation of actual flow behavior. However the some discrepancy is due to change in material properties during flow and pore pressure which is not accounted for.

ACKNOELEDGMENT

The authors are very thankful to DAM (Development Authority Muzaffarabad) for their collaboration and help during the field survey and devotion towards these long lasting issues and their mitigation strategies.

REFERENCES

- [1] Hiroshi P. Sato, Hiroyuki Hasegawa, Satoshi Fujiwara, Mikio Tobita, Mamoru Koarai, Hiroshi Une and Junko Iwahashi (2006) Interpretation of landslide distribution triggered by 2005 Northern Pakistan earthquake using SPOT 5 imagery. *Landslides* (2007) 4:113-122
- [2] Lewis A. Owen, Ulrich Kamp, Ghazanfar A. Khattak, Edwin L. Harp, David K. Keefer, and Mark A. Bauer landslide triggered by 8 October 2005 Kashmir earthquake. *Geomorphology* 94 (2008) 1-9
- [3] Geographical Survey Institute (GSI), Japan. Detection of crustal deformation of the northern Pakistan earthquake by satellite data
- [4] District census report, 1998
- [5] Kazuo Konagai, Johansson Jorgen, Takatsu Shigeki and Ikeda Takaaki: Huge landslides caused by massive earthquakes and long-lasting risks.
- [6] Report by JSCE-AIJ Joint investigation/ technical team for restoration and reconstruction of the affected areas by Pakistan earthquake on Oct. 8, 2005.
- [7] Dr. Navin Peiris, Dr. Tiziana Rossetto, Dr. Paul Burton, Mr. Suqlain Mahmood. EEFIT mission: October 8, 2005 Kashmir Earthquake
- [8] Metrological department, Pakistan (Data provided by Development Authority Muzaffarabad)
- [9] Matteo Berti, Rinaldo Genevois, Alessandro Simoni, Pia Rosella Tecca: Field Observations of a debris flow event in Dolomites. *Geomorphology* 29 (1999) 265-274
- [10] Keita Abe, Jorgen Johansson and Kazuo Konagai: A new method for run-out analysis and motion prediction of rapid and long-traveling landslides with MPM



GEOTECHNICAL ISSUES CAUSED BY THE MAY 12th 2008, WENCHUAN EARTHQUAKE, CHINA

Kazuo KONAGAI¹, Yoshiharu ISHIKAWA², Satoshi TSUCHIYA³ and Fawu WANG⁴

ABSTRACT: A devastating earthquake occurred in Longmen-Shan Mountainous terrain, Chendu, China on May 12, 2008. With the Grants-in-Aid for Scientific Research, Ministry of Education, Culture, Sports, Science and Technology, Japan, and the network of Japanese experts in the field of seismology, geology and earthquake engineering planned to organize a team (Leader: K. Konagai, the first author) asking collaboration from Chinese organizations and experts with the China Earthquake Administration (CEA) as its core, with the support from Ministry of Science and Technology of China. This report describes briefly findings obtained through the authors' reconnaissance, highlighting some geotechnical issues for better rehabilitations.

Key Words: Wenchuan Earthquake, geotechnical issues, rehabilitations

INTRODUCTION

An earthquake of magnitude 7.9 struck northwestern Sichuan province of China. Chinese Ministry of Civil Affairs stated that 69,197 were confirmed dead, and 18,222 listed as missing as of May 21st. This earthquake was remarkable in terms of length of activated fault in which a 280km long fault dislocation, a thrust formation appearing along the toe of steep ranges of Longmenshan Mountains, which was one of the longest fault offsets ever to appear inland. With this long fault in mountains, there is a serious concern that huge amount of debris deposits have been created in the zone along the fault stretch. In fact, a number of bare slopes were found exposed on satellite photographs including the world largest landslide with an area of about 50,000m² (Chigira et al., 2008). Large earthquakes that hit mountainous terrains often cause long-lasting problems of frequent debris flows. In Hietsu Earthquake, Japan (1858), a huge landslide mass of about 400 million m³ blocked the upper reach of Joganji River. It was estimated that debris flow as a result of failure of this landslide mass would have raised the level of Toyama plane, along lower reach of Joganji River, by about 1 to 2 meters. To control the debris mass flow, a number of check dams have been constructed so far and the current annual expenditure for debris flow control for Joganji River system reached 5 billion JPY. The October 8, 2005 Kashmir Earthquake, Pakistan is another case history. The earthquake induced slope failures created debris sources along the steep slopes. During monsoon of 2006, about 10 months after the earthquake, a debris flow occurred at Ghari Habibullah Khan leaving about 4 to 6 meters thick debris deposits at the exit of a canyon onto a flat plain along Kunhar River. Even within the city of Muzaffarabad, people living along valleys scratching terraces are suffering from debris from mountains rising behind, with their dwellings being half and/or entirely buried in debris. Future flows will most likely follow the gorges crossing roads and will suspend traffic. Clearing the debris

¹ Professor, Institute of Industrial Science, University of Tokyo

² Professor, Tokyo University of Agriculture

³ Professor, Shizuoka University

⁴ Assistant Professor, Disaster Prevention Research Institute, Kyoto University

remaining on the roads would be just a stopgap. One of the feasible ideas discussed among Japanese and Pakistani experts was to connect existing roads point-wise by constructing new bridges etc. A cost-effective bypass could be constructed allowing bi-directional traffic to be realized. Experiences are now being shared among these experts.

After the 2008 devastating Wenchuan Earthquake in Sichuan Province, international academic societies expressed great deal of condolences and showed great concerns to the related scientific issues. With the Grants-in-Aid for Scientific Research, Ministry of Education, Culture, Sports, Science and Technology, Japan (MEXT hereafter) and the network of Japanese experts in the field of seismology, geology and earthquake engineering planned to organize a team (Leader: K. Konagai, the first author) asking collaboration from Chinese organizations and experts with the China Earthquake Administration (CEA) as its core, with the support from Ministry of Science and Technology of China. Japanese nominees and experts from CEA have come to a firm common understanding that China-Japan joint investigation will contribute remarkably in learning lessons from the tragic devastations in a scientific manner and therefore in quick and rational rehabilitations.

Total seven sub-groups were organized to cover 7 subjects, respectively. They include (1) slope failures and remedial measures, (2) civil infrastructures and remedial measures, (3) houses and buildings, (4) seismology, (5) active fault, (6) geodesy and (7) rescue, restoration and economic damages. They have made total 20 reconnaissance trips. This report shows some findings from the authors' quick two-days survey (July 27-30, 2008). More details will appear in the MEXT final report.

BEICHUAN AREA

Slope failures

Beichuan is a county under the jurisdiction of Mianyang Municipality in Sichuan province. This town was most seriously damaged by the earthquake and was under strict security conditions being completely separated with a fence by the Chinese army. Fig. 1 shows the route for the authors' survey (July 27th) and locations of photos. Photo 1, the view of the downtown after the earthquake, was taken through the fence at the northern end of the route (31°49'09.7"N, 104°27'05.7"E presumed location from Google map). Some findings and/or indications from these photos are:

- (1) The shake must have been intense enough to destroy many houses and buildings to be sure, but two major slope failures on both sides of the city have certainly caused fatal and wide-spread damage to built-up downtown areas of the city.
- (2) The western slip surface is about 300 m high, and dips about 35 degrees east-northeast. The landslide mass from this west slope was about 400 m wide and surged about 430m of downtown area. The landslide reached its maximum thickness near its distal end because of being slowed down as it traveled further onto the built-up area. The total volume of the soil mass was estimated to be about 5,200,000 m³ presuming its average thickness as 30 m.
- (3) The eastern slip surface was about 300 m high, and dips about 40 degrees northwest. The landslide mass was about 400m long, 400 m wide and 20m thick. The volume of the landslide mass was presumably 3,200,000 m³. The landslide mass included much larger rocks than those in the mass from the west slope.
- (4) There are some dolomite rocks exposed along the eastern mountain slopes. Solubility of dolomite allows water to seep easily through its cracks and water enlarges the cracks in such a way that cavity systems are formed in its interior. Dolomite rocks are often weak enough and eventually break into pieces.

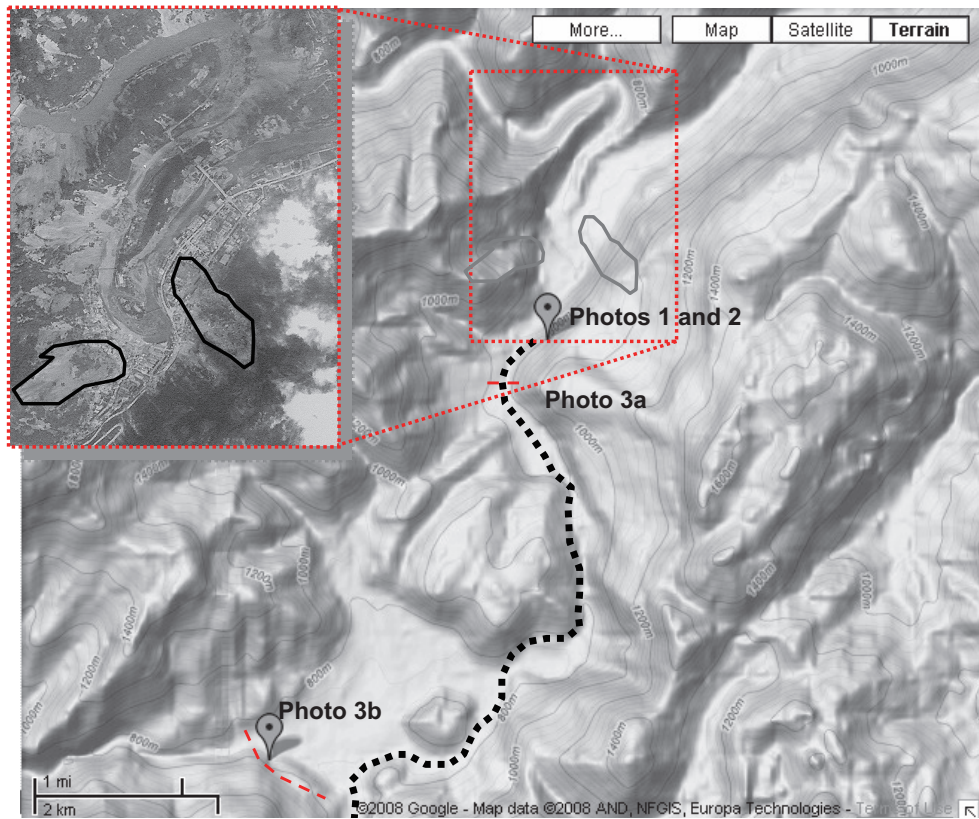


Fig. 1. Beichuan and its vicinity: Thick broken line shows the route for the authors' survey.



Photo 1. Downtown of Beichuan County. Two major built-up areas were completely destroyed by two major slope failures.



Photos 2a and 2b. South built-up area of Beichuan County. Photo 2a was taken on July 27th, 2008 while Photo 2b shows the same area in December, 2008, buried beneath thick debris mass. (Photo 2b by Maki, N., DPRI, Kyoto University)

At later date, on September 24th, it was reported that two-day heavy rain at Beichuan county triggered debris flow and larger parts of the southern half of the city was buried. As a consequence, the plan to preserve quake-devastated Beichuan as an earthquake museum was put on hold. Photo 2b (by Maki, N.) shows the debris mass remaining in the southern part of the city. Comparing Photos 2a and 2b, the

debris mass which have been carried over the three months (September, 2008 to December, 2008) is estimated to be about 10 to 12 m thick at this location.

Fault ruptures

Fault ruptures appeared in Beichuan and its vicinity. Densmore et al. (2007) described the detailed geomorphologic features of the terrains along the Longmen-Shan fault (see Fig. 2). One of the observed rupture (Point A in Fig. 2) appeared almost on this recognized fault trace, while the other (Point B in Fig. 2) appeared off the trace. As is often the case, the thrust faults seem to make up a wide brush, which extend across the central areas of Beichuan. Some serious devastations and landslides may have been due to fault offsets. To have a clear perspective on how the area should be rehabilitated, fault traces are to be precisely mapped.

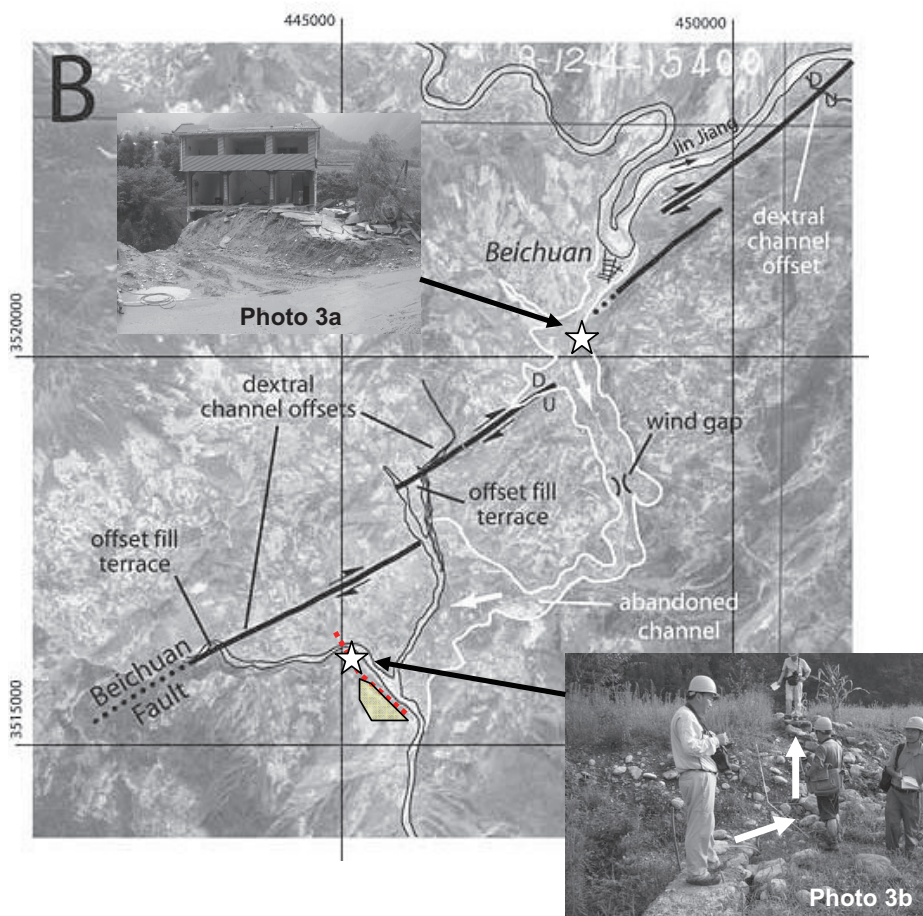


Fig. 2. Interpretation of fault traces in Beichuan and its vicinity by Densmore, A. et al. (2007): Thick lines show interpreted fault traces. Thin white lines show margins of abandoned channel of the Jin Jiang; white arrows show inferred flow direction. The Jin Jiang is now diverted at Beichuan and flows northeast, parallel to the Beichuan fault.

QINGCHUAN AREA

Being located near the northern end of recognized fault rupture, Qingchuan County has continuous aftershocks of high magnitude since the Wenchuan Earthquake. The shake there must have been responsible for a number of landslides and debris mass flows including the following two stopping flows of TongHe River and its tributaries. A large debris flow occurred on a mountain slope at TongHeKuo (Fig. 3 and Photo 4). The source area was about 400 m higher than the photo-shooting location. The debris mass rushed down the gully and surged up the hill, where the photo 4 was taken. After making a turn over the hill, it went down about 2km along the main stream of the TongHe River. The debris mass was reportedly responsible for the loss of about 400 people at TongHeKuo village. The mass stopped flows of both TongHe river and its tributary (Photo 4). Judging from the marks of maximum water level and from the estimated present water depths, the debris mass was estimated to be about 20 m at the merging section of TongHe River and the tributary. The flow has left an S-shaped trace along the valley and segregation was clearly observed. One more example is about 4km upstream side of the TongHe village (Photo 5). The landslide mass was responsible for complete destruction of four villages and about 400 lives were reportedly lost in the landslide mass. The maximum depth of the stopped water was estimated to be 25m. However, it was lowered to 10m after constructing an emergent spill way. The valley area between these two landslide masses has been called “ShiBan-Gou” (Slate-Valley in English). A lot of weathered slates were exposed on both sides of the valley.

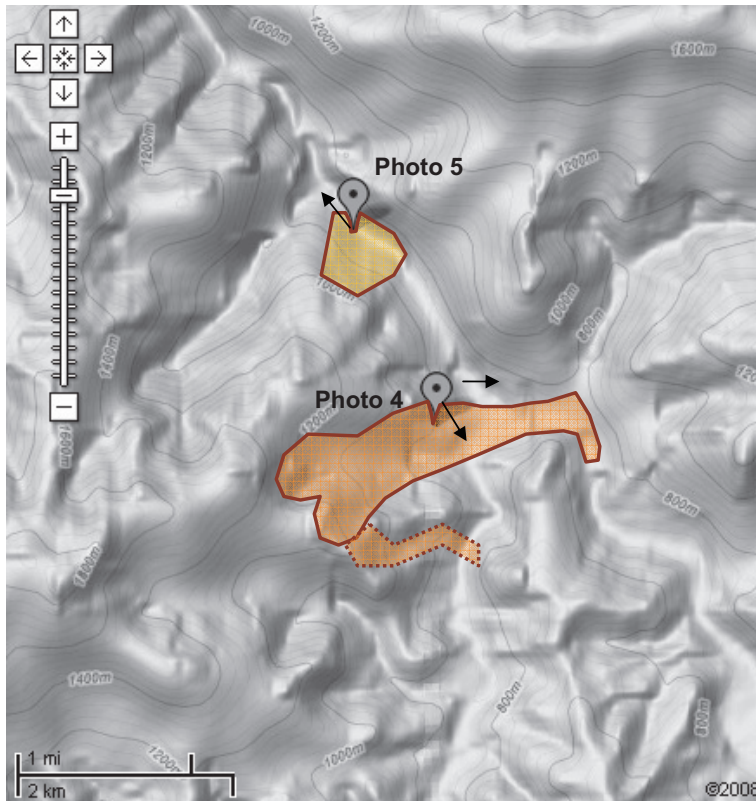


Fig. 3. Two major landslides at TongHeKuo, QingChuan County (from Google map)



Photo 4. Debris mass flowed down to TongHeKuo village: The debris mass is stopping waters of the major flow of TongHeKuo river (left) and its tributary (right). (Photo taken on July 28, 2008, at 32°23'55.1"N, 105°07'13.3"E: Location estimated from Google earth: See Fig. 3)



Photo 5. Landslide mass at “ShiBan-Gou” (Slate-Valley in English): (Photo taken on July 28, 2008, at 32° 25'55.5"N, 105° 06'32.2"E: Location estimated from Google earth: See Fig. 3)

YINGXIU AREA

YingXiu was one of the most severely devastated areas nearby the epicenter. At about 2 km southwest of YingXiu, the distal end of a large debris mass along NiuJuan Valley is reaching Ming Jiang River (Photo 6). The volume of the entire debris mass is estimated to be about 5 million m³. This flow left its marks along NiuJuan Valley and the flow along a curved channel had enough momentum to surge up along its outer bank. Assuming that the line connecting available traces of debris along banks represents inclined mud flow surface, the following equation is obtained.

$$\theta \cong \text{centrifugal force} / \text{gravitational force} = \left(\frac{mv^2}{R} \right) / (mg) \quad (1)$$

where, R = radius of curvature, and one obtains:

$$v \cong \sqrt{Rg\theta} \quad (2)$$

Necessary parameters for Eq. (2) at the curve in Photo 6 are roughly estimated from the photo and the topographical map (Fig. 4) as:

$$\theta \cong 0.13, \quad R \cong 400 \text{ m},$$

Substituting these parameters in Eq. (2) yields:

$$v \cong \sqrt{Rg\theta} = 22\text{m/s} \quad (3)$$

Sabo Technical Center uses the following equation for estimating debris velocity:

$$v \cong \sqrt{Rg\theta/\alpha} \quad \text{with } \alpha \text{ empirically set at } 10 \quad (4)$$

And the velocity will be:

$$v \cong 7\text{m/s} \quad (5)$$

Going up along the NiuJuan Valley, there is the point where the debris mass from the source area flowed down to the valley (Photo 7). The debris mass scraped off vegetations on this slope, and either surged or jumped about 40-45m up on the other side of the valley. NiuJuan Valle at this location is about 150m wide. These traces are to be carefully measured for estimating velocities of debris mass flows at different locations. Debris flows are long-lasting problems affecting seriously rehabilitation strategies for the devastated areas.

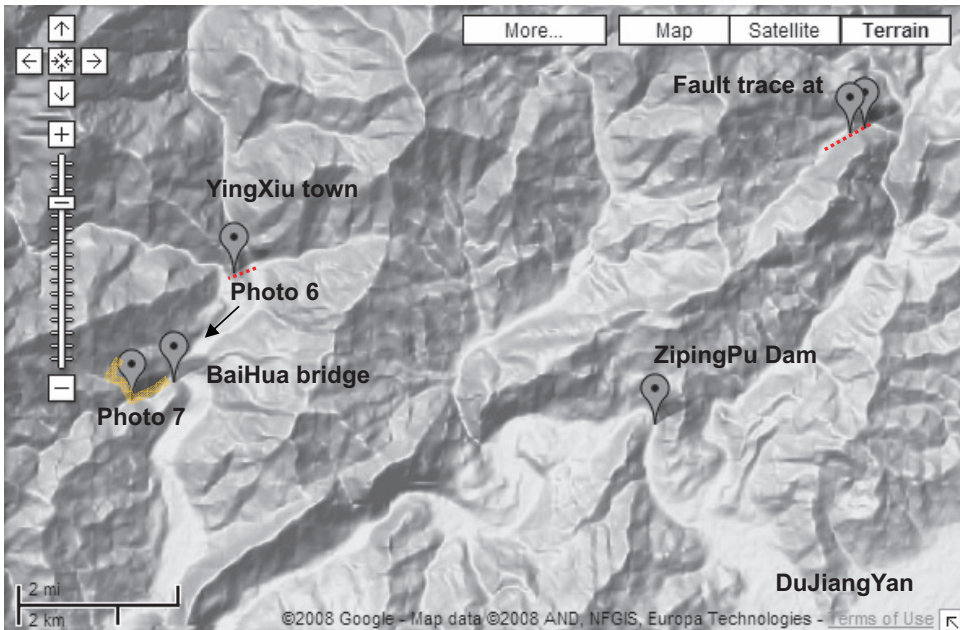


Fig. 4. YingXiu county and its vicinity:

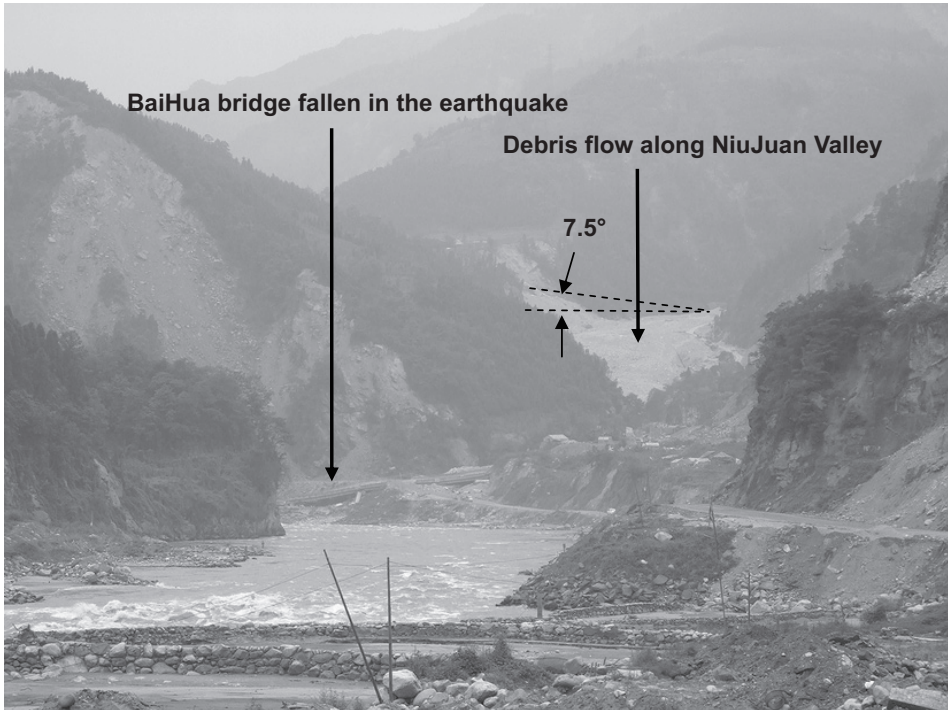


Photo 6. Debris mass flow reaching Ming Jiang River (Photo taken on July 29, 2008, at $31^{\circ} 03'09.1''N$, $103^{\circ} 28'43.2''E$: Location estimated from Google earth: See Fig. 4)

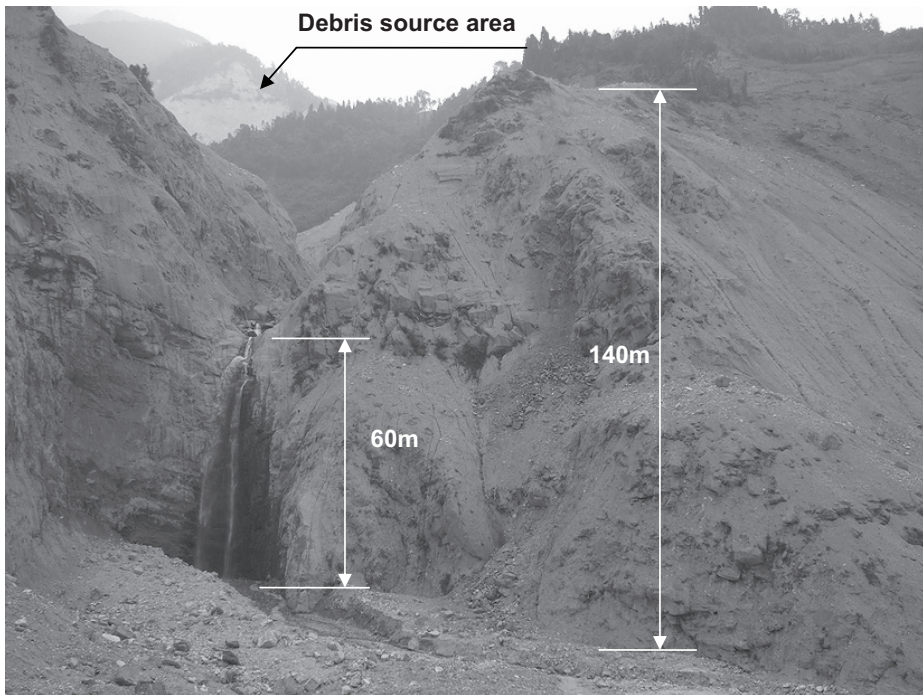


Photo 7. Debris trace: NiuJuan Valle at this location is about 150m wide. (Photo taken on July 29, 2008, at $31^{\circ} 02'27.4''N$, $103^{\circ} 27'48.5''E$: Location estimated from Google earth: See Fig. 4)

SUMMARY

The May 12th, 2008, Wenchuan Earthquake was remarkably large in terms of the length of the activated fault, affected areas, estimated cost of rehabilitation etc. With the Grants-in-Aid for Scientific Research, Ministry of Education, Culture, Sports, Science and Technology, Japan and the network of Japanese experts in the field of seismology, geology and earthquake engineering organized a team (with the first author as the leader) asking collaboration from Chinese organizations and experts with the China Earthquake Administration as its core. Based on the authors' first reconnaissance trip, this quick report summarized some geotechnical aspects of the damage.

It was shocking that a two-days heavy rain at Beichuan county on Sept. 23rd and 24th triggered a debris mass flow, and larger part of the southern half of the city was buried. Rehabilitation issues often attract less attention than issues that arise in the immediate aftermaths of earthquakes, and have never been given prominent coverage by news media. This event at Beichuan reminds us of some long-lasting issues after devastating earthquakes. Both the 1999 ChiChi earthquake, Taiwan and the 2005 Kashmir earthquake, Pakistan for example, formed a great number of debris deposits along their activated faults. Heavy rains in the monsoon of 2006 that followed the Kashmir earthquake were responsible for raising river beds. At Ghari Habibullah village, 4 to 5 kilometers west of the northern segment of the Muzaffarabad fault, about 4 to 6 meters of thick debris deposits were formed at the exit of a canyon onto a flat plain along the Kunhar River (Konagai, 2009). The ChiChi earthquake was followed by a number of typhoons in rapid succession. They included Toraji and Nari in 2001, Mindulle and Aere in 2004. About 3.9 typhoons on the average over the past ten years (1996-2005) have hit Taiwan, causing a three-fold increased risk of debris flows. As a result of these typhoons, an increase of river bed elevations of about 4 to 8 meters have been reported (W.F. Lee, 2007).

In order to have a clear perspective for dealing with long-lasting landform changes, monitoring landforms at different times is strongly recommended.

ACKNOWLEDGEMENT

This survey was granted by the Ministry of Education, Culture, Sports, Science and Technology, Japan. The authors are indebted to all experts from China Earthquake Administration, Institute of Mountain Disaster and Environment, Chinese Academy of Sciences. It is our sincere wish that MEX team and the abovementioned organizations, will be in tight collaborations beneficial for both Chinese and Japanese sides. Lastly, on behalf of the ERS members, we would like to extend hereby our deepest condolences to the families of those who have been killed or injured in the earthquake.

REFERENCES

- [1] Chigira, M., Wu, X., and Inokuchi, T. (2008): Characteristics and Distribution Pattern of landslides Induced by the 2008 Wengchan Earthquake, Sichuan, China, Proc. Management of Landslide Hazard in the Asia-Pacific Region, 248-256, Sendai, pp.11-15.
- [2] Konagai K. (2009), "Huge landslides caused by massive earthquakes and long-lasting geotechnical risks," Landslides – Disaster risk reduction --, Kyoji Sassa/ Paolo Canuti eds., Springer, ISBN 978-3-540-69966-8, pp.159-176.
- [3] Konagai, K., Tsuchiya, S., Ishikawa, Y., and Wang F (2008): Provisional report of landslides, debris mass flows in the May 12th 2008, Wenchuan Earthquake, SEISANKENKYU, 60(6), pp. 3-8.
- [4] Lee W.F. (2007), personal communication.
- [5] Densmore, A., Ellis, M., Li, Y., Zhou, R., Hancock, G., and Richardson, N. (2007): Active tectonics of the Beichuan and Pengguan faults at the eastern margin of Tibetan Plateau, TECTONICS, Vol. 26, TC4005, doi:10.1029/2006TC001987.



PROVISIONAL REPORT OF THE DAMAGE CAUSED BY THE JUNE 14th 2008, IWATE-MIYAGI EARTHQUAKE

Kazuo KONAGAI¹, Tomohiro FUJITA², Fumihiko NOMURA², Yuriko TOMIYASU²,
Masaki DATE³, Yoshimitsu TAJIMA⁴ and Toshihiko KATAGIRI⁵

ABSTRACT: A M7.4 Earthquake jolted south of the inland of Iwate Prefecture at 8:43 JST on Saturday morning, June 14. Even though the peak acceleration of 4022 cm/s^2 was the largest on records, damage to dwellings did not seem to be serious. Much more serious issues were about landslides and debris flows. The authors made several field surveys; first from June 15 to 17, second from July 12 to 14 and then from Sept. 8 to 9. The results from these surveys are shown in form of figures in this report. The latest version of this document is available at: <http://shake.iis.u-tokyo.ac.jp/home-new/>

Key Words: Iwate-Miyagi Earthquake, geotechnical issues, rehabilitations

INTRODUCTION

An earthquake of JMA magnitude 7.2 struck a border area between Iwate and Miyagi prefectures, Japan, on June 14th, 2008. The epicenter was located at $39^{\circ} 01.7'N$, $140^{\circ} 52.8'$ beneath mountain terrains with Kurikoma volcano. This earthquake was remarkable in that a number of debris flows were triggered, while less serious damages to dwellings were reported. Ministry of Land, Infrastructures, and Transport made quick estimate of property losses of around 12 million JPY and 2.94 million JPY for Miyagi and Iwate prefectures, respectively. The greater part of the losses was due to geotechnical hazards. The authors were members in the field reconnaissance first one from June 15 to 17, second from July 12 to 14, and then Sept. 8 to 9, have compiled the results in forms of figures shown below. The latest version of this document is available at: <http://shake.iis.u-tokyo.ac.jp/home-new/>. At this moment, the drawing reflects the authors own opinions and views, but the figures will be updated with the help of more detailed field information and other experts' opinions.

SLOPE FAILURES

Aratosawa landslide

Fig. 1 shows the bird's eyes view of a largest landslide at Aratosawa with Kurikoma Volcano rising behind. The terrain here is suggestive that similar landslides have been reactivated. A wide-spread and almost horizontal laminar structure of loose volcanic sand and ashes is exposed on the escarpment. When wet, some pieces of light-gray rock fragments taken from the toe of the landslide mass smelled strong hydrogen sulfide (see Fig. 3)

¹ Professor, Institute of Industrial Science, University of Tokyo

² Graduate student, ditto

³ Undergraduate student, ditto

⁴ Associate Professor, Department of Civil Engineering, University of Tokyo

⁵ Technical staff, Institute of Industrial Science, University of Tokyo



Fig. 1. Landslide at Aratosawa dam: (Photo by K. Konagai, June 15, 2008)

Fig. 2 shows a digital elevation model (DEM hereafter) of the landslide at Aratosawa. The road locations before (gray) and after the earthquake were drawn upon the DEM by using images from helicopter survey, photos (black lines), and field GPS survey (open circles) etc. The arrows show that Points P₁, P₂, P₃ and P₄ have respectively moved about 200m, 300m, 300m and 500m SSE towards the dam lake. The slide blocks are lined up in a succession. The cross-section A-A' (Figure 2b) shows a gradient of about 3-4 degrees. Even though the base slope was very gentle the soil masses have moved some 200 to 500 meters.

A rock piece from the landslide mass was taken at 38.8942°N, 140.8545°E, to determine specific gravities under different conditions (Fig. 3).

Specific gravity immediately after the sample was taken (18:00JST, June 16, 2008)	= 1.78 g/cm ³
Specific gravity after the sample was dried for 24 hours at 105° C in oven	= 1.18 g/cm ³
Specific gravity after the sample was again soaked up in water for three hours	= 1.69 g/cm ³

When soaked in water, the sample smelled hydrogen sulfide which is evidence that the materials were from volcanoes. It is remarkable that the specific gravity of the dried sample is quite small, indicating large volume of voids.

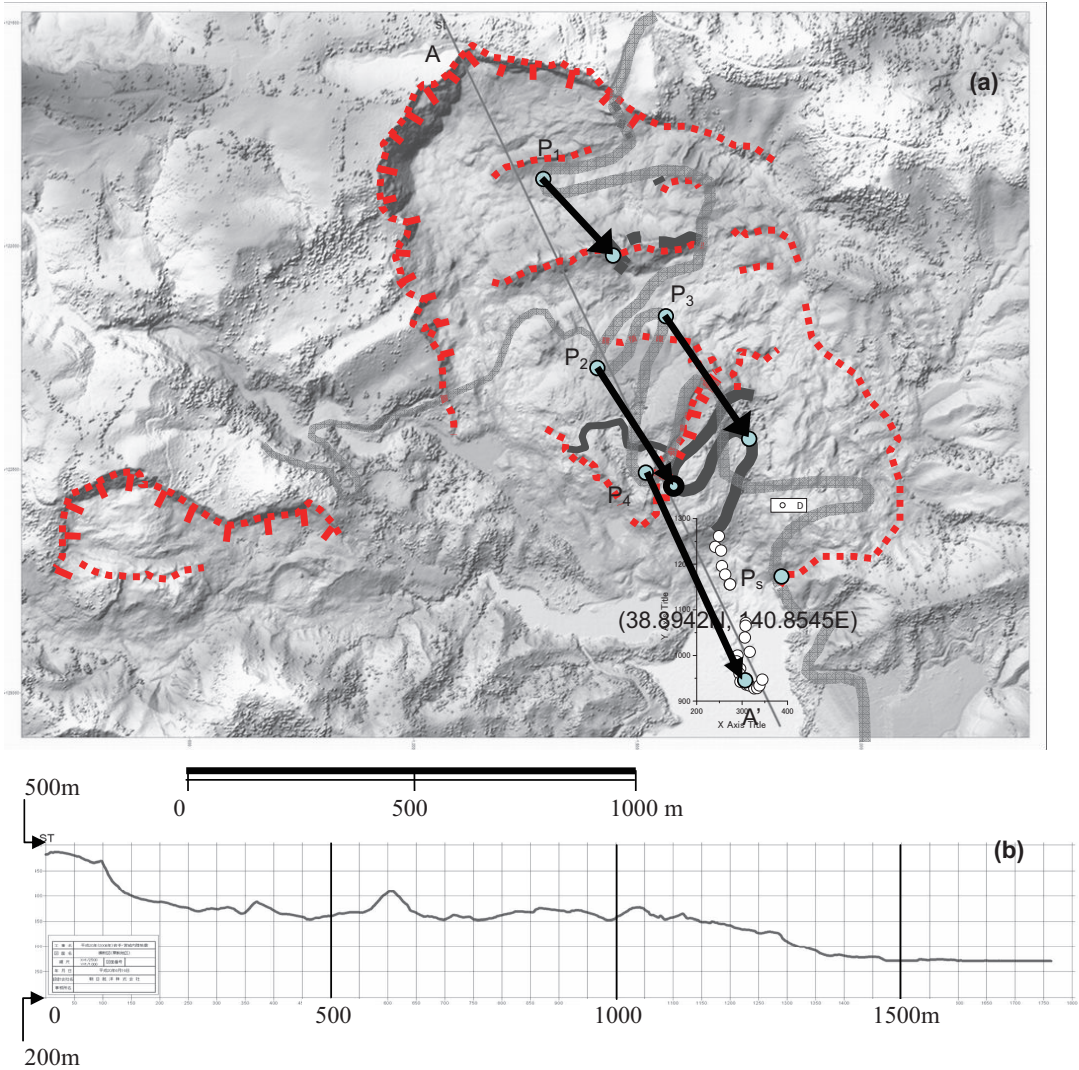
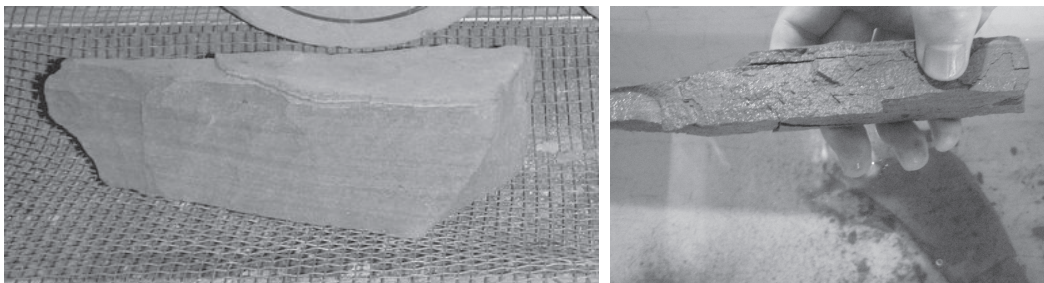


Fig. 2. Landslide behind Aratosawa dam: (Aero Asahi Co. provided the digital elevation model).



(a) Sample dried in oven

(b) Sample put again in water

Fig. 3. Rock sample taken for testing specific gravities under different conditions.

Seiche induced in the dam lake

The Aratosawa landslide mass also caused some remarkable seiche in the lake behind the Aratosawa dam. As shown in Table 1, the lake elevation increased from 268.5 m before the earthquake to 270.9 m after the earthquake. This increase in lake elevation is due to the plunge of the landslide mass and possibly also due to some tectonic deformation.

Table 1. Dam Lake elevations measured by Dam Management Office.

Date	Height [m]	Remark
06/14/2008	268.5	Before Earthquake
06/14/2008	270.9	After Earthquake, water level increased due to land-sliding and possibly due to tectonic deformation
07/12/2008	261.4	Reference elevation for measurements on July 12
07/13/2008	261.2	Reference elevation for measurements on July 13 (Lake is being emptied slowly)

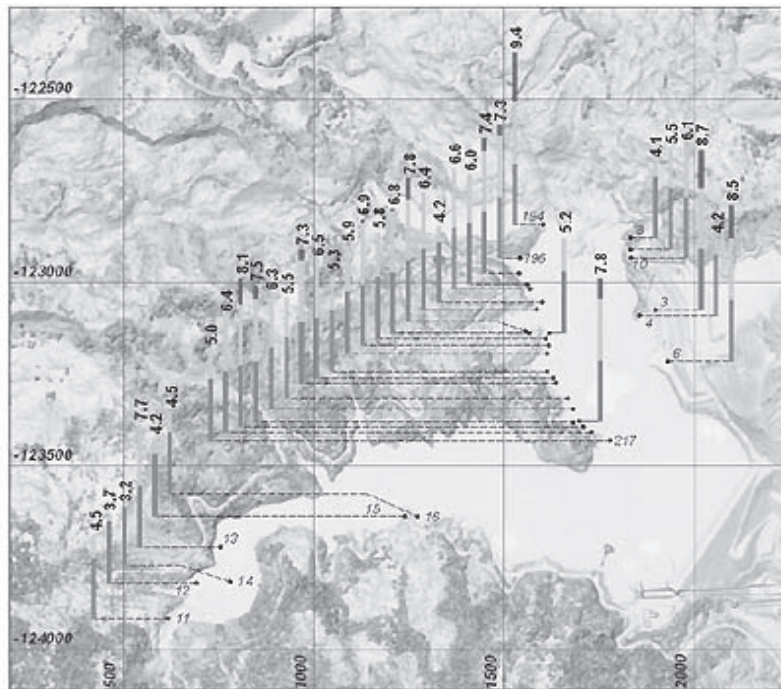


Fig. 4: Seiche high water marks above the lake elevation of 259.7m on July 12 and 13

DEBRIS FLOWS

Wet debris masses flowed along Dozo and Ura Rivers. A deep scar was created immediately beneath the snow remaining near the eastern peak of Mt. Komagatake (**Photo a**, 38.9584°N 140.8061°E). The debris flow from this source swept into Dozo River, and scoured sediment and vegetation from the channel.

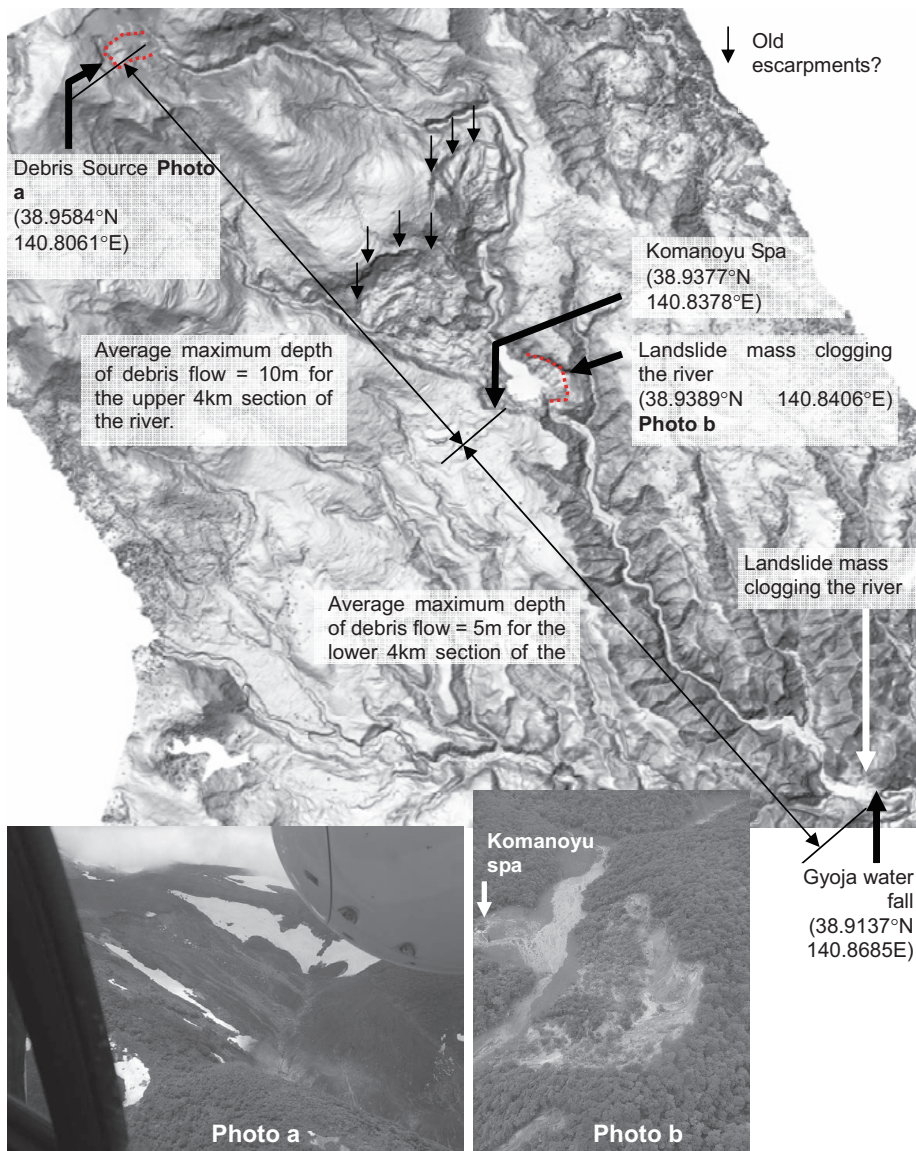


Fig. 5. Debris flow along Dozo and Ura Rivers: (DEM provided by Aero Asahi Co.)

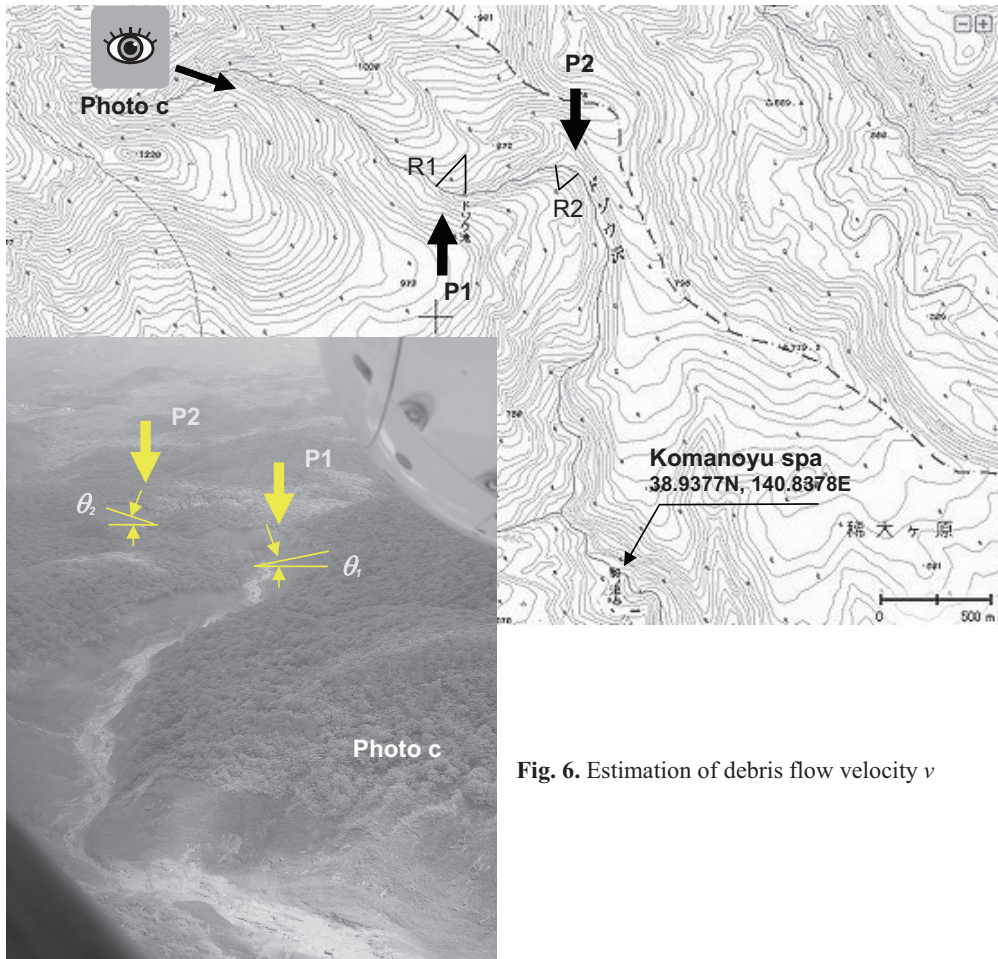


Fig. 6. Estimation of debris flow velocity v

The mud flow, with its channel clogged with another landslide mass (**Photo b**, 38.9389°N 140.8406°E, surged up to a hot spa resort “Komano-Yu” (**Photo b**, 38.9377°N 140.8378°E), where seven people were trapped in soil and rubble. The average maximum debris flow depth for the 4 km-long upper stream reach of Komanoyu spa was visually estimated to be about 10 m, while it was about half for the lower stream reach probably losing its momentum. The flow was stopped at Gyoja waterfall (38.9137°N 140.8685°E). (DEM provided by Aero Asahi Co.)

This wet flow along a curved channel had enough momentum to surge up along its outer wall (**Photo c**). Assuming that walls of the channel covered with mud show the inclined mud flow surface, the following equation is obtained.

$$\theta \cong \text{centrifugal force} / \text{gravitational force} = \left(\frac{mv^2}{R} \right) / (mg) \quad (1)$$

where, R = curvature radius, and one obtains:

$$v \cong \sqrt{Rg\theta} \quad (2)$$

Necessary parameters for Eq. (2) at Points #1 and #2 are roughly made out from the photo (left) and the topographical map (below) as:

$$\theta_1 \cong 0.12, \quad R_1 \cong 200 \text{ m},$$

$$\theta_2 \cong 0.3, \quad R_2 \cong 120\text{m},$$

Substituting these parameters in Eq. (2) yields:

$$v \cong \sqrt{Rg\theta} = 15 \sim 19\text{m/s} \quad (3)$$

This velocity is near to that estimated by Public Works research Institute (PWRI). Sabo Technical Center uses the following equation for estimating debris velocity:

$$v \cong \sqrt{Rg\theta/\alpha} \quad \text{where } \alpha \text{ is empirically set at } 10 \quad (4).$$

And the velocity will be:

$$v \cong 5 \sim 7\text{m/s} \quad (5)$$

CRACKED SHIN-TAMAYAMA TUNNEL

A 36m-long segment at 216m inside the eastern end (38.9006°N, 140.9230°E) of the 1220-m-long tunnel was diagonally cracked. Fig. 7 shows projections of the cracked south and north walls on a virtual screen. These cracks were all opened. Black arrows show that the eastern segment moved down with respect to the western segment, while gray ones show the opposite. Numbers in parentheses show these relative displacements in millimeters. If a deep-seated landslide was the cause, long-term monitoring will be a must for rational repairs.

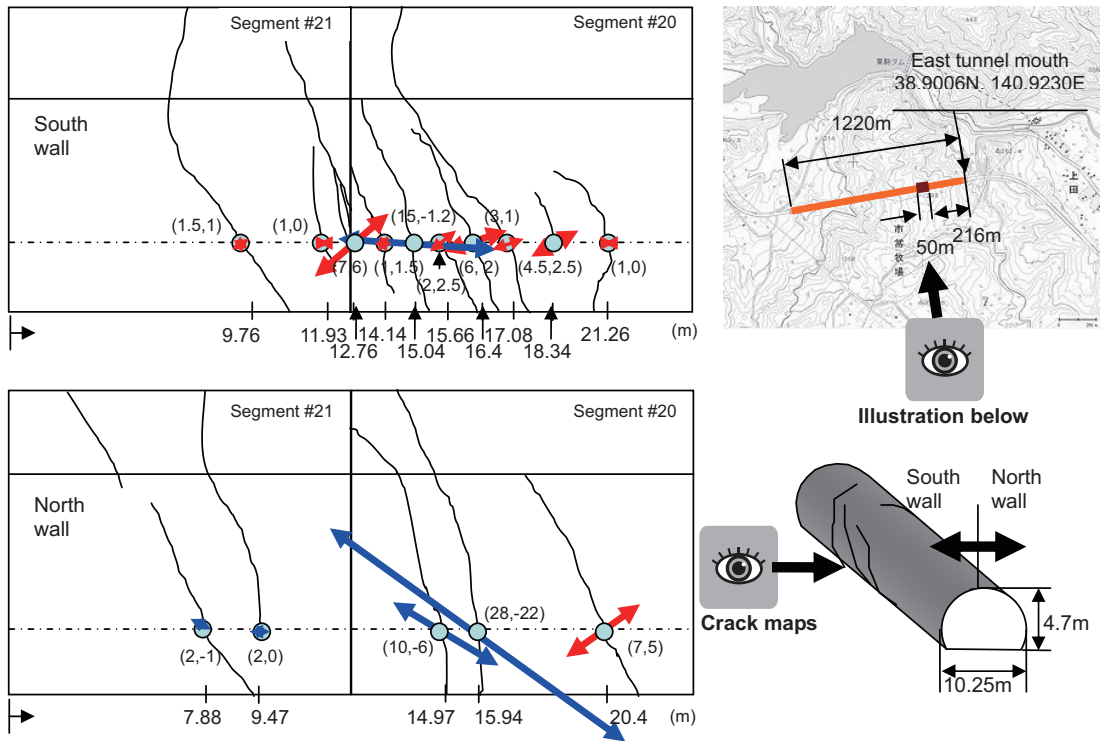


Fig. 7. Cracks in Shin-Tamayama Tunnel:

SUMMARY

This earthquake was remarkable in that a number of debris flows and landslides were triggered, while less serious damages to dwellings were reported. The largest landslide mass at Aratosawa was estimated to be around 50 to 70 million m³. Although the mass did not cause any loss of human lives luckily, but this volume was certainly extremely large among many recent earthquake-induced landslides. Weakly consolidated rocks of volcanic products were very light, having oven dried specific gravity of 1.18 g/cm³ indicating large volume of voids. These rocks must have been wet when the earthquake occurred because of the snow melting time, and the increase in excessive pore-water pressure may have accelerated the motion of the huge landslide mass. It is also noted that the landforms around the landslide mass suggest that the landslide may have been reactivated repeatedly. Among 23 deaths in this earthquake, 5 people were confirmed dead and 2 still missing at a hot spa resort “Komano-Yu”. A mud flow along Dozo River from Mt. Komagatake turned around and surged up to the spa because its channel was clogged with another landslide mass just nearby the spa. This wet flow along a curved channel had enough momentum to surge up along its outer walls. The marks that the flow has left on valley walls are to be carefully studied to learn important lessons from this tragedy.

ACKNOWLEDGEMENT

The authors are indebted to Mr. C. Karino, Head of Aratosawa Dam Office, and Mr. T. Ogata, Public Works Division, Miyagi Prefecture, for allowing us to survey the lake front area of the reservoir, and providing us with landform data of the dam area of its construction time.

REFERENCES

- [1] Konagai, K., Johansson, J., Tajima, Y., Tomiyasu, Y., Nomura, F. Date, M. and Katagiri, T. (2008): Provisional report of damage caused by the June 14th 2008, Iwate/Miyagi Prefectures Earthquake, SEISANKENKYU, 60(6), 9-14.



BUILDING DAMAGE DUE TO 2008 WENCHUAN EARTHQUAKE AND COOPERATIVE ACTIVITIES ON DAMAGE RESTORATION BY JAPANESE EXPERTS

Yoshiaki NAKANO¹, Masaki MAEDA², Joji SAKUTA³, and Masanobu SAKASHITA⁴

ABSTRACT: A destructive earthquake occurred on May 12, 2008, and caused extensive damage to Sichuan Province in China. Immediately after the event, Japanese scientific/engineering societies that had experiences and know-how on damage restoration of structures in the past major earthquakes jointly formed a liaison council to technically support the restoration of the hardest hit areas through mutual cooperation and sharing information. Since then, the council has been actively cooperating with Chinese experts from academic and engineering fields through damage investigations and extensive discussions on technical and practical issues for damage restoration. This paper briefly overviews damage to buildings and their restoration activities made in cooperation with Southwest Jiaotong University in Chengdu city, Sichuan Province.

Key Words: Sichuan (Wenchuan) Earthquake, Damage Restoration, Technical Support Liaison Council

INTRODUCTION

The Wenchuan Earthquake of magnitude 7.9 (USGS) jolted major cities in Sichuan Province, Central China at 14:28 local time on May 12, 2008. The damage is widespread and devastating, and more than 80,000 including missing people are reportedly killed mainly due to building collapse.

Immediately after the event, the following eight Japanese scientific/engineering societies (initially the first five societies listed below) jointly set up the Technical Support Liaison Council for Damage Restoration after Sichuan (Wenchuan) Earthquake (Council Chair: Dr. M. Hamada, Professor of Waseda University).

* Council member societies

1. JSCE (Japan Society of Civil Engineers)
2. AIJ (Architectural Institute of Japan)
3. JGS (The Japanese Geotechnical Society)
4. JAEE (Japan Association for Earthquake Engineering)
5. SSJ (Seismological Society of Japan)
6. CPIJ (The City Planning Institute of Japan)
7. AJG (The Association of Japanese Geographers)
8. ISSS (The Institute for Social Safety Science)

¹ Professor, Institute of Industrial Science, The University of Tokyo

² Associate Professor, Department of Architecture and Building Science, Tohoku University

³ Research Associate, Department of Architecture and Building Science, Tohoku University

⁴ Assistant Professor, Department of Architecture and Architectural Engineering, Kyoto University

The major purpose of the Council's activity is to form a technical support team in close cooperation with eight societies that are well experienced in post-earthquake activities and to help researchers, engineers, and practitioners in the affected area restore damaged structures and communities through sharing knowledge and experiences of recent damaging earthquakes such as 1995 Hyogo-Ken Nambu (Kobe), 2004 Niigata-Ken Chuetsu, and 2008 Iwate-Miyagi Nairiku earthquakes.

After the earthquake, the Council dispatched technical support teams during May 28 through June 1 and June 20 through 25, and organized a series of special lectures on engineering seismology and earthquake engineering at the Southwest Jiaotong University, Chengdu city, Sichuan Province, in September and October. In this paper, the damage observation of building structures and technical support activities for their restoration made during the second visit in June are briefly described.

BUILDING DAMAGE OBSERVATIONS

Damage surveys were primarily made in Dujiangyan city and Hanwang town of Mianzhu city. Figure 1 shows the surveyed areas. In especial, damage in Hanwang, where the seismic fault runs across the northern edge of the town, is extensive, and many buildings are found totally collapsed. The surveys were arranged by the Southwest Jiaotong University, which was the Chinese counterpart for the technical support activities. During surveys, two major structural types, brick structures and RC frames with URM (unreinforced masonry) walls, are found. In the subsequent sections, major damage patterns found during surveys are briefly described for each structural type.

Brick buildings

Brick buildings are most seriously damaged and they often sustain partial or total collapse, resulting in the primary source of human damage. They have UR brick walls having RC ring beams and precast concrete hollow-core slabs above the walls. The major cause of the fatal damage is attributed to the low resistance and brittleness of URM walls and poorly detailed joints between precast concrete members and RC beams. Photos 1 and 2 show typical damage to brick buildings.

RC buildings

In RC buildings, several damage patterns are found. They include damage to UR brick walls, shear failure in columns, flexural compression failure at column top and/or bottom, beam-column joint failure, and structural damage resulting from soil/ground failure underneath.

Damage to UR brick walls

Reinforced concrete shear walls are much less frequently provided in RC buildings than UR brick walls. Lightly reinforced small-sized columns (tie columns) are often placed later between UR brick walls so that the walls should serve as the form in casting concrete of RC tie columns. During the surveys, shear cracks and failure of brick walls are found in many buildings as shown in Photo 3. It



Figure 1. Surveyed areas

should be noted, however, that lath-mortar finishing on the exterior surface of UR brick walls is found to help avoid their out-of-plane failure, although they are heavily cracked. Such efforts therefore should be encouraged to minimize falling hazard to residents and users during and after major earthquakes.

Shear failure in RC column

Shear failures in RC columns shortened by partial height UR brick walls are found in several buildings, as have been found elsewhere in the past damaging earthquakes. Photo 4 shows a typical shear failure in the first story of a building in Dujiangyan city. Photo 5 shows another failure, where the column is shortened and failed in shear leaving vertical cracks along the interface between the column and brick wall. The damage is attributed to the presence of partial height brick walls, which are generally neglected in the structural design but significantly affect the building's behavior during strong shaking.



Photo 1. Seriously damaged brick buildings (Hanwang town of Mianzhu city)

Flexural compression failure in RC column

Seriously damaged RC buildings often show

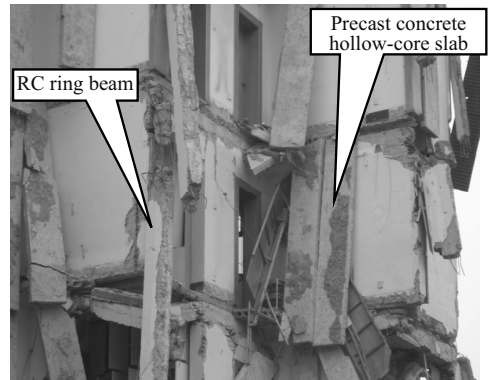


Photo 2. Partially collapsed brick buildings with precast concrete hollow-core slabs (Dujiangyan city)



Photo 3 Failed brick wall (left) and survived brick wall (right)



Photo 4. Typical shear failure in RC short columns



Photo 5. Shear failure in RC column shortened by partial height brick wall



flexural compression failure at the top and bottom of their columns. Photos 6 and 7 show the damage to columns in the first story of a six story apartment building in Dujiangyan city. Hooks of lateral reinforcement are pulled out of crushed concrete core. Main rebars buckle and fracture as shown in the photos. As will be found later in this paper, the building is employed for a sample building to investigate possible restoration schemes and to discuss their feasibility with Chinese engineers.



Photo 6. Soft first story of a 6 story RC apartment house

Damage to RC beam-column joints

Damage to beam-column joints are less frequently found than other failure patterns such as shear failure in columns, flexural compression failure in columns. Photo 8 shows the damage to beam-column joints of RC apartment buildings, which were under construction at the time of the earthquake.

Photo 8 shows the damage to beam-column joints of RC apartment buildings, which were under construction at the time of the earthquake.

Structural damage due to soil failure

Structural damage due to soil failure underneath a building resulting in the differential settlement is found in some buildings located at the foot of a mountain slope in Dujiangyan city. Photo 9 shows damage to a retaining wall, causing soil outflow and differential settlement of superstructures.

SINO-JAPAN SEMINAR ON RESTORATION OF DAMAGED BUILDINGS

Along with the aim of the liaison activities, the Council, in corporation with Architectural Institute of Japan (AIJ), dispatched an expert team on building damage assessment and restoration led by the author during the period of June 20 through 25 following the first preliminary surveys in May. After two-day surveys of affected areas in Dujiangyan city and Hanwang town of Mianzhu city, the Sino-Japan Seminar on Techniques for Rehabilitation and Reconstruction after the Sichuan (Wenchuan) Earthquake was held on June 24 at the Southwest Jiaotong University (SJU).

Outline of the seminar

The purpose of the seminar is primarily to present concrete strategies and solutions for damage restoration and to discuss their feasibility and applicability with seminar participants in detail. To this



Photo 7. Flexural compression failure at the top and bottom of columns

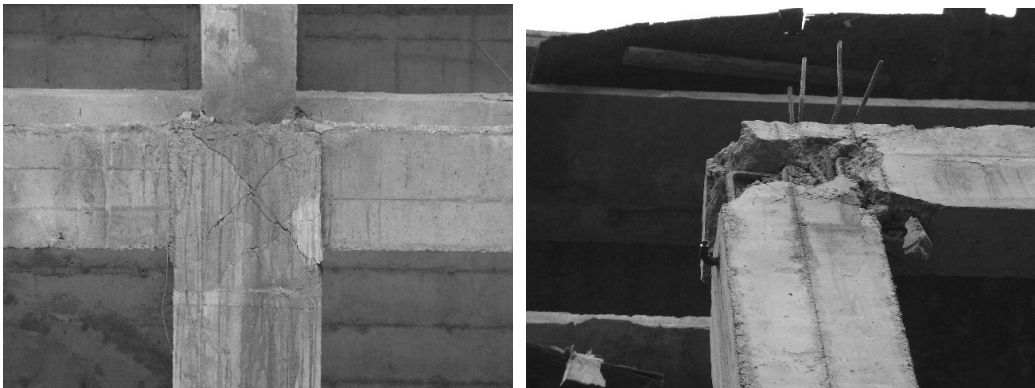


Photo 8. Failure in beam-column joint



Photo 9. Structural damage due to failure in retaining wall

end, an example building is selected from those inspected during the field surveys considering Chinese side requests and then restoration schemes for the building are investigated and proposed by the Japanese side in the seminar.

In the seminar, summaries of damage surveys and basic ideas widely applied in Japan to restore earthquake-damaged buildings are first presented. Then restoration scheme candidates for buildings damaged by the Wenchuan Earthquake are proposed by the Japanese side and their applicability, problems to be solved from the practical design and construction point of view in China are discussed in detail.

Example building

The example building is a six story RC apartment building in Dujiangyan city, which appeared earlier in Photos 6 and 7. The building was under construction but its structural construction was already completed at the time of the earthquake. The first story designed for a parking garage has no walls, while the upper stories have dwelling units with UR brick walls as shown in Photo 10 and Figure 2.



Photo 10. Example six story RC apartment building (See also Photos 6 and 7)

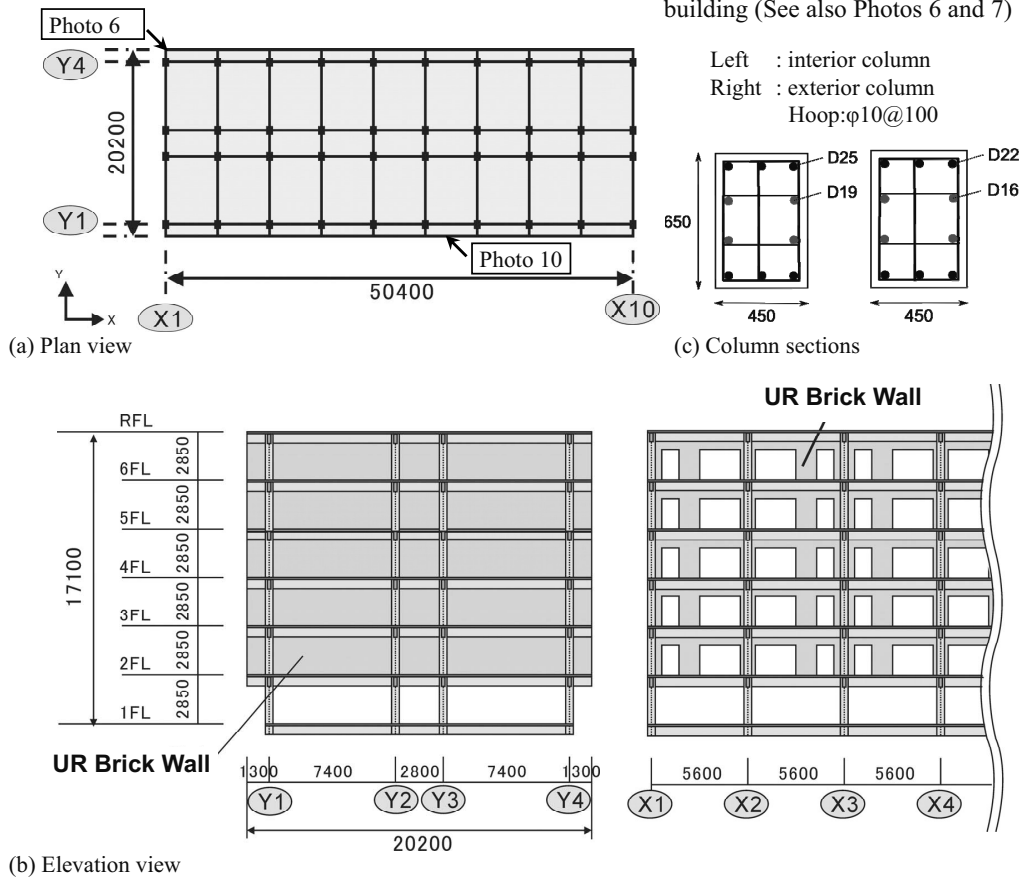


Figure 2. Structural configuration and column size of example RC building

Almost all columns in the first story form plastic hinges both at their top and bottom, causing concrete crushing and rebar buckling (Photos 6 and 7) resulting in the soft first story mechanism with a residual lateral drift of approximately 10% of the story height. No major damage is, however, found in upper stories.

The observed damage is rated [unsafe] based on the Japanese post-earthquake quick inspection manual (JBDPA1997) and [heavy damage] based on the Japanese post-earthquake damage evaluation guidelines (JBDPA 2001, Nakano et al. 2004). The building therefore is identified to be [no occupancy] and needs to be shored to avoid life-threatening risk and further damage progress due to aftershocks.

Restoration strategies

To understand the fundamental seismic performance of the building, the Japanese seismic evaluation procedure (JBDPA 2001, Nakano et al. 2004) is applied and the seismic capacity index I_s of the first story is evaluated. The basic concept and procedure of the Japanese Standard (JBDPA 1977, 1990, 2001, 2005) can be found in Appendix of this paper.

Table 1 summarizes the result. The building is found ductile with F index (ductility index, see also Appendix) of 2.6, which is consistent with observed damage with a large lateral residual displacement. In the Standard, the required seismic capacity index is recommended to be equal or larger than 0.6 for standard RC buildings in Japan as is shown in the Appendix. The criteria value is determined considering results on non-linear response analyses of typical RC buildings, and studies on the relationship between observed damage to buildings and their seismic capacity indices after major earthquakes in Japan including 1968 Tokachi-Oki Earthquake, 1978 Miyagi-Ken-Oki Earthquake, 1995 Hyogo-Ken Nambu (Kobe) Earthquake, etc.

To restore the damage, the following six schemes are investigated and proposed in the seminar. Table 2 summarizes and illustrates the basic ideas of the schemes and their expected post-restoration performance, where the capacity recovering factor ψ (i.e., the reduction factor to take into account of damage prior to restoration defined in the Guidelines (JBDPA 2001) and Nakano et al. (2000)) is conservatively assumed 0.7 herein.

Scheme 1 aims primarily to repair the damaged columns after re-centering the building, replacing buckled rebars with new rebars, and re-cast concrete in the damaged region. Since the performance may not be fully recovered to the original due to extensive damage and hence the seismic capacity index I_s after restoration ($\psi=0.7$ assumed) is lower than the original value of 0.67, the restored building is likely to collapse when subjected to the future shaking with intensity similar to the main event on May 12.

Scheme 2 aims to repair and upgrade flexural strength and confinement of columns by RC jacketing after re-centering the building. In Scheme 2, the flexural strength after restoration is estimated neglecting reinforcement in the original section, which is found buckled in the survey, while the whole section including repaired inner (i.e., original) section is assumed effective on the shear strength. As is found in Table 2, the expected performance may be better than the original, but both

Table 1. Seismic capacity index of example building prior to damage

Location	C	F	E_o	I_s
Interior	0.14	2.60	0.67	0.67
Exterior	0.12	2.99		

Note: $I_s = E_o \times S_D \times T$ (See also Appendix)

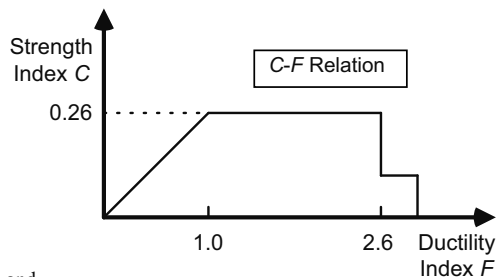
$$E_o = (0.14 + 0.12) \times 2.6 = 0.67$$

E_o : basic structural capacity index defined by $C \times F$

C : strength index defined in terms of shear coefficient

F : ductility index (ranging from 1.0 to 3.2) defined mainly by shear-to-flexure strength ratio, yielding displacement, height-to-depth ratio etc.

S_D and T : reduction factors for E_o to allow for irregularity and deterioration of building (both assumed 1.0 herein)



Schemes 1 and 2 need re-centering of the building, which may not be necessarily easy and requires well-experienced engineers with high-level skills.

Then Schemes 3 and 4, which do not employ re-centering of the building, are proposed to facilitate the restoration work. It should be noted, however, that the column size after Schemes 3 and 4 would be almost twice as large as the original since the new RC element around the original section needs to be large enough to jacket the tilted column and new reinforcement. In Scheme 3, as is

Table 2. Restoration scheme candidates

Scheme (F-: flexural / S-: shear)	General description	Expected difficulties ^{*1}	Expected performance ^{*2}	<i>I_s</i> Index ^{*3}
0. Original	Prior to damage	-	-	0.67
1. Repair	Repair to initial configuration after re-centering	(1)	(a)	0.47
2. F-strengthening	RC jacketing ^{*4} after re-centering	(1) (2)	(b)	0.71
3. F-strengthening	RC jacketing ^{*4} without re-centering	(2)	(b)	1.04
4. F- and S-strengthening	Scheme 3 and steel jacketing	(2)	(b)	1.19
5. Repair & strengthening with new wing walls	Scheme 1 and wing walls	(1)	(b)	0.60
6. Repair & strengthening with new shear walls	Scheme 1 and shear walls	(1)	(b)	0.35

*1 Expected difficulties and necessary construction works

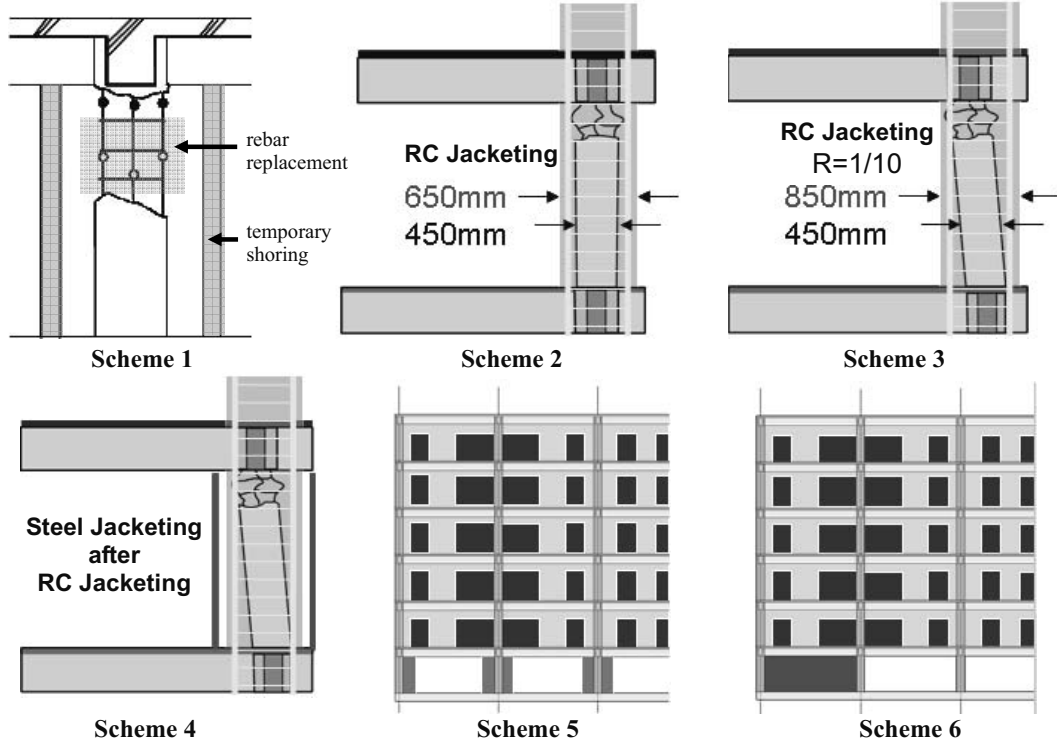
(1) Jack-up and re-centering of building; (2) Anchorage of longitudinal rebars for jacketing and arrangement of shear reinforcement in beam-column joints

*2 Expected post-restoration performance

(a) Damage expected under future major earthquake; (b) Higher resistance and stiffness expected but careful examination needed on their vertical distribution

*3 The strength index *C* is evaluated assuming the building weight per unit area is 10 kN/m². The capacity recovering factor ψ after restoration (i.e., reduction factor due to damage prior to restoration) employed in the Guidelines (JBDPA 2001, Nakano et al. 2000) is assumed 0.7 in this study.

*4 The amount of new reinforcement is assumed the same as the original. The column size of Schemes 1, 5, and 6: 450 x 650 mm; Scheme 2: 650 x 850 mm; Scheme 3: 850 x 850 mm; Scheme 4: > 850 x 850 mm.



assumed in Scheme 2 above, the flexural strength is estimated neglecting reinforcement in the original section while the whole section is assumed effective on the shear strength. It should also be noted that it is more favorable to provide cross-ties to confine such a large size section although difficult due to the presence of the original section. Scheme 4 therefore aims to provide flexural, shear, and confinement strength higher than those expected in the earlier Scheme 3 through employing steel jacking after RC jacking.

In Schemes 5 and 6, additional lateral resisting elements are provided in the first story as shown in Figure 3. Scheme 5 aims to increase in lateral resistance through providing wing walls in each column, while Scheme 6 provides six sets of RC shear walls which are expected to provide high lateral resistance. In both cases, the contribution of new sections is simply estimated by the product of the sectional area A_w and the ultimate shear strength τ_u of the wall, where τ_u is assumed 2 N/mm^2 . Since the original structure is designed to absorb seismic energy through large plastic deformation rather than high lateral resistance, I_s index after scheme 6 is still much lower than the original and the six sets of new shear walls may not be sufficient to fully improve the overall behavior of the structure as shown in Table 2.

Discussions in the seminar

More than ninety participants including researchers, engineers, and SJU students attended the seminar, and the applicability of the proposed restoration schemes are discussed as well as other general issues related to restoration techniques. Photo 11 shows snapshots from the seminar.

In the seminar, the Japanese side emphasized that the continuous distribution of strength and stiffness, smooth transfer of actions through structural members and their interface under seismic

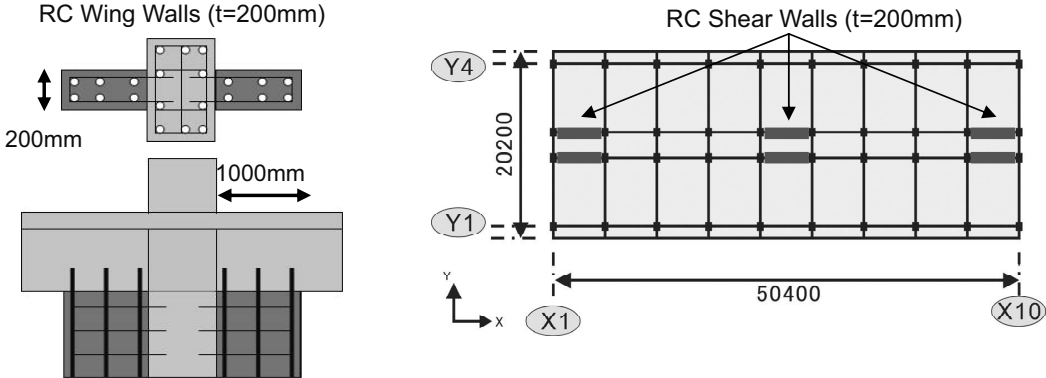


Figure 3. Location of wing walls for Scheme 5 (left) and shear walls for Scheme 6 (right)



Photo 11. Discussions in the Seminar

excitations, anchorage of new reinforcement into existing RC members etc. were of highest priority in re-designing the damaged buildings, although the restoration proposals were made only in the first story for simplified discussions. It was also pointed out that the buckling of column reinforcing bars associated with flexural compression failure could be observed in areas close to their interface between column ends and adjacent beams, and the confinement of beam-column joints using additional lateral reinforcement therefore is recommended to effectively eliminate further damage.

After long and enthusiastic discussions, the Chinese participants concluded that Scheme 3 would be most realistic and practical if the oversized section after repair can be accepted by the residents, and that Scheme 2 may be the second best solution to restore the building if Scheme 3 is not accepted. It was also very interesting for Japanese participants to learn that Schemes 5 and 6 were much less acceptable by the Chinese participants although they might be most likely to be accepted in Japan. This is mainly because the mixture of different structural types (i.e., RC frames with shear walls in the first story and RC moment resisting frames in the upper stories) is not specified in the Chinese structural design code while it may be accepted in Japan if its effects by the change in stiffness and strength distribution along building's height on structural behavior are carefully taken into account.

CONCLUSIONS

Typical structural damage to URM and RC buildings due to the Wenchuan Earthquake and liaison activities for their damage restoration by the Japanese experts in close cooperation with Southwest Jiaotong University (SJU) are briefly presented. In especial, possible solutions for damage restoration of an example RC building in Dujiangyan city, which were proposed and discussed in the seminar held at SJU, are highlighted.

The central Chinese government has high-level background on seismic design and restoration techniques, but there still remain various types of difficulties even on the technical aspects as has been usually found in the earthquake aftermath elsewhere since such a devastating disaster and its aftermath are always the first experience to researchers and engineers in the most affected areas. The author therefore sincerely and deeply wishes that continued cooperative efforts, sharing information and experiences such as those having been done by the Council would effectively help restore damaged structures and communities.

ACKNOWLEDGMENT

The local arrangement for field surveys in the affected areas and workshop was coordinated by Professors Shi Chun Zhao and Jian Jing Zhang of Southwest Jiaotong University, China, and Dr. X. Wu of Oyo Corporation, Japan. The authors gratefully acknowledge their valuable support without which the activity could not be completed.

APPENDIX: BASIC CONCEPT OF JAPANESE STANDARD FOR SEISMIC EVALUATION OF EXISTING RC BUILDINGS

The Standard for Seismic Evaluation (JBDPA 1977, 1990, 2001), designed primarily for pre-earthquake existing RC buildings in Japan, defines the following structural seismic capacity index I_s at each story level in each principal direction of a building.

$$I_s = E_o \times S_D \times T \quad (1)$$

where,

E_o : basic structural seismic capacity index, calculated by the product of Strength Index (C), Ductility Index (F), and Story Index (ϕ) at each story and each direction when a story or a building reaches the ultimate limit state due to lateral force ($E_o = \phi \times C \times F$)

C : index of story lateral strength expressed in terms of story shear coefficient

F : index of story ductility, calculated from the ultimate deformation capacity normalized by the story drift of 1/250 when a typical-sized column is assumed to fail in shear. F is dependent on the failure mode of a structural member and its sectional properties such as bar arrangement, member's geometry size etc. F is assumed to be in the range of 1.27 to 3.2 for ductile columns*, 1.0 for brittle columns* and 0.8 for extremely brittle short columns. (* Note: The Standard of 1990 version is applied in this study and F index of columns is evaluated as shown above.)

ϕ : index of story shear distribution during earthquake, estimated by the inverse of design story shear coefficient distribution normalized by the base shear coefficient. The value of $\phi = (n+1)/(n+i)$ is basically employed for the i -th story of an n story building.

S_D : reduction factor to modify E_o index due to stiffness discontinuity along stories, eccentric distribution of stiffness in plan, irregularity and/or complexity of structural configuration, basically ranging from 0.4 to 1.0

T : reduction factor to allow for time-dependent deterioration grade after construction, ranging from 0.5 to 1.0

A required seismic capacity index I_{so} , which is compared with I_s to identify structural safety against an earthquake, is defined as follows.

$$I_{so} = E_s \times Z \times G \times U \quad (2)$$

where,

E_s : basic structural seismic capacity index required for the building concerned. Considering past structural damage due to severe earthquakes in Japan, the standard value of E_s is set 0.6 (see also Figure A1.).

Z : factor allowing for the seismicity

G : factor allowing for the soil condition

U : usage factor or importance factor of a building

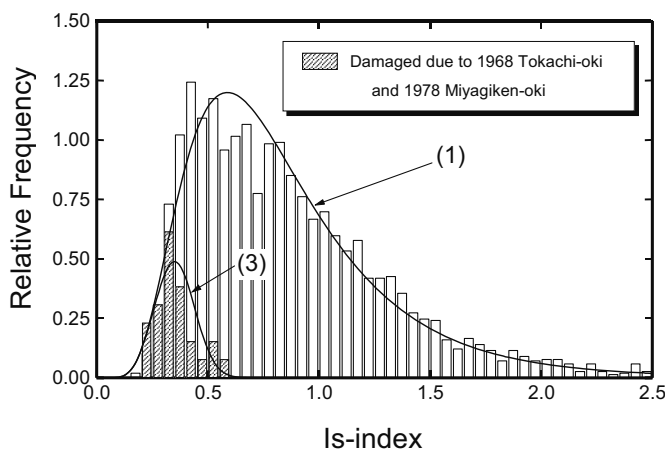
Typical I_{so} index is 0.6 considering $E_s = 0.6$ and other factors of 1.0. As can be found in Figure A1., buildings with I_s larger than 0.6 successfully survived the 1968 Tokachi-Oki and 1978 Miyagi-Ken-Oki earthquakes. It should be noted that $C_T \times S_D$ defined in Equation(3) is required to equal or exceed $0.3 Z \times G \times U$ in the Standard to avoid fatal damage and/or unfavorable residual deformation due to a large response of structures during major earthquakes.

$$C_T \times S_D = \phi \times C \times S_D \quad (3)$$

Seismic rehabilitation of existing buildings is basically carried out in the following procedure.

(1) Evaluate seismic capacity of the structure concerned (I_s and $C_T \times S_D$)

- (2) Determine required seismic capacity (I_{so})
- (3) Compare I_s with I_{so} and $CT \times SD$ with $0.3 Z \times G \times U$
- * If $I_s < I_{so}$ or $CT \times SD < 0.3 Z \times G \times U$ and therefore rehabilitation is required, the following actions (4) through (6) are needed.
- (4) Select rehabilitation scheme(s)
- (5) Design connection details
- (6) Re-evaluate the rehabilitated building to ensure the capacity of re-designed building equals or exceeds the required criteria



NOTE: I_s indices of more than 1,600 existing RC buildings in Shizuoka prefecture, Japan, together with those of damaged buildings were evaluated and plotted in this figure. The horizontal axis [I_s -index] indicates seismic index of structure which signifies the seismic capacity of a building calculated in accordance with the Standard. The vertical axis indicates relative frequencies of I_s index. Bars shown in blank correspond to existing buildings in Shizuoka prefecture, which are prior to damaging earthquakes, while those in hatched correspond to buildings damaged in the past earthquakes in 1968 and 1978 in Japan. Curves in the figure were obtained from a probabilistic study.

Figure A1. I_s index vs. observed damage in the past major earthquakes in Japan (Okada and Nakano 1988)

REFERENCES

- JBDPA/The Japan Building Disaster Prevention Association (1977, 1990, 2001, and 2005 (English version)). "Standard for Seismic Evaluation of Existing Reinforced Concrete Buildings".
- JBDPA/The Japan Building Disaster Prevention Association (1991, 2001). "Guidelines for Post-earthquake Damage Evaluation and Rehabilitation of RC Buildings" (in Japanese).
- JBDPA/The Japan Building Disaster Prevention Association (1997). "Post-earthquake Quick Inspection Manual for Damaged Buildings" (in Japanese).
- Nakano, Y. (2000). "Temporary Restoration Guide of RC School Buildings Damaged by the 21.9.99 Chichi Earthquake", *Series on Innovation in Structures and Construction / Implication of Recent Earthquakes on Seismic Risk*, Vol. 2, 51-66.
- Nakano, Y., Maeda, M., Kuramoto, H., and Murakami, M. (2004). "Guideline for Post-earthquake Damage Evaluation and Rehabilitation of RC Buildings in Japan", *Proc., the 13th World Conference on Earthquake Engineering* (CD-ROM).
- Okada, T. and Nakano, Y. (1988). "Reliability Analysis on Seismic Capacity of Existing Reinforced Concrete Buildings in Japan" *Proc., the 9th World Conference on Earthquake Engineering*, Vol. VII, 333-338.



EFFECT OF STATIC SHEAR STRESS ON UNDRAINED CYCLIC BEHAVIOR OF SATURATED SAND

Gabriele CHIARO¹, Takashi KIYOTA², L.I.N. DE SILVA³,
Takeshi SATO⁴ and Junichi KOSEKI⁵

ABSTRACT: To investigate the effect of static shear stress on the undrained cyclic behavior of saturated sand, a series of torsional shear tests was conducted on saturated Toyoura sand specimens up to extremely large strain level of about 100%. After being isotropically consolidated, the specimens were subjected to drained monotonic torsional shear stress, and then, undrained cyclic torsional shear stress was applied. The amplitude of combined static and cyclic shear stress was kept constant by correcting the measured value for the effect of membrane force. The test results revealed that the effective stress path and the stress-strain curve during the cyclic shear loading were affected by the initial static shear stress. Accumulation of shear strain was clearly noticed in the same direction where previously static shear stress was applied. Progressive localization of specimen deformation was observed.

Key Words: Large strain, Liquefaction, Membrane force, Sand, Static shear stress, Torsional shear test

INTRODUCTION

Extremely large deformations could be observed on liquefied gentle slope of sand, following earthquake events, such as the 1964 Niigata and 1983 Nihonkai-Chubu earthquakes (Hamada et al., 1994). Even though the gradient of slopes was merely of some percents, their lateral spreading achieved several meters. Due to liquefaction, flow of slope can occur when the mobilized shear stress of soil in its liquefied state exceeds the shear stress required for the static equilibrium of soil mass. Once deformations produced by flow liquefaction are triggered, they may become extremely large depending on the acting static shear stress.

Many laboratory tests under different conditions (in term of density, confining pressure, stress ratio, severity of liquefaction, etc...) have shown that large deformation always occurs after liquefaction of sand, and it can be developed when the effective mean principal stress in sand momentarily achieves zero state during undrained loading (e.g., Koseki et al., 2005 and 2007; Kiyota et al. 2008). These cyclic torsional or triaxial tests were carried out on isotropically consolidated specimens, in which there is no static shear stress; this zero static stress state represents the stress conditions of level ground.

Towhata (2008), regarding the effects of initial static shear stress combined with cyclic torsional shear stress, pointed out that in case of one-way loading (the shear stress is always positive), the

¹ Ph.D. Student, Department of Civil Engineering, University of Tokyo

² Assistant Professor, Tokyo University of Science

³ Post Doctoral Research Fellow, Institute of Industrial Science, University of Tokyo

⁴ Research Support Promotion Member, Institute of Industrial Science, University of Tokyo

⁵ Professor, Institute of Industrial Science, University of Tokyo

specimen maintained its stability and liquefaction was not achieved. In case of two-way loading the specimen easily liquefied and developed large shear deformation. However, due to mechanical limitation of the employed apparatus the shear strain level could not exceed 10%.

On the other hand, Yasuda et al. (1992), by conducting shaking table tests with different sloping ground surface and thickness of liquefied sand layer, showed that permanent ground displacement would not occur along any specific surface of rupture, but would occur throughout a liquefied layer because of a fall of shear strength and shear modulus due to liquefaction.

Since the soil in a sloping ground is always subjected to an initial driving shear stress prior to seismic loading, and because properties of liquefied soil under extremely large deformation are not understood well, in the present study, in order to investigate the effect of initial static shear stress level on the undrained cyclic behavior of saturated Toyoura sand, a series of undrained cyclic torsional shear tests was performed up to a double amplitude of shear strain of about 100%.

TEST APPARATUS

To achieve extremely large torsional shear displacements, a fully automated torque loading device on hollow cylindrical specimens (Fig. 1), developed by Koseki et al. (2007) and Kiyota et al. (2008), was employed in this study.

It is capable of achieving double amplitude torsional shear strain levels exceeding 100% by using a belt-driven torsional loading system that is connected to an AC servo motor through electro-magnetic clutches and reduction gears.

To evaluate large torsional deformations, a potentiometer with a wire and a pulley was employed, as illustrated in Figs. 1b) and 1c). The torque and axial load were detected by using a two-component load cell which is installed inside the pressure cell.

The hollow cylindrical specimen was 150mm in outer diameter, 90mm in inner diameter and 300mm in height.

TEST PROCEDURE

The material employed in this study was Toyoura sand, a uniform sand with negligible fines content under $75\mu\text{m}$ (Table 1). Several specimens, as listed in Table 2, were prepared by pluviation air-dried sand particles through air. Their initial relative density of about 43% was obtained by using a funnel and keeping constant the height of pluviation. After saturating the specimens with pouring carbon dioxide and then pouring de-aired water, they were isotropically consolidated by increasing the effective stress state up to 100kPa, with a back pressure of 200kPa. Subsequently, the stress state was changed by applying drained monotonic torsional shear stress up a specified value. Finally, undrained cyclic torsional loading, with constant double amplitude of shear stress of 32kPa, was applied at a constant shear strain rate of 2.5 %/min. The loading direction was reversed when the amplitude of combined shear stress, which was corrected for the effect of membrane force, reached the target value. For all the duration of torsional loading, both monotonic and cyclic cases, the vertical deformation of the specimen was kept to be zero by using a mechanical locking devices for the vertical displacement of loading shaft.

Table 1 Material properties

Material	Specific gravity, G_s	Maximum void ratio, e_{max}	Minimum void ratio, e_{min}	Mean diameter, D_{50} (mm)	Fines content, F_C (%)
Toyourea sand	2.656	0.992	0.632	0.16	0.1

Table 2 Test conditions

Test	Relative density, D_r	Static Shear Stress, τ_s	Combined static and cyclic shear stress, $\tau = \tau_s \pm \tau_{CL}$	Type of loading
Test SH05	43.3%	5kPa	+21 / -11kPa	Two-way
Test SH10	44.3%	10kPa	+ 26 / -6kPa	Two-way
Test SH15	41.9%	15kPa	+ 31 / -1kPa	Two-way
Test SH20	43.2%	20kPa	+36 / +4kPa	One-way

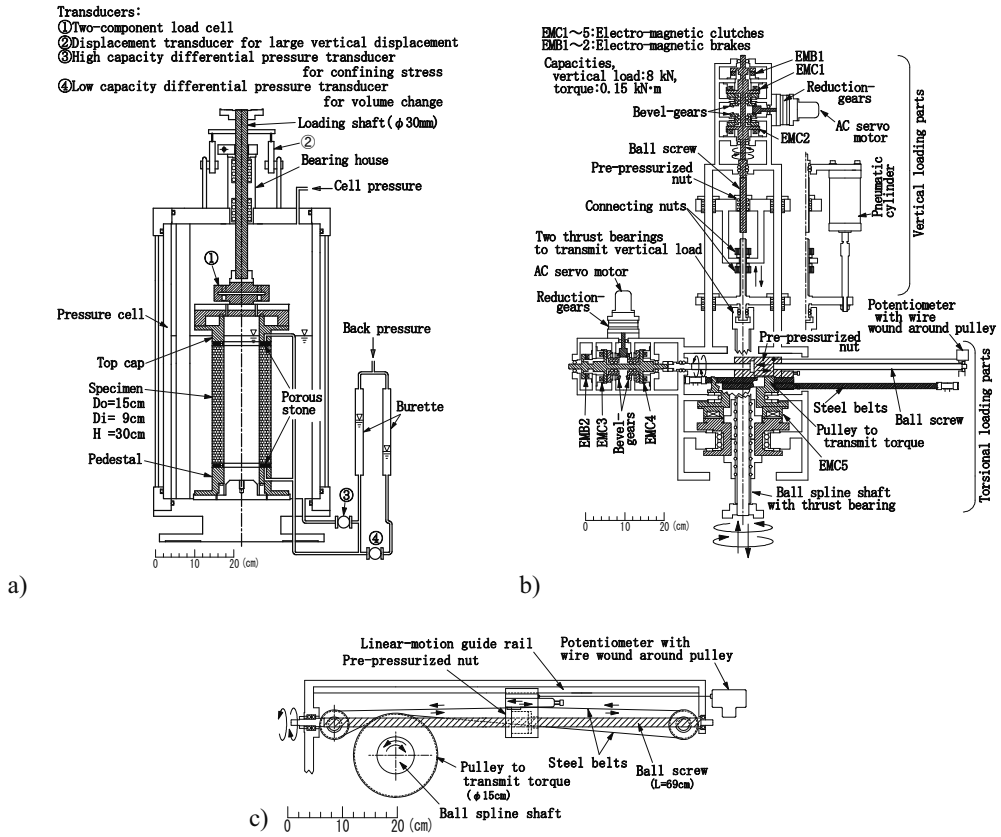


Figure 1 a) Torsional shear test apparatus on hollow cylindrical specimen; b) loading device and c) plan view of torque-transmission part.

TEST RESULTS

Correction for membrane force

As Koseki et al. (2005 and 2007) among others pointed out, in torsional shear tests on hollow cylindrical specimen due to the presence of inner and outer membranes, the effect of membrane force can not be neglected. Furthermore, it becomes significantly important when shear strain reach extremely high level as Kiyota et al. (2008) indicated.

Usually, the membrane force has been corrected based on the linear elasticity theory, which uses the Young's modulus of the membrane. The theoretical apparent shear stress, τ_m , induced by the inner and the outer membranes can be evaluated as:

$$\tau_m = \frac{t_m E_m (r_o^3 + r_i^3) \theta}{(r_o^3 - r_i^3) h} \quad (1)$$

where θ is the rotational angle of the top cap detected by external potentiometer; h is the height of the specimen; r_o and r_i are the outer and inner radii of the specimen; t_m and E_m are, respectively, the thickness (=0.3 mm) and the Young's modulus (=1492 kPa) of the membrane.

In order to confirm the validity of Eq. (1) in correcting for effect of membrane force, a special test was performed by filling water between the inner and outer membranes and shearing it cyclically under undrained condition up to single amplitude shear strain of 50% (Photo 1).

Figure 2 shows both experimental and theoretical relationships between shear strain and apparent shear stress that is induced by the membranes due to torsional deformation. As expected, the deviation of the actual membrane deformation from the uniform one that is assumed in the theory became larger with increase in the strain level. Hence, in this study, the shear stress was corrected for the effect of membrane force by employing the polynomial approximation of the measured relationship between γ and τ_m as shown in Fig. 2.

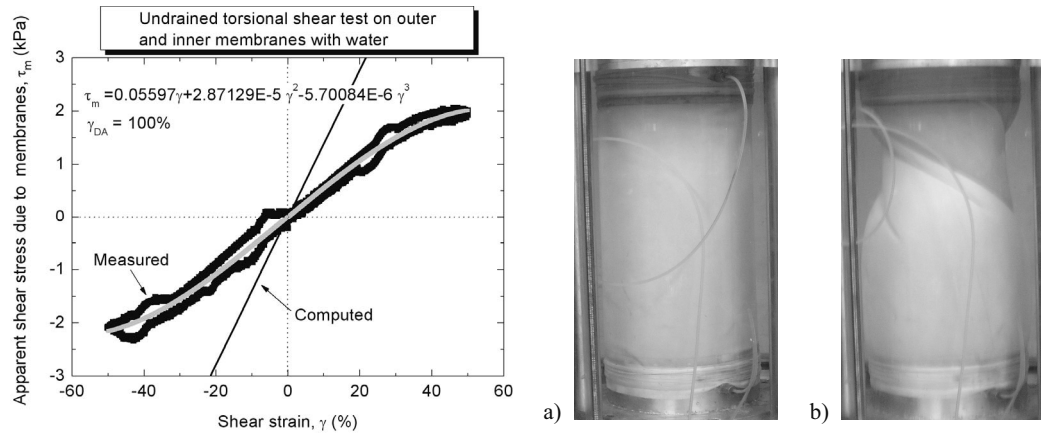


Figure 2 Relationships between apparent shear stress due to membrane force and shear strain

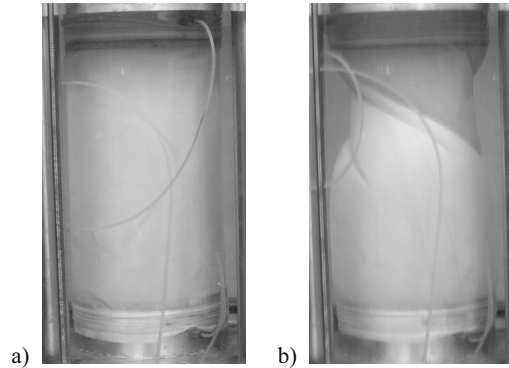


Photo 1 Deformation of water specimen: a) before test ($\gamma=0\%$) and b) at $\gamma=50\%$

Two-way loading test results

During each cycle of loading in some tests, the combined static and cyclic shear stress value is reversed from positive ($\tau = \tau_S + \tau_{CL} > 0$) to negative ($\tau = \tau_S - \tau_{CL} < 0$), or vice versa; this type of loading will be called hereafter as two-way loading.

Typical two-way loading test results on Toyoura sand specimens, in which static shear stress with magnitude of 5, 10 and 15kPa, respectively, was applied before undrained torsional loading, are shown in Figs. 3, 4 and 5.

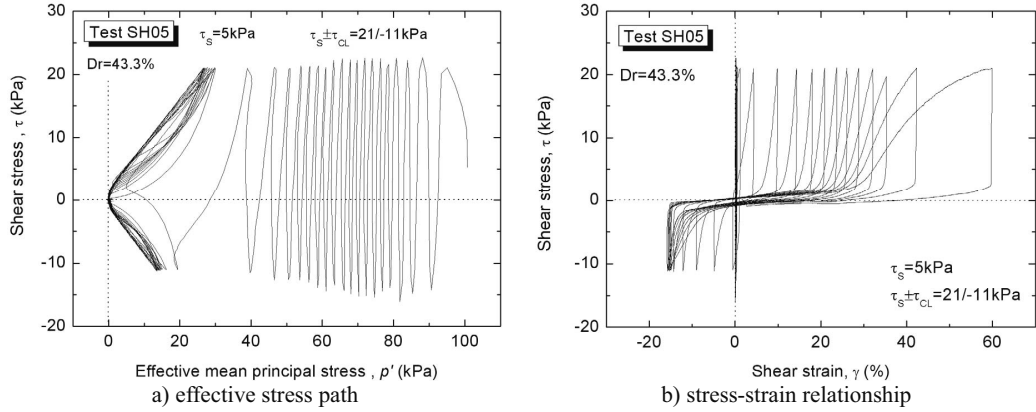


Figure 3 Typical test result on Toyoura sand applying static shear stress ($\tau_s=5\text{kPa}$)

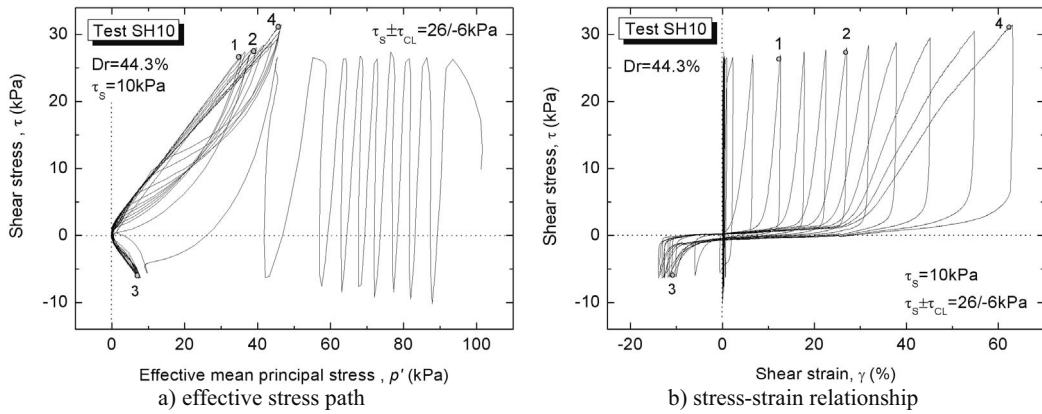


Figure 4 Typical test result on Toyoura sand applying static shear stress ($\tau_s=10\text{kPa}$)

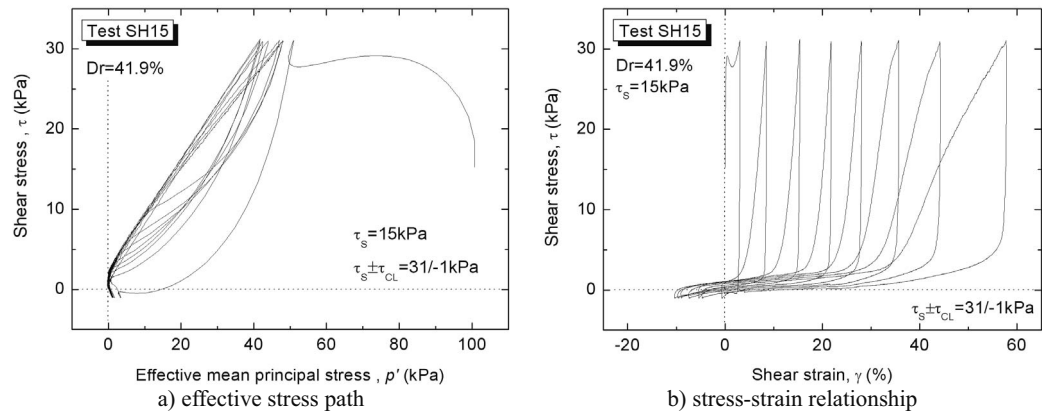


Figure 5 Typical test result on Toyoura sand applying static shear stress ($\tau_s=15\text{kPa}$)

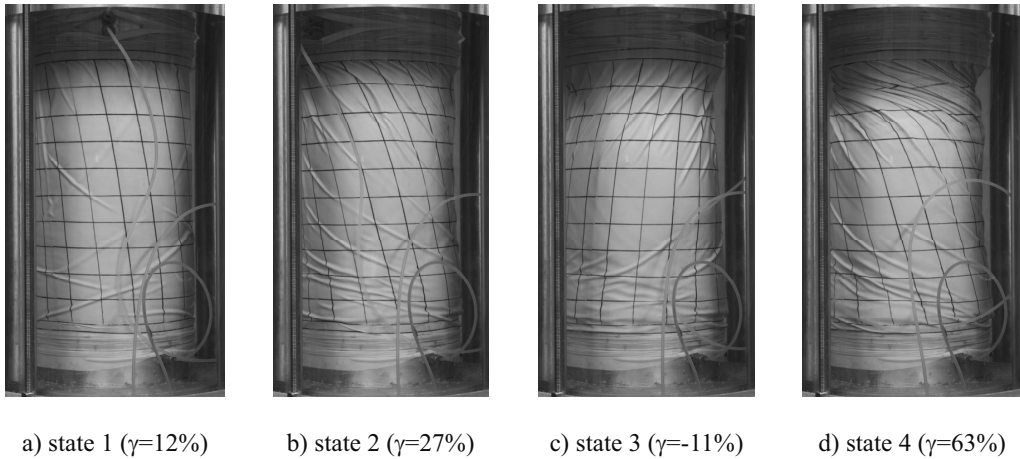


Photo 2 Specimen deformation at states 1 through 4 shown in Fig. 4

The cyclic mobility was observed in Figs. 3a), 4a) and 5a) where the effective stress recovered repeatedly after achieving the state of zero effective stress (i.e., liquefaction). It was accompanied with a significant development of double amplitude shear strain, γ_{DA} , as shown in Figs. 3b), 4b) and 5b).

It was found that the pre-liquefaction behavior of saturated sand was affected by the amount of static shear stress, (e.g., number of cycles to cause liquefaction decreased with the increase in the static shear stress). It should be noted that significant shear strain was induced when the effective stress became almost 40% of the initial effective stress level before dropping suddenly to the zero effective stress state. In the post-liquefaction state, the shear strain increased with the number of cycles; this process clearly depended on the applied static shear stress, in the sense that accumulation of shear strain was noticed in the same direction where the previously monotonic drained shear stress was applied.

Specimen deformation at several states as numbered 1 through 4 in Fig. 4 is shown in Photo 2. At state 1 ($\gamma=12\%$), the deformation was almost uniform except for the regions close to the pedestal and the top cap that are affected by the end restraint; the outer membrane appeared slightly wrinkled. At state 2 ($\gamma=27\%$), the outer membrane was visibly wrinkled; in the region near the top cap the deformation of the specimen started to localize due to water film formation. At state 3 ($\gamma=-11\%$), the localization of specimen deformation developed clearly in the upper part of the specimen. At state 4 ($\gamma=63\%$), the specimen was almost twisted near the top cap.

One-way loading test results

The type of loading in which the combined shear stress (static + cyclic, $\tau_s \pm \tau_{CL}$) is always positive or achieves zero state momentarily during the undrained torsional shear loading, is herein called one-way loading.

Fig. 6 shows test results with one-way loading. As indicated in Fig 6a), the state of zero effective stress was not reached even after applying 208 cycles. Figs. 6b) and c) show that a large shear strain level exceeding 50% was achieved, even though cyclic mobility did not occur.

In addition, a peculiar behavior of Toyoura sand under cyclic torsional loading was observed once the shear strain achieved a level of about 21%. In Fig. 6d) a drop of shear stress exceeding the target value of control could be observed. Also the shear strain suddenly shifted of same percents, Figs. 6b), c) and d).

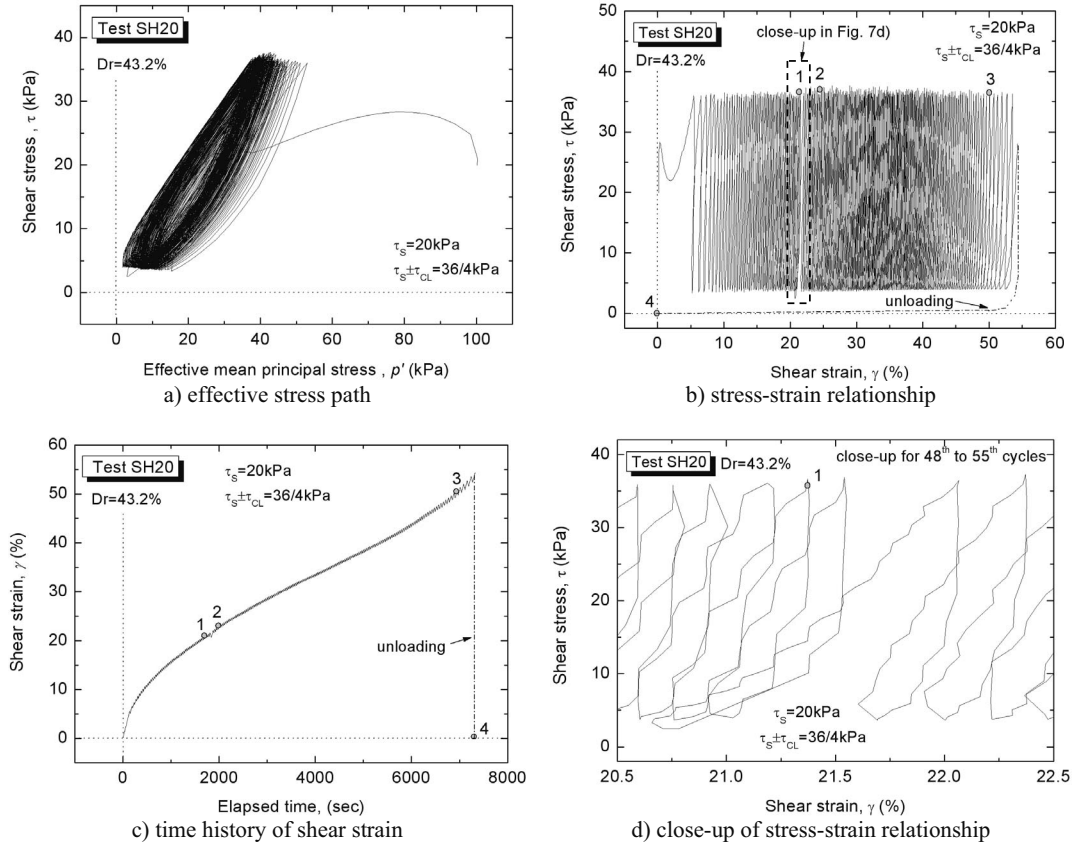


Figure 6 Typical test result on Toyoura sand applying static shear stress ($\tau_s = 20 \text{ kPa}$)

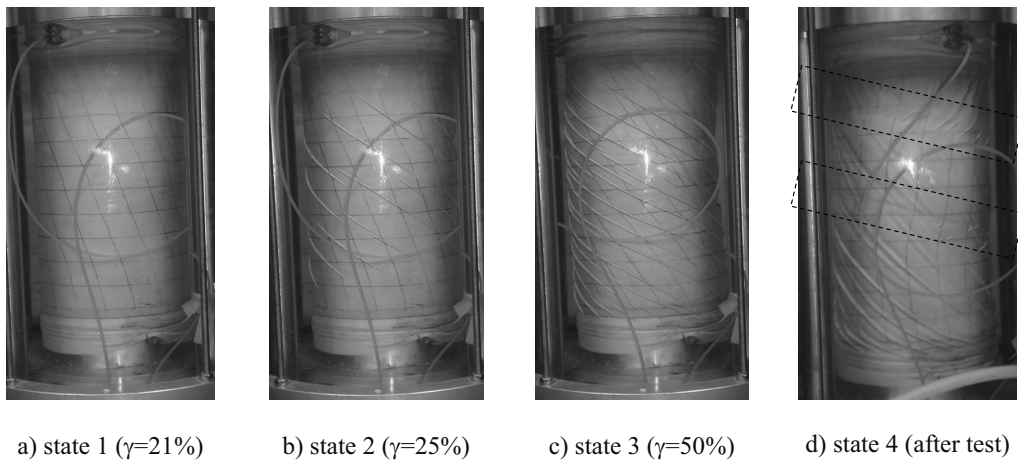


Photo 3 Specimen deformation at states 1 through 3 shown in Fig. 6

Specimen deformation at several states as numbered 1 through 4 in Fig. 6 is shown in Photo 3. The sequence of state 1 ($\gamma=21\%$) and state 2 ($\gamma=25\%$) shows specimen deformation before and after the above described phenomenon.

At state 1 ($\gamma=21\%$) the deformation was rather uniform except for the zones near the top cap and pedestal due to the effect of end restraint. At state 2 ($\gamma=25\%$) the outer membrane was wrinkled at several locations due to local drainage. At state 3 ($\gamma=50\%$) the membrane was extensively wrinkled from the bottom to the top. At state 4 (after test), when zero shear strain state was recovered while keeping undrained condition, formation of a spiral shear band could be observed (Photo 3d).

The results of this one-way loading test indicate that, when the combined shear stress can not reach zero state, liquefaction (i.e., the zero effective stress state) does not occur. However, this does not mean that sand is very resistant against seismic loading, in fact a significant magnitude of combined shear stress may cause failure as evidenced with the formation of shear band.

CONCLUSIONS

Since the soil in a sloping ground is always subjected to an initial driving shear stress prior seismic loading, in order to investigate the effect of static shear stress on the cyclic behavior of liquefied sand, a series of undrained cyclic torsional shear tests was conducted on saturated Toyoura sand specimens up to extremely large deformation. From the present study, analyses of test results revealed that:

- a) by employing the modified torque loading devices undrained cyclic torsional tests could be conducted on saturated Toyoura sand up to double amplitude of about 100%;
- b) in using hollow specimens, due to the presence of inner and outer membranes, correction for effect of membrane force on the measured value of shear stress is indispensable;
- c) saturated loose Toyoura sand undergoing cyclic torsional shear stress behaved in two different ways depending on the value of combined shear stress (static + cyclic). In case of two-way loading, the sand easily liquefied and large deformation was developed while showing cyclic mobility. On the other hand, in case of one-way loading, liquefaction did not occur, while under large shear strain levels formation of shear bands was clearly observed;
- d) both the effective stress path and the stress-strain curve were affected by the initial static shear stress level. In particular, two-way loading tests revealed that, by increasing the initial amount of static shear stress, large shear strain levels could be achieved by applying less cycles;
- e) accumulation of shear strain was clearly noticed in the same direction where previously monotonic drained shear stress was applied;
- f) under extremely large strain level localization of specimen deformation was also observed. In two-way loading tests, they were visible in the region near the top cap where the specimen was almost twisted due to water film formation; whereas, in case of one-way loading, due to local drainage the outer membrane was extensively wrinkled along the whole specimen height.

REFERENCES

- Hamada, M., O'Rourke, T.D. and Yoshida, N. (1994): Liquefaction-induced large ground displacement, *Performance of Ground and Soil Structures during Earthquakes, 13th ICSMFE, JGS*, 93-108
- Kiyota, T., Sato, T., Koseki, J., and Mohammad, A. (2008): Behavior of liquefied sands under extremely large strain levels in cyclic torsional shear tests, *Soils and Foundations*, **48** (5), 727-739
- Koseki, J., Kiyota, T., Sato, T. and Mohammad, A.M. (2007): Undrained cyclic torsional shear tests on sand up to extremely large strain levels, *International Workshop on Earthquake Hazard and Mitigation, Guwahati, India, 7-8 December 2007*, 257-263
- Koseki, J., Yoshida, T. and Sato, T. (2005): Liquefaction properties of Toyoura sand in cyclic

- torsional shear tests under low confining stress, *Soils and Foundations*, **45** (5), 103-113.
- Towhata, I. (2008): Geotechnical Earthquake Engineering, Springer
- Yasuda, S., Nagase, H., Kiku, H. and Uchida, Y. (1992): The mechanism and a simplified procedure for the analysis of permanent ground displacement due to liquefaction, *Soils and Foundations*, **32** (1), 149-160.



A CYCLIC ELASTO-PLASTIC CONSTITUTIVE MODEL TO DESCRIBE DRAINED AND UNDRAINED TORSIONAL SHEAR BEHAVIOR OF SAND

Laddu Indika Nalin DE SILVA¹, Junichi KOSEKI² and Takeshi SATO³

ABSTRACT: A cyclic elasto-plastic constitutive model to describe the drained and undrained torsional shear behavior of sand is proposed. Stress-strain relationship under cyclic drained loading is modeled by incorporating a hyperbolic type stress-strain relationship with extended Masing's rules considering the damage to plastic shear modulus at large shear stress levels and hardening of the material with cyclic loading. Undrained cyclic shear behavior is modeled by assuming that the total volumetric strain increment during undrained loading, which consists of dilatancy and consolidation/swelling components, is equal to zero. Applicability of the proposed model is verified by simulating the results of a series of drained and undrained cyclic torsional shear tests on Toyoura sand. The stress-strain relationship, effective stress path and the liquefaction strength curve during cyclic loading are reasonably simulated by the proposed model.

Key Words: Hyperbolic stress-strain relationship, damage, hardening, stress-dilatancy relationship, liquefaction, cyclic torsional shear

INTRODUCTION

Soils are frequently subjected to large cyclic loadings due to traffic, sea waves and earthquakes. The type of loading condition can be drained, partially drained or undrained depending on the local soil conditions and frequency of loading. Among other issues associated with cyclic loading, liquefaction has been given a great deal of attention as the damage caused by liquefaction is disastrous and costly.

Therefore, researchers have been developing constitutive models based on various approaches to describe the behavior of soils under cyclic loading. One framework of cyclic elasto-plastic modelling to model the stress-strain relationship of soils under drained conditions is to model the monotonic loading curve (skeleton curve or backbone curve) by an appropriate type of function (usually hyperbolic) and apply the well known Masing's rule (Masing, 1926) with appropriate modifications to model the subsequent cyclic loading branches.

Tatsuoka et al. (2003) utilized the above approach successfully to simulate the stress-strain relationship of Toyoura sand subjected to cyclic plane strain compression under drained condition. Balakrishnaiyer (2000) employed a similar approach as above to successfully simulate the drained stress-strain relationship of Chiba gravel subjected to cyclic triaxial loading. The applicability of the above approach in simulating the stress-strain relationship of Toyoura sand subjected to drained cyclic torsional shear loadings was investigated by Hong Nam (2004).

¹ Post doctoral research fellow

² Professor

³ Research support promotion member

However, it should be noted that all the models as described above are capable of reasonably simulating the stress-strain relationship of soils under drained condition well before its peak state (or less than 1 % of strain). In order to simulate large cyclic behavior with stress states closing its peak state, some modifications to the original concept may be necessary as the experimental evidences show damage to the soil structure at large stress levels causing reduction of plastic modulus of soil and hardening behavior of soil with subsequent cyclic loadings. In addition, there has been no attempt so far to the authors' knowledge to extend this approach to model the cyclic undrained behavior of soil.

In view of the above, it has been attempted in the present study to model the stress-strain relationship of sand subjected to large cyclic drained torsional shear loading by utilizing the same approach as proposed by Tatsuoka et al. (2003), while considering the damage to plastic properties at higher stress levels and hardening with subsequent cyclic loadings. The proposed model is employed to simulate the stress-strain relationship of Toyoura sand under drained cyclic torsional shear loading and it was combined with an empirical stress-dilatancy relationship to simulate the volumetric strain of sand under the same loading condition. Finally, a model is proposed to simulate the undrained cyclic torsional shear behavior of sand and hence liquefaction strength curve of Toyoura sand was obtained.

MODELLING OF DRAINED CYCLIC TORSIONAL SHEAR BEHAVIOR OF SAND

Modelling of skeleton curve

Hyperbolic type equations are widely employed to model non-linear stress-strain behavior of soil under drained condition. A typical hyperbolic equation has only two parameters with clear physical meanings namely, initial stiffness and peak strength, which can be determined in the laboratory. However, it was observed that the simulation using the above hyperbolic equation is not in good agreement with actual test data particularly at small strains (Tatsuoka and Shibuya, 1991a). Therefore, modified hyperbolic models have been proposed with more numbers of parameters. Tatsuoka and Shibuya (1991b) proposed a hyperbolic equation using parameters that are modeled as functions of strain to simulate stress-strain relations for wide range of strain. This equation is called as the Generalized Hyperbolic Equation (GHE) and takes the form as shown in Equation (1).

$$Y = \frac{X}{\frac{1}{C_1(X)} + \frac{|X|}{C_2(X)}} \quad (1)$$

in which, the normalized plastic shear strain and shear stress, $X = \gamma_{z\theta}^p / \gamma_{z\theta r}$ and $Y = \tau_{z\theta} / \tau_{z\theta max}$ are selected in the present study to model the torsional shear behavior of sand. $\gamma_{z\theta}^p$ is the plastic shear strain component, which was computed by subtracting the elastic shear strain component from total shear strain. Elastic shear strain component was evaluated by employing the recently developed IIS model (Hong Nam et al., 2005). $\gamma_{z\theta r}$ is the reference shear strain taken as the ratio of peak shear stress ($\tau_{z\theta max}$) and maximum quasi-elastic shear modulus ($G_{z\theta max}$). $\tau_{z\theta max}$ and $G_{z\theta max}$ of Toyoura sand of 75 % relative density at 100 kPa consolidation pressure was determined as 85 kPa and 100 MPa, respectively.

$C_1(X)$ and $C_2(X)$ are functions of strain, which can be determined by fitting to experimental data (refer to Hong Nam, 2004 for the details). Note that, $C_1(X = 0)$ represent the ratio of initial plastic shear moduli and initial quasi-elastic shear modulus, and $C_2(X = \infty)$ represent the normalized peak strength of the material.

Typical simulation of monotonic stress-strain relationship (skeleton curve) using the above equation along with the parameters used is shown in Fig. 1. It can be stated that the GHE can well simulate the skeleton curve of sand under torsional shear loading.

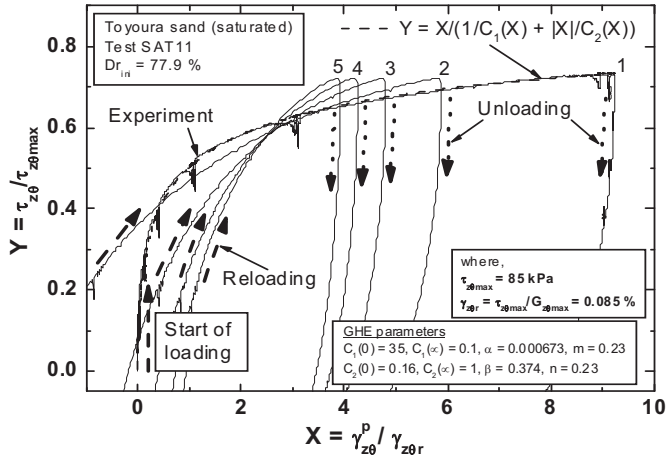


Figure 1. Modelling of skeleton curve of sand under torsional shear

Modelling of subsequent cyclic loading

Subsequent cyclic loading can be modeled by employing the extended Masing's rules (Tatsuoka et al, 2003). When the soil is subjected to cyclic loadings, rearrangement of particles takes place within the soil specimen. Tatsuoka et al. (2003) proposed a concept known as "drag" to take the particle rearrangement into account, in which the corresponding monotonic loading curve in opposite direction is dragged by an amount β when applying the Masing's rule during cyclic loading (extended Masing's rule). Refer to Fig. 2a for a schematic illustration of the concept of dragging and extended Masing's rule. Note that, the extended Masing's rule consists of several sub rules depending on the location of the current and previous turning points (refer to Tatsuoka et al., 2003 for the detailed explanation of these sub rules).

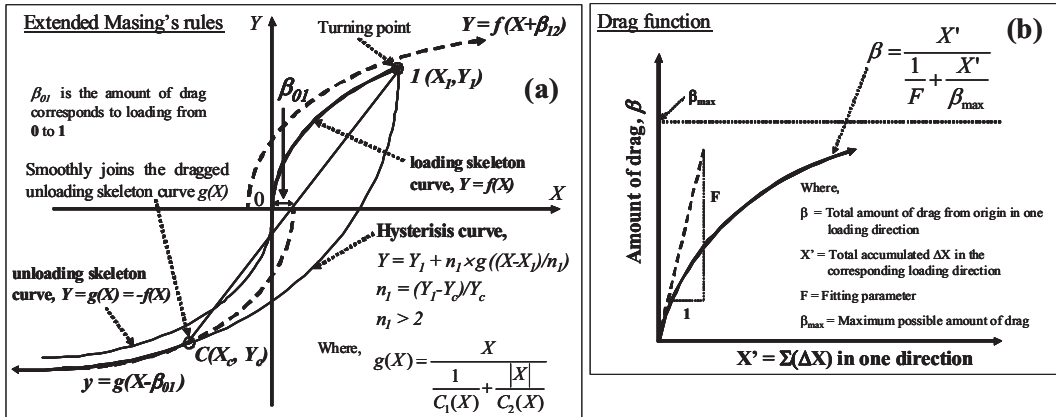


Figure 2. Application of extended Masing's rule in modeling the subsequent cyclic loadings

The amount of drag in a particular loading direction is assumed to be empirically related to the total accumulated normalized plastic shear strain, $X' = \Sigma(\Delta X)$, in the same direction up to the current turning point as schematically shown in Fig. 2b. Hong Nam (2004) suggested the values of the parameters F and β_{max} that are defined by the hyperbolic equation shown in Fig. 2b to be 0.45 and 3.13, respectively for cyclic torsional shear loading. The same values were employed in the current study.

Hardening and damage

Monotonic and cyclic stress-strain relationships of Toyoura sand specimens with similar densities under torsional shear loading are compared in Fig. 3. Although the peak strength values of the tests are similar to each other, effects of hardening due to the application of cyclic loading on the pre-peak behavior are evident.

Since the GHE tends to reach its asymptotic value near the peak stress state, the effects of drag in simulating the hardening behavior at higher stress levels is not significant; hence the simulation results start deviating from the experiment data when the stress state is closing its peak.

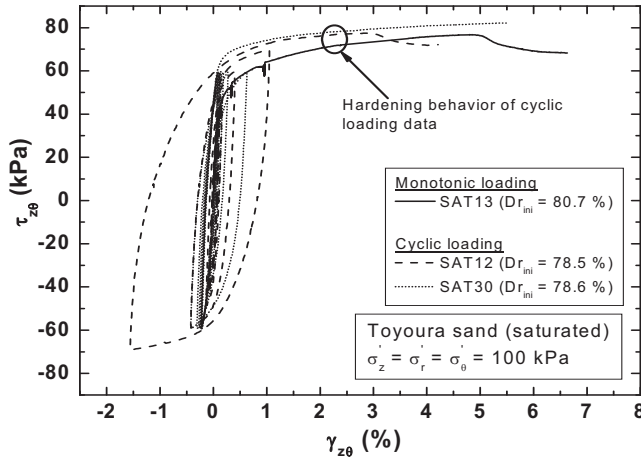


Figure 3. Hardening due to cyclic loading

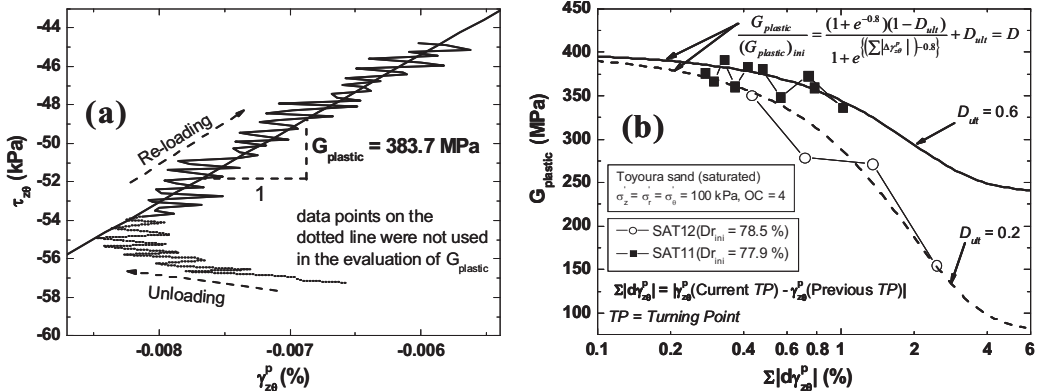


Figure 4. Damage to plastic shear modulus during large amplitude cyclic loading

In addition to the hardening due to cyclic loading, the soil fabric will undergo damage when subjected to higher shear stress levels. In order to further investigate the damage, plastic shear modulus ($G_{plastic}$) values at each turning point during cyclic loading were evaluated as typically shown in Fig. 4a. Note that the plastic shear modulus values were evaluated by linearly fitting to the linear portion of the shear stress versus plastic shear strain relationship when the specimen starts showing the plastic deformation at each turning point. These plastic shear moduli values were plotted against the accumulated γ_{z0}^p between the current and previous turning points ($\sum |d\gamma_{z0}^p|$) as shown in Fig. 4b. Results show good correlation between $G_{plastic}$ and $\sum |d\gamma_{z0}^p|$ showing possible damage to soil fabric.

In the method proposed by Tatsuoka et al. (2003), a unique skeleton curve for a particular loading

direction was used when modeling the hysteresis curves using the extended Masing's rules. In order to consider in addition the effects of above hardening and damage in such modeling, the use of non-unique skeletons curves when applying the extended Masing's rule is proposed in the current study.

Hardening behavior with cyclic loading is taken into account by multiplying $C_2(X)$ of Eq. (1) by a hardening factor "S" (refer to Eq. (2)). The hardening factor "S" is assumed to be a function of the total normalized plastic shear strain that has been accumulated up to the current turning point, $\sum|\Delta X|$.

$$S = 1 + \frac{\left(\sum |\Delta X| \right)_{\text{Upto current turning point}}}{\frac{\beta_{\max}}{F} + \frac{\left(\sum |\Delta X| \right)_{\text{Upto current turning point}}}{(S_{ult} - 1)}} \quad (2)$$

where, S_{ult} = the highest value for S (taken as 1.35 and 1.15 for constant stress amplitude cyclic loading and varying stress amplitude cyclic loadings, respectively). When hardening and damage are considered in the model, the drag parameters F and β_{\max} are modified into 0.15 and 12.0, respectively. These parameters were determined by trial and error. It should be emphasized that more experimental investigations on this issue is required for better understanding of the phenomenon.

Damage to the plastic shear moduli is taken into account by multiplying $C_1(X)$ of Eq. (1) by a damage factor "D" (refer to Eq. (3)). Experimental evidences as shown in Fig. 4 suggest that the damage factor "D" can be taken as a function of the accumulated plastic shear strain between the current and previous turning points ($\sum|d\gamma_{z\theta}^p|$).

$$D = \frac{(1 + e^{-0.8})(1 - D_{ult})}{1 + e^{\left\{ \left(\sum |d\gamma_{z\theta}^p| \right)^{-0.8} \right\}}} + D_{ult} \quad (3)$$

where, D_{ult} = the ratio of plastic shear modulus at peak shear strain and the initial plastic shear modulus (D_{ult} is taken as 0.2). Note that the initial plastic shear modulus was evaluated by linearly fitting to the initial linear portion of the shear stress versus plastic shear strain relationship when the specimen starts showing the plastic deformation. It is assumed that $D = 1$ (no damage) until the stress state first exceeds the phase transformation stress state at which volumetric behavior changes from contractive to dilative, as will be explained later in details. Note that factors "S" and "D" are constants for a particular loading branch but varies with different branches.

STRESS-DILATANCY RELATIONSHIP

Modeling of stress-strain relationship as discussed above is not sufficient to describe the volumetric behavior of soil. Therefore, a relationship that deals with the ratio of plastic volumetric and shear strain increments to a shear stress ratio is required in addition to the stress-strain relationship. This relationship is known as the stress-dilatancy relationship.

There are various theoretical stress-dilatancy relationships available for triaxial and plane strain loading conditions. It should be noted that all those stress-dilatancy relations are originally developed for monotonic loading conditions. Pradhan and Tatsuoka (1989) experimentally investigated the stress-dilatancy relationships of sand subjected to cyclic loading conditions and modified the available stress-dilatancy relationships to apply for cyclic loading conditions.

However, it should be noted that the theoretical stress-dilatancy relations were derived mostly for either cyclic triaxial ($d\varepsilon_2 = d\varepsilon_3$) or cyclic plane strain (or simple shear) ($d\varepsilon_2 = 0$) loading conditions. Therefore, in order to deal with more general deformation mode such as torsional shear, an empirical

stress-dilatancy relationship is employed in the present study.

As shown in Fig. 5, results from cyclic torsional shear experiment suggest that unique relationships between the shear stress ratio ($\tau_{z\theta}/p'$) and the dilatancy ratio ($-d\varepsilon_{vol}^p/d\gamma_{z\theta}^p$) exist for $d\gamma_{z\theta}^p > 0$ and $d\gamma_{z\theta}^p < 0$, respectively. Higher dilatancy ratios can be observed immediately after the reversal of loading direction. In addition, the effects of over-consolidation alter the stress-dilatancy relationship during virgin loading as shown in Fig. 5b. Therefore, the following bilinear equation can be proposed by referring to the experiment data as shown in Fig. 5 to model the stress-dilatancy relationship during subsequent cyclic loadings.

$$\frac{\tau_{z\theta}}{p'} = R_k \left(-\frac{d\varepsilon_{vol}^p}{d\gamma_{z\theta}^p} \right) + C \quad (4)$$

where, the average value of R_k is taken as 1.5 and the average value of C is taken as 0.46 and -0.46 for $d\gamma_{z\theta}^p > 0$ and $d\gamma_{z\theta}^p < 0$, respectively. In order to consider the stress-dilatancy relationships immediately after the reversal of loading direction, R_k is taken as 0.33 and C is taken as -0.18 and 0.18 for $d\gamma_{z\theta}^p > 0$ and $d\gamma_{z\theta}^p < 0$, respectively (refer to Fig. 5a and 5b).

Stress-dilatancy relationship of normally consolidated Toyoura sand during virgin loading (refer to Fig. 5a) is modeled separately (Nishimura, 2002) by taking R_k as 1.3 and C as 0.60, while that of over-consolidated Toyoura sand (refer to Fig. 5b) will be discussed later.

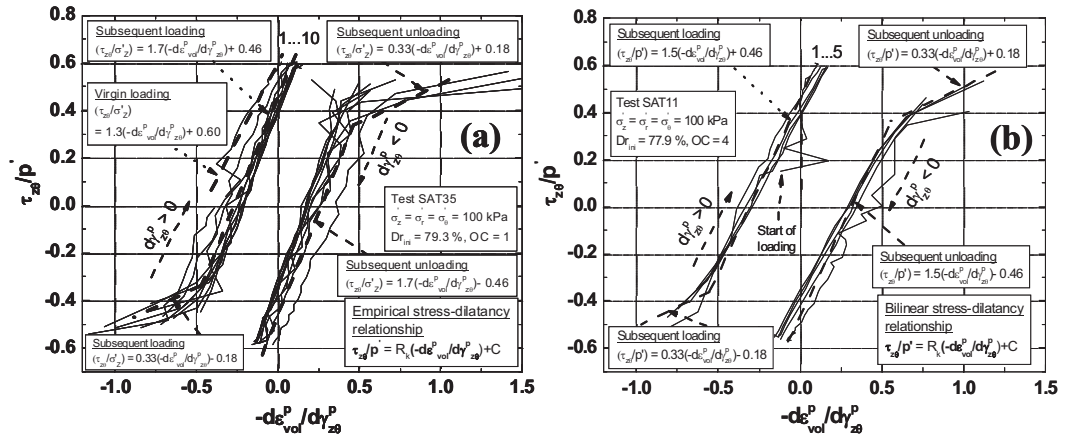


Figure 5. Bilinear stress-dilatancy relationship

Effects of hardening and damage on stress-dilatancy relationship

It can be seen in Fig. 5 that the effects of hardening and damage cause slight variations in the stress-dilatancy relationship during subsequent cyclic loadings. Note that the $|C|$ values during constant stress amplitude cyclic torsional loading becomes smaller with subsequent cyclic loadings as shown in Fig. 5a and 5b (1..10 in Fig. 5a corresponds to the cyclic number). Furthermore, the $|C|$ value can even become larger, depending on the accumulated strain during the previous reloading/re-unloading branch.

Considering the above factors, the bilinear stress-dilatancy model as proposed before was further modified as shown below by introducing the damage factor D .

$$\frac{\tau_{z\theta}}{p'} = (R_{\max} \times D) \times \left(-\frac{d\varepsilon_{vol}^p}{d\gamma_{z\theta}^p} \right) + \frac{C_{\min}}{D} \quad (5)$$

where, R_{max} = the maximum value of R_k in Eq. 4 ($R_{max} = 1.5$ was selected). C_{min} = the minimum value of C ($C_{min} = \pm 0.36$ was assumed for $d\gamma_{z\theta}^p > 0$ and $d\gamma_{z\theta}^p < 0$, respectively). Two boundary conditions were specified for $R_{max} \times D$ value and $|C_{min}/D|$ value by referring to the experimental data. If $R_{max} \times D$ value becomes less than 1.00, $R_{max} \times D = 1.00$ was used. If $|C_{min}/D|$ becomes greater than 0.50, $|C_{min}/D| = 0.50$ was used.

Therefore, $R_{max} \times D$ value in Eq. 5 varies between 1.5 and 1.0, and $|C_{min}/D|$ value varies between 0.36 and 0.50 depending on the accumulated strain between current and previous turning points (i.e. damage parameter, D). Note that the above modification was applied only to the main body of the bilinear stress-dilatancy relationship. The stress-dilatancy relationships immediately after the stress-reversal as shown in Fig. 5 was not modified (i.e. $R_k = 0.33$ and $C = \pm 0.18$ for $d\gamma_{z\theta}^p > 0$ and $d\gamma_{z\theta}^p < 0$, respectively). Furthermore, the stress-dilatancy relationship during virgin loading was also not modified.

The value of $d\gamma_{z\theta}^p$ in Eq. 5 can be obtained from the simulation of stress-strain relationship. Then, ε_{vol}^p can be evaluated by numerically integrating $d\varepsilon_{vol}^p$ in Eq. 5.

MODELLING OF UNDRAINED CYCLIC TORSIONAL SHEAR BEHAVIOR

One framework for modeling the undrained torsional shear behavior of soil is to assume that the total volumetric strain increment ($d\varepsilon_{vol}$) during undrained loading, which is equal to zero, consists of a volumetric strain component purely due to shear stress (or dilatancy, $d\varepsilon_{vol}^d$) and a volumetric strain component purely due to consolidation/swelling of the soil ($d\varepsilon_{vol}^c$) due to the change in mean effective stress (p'). Hence the following equation is assumed to be valid during the cyclic undrained loading.

$$d\varepsilon_{vol}^c + d\varepsilon_{vol}^d = 0 \quad (6)$$

$d\varepsilon_{vol}^d$ can be evaluated by combining the modeling of stress-strain relationship during cyclic drained loading with the stress-dilatancy relationship. It is assumed that there exists a unique relationship between $(\tau_{z\theta}/p')/(\tau_{z\theta}/p')_{max}$ and $\gamma_{z\theta}^p/\gamma_{z\theta}^p$ (where, $\gamma_{z\theta}^p = (\tau_{z\theta}/p')_{max}/(G_{z\theta}/p'_o)$) among drained and undrained loadings (note that p' is kept constant, hence $p' = p'_o$ in drained tests), hence the same stress-dilatancy relationship as proposed in Eq. 5 can be employed to evaluate $d\varepsilon_{vol}^d$ during undrained loading.

However, accurate determination of $(\tau_{z\theta}/p')_{max}$ of dense sand subjected to drained and undrained torsional shear loadings is a difficult task in the current study because the capacity of shear strain measurement employed is limited to about 5 % of single amplitude shear strain. Therefore, GHE parameters for undrained loading are determined by slightly modifying the drained parameters for better simulation of the undrained behavior.

Effects of over-consolidation on stress-dilatancy relationship

It is evident from Fig. 5b that the effects of over-consolidation significantly affect the stress-dilatancy relationship during virgin loading and its effects vanish with subsequent cyclic loadings. Note that p' is kept constant during drained cyclic torsional shear tests in the current study. However, during cyclic undrained loading, the specimen is continuously subjected to over-consolidation, which may have significant effects on the stress-dilatancy relationship, which is proposed in Eq. 5.

During undrained cyclic loading, firstly, the soil is subjected to over-consolidation until the stress state exceeds the phase transformation stress state for the first time (i.e. the first instance where the volumetric behavior changes from contractive to dilative ($dp' > 0$)). Phase transformation stress state for virgin loading is taken as $|\tau_{z\theta}/p'| = C = 0.60$, and for subsequent cyclic loadings, it is determined as $|\tau_{z\theta}/p'| = C = 0.50$. Note that, in Eq. 4, the average value of C is taken as 0.46, while $C = 0.50$ corresponds to the maximum value of C during subsequent cyclic loading (i.e. the boundary value of

$|C_{min}/D|$ in Eq. 5). Then the soil will enter the stage of cyclic mobility. The stress-dilatancy relationships during these two stages will be addressed separately in the current study.

After the stress state enters the cyclic mobility for the first time, the stress-dilatancy relationship during cyclic torsional loading can be modeled by the modified bilinear stress-dilatancy relationship as expressed in Eq. 5. Before the stress state exceeds the phase transformation stress state for the first time (before cyclic mobility), the effects of over-consolidation need to be taken into account for better simulation of the cyclic undrained behavior. Oka et al. (1999) proposed a stress-dilatancy equation to consider the effects of over-consolidation. A similar equation was employed in the current study as shown in Eq. 7.

$$\left(-\frac{d\varepsilon_{vol}^p}{d\gamma_{z\theta}^p} \right) = D_k \left(\frac{\tau_{z\theta}}{p'} - \left(\frac{\tau_{z\theta}}{p'} / \ln(OC) \right) \right) / (R_s) \quad (7)$$

where, $D_k = \left[\tau_{z\theta} / p' / (C_s \times \ln(OC)) \right]^{1.5}$, OC = over-consolidation ratio, R_s and C_s are taken as 2.2 and 0.50, respectively.

Eq. 7 is employed when D_k is less than or equal to 1.0 during cyclic undrained loading until the stress state first exceeds the phase transformation stress state. When $D_k = 1$, Eq. 7 becomes identical to Eq. 4 with R_k and C being replaced by R_s and C_s , and follows the stress dilatancy relationship given by Eq. 4 afterwards. Therefore $D_k = 1$ denotes the over-consolidation boundary surface.

The above equation was used in the drained tests as well, if the specimen is subjected to over-consolidation.

Evaluation of $d\varepsilon_{vol}^e$

Experimental evidences as shown in Fig. 6a suggests that the quasi-elastic bulk moduli ($K = dp' / d\varepsilon_{vol}^e$) can be expressed as a function of p' for a given density as shown in Eq. 8 (note that the effect of the change in void ratio during consolidation from $p' = 100$ kPa to 400 kPa on the K value is considered implicitly in the equation, i.e. $f(e) = f(e_o)$).

$$\frac{K}{f(e)} = \frac{K_o}{f(e_o)} \left(\frac{p'}{p_o} \right)^{m_k} \quad (8)$$

where, K_o is the bulk modulus at a reference stress state p'_o and m_k is the parameter to express the stress state dependency of K . According to the experiment data as shown in Fig. 6a, K_o at $p'_o = 100$ kPa is obtained as 80 MPa for a Toyoura sand specimen of about 75 % relative density. The average value of m_k is 0.643. Note that, the K_o values for other densities as shown in Fig. 6a were evaluated by assuming that the K_o values normalized by the void ratio function $f(e_o)$ (Hardin and Richart, 1963) at the same reference stress state are unique among different densities.

Since it is believed that the swelling behavior of sand is nearly elastic, the total volumetric strain due to swelling (ε_{vol}^e) is evaluated by integrating its increment ($d\varepsilon_{vol}^e$) given by Eq. 8, and compared with the corresponding experiment data as shown in Fig. 6b. However, it can be observed from Fig. 6b that the specimen exhibits generation of some plastic volumetric strain even during swelling.

Therefore, in order to take the generation of plastic volumetric strain into account, K_o at $p'_o = 100$ kPa is taken as 58 MPa for a Toyoura sand specimen of about 75 % relative density and the value of m_k is taken as 0.9. It can be observed that ε_{vol}^e evaluated by applying the above parameters in Eq. 8 reasonably matched with the experiment data as shown in Fig. 6b.

Then, by combining Eqs. 6 and 8, we can get the following relationship between dp' and $d\varepsilon_{vol}^d$.

$$dp' = K_o \left(p' / p_o \right)^{m_k} \times (-d\varepsilon_{vol}^d) \quad (9)$$

Therefore, the stress path and stress-strain relationship of sand subjected to undrained cyclic torsional shear loading can be modeled by employing Eq. 9.

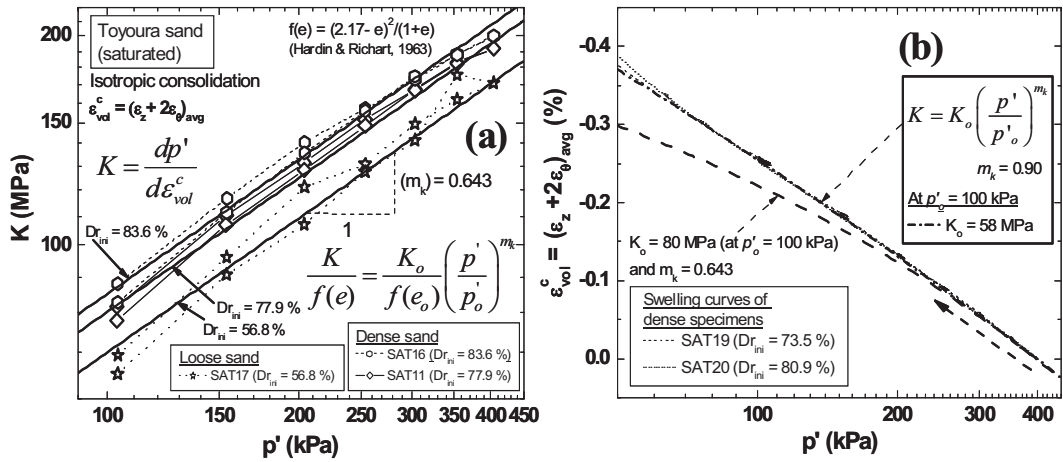


Figure 6. Modelling of the swelling behavior of sand

SIMULATION OF TEST RESULTS AND DISCUSSION

Simulation of cyclic drained behavior of sand

Simulation results of stress-strain relationships of sand subjected to drained cyclic torsional shear loading are shown in Figs. 7, 8 and 9. In order to illustrate the improvement achieved, first the simulation was carried out by employing the original Masing's rule (Case 1) (without the drag) as shown in Fig. 7. It can be seen in Fig. 7a that the original Masing's rule is not capable of simulating the constant stress amplitude cyclic loading and ended up tracing an identical curve for subsequent cyclic loadings, while experimental data shows hardening behavior with the subsequent cyclic loading. In addition, the simulation results of varying stress amplitude cyclic loading start deviating from the experiment data when the stress states become closer to the peak strength as shown in Fig. 7b.

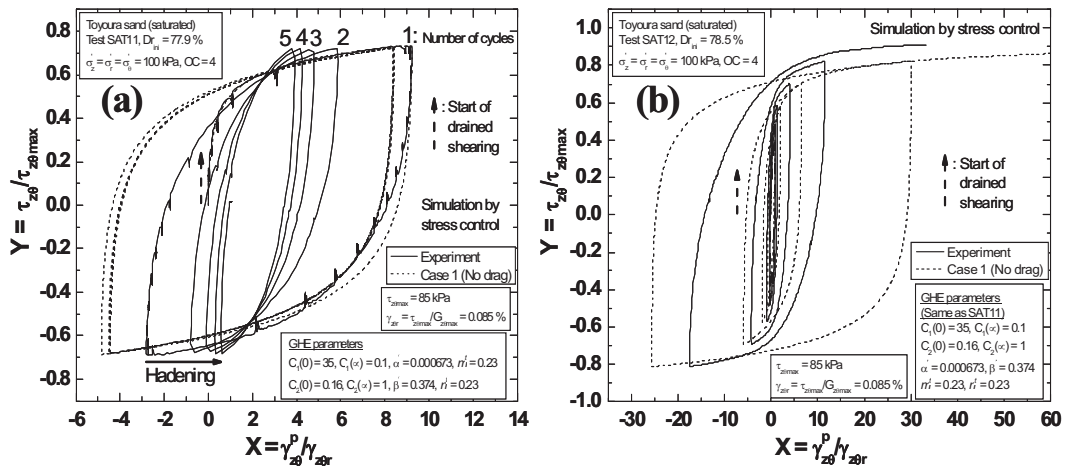


Figure 7. Simulation of stress-strain relationship using the original Masing's rule

Then the concept of drag is introduced into the simulation as shown in Fig. 8 (Case 2). It can be seen that, except for the first cycle, no significant improvement can be observed in the simulation of constant stress amplitude cyclic loading as shown in Fig. 8a. On the other hand, simulation is improved up to a certain extent in case of varying stress amplitude cyclic loading as shown in Fig. 8b. However, the simulation results start deviating from the experiment data when the stress state is closing its peak.

Finally, simulation is further modified by introducing the hardening and damage into the model as shown in Fig. 9 (Case 3). It can be seen that the simulation results of constant and varying stress amplitude cyclic loadings (Fig. 9a and Fig. 9b, respectively) are reasonably consistent with the experiment data after introducing hardening and damage to the extended Masing's rules.

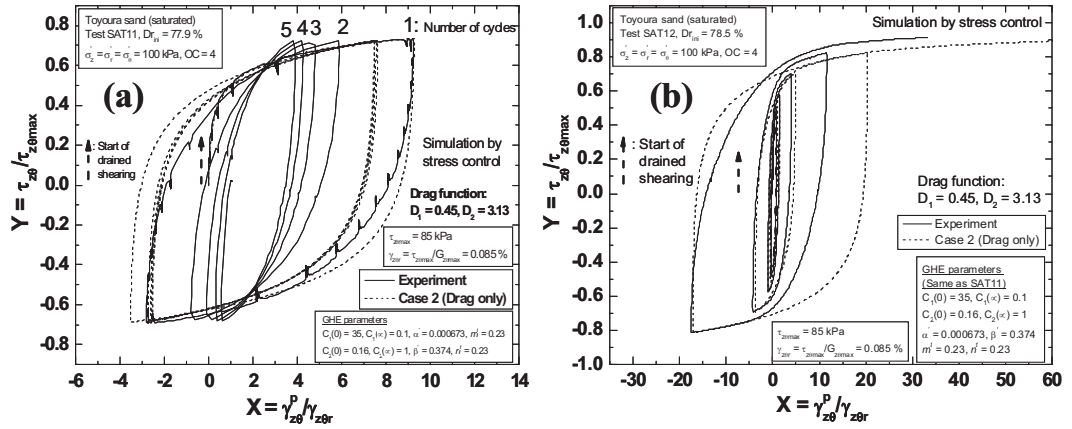


Figure 8. Simulation of stress-strain relationship using the Extended Masing's rule

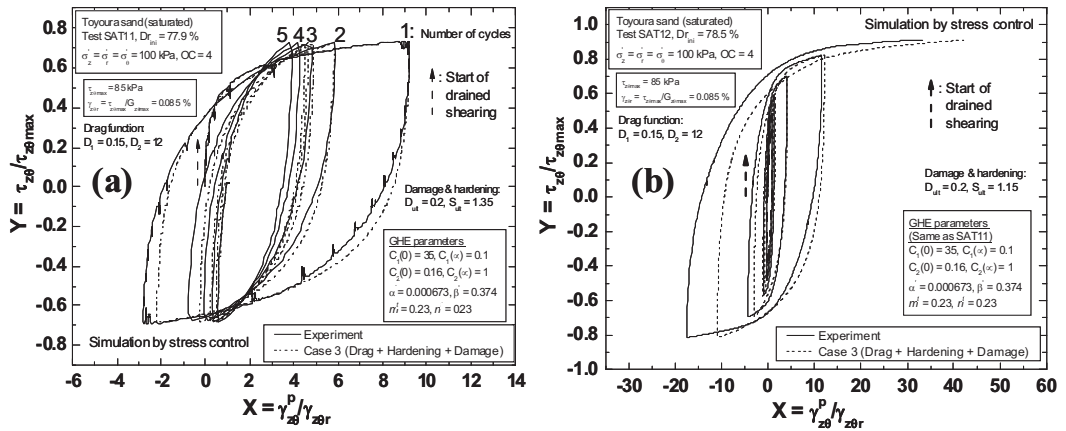


Figure 9. Simulation of stress-strain relationship with hardening and damage

Simulation of volumetric behavior of sand

Simulation of ε_{vol}^p during drained cyclic torsional shear loading was carried out, first by employing the bilinear stress-dilatancy relationship (Eq. 4)(denoted as Case A), and then by employing the modified bilinear stress-dilatancy relationship (Eq. 5)(Case B) in order to illustrate the improvement achieved. $d\gamma_{z\theta}^p$ values in Eqs. 4 and 5 were computed by using the Case 3 stress-strain simulation since it is reasonably consistent with the experiment data.

Comparison of simulation of ε_{vol}^p with corresponding experiment data of two typical experiments are shown in Fig. 10a and Fig. 10b. It is evident that hardening of the material due to constant stress amplitude cyclic torsional loading causes reduction of the accumulation of ε_{vol}^p with subsequent cyclic loadings as shown in Fig. 10a. However, simulation of ε_{vol}^p by using bilinear stress-dilatancy model (Case A of Fig. 10a) do not well conform with the experiment data showing nearly constant accumulation of ε_{vol}^p with subsequent cyclic loadings.

In addition, the large accumulation of ε_{vol}^p immediately after the reversal of loading direction at large shear stress levels as shown in Fig. 10b can not be well simulated by employing the bilinear stress-dilatancy model (Case A of Fig. 10b).

On the other hand, It can be observed that the simulation is significantly improved when the slight variations in stress-dilatancy relationship due to hardening and damage is taken into account by employing the modified bilinear stress-dilatancy model as shown in Case B of Fig. 10a and Fig. 10b.

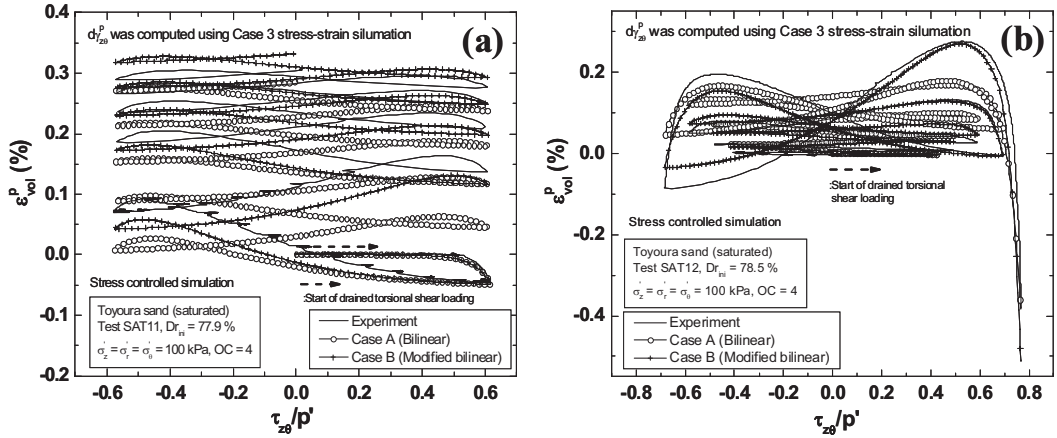


Figure 10. Simulation of volumetric strain

Simulation of liquefaction behavior of sand

Fig. 11 shows the comparison of experimentally obtained stress paths and stress-strain relationships of a typical undrained cyclic torsional shear test (refer to Fig. 11a and Fig. 11b, respectively) and its simulation (Note that, the elastic strain component can be neglected compared to the total shear strain, hence $\gamma_{z\theta} \approx \gamma_{z\theta}^p$ is assumed in the comparison of experiment data with its simulation).

First, the simulation of stress path and stress-strain relationship was carried out by employing the modified bilinear stress-dilatancy relationship to evaluate $d\varepsilon_{vol}^d$ as shown in Fig. 11c and Fig. 11d. The effect of change of over-consolidation ratio on stress-dilatancy relationship was not considered in the above simulation.

Then the effect of over-consolidation on the stress-dilatancy relationship was taken into account in the simulation by employing Eq. 7 within the over-consolidation boundary surface ($\tau_{z\theta} < \pm p' \times C_s \times \ln(OC)$) as shown in Fig. 11e and Fig. 11f.

It is clear from Fig. 11e and Fig. 11f that the simulation of both stress path and stress-strain relationship is improved after introducing the effects of over-consolidation on stress-dilatancy relationship in the simulation.

However, experimentally obtained stress-strain relationship of dense Toyoura sand (refer to Fig. 11b) shows continuous and more regular increase in the shear strain amplitude even after the stress path enters the steady state of cyclic mobility, while simulation results show reasonable agreement with the experiment data until the stress path enters the steady state, and ended up tracing a closed loop after the stress path enters the steady state. Further modifications that might consider the strain

softening behavior of sand would be required in the simulation to address the above issue, which is out of the scope of the current study.

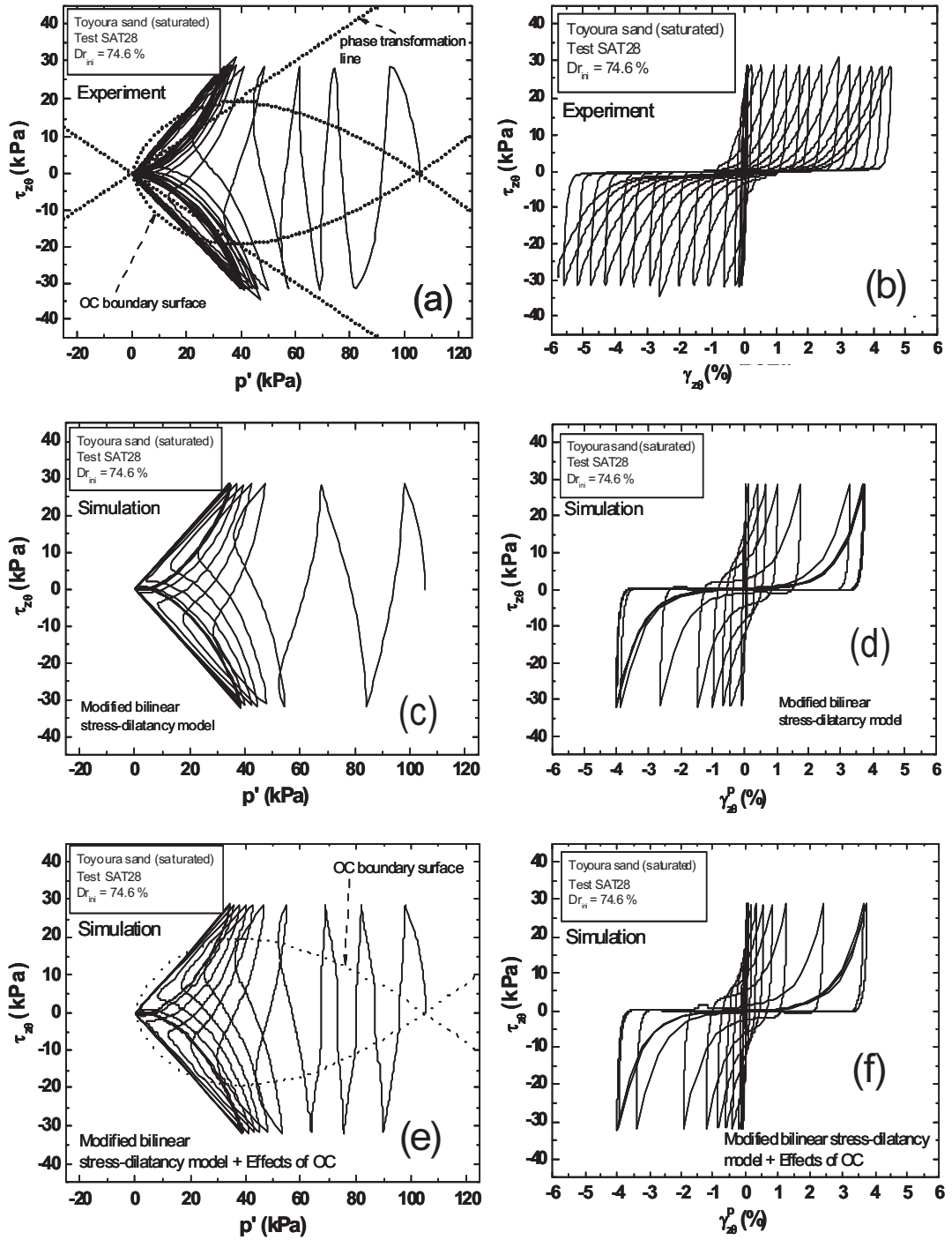


Figure 11. Simulation of the liquefaction behavior of sand

Fig. 12 shows the liquefaction resistance curves of dense Toyoura sand obtained from the experimental and simulation results. Liquefaction resistance is defined as the number of cycles required to induce a double amplitude shear strain (DA) of 6 %. It can be seen that simulation could be significantly improved when the modified bilinear stress-dilatancy relationship was employed in the simulation, while considering the effects of over-consolidation.

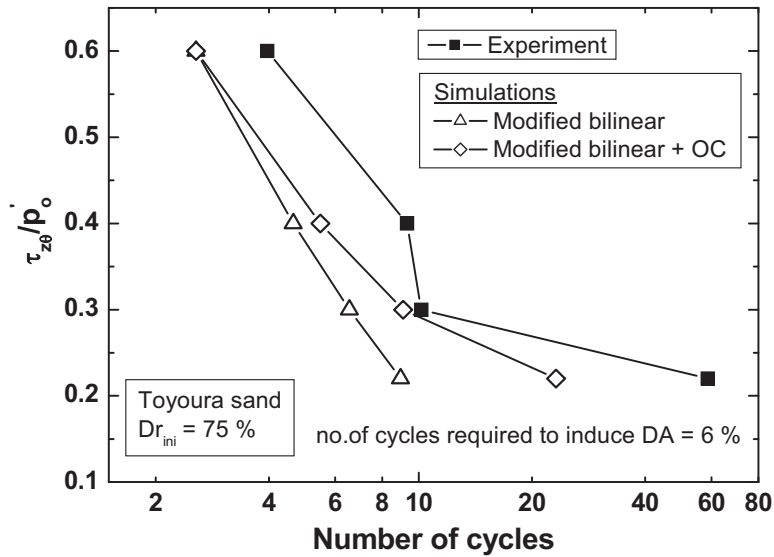


Figure 12. Liquefaction resistance curve

CONCLUSIONS

A cyclic elasto-plastic constitutive model based on a hyperbolic type stress-strain relationship, extended Masing's rules and an empirical stress-dilatancy relationship is proposed to simulate the drained and undrained cyclic torsional shear behavior of sand. The main findings of the current study could be summarized as follows.

- Stress-strain relationship of Toyoura sand subjected to drained cyclic torsional shear loading could be reasonably simulated by the proposed model after considering the hardening behavior due to cyclic loading, and damage to plastic shear modulus at higher shear stress levels.
- An empirical bilinear stress-dilatancy relationship that varies with the amount of damage to the plastic shear modulus of the material is proposed. Accumulation of plastic volumetric strain due to the application of drained cyclic torsional shear loading could be reasonably simulated by the proposed stress-dilatancy relationship.
- The proposed model is capable of reasonably simulating the liquefaction behavior of dense sand until the specimen enters the steady state. Liquefaction resistance of dense Toyoura sand could be reasonably reproduced by the proposed model.

REFERENCES

- Balakrishnayer, K. (2000). "Modelling of deformation characteristics of gravel subjected to large cyclic loading." *Ph.D. thesis*, Department of civil engineering, The University of Tokyo, Japan.
- Hardin, B. O. and Richart, F. E., Jr. (1963). "Elastic wave velocities in granular soils." *Journal of soil mechanics and foundation division*, Vol. 89, No. 1, ASCE, 33-65.

- Hong Nam, N. and Koseki, J. (2005). "Quasi-elastic deformation properties of toyoura sand in cyclic triaxial and torsional loadings." *Soils and Foundations*, Vol. 45, No. 5, 19-38.
- HongNam, N. (2004). "Locally measured quasi-elastic properties of toyoura sand in cyclic triaxial and torsional loadings and their modeling." *PhD thesis*, Dept. of Civil Engineering, The University of Tokyo, Japan.
- Masing, G. (1926). "Eigenspannungen und verfestigung beim messing." *Proceedings of the Second International Conference of Applied Mechanics*, 332-335.
- Nishimura, S. (2002). "Development of three dimensional stress-strain model of sand undergoing cyclic undrained loading and stress-axes rotation." *M.Eng thesis*, Dept. of Civil Engineering, The University of Tokyo, Japan.
- Oka, F., Yashima, A., Tateishi, Y., Taguchi, Y. and Yamashita, S. (1999). "A cyclic elasto-plastic constitutive model for sand considering a plastic-strain dependence of the shear modulus." *Geotechnique*, Vol. 49, No. 5, 661-680.
- Pradhan, T.B.S. and Tatsuoka, F (1989). "On stress-dilatancy equations of sand subjected to cyclic loading." *Soils and Foundations*, Vol.29, No.1, 65-81.
- Tatsuoka, F. and Shibuya, S. (1991a). "Modelling of non-linear stress-strain relations of soils and rocks- Part 1: Discussion of hyperbolic equation." *Seisan-kenkyu, Journal of IIS*, The University of Tokyo, Vol. 43, No. 9, 409-412.
- Tatsuoka, F. and Shibuya, S. (1991b). "Modelling of non-linear stress-strain relations of soils and rocks- Part 2: New Equation." *Seisan-kenkyu, Journal of IIS*, The University of Tokyo, Vol. 43, No. 10, 435-437.
- Tatsuoka, F., Masuda, T., Siddiquee, M. S. A. and Koseki, J. (2003). "Modeling the stress-strain relations of sand in cyclic plane strain loading." *Journal of Geotechnical and Geoenvironmental Engineering*, Vol. 129, No. 6, ASCE, 450-467.



USE OF GRANULAR MATERIAL MADE FROM RECYCLED GLASS AS COUNTERMEASURE AGAINST EARTHQUAKE-INDUCED UPLIFT OF UNDERGROUND PIPES

Tomonori MIKAMI¹, Junichi KOSEKI², Takeshi SATO³ and Chihiro YAJIMA⁴

ABSTRACT: In order to study the validity of use of granular materials made from recycled glass as a countermeasure against earthquake-induced uplift of underground pipes, their permeability test was conducted, while referring to the results from relevant centrifugal model tests. Moreover, an estimation method on the validity of use of granular materials as the countermeasure against earthquake-induced uplift of underground pipes was proposed.

Key Words: granular material, liquefaction, underground pipe, recycled glass, permeability

INTRODUCTION

In Japan, a lot of transparent and brown colored glass bottles are recycled. However, a lot of other colored glass bottles are not recycled. It is difficult to reproduce uniformly-colored glass bottles from them because there are various kinds of other colored glass bottles. Thus, these glass bottles become wastes after single use. The total amount of the waste of glass bottles in Japan was 580,000 ton/year as of 2006 (GBRPA,2009). Therefore, granular materials made from recycled glass bottles have been developed for their effective re-use.

Since the above material having diameters in the range of 5 to 10 mm has a high permeability, it can be used as a countermeasure against earthquake-induced uplift of underground pipes. In order to confirm its applicability, Sugita et al. (2008) conducted a series of centrifugal model tests. Based on these results and permeability test results conducted by the authors, seismic behavior of the above material in prototype scale was estimated. Moreover, an estimation method on the validity of use of granular materials as the countermeasure against earthquake-induced uplift of underground pipes was investigated.

TEST CONDITIONS AND PROCEDURES

Model test conditions conducted by Sugita et al. (2008) are shown in Table 1. Granular materials made from recycled glass bottles are called simply as “Glass” below. Particle size distributions of backfill materials used in these tests are shown in Fig. 1.

In this study, the idea of particle size in prototype was used in order to take the “particle size effect”

¹ PhD Student, Graduate School of Engineering, University of Tokyo

² Professor, Institute of Industrial Science, University of Tokyo

³ Research Support Promotion Member, Institute of Industrial Science, University of Tokyo

⁴ Glass Resourcing Co.,Ltd.

into account. In usual centrifugal model tests conducted under a centrifugal acceleration of nG , a model having a geometrical scale of $1/n$ is employed. However, as the geo-material model, the same material as used for the prototype is frequently employed, since it is in general difficult to reduce its geometrical scale without changing its mechanical properties. The effect due to the disagreement between the geometrical scales of the model and the geo-material is called herein as “particle size effect”. In this study, the prototype Glass to be examined is relatively coarse as mentioned above. If the same material is used in centrifugal model tests, the uplifting displacement of underground pipe might be underestimated because relative larger particles can hardly move into the space under the pipe model when it starts to uplift. Therefore, the particle size effect should be considered properly in these tests.

Table 1. Test conditions (Sugita et al., 2008)

case	Backfill material	Degree of compaction	Centrifugal acceleration	Excitation condition	Pore fluid
06-00	Glass 1	91.3(%) [*]	25G	sin ^{***} , 10G	solution of methyl cellulose (25cs)
	Glass 2	91.3(%) [*]		25Hz,	
	Glass 3	91.2(%) [*]		20cycles	
07-00	Toyoura sand	96.6(%) ^{**}	15G	sin ^{***} , 8G	solution of methyl cellulose (3cs)
	Glass 4	82.6(%) ^{**}		30Hz,	
	Fine sand	87.5(%) ^{**}		40cycles	
08-00	Glass 4	89.9(%) ^{**}	15G	sin ^{***} , 8G	solution of methyl cellulose (3cs)
	Glass 5	89.9(%) ^{**}		30Hz,	
	Glass 6	89.9(%) ^{**}		40cycles	

- * for the maximum density evaluated at compaction energy of about 550 kJ/m³
- ** for the maximum density evaluated at compaction energy of about 2500 kJ/m³
- *** sin: sinusoidal

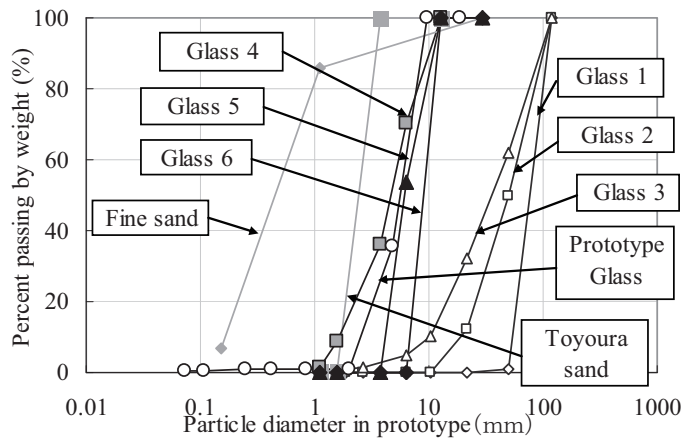


Figure 1. Particle size distributions

Figure 2 shows cross-sections of models in these tests. Synthetic rubber was used to model the original ground which was supposed to be soft ground like peat. Young’s modulus of the synthetic

rubber (≈ 1.1 to 1.2 MN/m^2) was almost the same as that of typical peat ground. Its bottom was fixed to the base of the sand box. A gravel was placed below the original ground in order to make their saturation easily. In order to adjust the depth of the backfill layers, dense silica sand was placed between the backfill layers and the gravel layers.

In case 06-00, synthetic rubbers at both ends could not deform freely because these rubbers together with adjacent silica sand layers were constrained by the ends of the rigid sand box. Therefore, in cases 07-00 and 08-00, dummy backfill layers were added near the ends of the sand box in order to reduce the end restraint effect.

Underground pipe models used in these tests were 21 mm in diameter and 194.5 mm in length in case 06-00, and 30 mm in diameter and 295 mm in length in cases 07-00 and 08-00. Apparent unit weight of these pipes was adjusted to 8 kN/m^3 .

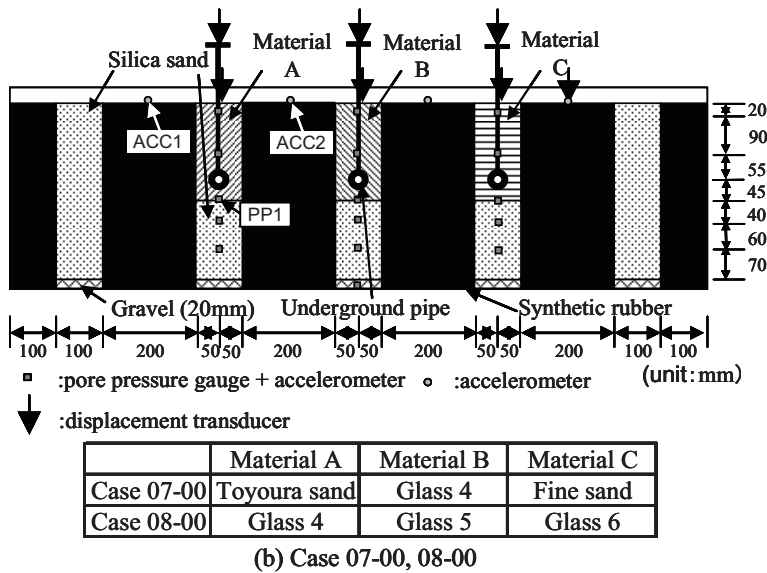
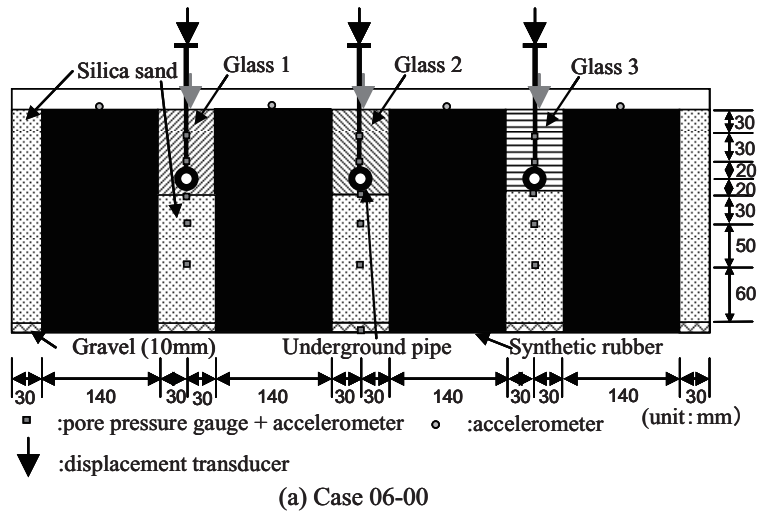


Figure 2. Cross-sections (Sugita et al., 2008)

Permeability tests on all of the backfill materials using water as pore fluid were conducted by the authors based on JIS A 1218. In addition, solutions of methyl cellulose with different viscosities were also used in permeability tests on Toyoura sand in order to evaluate the relationship between the viscosity of pore fluid and the permeability coefficient. Figure 3 shows the relationship between the viscosity of pore fluid and the permeability coefficient. These results revealed that the permeability coefficient was approximately in inverse proportion to the viscosity of pore fluid.

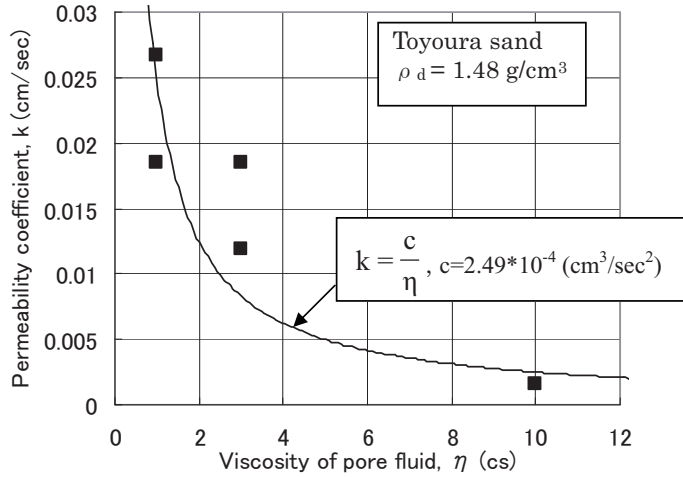


Figure 3. Relationship between permeability coefficient and viscosity of pore fluid

Table 2. Permeability coefficient in prototype

case	backfill material	Degree of compaction	permeability coefficient in prototype (cm/sec)
06-00	Glass 1	93.7(%)	$4.8 \cdot 10^{-1}$
	Glass 2	92.5(%)	$4.0 \cdot 10^{-1}$
	Glass 3	90.3(%)	$2.6 \cdot 10^{-1}$
07-00	Toyouira sand	93.7(%)	$1.4 \cdot 10^{-1}$
	Glass 4	80.1(%)	$1.2 \cdot 10^{-1}$
	Fine sand	92.8(%)	$1.3 \cdot 10^{-3}$
08-00	Glass 4	89.9(%)	$1.0 \cdot 10^{-1}$
	Glass 5	89.9(%)	$6.0 \cdot 10^{-1}$
	Glass 6	90.0(%)	$1.1 \cdot 10^0$
Prototype Glass		92.2(%)	$0.3 \cdot 10^0$

In the centrifugal model tests, the permeability in prototype as listed in Table 2 was evaluated using Eq. (1), which was derived based on the relationship shown in Figure 3.

$$k_p = k_{mw} \times \frac{\eta_w}{\eta} \times \frac{n_c}{n_g} \quad (1)$$

in which k_p : permeability coefficient in prototype, k_{mw} : measured permeability coefficient of the material using water as pore fluid, η_w : viscosity of water, η : viscosity of pore fluid used in the centrifugal model test, n_c : centrifugal acceleration, and n_g : gravitational acceleration.

It should be noted that backfill material in cases 07-00 and 08-00 had smaller particle sizes than the prototype Glass. Therefore, less viscous pore fluid was used in these cases to compensate for the change in the measured permeability coefficient due to different gradations.

TEST RESULTS -UPLIFT OF UNDERGROUND PIPES-

Figure 4 shows the time histories of uplifting displacement of underground pipes in prototype.

In case 06-00, the pipe backfilled by Glass 3 uplifted a little by about 20 mm. Permeability coefficients of Glass 1, Glass 2 and Glass 3 were 0.48 cm/sec, 0.40 cm/sec and 0.26 cm/sec respectively. It could be inferred that uplift of underground pipes hardly occur under these conditions of permeability and compaction. On the other hand, as mentioned before, the particle size effect might be more predominant in this case.

In case 07-00, underground pipe in backfill of Glass 4 uplifted significantly by larger than 300 mm. The degree of compaction of Glass 4 was lower than that of Toyoura sand (Table 1), although the particle size distribution and permeability of Glass 4 were similar to those of Toyoura sand (Fig. 1 and Table 2). Therefore such severe uplifting displacement could be due to lower degree of compaction.

In case 08-00, the pipe in backfill of Glass4 uplifted a little by about 20 mm. The permeability of this material was lower than those of Glass 5 and Glass 6 (Table 2) because the particle size of this material was finer (Fig. 1). Therefore this small uplift could be due to lower permeability. The pipe in backfill of Fine sand in case 07-00 uplifted significantly by larger than 300mm. Such severe uplifting displacement could be also due to low permeability.

On the other hand, the pipe in the backfill of Glass 4 started uplifting during tapered excitation after the main excitation. In this case, 40 cycles were applied at a prototype frequency of 2Hz, while 20 cycles were applied at a prototype frequency of 1Hz in cases 06-00 and 07-00. Thus the total shaking duration in prototype in case 08-00 was the same as that in cases 06-00 and 07-00. Therefore the uplift of the pipe in the backfill of Glass 4 might be due to the effect of the larger number of cycles.

Relationships between the residual uplifting displacements of underground pipes in prototype and the permeability coefficients in prototype are shown in Fig. 5.

In case 07-00, the residual uplifting displacements of underground pipes could not be measured due to the overscaling of displacement transducers. Therefore, the residual uplifting displacements were evaluated as Eq.(2) in case 07-00. This evaluation could result into underestimation of the residual uplifting displacement, since settlements of underground pipes during the stage of reducing centrifugal acceleration was neglected. However, considering the possible error in the data measured with the displacement transducer due to inclination of its target, the accuracy of this evaluation was considered to be acceptable.

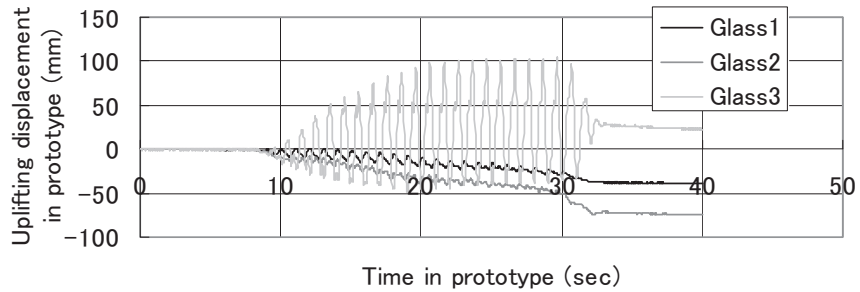
$$D_{res} = D_1 - D_2 \quad (2)$$

in which D_{res} : residual uplifting displacement, D_1 : uplifting displacement measured by a ruler after the tests, and D_2 : uplifting displacement (negative value) measured by displacement transducer during application of centrifugal acceleration and consolidation.

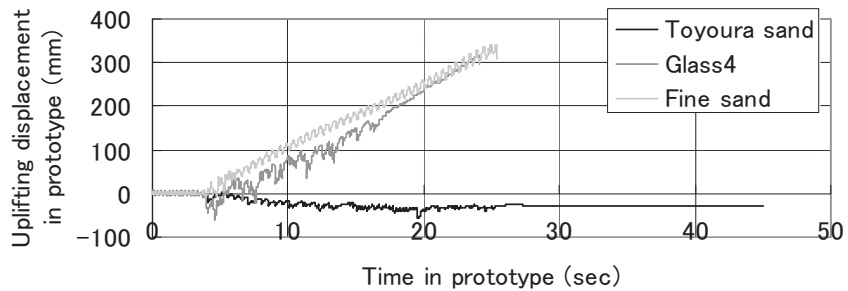
The test results using Glass 4 as the backfill material exhibited that employing enough compaction with the degree of compaction around 90% or more is effective in reducing the uplifting displacement.

In cases where the degrees of compaction are around 90%, when the permeability coefficients exceeded about 0.1 cm/sec, uplift of underground pipes hardly occurred. Therefore the prototype Glass having diameters in the range of 5 to 10 mm, would not cause uplift of underground pipes under the backfill condition employed in these tests because the permeability coefficient of this material was about 0.3 cm/sec (Table 2). Moreover, it could be inferred that in cases where the degrees of compaction are around 90%, the relationship between the uplifting displacement and the permeability

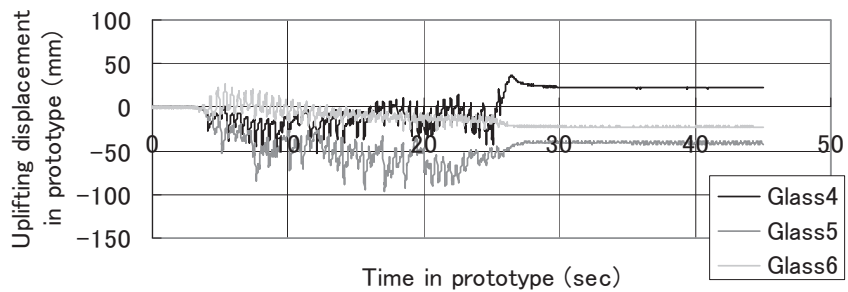
coefficient could be approximated by the broken curve as shown in Figure 5. Based on the curve, validity of use of granular materials as countermeasure against earthquake-induced uplift of underground pipes under the prototype backfill condition employed in these tests would be estimated.



(a) case 06-00



(b) case 07-00



(c) case 08-00

Figure 4. Time histories of uplifting displacement in prototype

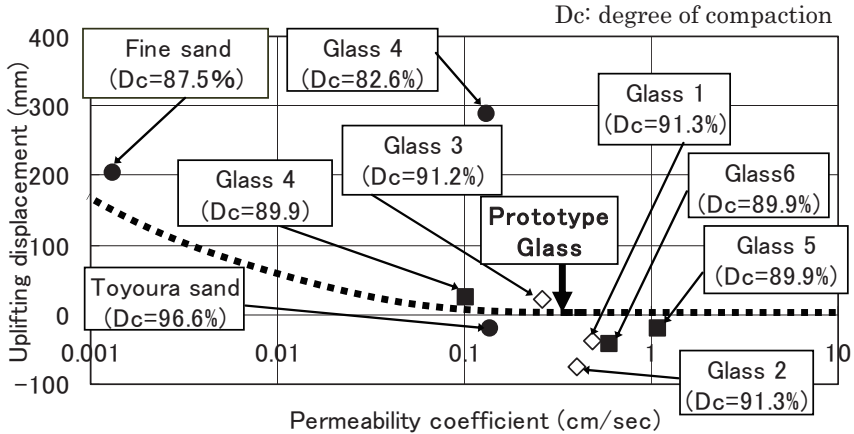


Figure 5. Relationship between uplifting displacement and permeability coefficient

TEST RESULTS -SETTLEMENTS OF GROUND SURFACE-

Figure 6 shows the time history of settlements of the ground surface in prototype in case 08-00. The residual settlement of Glass 4 ground occurred hugely by about 700 mm. However, this value was possibly overestimated due to the movement of the target during shaking. In these tests, settlements at ground surface were displacements of targets set on ground surface measured by displacement transducers that were fixed to the top of the sand box. If the displacement transducers touch on the ground surface directly caused by the movement of targets, displacement transducer can stick into the ground easily. In Glass 4 ground, a dent due to the sticking of the displacement transducer was observed after the test.

On the other hand, residual settlements of Glass 5 and Glass 6 also occurred significantly by larger than 200 mm. Therefore, it is important to reduce not only earthquake-induced uplift of underground pipes but also settlements at ground surface in order to use granular materials as backfills of underground pipes.

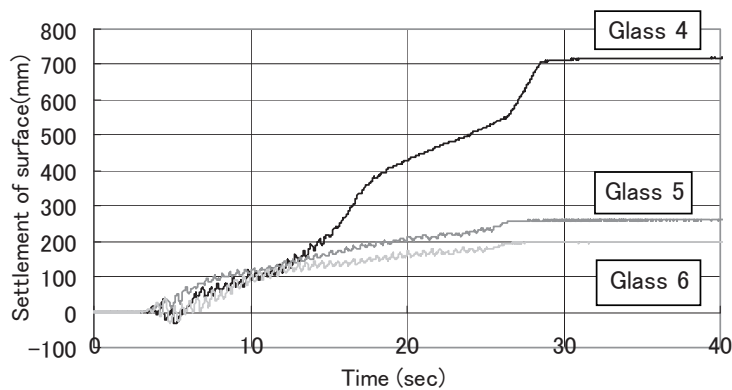


Figure 6. Time history of settlement at ground surface

TEST RESULTS -EXCESS PORE PRESSURE-

Figure 7 shows the time history of excess pore pressure measured at PP1 in case 08-00, Glass 4 (see Fig. 2 for the location of pore pressure gage). As typically shown in this figure, all of the time histories of measured pore pressure in the present model tests were with very spiky wave forms.

Dynamic pore fluid pressure in the backfill that was restricted by the synthetic rubbers could be generated during shaking. Therefore such dynamic pore fluid pressure might be one of the reasons for the spiky wave forms, while the amplitudes of the spikes were larger than those of the theoretical dynamic pore fluid pressures.

Figure 8 shows the time histories of response accelerations measured at ACC1 and ACC2 in case 08-00. They were different from each other. It could be due to the different degrees of end resistant effects. Therefore it could be inferred that horizontal cyclic loading was also applied on the backfill ground during shaking. Such horizontal cyclic loading might increase the amplitudes of the spikes of excess pore pressure.

In many of the model tests focusing on liquefaction, the degree of liquefaction has been evaluated based on excess pore pressure ratio. However, in the present model tests, the degree of liquefaction could not be properly evaluated due to the spiky wave forms as mentioned above. Therefore rational estimation techniques of degree of liquefaction should be studied more in the future.

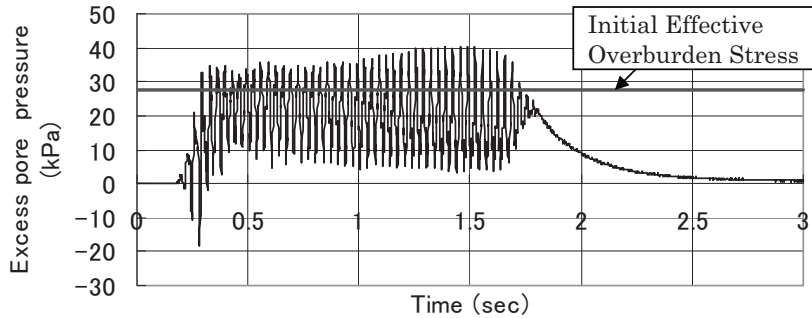


Figure 7. Time history of excess pore pressure (PP1, Glass 4, case 08-00)

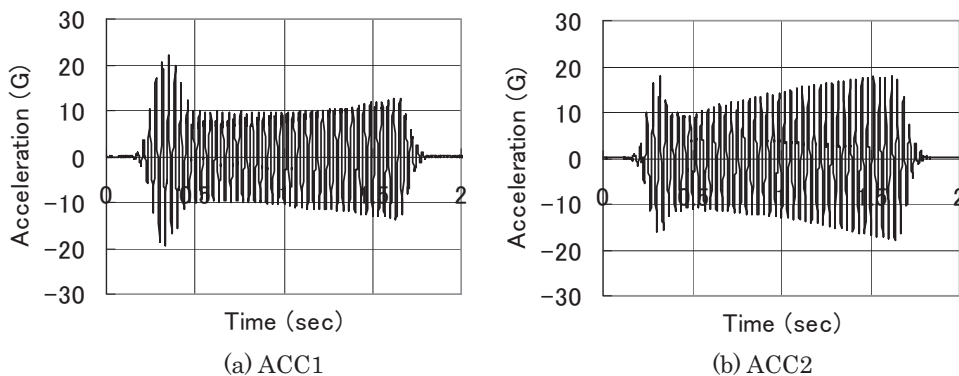


Figure 8. Time history of response acceleration of synthetic rubber (ACC1 and ACC2, case 08-00)

CONCLUSIONS

When the degree of compaction of backfill material was over 90% with permeability coefficient exceeding 0.1cm/sec, liquefaction did not occur under the conditions employed in the present model tests. Therefore the granular material made from recycled glass bottles having diameters in the range of 5 to 10 mm could be used as a countermeasure against earthquake-induced uplift of underground pipes, because the permeability coefficient of this material is about 0.3 cm/sec.

Residual settlements of surfaces occurred severely in some model backfill ground. Therefore, not only resistance to earthquake-induced uplift of underground pipes but also resistance to settlements of surfaces should be secured in using granular materials as backfills of underground pipes.

ACKNOWLEDGEMENTS

The authors wish to thank Public Works Research Institute for providing the model test results that were analyzed in the present study

REFERENCES

Glass Bottle Recycling Promoter Association (2009), <http://www.glass-recycle-as.gr.jp/index.html> (in Japanese)

Sugita, H., Sasaki, T., Ishihara, M. and Mizuhashi, M (2008). "Centrifugal model tests on the use of granular material made from recycled glass bottles as backfill of sewage pipes", *Technical Note of PWRI*, No.4110 (in Japanese)

Japanese Geotechnical Society (2004). "Countermeasures against liquefaction". (in Japanese)



SURVEY ON DAMAGE TO ROADS IN AKITA PREFECTURE CAUSED BY 2008 IWATE- MIYAGI NAIRIKU EARTHQUAKE

Yukika TSUTSUMI¹, Junichi KOSEKI², Reiko KUWANO³,
Takashi KIYOTA⁴ and Tomonori MIKAMI⁵

ABSTRACT: On June 14, 2008, the main shock of the Iwate- Miyagi Nairiku earthquake with a JMA magnitude of 7.2 hit the mountainous areas in Iwate, Miyagi and Akita prefectures, Japan. Based on a site investigation performed four days after the earthquake, the following damage to roads in Akita prefecture was reported: a road closing caused by slope failure adjacent to a bend of a river, settlement of approach embankments for highway bridges due to large displacement of reinforced soil retaining walls having low stability, a failure of a road constructed by cut and fill, and a large slope failure including road embankment.

Key Words: Iwate-Miyagi Nairiku earthquake, Site investigation, Slope failure, Road embankment, Reinforced soil retaining wall

INTRODUCTION

At 8:43 am on Saturday, June 14, 2008, the main shock of the Iwate-Miyagi Nairiku earthquake measuring a magnitude specified by the Japan Meteorological Agency, M_{JMA} , of 7.2 (JMA, 2008) with an epicentral depth of 8 km struck mountainous areas in Iwate, Miyagi and Akita prefectures, Japan. It caused 13 casualties, 10 missing persons, 451 injuries, 2,352 collapsed houses, and 48 sediment disasters as of November 19, 2008 (Cabinet Office, Government of Japan, 2008). It was pointed out that, on the whole, the number of collapsed houses was smaller, while the number of sediment disasters was larger than the data in the past large earthquakes. Mostly, these severe effects occurred in Oshu city in Iwate prefecture and Kurihara city in Miyagi prefecture.

The authors conducted a site investigation in Akita prefecture on June 18, 2008, four days after the earthquake. This paper briefly summarizes typical results of the investigation, focusing on damage to roads and its possible causes from a geotechnical point of view.

OVERVEIW OF INVESTIGATED AREA

Figure 1 shows location of the investigated area in this report and those of another survey in Iwate and

¹ Technical staff, Institute of Industrial Science, University of Tokyo

² Professor, Institute of Industrial Science, University of Tokyo

³ Associate professor, Institute of Industrial Science, University of Tokyo

⁴ Research associate, Tokyo University of Science

⁵ Graduate student, Department of Civil Engineering, University of Tokyo

Miyagi prefectures on July 1-2, 2008, which are indicated by dotted rectangles, and epicenters of the main shock and aftershocks that are marked with symbols “X”. In Akita prefecture, there were 21 injuries, 12 collapsed houses and 2 sediment disasters as of July 28, 2008 (Akita prefecture, 2008). Most of them occurred in Yuzawa city that was included as the major investigated area in this paper (Figure 2).

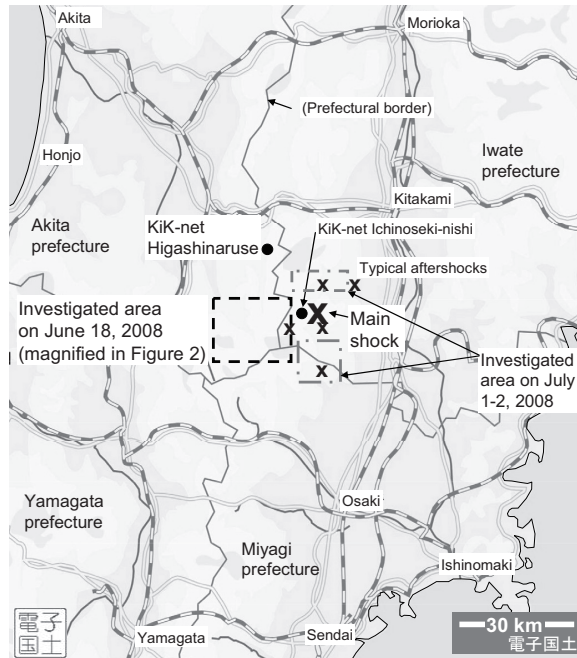


Figure 1. Locations of investigated areas and epicenters of main shock and aftershocks

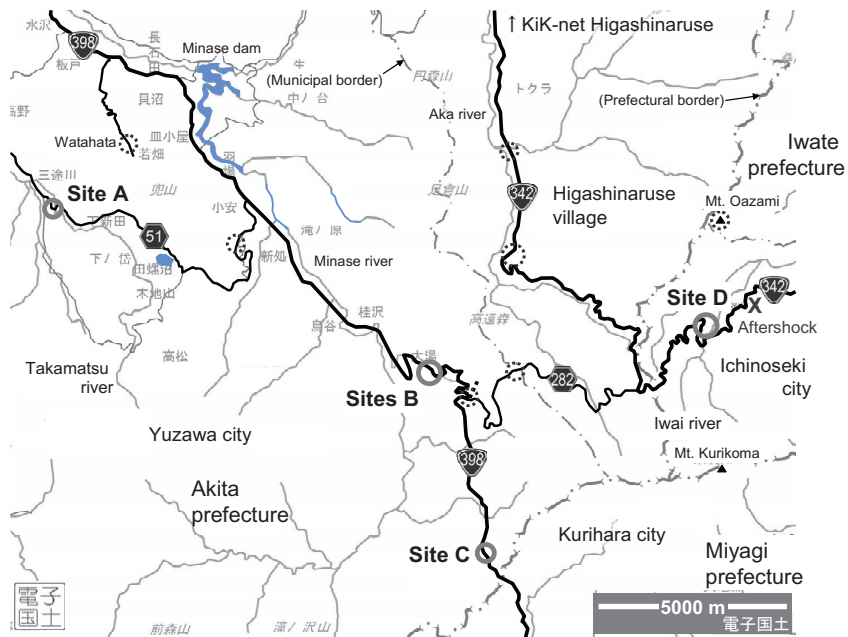


Figure 2. Locations of sites investigated on June 18, 2008

As shown in Figure 2 with solid and dotted circles, 11 sites along national highway route Nos. 342 and 398, and prefectural road Nos. 51 and 282 were investigated in detail. In addition, a site where strong motion seismograph was set by National Research Institute for Earth Science and Disaster Prevention (NIED) along national highway route No. 342 in Higashinaruse village (KiK-net Higashinaruse in Figure 1) was also visited. In this paper, the following typical damage to roads at 4 sites is reported as its representative: a road closing caused by slope failure, settlement of approach embankments for highway bridges, a failure of a road constructed by cut and fill, and a large slope failure including road embankment. The results of the investigation at the other 8 sites and those of another survey in the areas shown in Figure 1 are uploaded to the authors' website in Japanese (<http://soil.iis.u-tokyo.ac.jp/Investigations-j.htm>).

ROAD CLOSING CAUSED BY SLOPE FAILURE

A north facing slope adjacent to a bend of Takamatsu river at west side of Kurotaki bridge along prefectural road No. 51 (N 39° 1' 22.0" latitude, E 140° 35' 10.0" longitude) failed and the road was completely closed due to collapsed soil and trees as shown in Photo 1 (site A in Figure 2). Inclination of the original slope was about 30 degrees and the dimensions of failed area were approximately 30 m in width and 40 m in length. Figure 3 represents detailed locations of the failed slope in Photo 1, Takamatsu river and Kurotaki bridge. Collapsed soil flowed into the south side of Kurotaki bridge and caused a closure of the river course of Takamatsu river, while no damage to abutment of the bridge on the side of the failure was observed as shown in Photos 2 a) and b). By removing the collapsed soil and trees, prefectural road No. 51 was re-opened under two-way alternate traffic condition on August 7, 2008 (Yuzawa city, 2008).

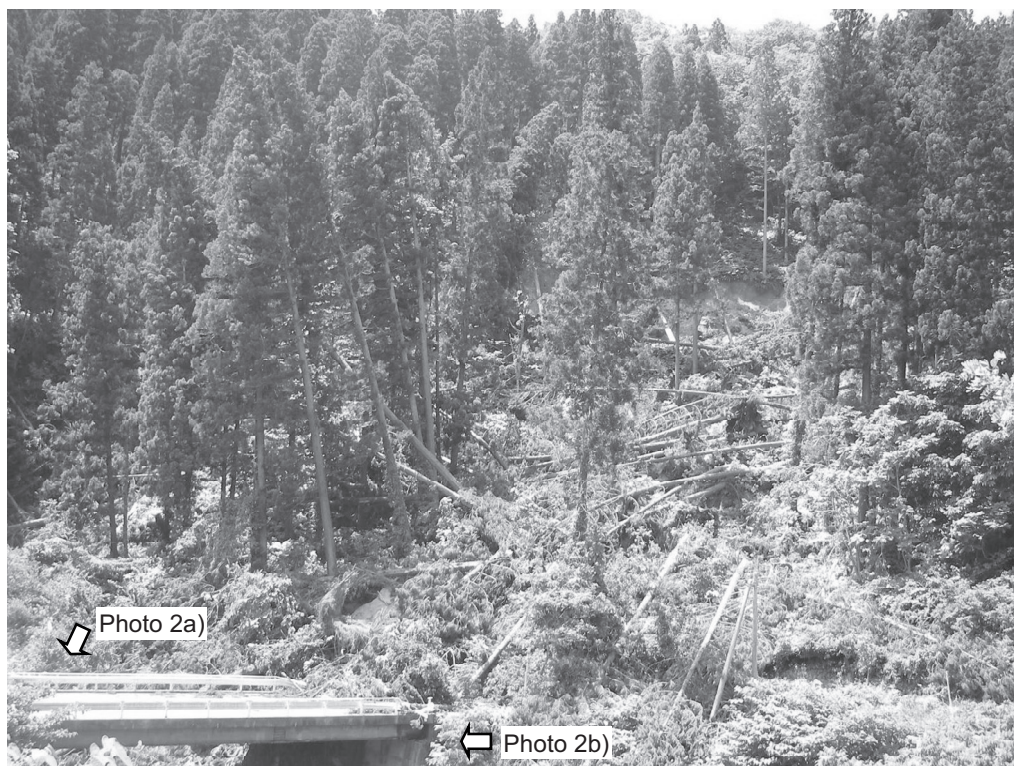


Photo 1. Slope failure at west side of Kurotaki bridge along prefectural road No. 51 (site A in Figure 2)

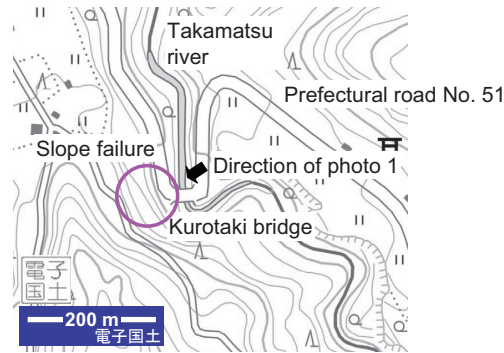


Figure 3. Detailed location of slope failure in Photo 1



Photo 2. a) River course closure of Takamatsu river due to collapsed soil
b) Abutment of Kurotaki bridge on the side of slope failure

SETTLEMENT OF APPROACH EMBANKMENT FOR HIGHWAY BRIDGE

Settlement of approach embankments for two bridges, Shirakaba bridge and Tochinoki bridge, which are located adjacent to each other along national highway route No. 398 was observed at site B in Figure 2 (N 38° 59' 6.5" latitude, E 140° 42' 2.8" longitude). Photo 3 and Photo 5 show the settlement of approach embankments at east side of Shirakaba bridge and at south side of Tochinoki bridge, respectively.

As shown in Photo 3, the settlement of the embankment for Shirakaba bridge was about 10 cm at the maximum, and it was accompanied by horizontal residual displacement with large cracks formed along the center line of the road with the maximum opening width of about 25 cm. The embankment was supported by a newly constructed gravity type retaining wall which did not suffer any damage and an old reinforced soil retaining wall using horizontal steel strips and concrete skins (so-called "Terre Armee" method) which suffered extensive opening of inclined concrete skins at the top (Photos 4 a) and b)). It can be estimated from the existence of vegetation from the opening that the reinforced soil retaining wall had displaced and its stability had been originally low before the earthquake. Accordingly, the damage to the embankment shown in Photo 3 was possibly caused by large displacement of the old reinforced soil retaining wall that exhibited low stability during the earthquake.



Photo 3. Settlement of approach embankment for Shirakaba bridge along national highway route No. 398 (site B in Figure 2)

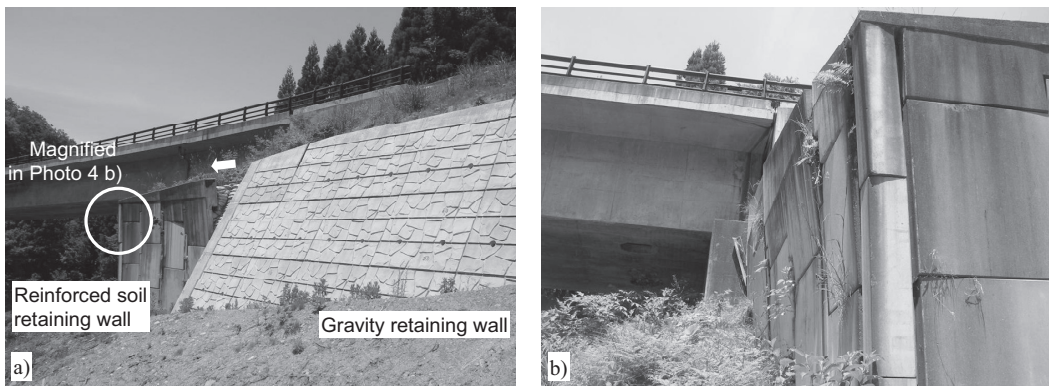


Photo 4. a) Retaining walls supporting approach embankment for Shirakaba bridge
 b) Damage to reinforced soil retaining wall in a)

The amount of the maximum settlement of the embankment for Tochinoki bridge in Photo 5 was approximately 20 cm. As shown in Photo 6 a), a reinforced soil retaining wall by “Terre Armee” method having a length of about 30 m supported the embankment. As the retaining wall had already deformed and overhanged largely, additional reinforcement had been executed by using H-shaped steel piles and concrete beams, or tie rod and anchoring at the time of the earthquake. At the foot of the reinforcement concrete beam as indicated in Photo 6 a) with a circle, a crack that was possibly caused due to the earthquake was observed as shown in Photo 6 b). The same type of reinforcement structure was adopted on the opposite side of the embankment, while adding anchoring at the wing of the abutment. Between the reinforcement frame and the wing of the abutment, outflow of backfill soil due possibly to the earthquake was observed as shown in Photo 7. It can be inferred from the above facts that large deformation and displacement of the reinforced soil retaining wall that was under the execution of additional reinforcement work caused the settlement of the embankment with outflow of backfill soil.



Photo 5. Settlement of approach embankment for Tochinoki bridge along national highway route No. 398 (site B in Figure 2)

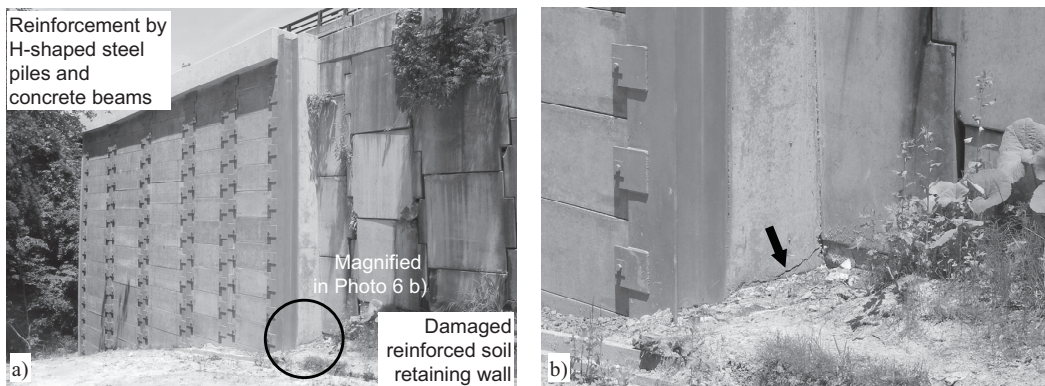


Photo 6. a) Reinforcement of approach embankment for Tochinoki bridge and adjacent reinforced soil retaining wall, b) Crack in reinforcement concrete beam of approach embankment



Photo 7. Outflow of backfill soil between reinforcement frame and original wing of Tochinoki bridge

FAILURE OF ROAD CONSTRUCTED BY CUT AND FILL

As shown in Photo 8, an embankment supported by a gravity type retaining wall along national highway route No. 398 collapsed at around the border between Akita and Miyagi prefectures (N 38° 56' 33.6" latitude, E 140° 43' 4.2" longitude, site C in Figure 2). Due to the collapse of the embankment, a large gap in the pavement was formed with the maximum width of about 30 cm at the center of the road. Photo 9 shows the tilting and settlement at the shallower part of the gravity type retaining wall that was constructed on slope with the maximum height of 4 m. The amount of maximum horizontal displacement at the top of the retaining wall was approximately 50 cm. On the opposite side of the road, cracks were formed in shotcrete on a cut slope as shown in Photo 10.



Photo 8. Collapse of embankment along national highway route No. 398 (site C in Figure 2)



Photo 9. Tilting and settlement of gravity type retaining wall in Photo 8



Photo 10. Cracks in shotcrete on cut slope

LARGE SLOPE FAILURE INCLUDING ROAD EMBANKMENT

As shown in Photo 11, a large slope failure including a road embankment occurred at an east facing slope along national highway route No. 342 in Ichinoseki city, Iwate prefecture (N 38° 59' 43.5" latitude and E 140° 47' 4.2" longitude, site D in Figure 2). The dimensions of the slope failure were about 90 m in width, 290 m in length and the height of the main scarp was about 30 m. A trace of puddle was observed at the surface of collapsed soil that remained at the north part of the slope. Collapsed soil flowed into Iwai river and made the river course closed as shown in Photo 12.



Photo 11. Large slope failure including embankment along National Highway route No. 342 (site D in Figure 2)



Photo 12. River course closure at Iwai river due to slope failure in Photo 11

It was observed that the total volume of collapsed soil was rather small, considering the dimension of the slope failure. Figure 4 shows a result of topographical analysis of slope failures including the one shown in Photo 11 based on aerial photo survey (GSI, 2008). According to the above observation and the relevant analysis results, it is estimated that the lower gentle slope was involved in a slope failure which occurred initially at the upper steep slope with partially deep sliding surfaces as schematically shown in Figure 5.

A section of the national highway route No. 342 between “Sukawa-onsen” and “Shinyu” in Ichinoseki city for a total length of 15.3 km, which included the slope failure explained above, was still completely closed for rehabilitation work as of December 22, 2008 and will be opened in autumn, 2010 (Iwate prefecture, 2008).

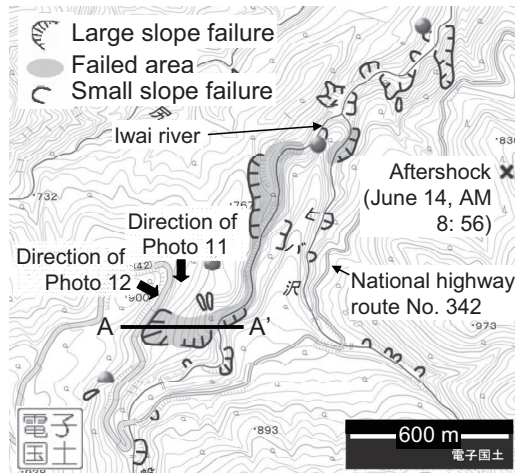


Figure 4. Topographical map including slope failure in Photo 11 (modified from GSI, 2008)

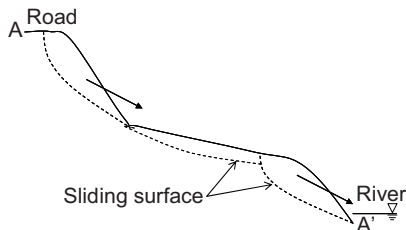


Figure 5. Estimated topography of cross section A-A' in Figure 4

CONCLUSIONS

Based on a site investigation performed four days after the earthquake, the following damage to roads in Akita prefecture was identified: a road closing caused by slope failure adjacent to a bend of a river, settlement of approach embankments for highway bridges due to large displacement of reinforced soil retaining walls having low stability, a failure of a road constructed by cut and fill, and a large slope failure including road embankment.

ACKNOWLEDGEMENTS

The authors express their deep appreciations to Mr. N. Ito at Development and Promotion Bureau of Ogatsu, Akita prefecture for his help in conducting the survey.

REFERENCES

- Akita prefecture. (2008), "Information related to the Iwate-Miyagi Nairiku Earthquake in Akita prefecture as of July 28, 2008", <http://www.pref.akita.lg.jp/> (in Japanese)
- Cabinet Office, Government of Japan. (2008), "Preliminary report in disaster situation as of November 19, 2008, the Iwate-Miyagi Nairiku Earthquake in 2008", <http://www.bousai.go.jp/saigaiinfo.html> (in Japanese)
- Geographical Survey Institute (GSI). (2008), "Map providing information related to the Iwate-Miyagi Nairiku Earthquake in 2008", <http://zgate.gsi.go.jp> (in Japanese)
- Iwate prefecture. (2008), "Information about closure of national highway route No. 342 in Ichinoseki city as of December 22, 2008", <http://www.pref.iwate.jp/> (in Japanese)
- Japanese Metrological Agency (JMA). (2008), "Preliminary report in disaster situation as of July 31, 2008, the Iwate-Miyagi Nairiku Earthquake in 2008", http://www.seisvol.kishou.go.jp/eq/2008_06_14_iwate-miyagi/index.html (in Japanese)
- Yuzawa city. (2008), "Preliminary report on damage caused by the Iwate-Miyagi Nairiku Earthquake in 2008 as of July 31, 2008", <http://aios.city-yuzawa.jp/> (in Japanese)



SMALL STRAIN SHEAR STIFFNESS OF TOYOURA SAND OBTAINED FROM VARIOUS WAVE MEASUREMENT TECHNIQUES

Ruta Ireng WICAKSONO¹ and Reiko KUWANO²

ABSTRACT: This paper compiles the values of shear modulus on Toyoura sand evaluated in laboratory tests by 6 researchers using various techniques in Institute of Industrial Science, the University of Tokyo in the last 5 years. In total, six measurement techniques including static, Trigger Accelerometer (TA) with S wave, TA with P wave, Bender Element, S type Plate Transducer (PT) method and P type PT method were performed in this study. As the results, for each measurement method the values of normalized shear modulus ($G/f(\epsilon)$) were in a good agreement having the deviation at largest of about 7.6%. Further study on the TA methods employing accelerometers inside and outside the specimens was reported. Additionally, the shear modulus values resulted from this study and those from International Parallel Test on the Measurement of G_{\max} using Bender Elements organized by TC-29 were compared.

Keywords: small strain, cyclic loading, trigger accelerometer, bender element, plate transducer

INTRODUCTION

In the field at construction sites, wave measurement techniques such as the cross-hole and down-hole methods, have been used for a long time to obtain small strain stiffness of the ground (Stokoe & Hoar, 1978). Meanwhile, in mega project of Akashi Kaikyo Bridge, Tatsuoka & Kohata (1995) presented stiffness modulus by employing pressure meter and plate loading tests as an in-situ static measurement that yields the shear modulus in larger strain.

For long time a laboratory measurement has become the reference standard for determining the properties of geomaterials. To develop a greater confidence of the results from an in-situ test, it is helpful to compare the field results with the laboratory ones. In case of a laboratory static measurement, established method of vertically and torsionally cyclic loading performed by triaxial and torsional apparatuses respectively has been employed in obtaining the stiffness modulus values. Additionally, in most of the studies (Dyvik and Madshus (1985), Mohsin and Airey (2003), and Lee and Santamarina (2005)), a bender element was employed to measure the shear wave velocity in a laboratory.

From those kinds of measurement, a disputable issue emerges in decades to the definitions of “static properties” and “dynamic properties”. Woods (1991) proposed not to use “dynamic properties”, since dynamic concerns the loading condition. He also suggested that there is no more different from

¹ Graduate student, The University of Tokyo, Japan, ruta@iis.u-tokyo.ac.jp

² Associate Professor, The University of Tokyo, Japan, kuwano@iis.u-tokyo.ac.jp

each other except for the strain levels. However, precise static small strain measurements in the laboratory tests have bridged the gap of strain levels between “dynamic” and “static” behavior (Tatsuoka and Shibuya, 1992). Following the pioneer work by Tanaka et al. (2000), AnhDan and Koseki (2002) found that the difference on dynamic and static properties is not only caused by strain level but also by some other factors like grain size and wave length. Nevertheless, in accordance with the definition by Tatsuoka and Shibuya (1991), in this paper the terms of static and dynamic measurements are used with respect to the effects of inertia to the soil particles during the testing.

Geotechnical Engineering Laboratory in Institute of Industrial Science (IIS), The University of Tokyo has been taking part together with other labs around the world exploring the soil and geotechnical-related behaviors both in field and laboratory. Particularly in laboratory work, small strain stiffness measurement has been becoming one of hot topics in this lab, while several researchers have been performing this work with various techniques on Toyoura sand.

With respect to that, this study aims to compile and comprehensively to compare the values of shear modulus of Toyoura sand from those works in the last 5 years. Triaxial Compression (TC) and Torsional Shear (TS) tests were performed to observe small strain cyclic loading which is known as a static measurement. Meanwhile for a dynamic measurement, independent tools of Trigger Accelerometer (TA), Bender Element (BE), and Plate Transducer (PT) were employed, that were attached to triaxial and torsional apparatuses as additional tools.

MATERIAL, APPARATUS, AND TESTING PROCEDURES

Material

Material used in this study was Toyoura sand from batch H owned by the Geotechnical Engineering Laboratory in IIS. This sand was taken from Toyoura Beach, Yamaguchi, Japan. Toyoura sand is fine uniform sand that has been widely used in geotechnical engineering laboratories all over Japan. Its mean diameter (D_{50}) is 0.2 mm. The specific gravity G_s is 2.635. The maximum void ratio e_{\max} is 0.966 and the minimum void ratio e_{\min} is 0.600.

Apparatus

In this study, both fully automated triaxial and torsional apparatuses were employed. Small, medium, and large scales of apparatus size were used appropriately adapting to the specimen size. Figure 1 shows the schematic figure of the triaxial apparatus used in this study, while that only in loading system and specimen shape the torsional apparatus differs.

As shown in Figure 1, the basic components of the system consist of a triaxial cell with a pneumatic cell pressure system, loading system, transducers and a personal computer equipped with a control and measurement program. A personal computer is connected to the apparatus through cards having 2 major functions of data acquisition and feed back control units. External Displacement Transducer (EDT) is utilized to measure the overall height of the specimen. A High Capacity Differential Pressure Transducer (HCDPT) is used to measure effective confining pressure in the cell. A Low Capacity Differential Pressure Transducer (LCDPT) which is connected with 2 water-filled burettes is employed to measure the volumetric strain of the specimen. One burette is connected to the specimen, while the other performs as a reference. The volume change is evaluated by measuring the difference in the water-head between those burettes.

A set of tools such as TA, BE, or PT was used for a dynamic measurement which is independently attached to the triaxial or the torsional apparatus. Figures 2a and 2b show the photos of TA and BE attached to the triaxial apparatus. Meanwhile, the units of PT where their positions on top cap and pedestal respectively are replaceable with those of BE, is shown in Figure 2c.

Those dynamic measurement tools are connected to several supporting devices including function generator, signal amplifier, charge amplifier, and digital oscilloscope. The function generator is employed to produce the P and the S waves signal. Both excitation types of pulse and sinusoidal waves can be generated and are sent to a trigger or a transmitter through a signal amplifier. To magnify the signal captured by the sensor, a charge amplifier is used and then its output is connected to a digital

oscilloscope for recording.

Additionally, a pair of widely used Local Deformation Transducer (LDT) after Goto et al. (1991) was employed to perform small strain cyclic loading. As shown in Figure 2b, the LDT is attached to the specimen through 2 pairs of hinge that are fixed with glue on the membrane. The length of the LDT varies with the size of the specimen.

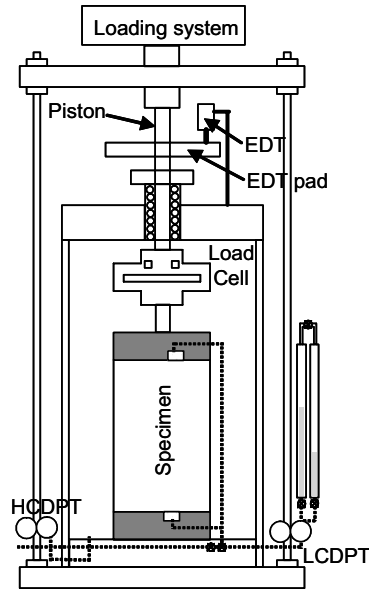


Figure 1. Schematic figure of TC apparatus

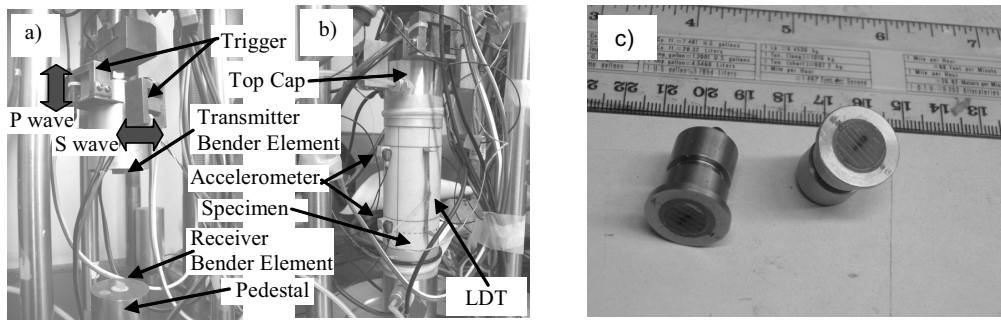


Figure 2. a) Trigger and Bender Element positions; b) Accelerometer & LDT position; c) Plate transducer

Testing Procedures

Air dried Toyoura sand was pluviated through air from a certain height to obtain the designed dry density. Cylindrical specimen at several sizes for TC test and hollow specimen for TS test were prepared under both dry and saturated conditions. After completing the preparation stage, the specimen was subjected stepwise to several stress levels under specific condition of isotropic consolidation in some cases, while that of anisotropic one in other cases.

At each stress level, the work of probing small strain stiffness by the ways of static and dynamic measurements was carried out. Among the static and dynamic measurements, a stage with constant

stress state in a couple minutes for stabilization was conducted. For static measurement, a cyclic loading stage was conducted under drained condition by changing the vertical stress in TC test case, while that by changing the shear stress in TS test case. For dynamic measurement, the elastic wave that propagates through the specimen was produced and was captured respectively by the trigger/transmitter and the sensors. A digital oscilloscope was employed in recording the wave time history.

Table 1 summarizes some important information of researchers, apparatuses, specimen size, the condition of specimen, specimen density, and the observed gain.

Table 1 Data of specimens

#	Researcher	Apparatus	Specimen size*	Condition	Dr**	Observed gain
A1	Wicaksono, R.I.	Triaxial	$\varnothing = 100$; h = 200	Dry	88.5	E_{TC}, E_{TA-P}
A2	Wicaksono, R.I.	Triaxial	$\varnothing = 50$; h = 100	Saturated	67.8	$E_{TC}, G_{BE}, G_{TA-S}, E_{TA-P}$
A3	Wicaksono, R.I.	Triaxial	$\varnothing = 50$; h = 100	Dry	86.9	$E_{TC}, G_{BE}, G_{TA-S}, E_{TA-P}$
A4	Wicaksono, R.I.	Triaxial	$\varnothing = 300$; h = 600, $t_{membrane} = 0.8$	Dry	74.5	$E_{TC}, G_{TA-S}, E_{TA-P}$
B1	De Silva, L.I.N.	Torsional	$\varnothing_{outer} = 150, \varnothing_{inner} = 90$; h = 300	Saturated	77.9	G_{TS}
B2	De Silva, L.I.N.	Torsional	$\varnothing_{outer} = 150, \varnothing_{inner} = 90$; h = 300	Saturated	56.8	G_{TS}
B3	De Silva, L.I.N.	Torsional	$\varnothing_{outer} = 150, \varnothing_{inner} = 90$; h = 300	Dry	74.9	E_{TS}
B4	De Silva, L.I.N.	Torsional	$\varnothing_{outer} = 150, \varnothing_{inner} = 90$; h = 300	Dry	38.3	E_{TS}
B5	De Silva, L.I.N.	Torsional	$\varnothing_{outer} = 150, \varnothing_{inner} = 90$; h = 300	Dry	68.6	G_{TA-S}
C1	Mulmi, S.	Triaxial	$\varnothing = 50$; h = 180	Dry	91.0	$E_{TA-P}, G_{BE}, G_{TA-S}$
C2	Mulmi, S.	Triaxial	$\varnothing = 30$; h = 100	Dry	83.6	E_{TC}, G_{BE}
C3	Mulmi, S.	Triaxial	$\varnothing = 40$; h = 100	Dry	82.0	E_{TC}, G_{BE}
C4	Mulmi, S.	Triaxial	$\varnothing = 50$; h = 100	Dry	88.3	G_{PT-S}
C5	Mulmi, S.	Triaxial	$\varnothing = 50$; h = 100	Dry	86.6	E_{PT-P}
D1	Enomoto, T.	Triaxial	$\varnothing = 300$; h = 600, $t_{membrane} = 0.8$	Dry	98.4	E_{TC}, G_{TA-S}
D2	Enomoto, T.	Triaxial	$\varnothing = 300$; h = 600, $t_{membrane} = 2.0$	Dry	98.8	E_{TC}, G_{TA-S}
E1	Kiyota, T.	Triaxial	$\varnothing = 50$; h = 100	Saturated	85.0	E_{TC}, G_{TA-S}
E2	Kiyota, T.	Torsional	$\varnothing_{outer} = 150, \varnothing_{inner} = 90$; h = 300	Saturated	70.5	G_{TA-S}
F1	Tsutsumi, Y.	Triaxial	$\varnothing = 50$; h = 100	Dry	42.1	$E_{TC}, G_{BE}, G_{TA-S}, E_{TA-P}$
F2	Tsutsumi, Y.	Triaxial	$\varnothing = 50$; h = 100	Dry	73.5	$E_{TC}, G_{BE}, G_{TA-S}, E_{TA-P}$
F3	Tsutsumi, Y.	Triaxial	$\varnothing = 50$; h = 100	Dry	77.9	$E_{TC}, G_{BE}, G_{TA-S}, E_{TA-P}$
R47	Wicaksono, R.I.	Triaxial	$\varnothing = 300$; h = 600, $t_{membrane} = 0.8$	Dry	98	$E_{TC}, G_{TA-S}, E_{TA-P}$

* Specimen size in mm; ** Relative density (Dr) in %

Source: Data A1- A3 (Wicaksono, 2007a); Data B (De Silva et al., 2005); Data C1 - C3 (Mulmi et al., 2008a) ; Data C4 - C5 (Mulmi et al., 2008b), Data D (Enomoto, 2008), Data E (Kiyota, 2008), Data F (Tsutsumi et al., 2006)

DATA PREPARATION

In this study, values of Young's modulus (E) and shear modulus (G) were observed from static and dynamic measurements. The values of E were observed from the cyclic loading of TC test, and as well, from evaluating of P wave velocity obtained from TA method with P wave and P type PT method that result in the values of E_{TC} , E_{TA-P} , and E_{PT-P} , respectively. Note that the value of E_{PT-P} was observed indirectly as explained next in this section. Meanwhile, the values of G were observed from the TS test, the TA with S wave, the BE, and the S type PT methods that result in the values of G_{TS} , G_{TA-S} , G_{BE} , and G_{PT-S} , respectively.

In static measurement, the values of E and G are observed by employing Equations 1 and 2 for the data obtained from TC and TS tests, respectively, as follows:

$$E = \frac{\Delta\sigma_v}{\Delta\varepsilon_v} \quad (1)$$

$$G = \frac{\Delta\tau}{\Delta\gamma} \quad (2)$$

where $\Delta\varepsilon_v$ is the increment of vertical strain corresponding to the increment of vertical stress ($\Delta\sigma_v$) during the cyclic loading in TC test. Meanwhile, $\Delta\gamma$ is the increment of shear strain corresponding to

the increment of shear stress ($\Delta\tau$) during the cyclic loading in TS test.

In dynamic measurement with the TA method using P wave, by presuming that the triggers are fixed to the top cap rigidly, an unconstrained wave in longitudinal direction that propagates in the rod is assumed. Hence, the value of E is observed by employing Equation 3 after evaluating P wave velocity (V_p) and by knowing density of the specimen (ρ), as follows:

$$E = \rho \cdot V_p^2 \quad (3)$$

With the TA method using S wave, under similar presumption about the behavior of the triggers and the top cap as previously, the elastic wave that propagates in torsional direction on the transverse section of the rod is assumed. Since the stiffness that controls shear wave in the rod is the same as in an infinite continuum, the velocity of torsional wave is the same as for body S wave (Santamarina, 2001). Meanwhile in the BE and the S type PT methods, S wave that propagates from the source to the receiver is considered as point to point propagation in an infinite continuum. Therefore, after evaluating S wave velocity (V_s) and by knowing density of the specimen (ρ), the value of G is observed by employing Equation 4, as follows:

$$G = \rho \cdot V_s^2 \quad (4)$$

Meanwhile, in case of the P type PT method where the transmitter and the receiver transducers are installed at the center of the top cap and the pedestal respectively, a constrained wave in longitudinal direction propagating in the rod is assumed. From this, the value of constrained modulus (M) is observed with Equation 5 and then for comparison the value of M is converted into the value of E using Equation 6, respectively as follows:

$$M = \rho \cdot V_p^2 \quad (5)$$

$$E = \frac{M(1-2\nu)(1+\nu)}{(1-\nu)} \quad (6)$$

where ν is Poisson's ratio (= 0.17 for Toyoura sand (Hoque, 1996)).

To compare the values among those moduli comprehensively, the values of E are converted to those of G considering the isotropic condition by employing Equation 7, as follows:

$$G = \frac{E}{2(1+\nu)} \quad (7)$$

Additionally, to neglect the effects of density (ρ) or void ratio (e), the values of G are normalized with a void ratio function, $f(e)$, that was proposed by Hardin and Richart (1963) as in Equation 8 as follows:

$$f(e) = \frac{(2.17 - e)^2}{(1 + e)} \quad (8)$$

TEST RESULTS AND DISCUSSIONS

Shear Modulus with Various Measurement Techniques

All the graphs in Figures 3 to 7 are plotted between the normalized values of shear modulus ($G/f(e)$) versus the stress parameter. The hollow and solid symbols refer to the values of $G/f(e)$ obtained with

the tests under dry and saturated conditions, respectively. Different values observed by different researchers are described with symbols in different shapes, instead of different colors.

Figure 3 shows the normalized values of statically measured shear modulus versus the stress parameter. The data were contributed by all the six researchers by employing triaxial and torsional apparatuses. All the data were plotted along the curve fitting with the deviation of about 3.7%.

Figure 4 shows the values of $G/f(e)$ observed with bender element. In this study, S wave produced by the bender element propagated from top cap to pedestal through the soil. After performing simple linear regression, it was found that the values of G_{BE} were spread with the deviation of 2.9%.

Figure 5 shows the values of $G/f(e)$ resulted from TA with S wave. Using the tools of the TA with S, no significant difference of $G/f(e)$ values was observed between those were combined with triaxial and those with torsional apparatus, except to those of data D1 showing distinctively higher values. However, all of the values excluding those of data D1 were fit to the linear curve with the deviation of 7.6%.

Figure 6 shows the values of $G/f(e)$ observed by TA with P wave method. The values of data A2 seemed to be unreliable as compared to others to the fact that the values were observed with the specimen under saturated condition. It is occurred due possibly to that the velocity of P wave propagating inside the specimen under saturated condition is affected by the existence of pore water. By ignoring the values of data A2, those of $G_{TA-P}(f(e))$ were fit to the regression line with the deviation of 4.1%.

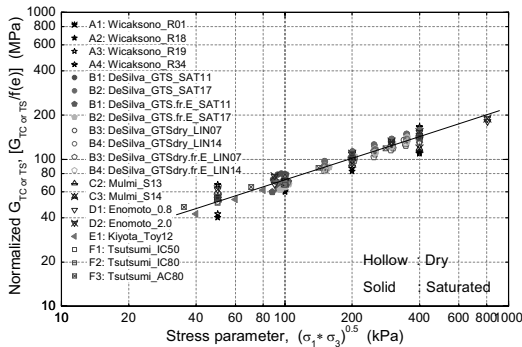


Figure 3. Normalized G_{TC} or T_S values versus stress parameter

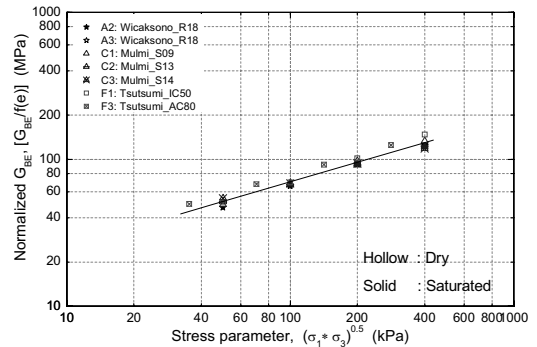


Figure 4. Normalized G_{BE} values versus stress parameter

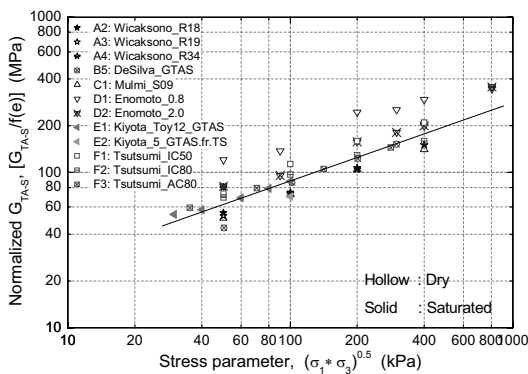


Figure 5. Normalized G_{TA-S} values versus stress parameter

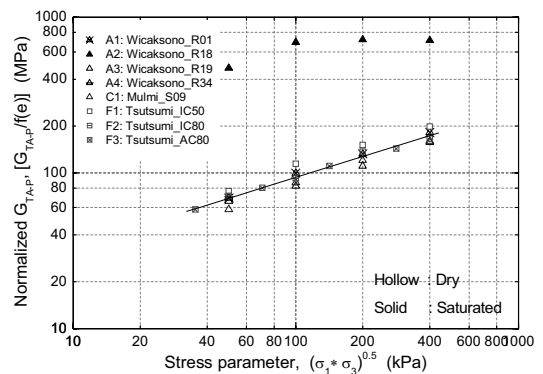


Figure 6. Normalized G_{TA-P} values versus stress parameter

Figure 7 shows the values of $G_{PT-S}/f(\epsilon)$ and $G_{PT-P}/f(\epsilon)$ versus the stress parameter. Since the tools of PT method are relatively new in this laboratory, to date only one researcher has been utilizing them to measured small strain stiffness. The values of G_{PT-P} were obtained originally from those of M_{PT-P} by considering Equation 6. However, the values of $G_{PT-S}/f(\epsilon)$ and $G_{PT-P}/f(\epsilon)$ seemed to be plotted in a good agreement having the deviation of 3.6%.

After comparing each data obtained from each method among the researchers, then the comprehensive comparison was performed to all the results showed in this study. For the simplicity, all of the data were represented by their fitting lines as shown in Figure 8. Three lines of shear modulus from the static, the BE, and the PT methods were in a good agreement. Meanwhile, the fitting lines of shear modulus from the TA method with S wave and that with P wave were in a good agreement. However, in average the values of shear modulus obtained with the TA methods resulted in about 30% higher than those with the BE and the PT methods.

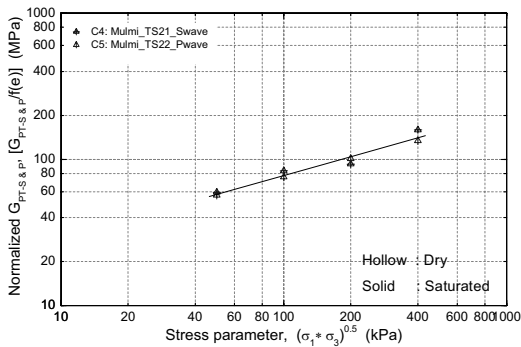


Figure 7. Normalized $G_{PT-S \& P}$ values vs. stress parameter

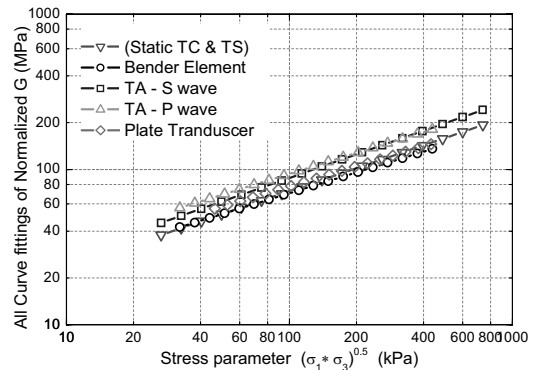


Figure 8. All Curve Fittings of the data

The phenomenon of the values of shear modulus resulted from the TA measurements are larger than those resulted from the static measurement, is in accordance with the previous study on Toyoura sand and Hime gravel ($D_{50}=1.7$ mm) (Wicaksono, 2008). Maqbool (2005) inferred that the difference between statically and dynamically measured stiffness moduli is due possibly to the effects of heterogeneity of the specimen. Furthermore, AnhDan and Koseki (2002) found that the difference on dynamic and static properties is not only caused by strain level but also by some other factors like grain size and wave length.

Additionally, on coarser material (Hime gravel), the dynamic measurement using the BE method appears to underestimate as compared to that using the TA method is due possibly to the effects of bedding error at both the top-end and the bottom-end of the specimen. Nevertheless, it is not significant in case with Toyoura sand (Wicaksono, 2007b).

Wave Propagation Measured Inside and Outside the Specimen

The facts obtained above may lead to the question on the reliability of TA methods which attaches accelerometers on the membrane on the side of specimen. Considering this, further study on TA methods was performed by putting the accelerometers both outside and inside the specimens.

Large scale triaxial apparatus was employed to conduct test R47 having the specimen size similar to that of test A4 (Table 1). As described by the schematic figures and photos shown in Figure 9, four accelerometers were installed inside the specimen having the position so that were possible to measure travel time of P and S waves, while usual manner of attaching accelerometers outside the specimen was also conducted for comparison. Cables of the inside accelerometers were managed to go out from the specimen through a hole at the pedestal like that of the drainage line. Similar to the common setting of TA method, two pairs of the accelerometers located inside and outside the specimens

respectively were set to capture the wave propagation simultaneously. Each pair of the accelerometers was put in 2 different locations (upper and lower) at certain vertical distance from the top cap.

As standard procedures in this study, after completing the cyclic loading stage, under constant stress stage the TA measurement was carried out. A series of elastic wave with several different frequencies generated by a function generator was employed. For comparison, in addition to those were produced by the function generator; a set of elastic wave was generated by hitting a hammer on the EDT pad attached to the loading piston (Figure 1).

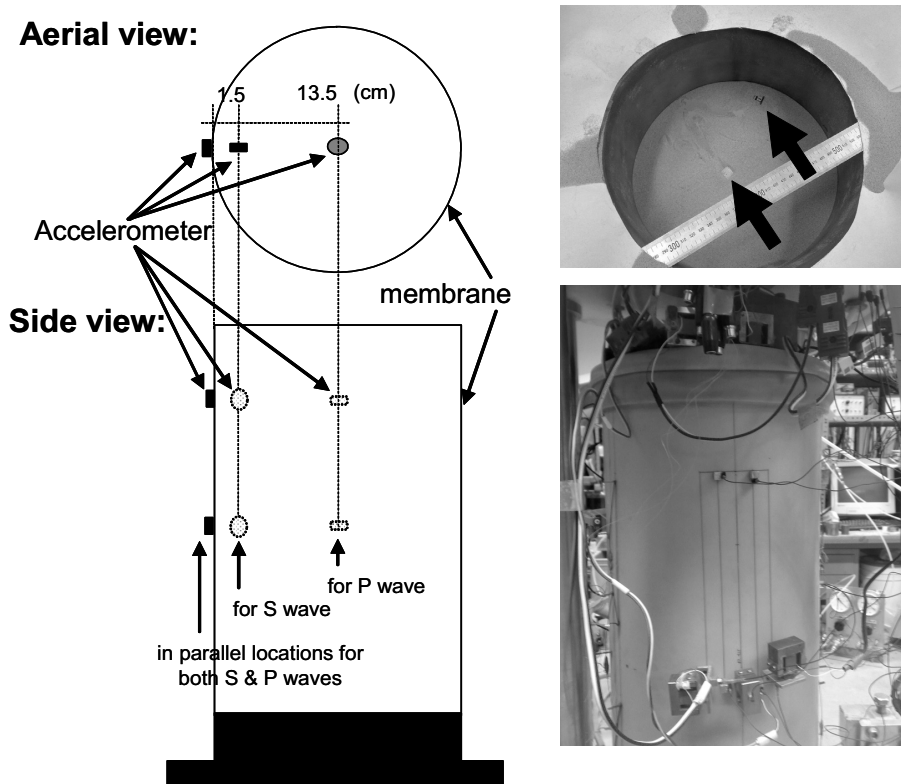


Figure 9. Schematic figures and photos for the location of the accelerometers

Figures 10 and 11 present the time history of wave propagation for both S and P waves with the wave sources of sine wave with 2 kHz in frequency and hitting by hammer, respectively. In those figures, the accelerometers defined with Ch.1 and Ch.2 are represented for those at upper and lower locations, respectively. Meanwhile, terms of “inside” and “outside” are used to indicate the accelerometers located inside and outside the specimens, respectively.

In general, faster wave velocity was observed in the waves measured inside the specimen as compared to those outside one. Despite Figure 10b shows that the rising point observed by the upper accelerometer located inside the specimen (Ch.1 - inside) was later than that located outside one (Ch.1 - outside), however by considering the first coming wave that assumed as near-field effects, the wave measured inside the specimen was still captured earlier. Meanwhile, with the P wave as shown in Figure 11, opposite polarities were observed between the first rising signal captured by the inside accelerometers and those by the outside ones. Those phenomena are not clear yet to be discussed until that more detailed and careful study observing the wave distribution on the cross section of the specimen is conducted.

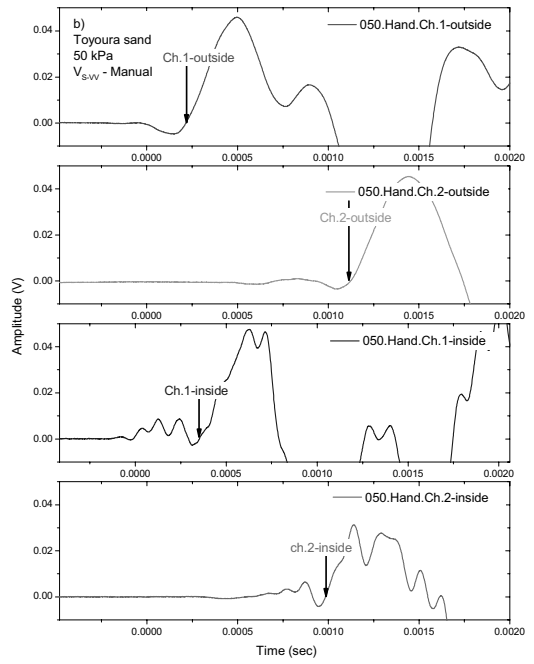
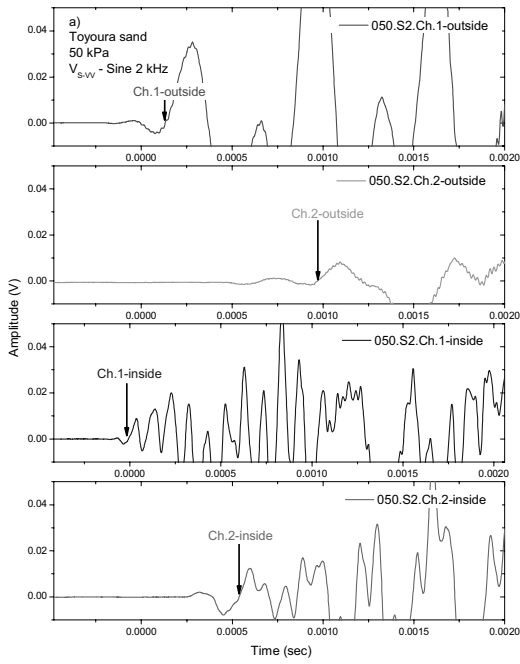


Figure 10. Time history of the input and the output V_s waves: a) Sine 2 kHz; b) hit by hammer

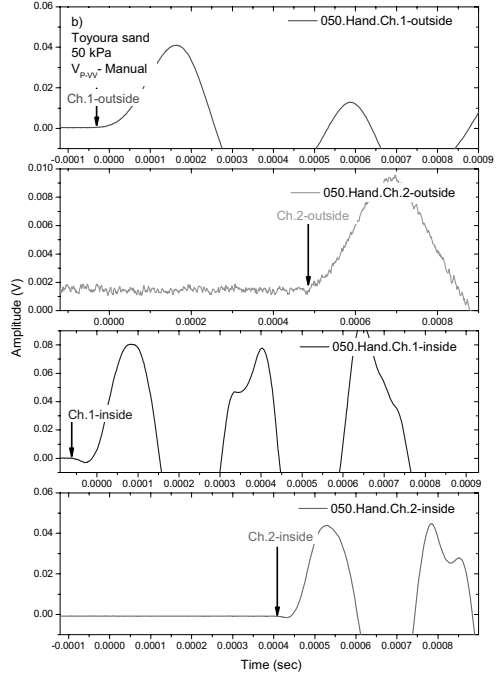
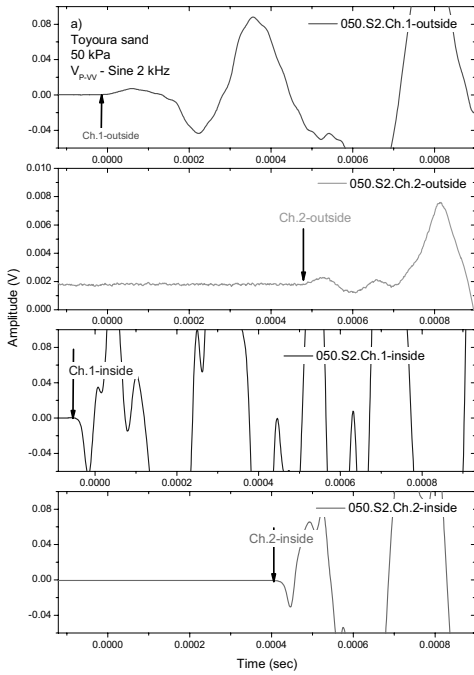


Figure 11. Time history of the input and the output V_p waves: a) Sine 2 kHz; b) hit by hammer

As the results of wave velocity measured inside and outside the specimens, Figures 12a and 12b show graphs plotting the values of wave velocity versus the confining stress obtained from the TA method with S and P waves respectively. The graphs compare between those employing the accelerometers inside the specimen and those outside one. In general these results suggested that for both S and P waves, slightly faster velocity of the wave propagation measured inside the specimen was observed as compared to that outside one. The scattering values of S wave velocity (V_s) between those captured by the inside and the outside accelerometers were fit to the regression line with the deviation of 2.8%, while those of P wave velocity (V_p) were with the deviation of 2.6%.

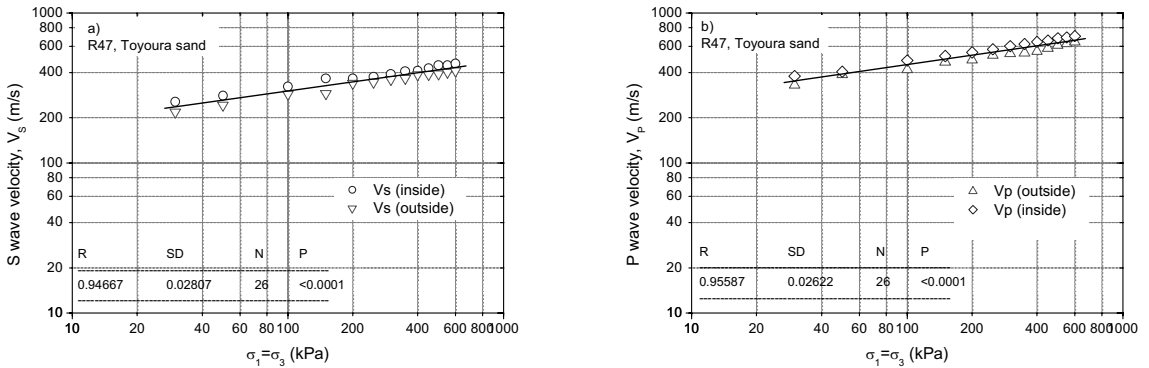


Figure 12. Wave velocity with accelerometers inside and outside the specimen: a) with TA-S wave; b) with TA-P wave

Comparison with the Result from Round Robin Test

In 2003, led by Japanese Geotechnical Society (JGS) the Technical Committee 29 (TC-29) of the Geomaterials of International Society of Soil Mechanics and Geotechnical Engineering (ISSMGE) that works on Stress-Strain and Strength Testing, started an international parallel test on the measurement of G_{max} using bender element. By 2005, a report of this round robin test works collecting data from 23 institutions of 11 countries was published. In this study, the report resulted from the round robin test was used for further comparison.

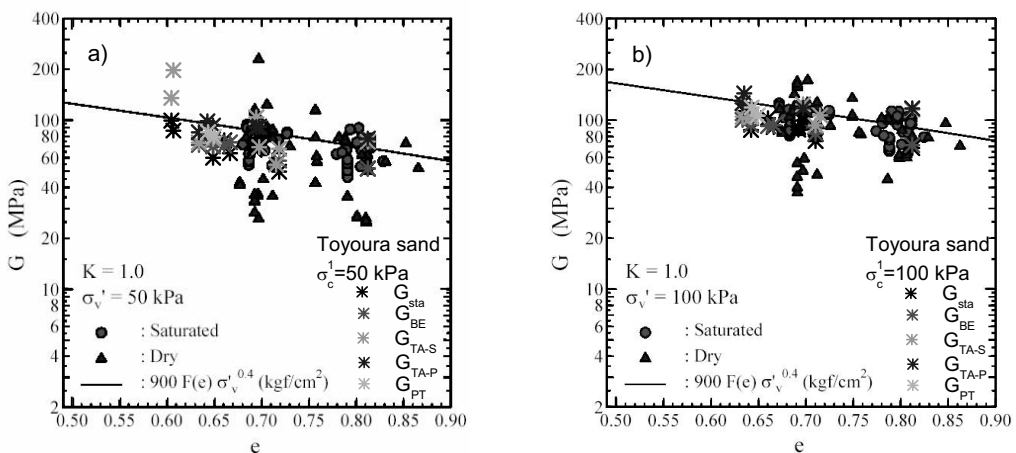


Figure 13. Comparison between results from this study and those from round robin test organized by TC-29, at the confining pressure (σ'_c) of: a) 50 kPa; b) 100 kPa

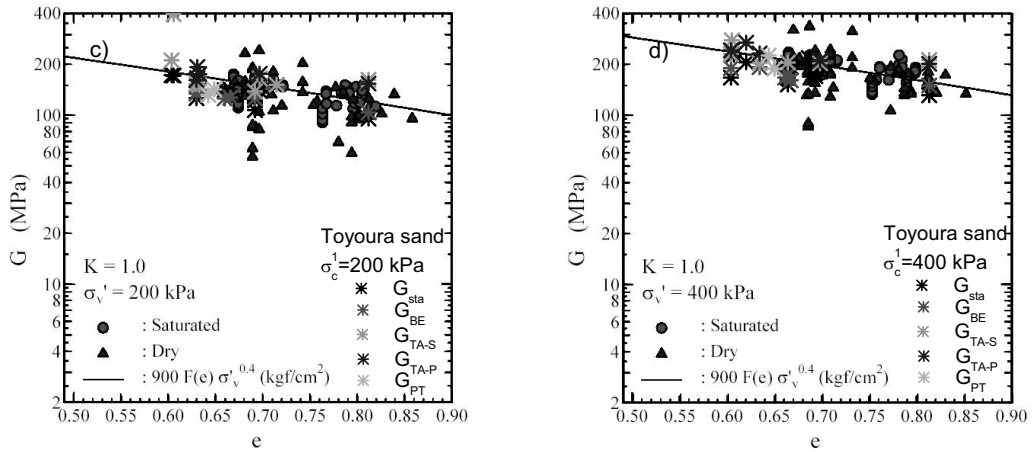


Figure 13 (continue). Comparison between results from this study and from round robin test organized by the TC-29, at the confining pressure (σ'_c) of: c) 200 kPa; d) 400 kPa

Figures 13a to 13d present the graphs of the comparison at the vertical stresses of 50, 100, 200, and 400 kPa, respectively. Data of this study are represented with star symbol with different colors for different measurement methods. It was observed that the results from this study were in a good agreement with those from the TC-29.

Considering the shear modulus values resulted from this study as presented in Figure 8, the fact was observed that those obtained from the TA methods were higher than those from other methods. However, when those of this study were compared with those of the TC-29 as shown in Figure 13, it seemed to that the scattering was plotted in the acceptable range. It suggests that by performing any techniques of small strain stiffness measurement especially on Toyoura sand, subjectively acceptable scattering on the shear modulus values is observed.

CONCLUSIONS

By considering different researchers with various techniques (in terms of specimen sizes, densities, dry and saturated conditions, apparatuses), small strain measurements using static, Trigger Accelerometer (TA), Bender Element (BE) and Plate Transducer (PT) methods on Toyoura sand yielded the values of normalized shear modulus having the deviation at largest of about 7.6%. However, the values of shear modulus obtained with the TA methods resulted in about 30% higher than those with the BE and the PT methods.

Instantly, further study on the TA methods with both S and P waves confirmed that with the deviation of about 3% the velocity of the wave propagation measured inside the specimen was observed faster than that outside one. To explain complicated phenomena regarding wave propagation inside the specimen, further detailed and careful study is needed.

By plotting results from this study and those from International Parallel Test on the Measurement of G_{max} using Bender Elements organized by the TC-29 in a graph for particular confining pressure, all of the G values seemed to be scattered in the acceptable range. The implication is that it suggests that by performing any methods of small strain stiffness measurement especially on Toyoura sand, subjectively acceptable scattering on the shear modulus values is observed.

ACKNOWLEDGMENT

The authors wish to extend special thanks to Dr. De Silva LIN, Mr. Mulmi S, Mr. Enomoto T, Dr. Kiyota T, Ms. Tsutsumi Y, Mr. Sato T, and Prof. Koseki J for help in supporting data, experiment work and discussion.

REFERENCES

- AnhDan, L.Q., Koseki, J., and Sato, T. (2002) "Comparison of Young's Moduli of Dense Sand and Gravel Measured by Dynamic and Static Methods", *Geotechnical Testing Journal*, ASTM, Vol. 25 (4), pp. 349-368.
- De Silva, L.I.N., Koseki, J., Sato, T., and Wang, L. (2005) "High capacity hollow cylinder apparatus with local strain measurements", *Proceedings of the Second Japan-U.S. Workshop on Testing, Modeling and Simulation, Geotechnical Special Publication*, ASCE, Vol. 156, pp. 16-28
- Dyvik, R. and Madshus, C. (1985) "Laboratory Measurements of G_{max} using Bender Elements", *Advance in the Art of Testing Soils under Cyclic Conditions*, ASCE, New York, 186-196.
- Enomoto, T. (2008) "Small Strain Measurement on Toyoura Sand using Large Apparatus in IIS" (personal communication).
- Goto, S., Tatsuoka, F., Shibuya, S., Kim, Y.S., and Sato, T., (1991) "A Simple Gauge for Local Small Strain Measurements in the Laboratory", *Soils and Foundations*, 31 (1), 169-180.
- Hardin, B.O. and Richart, F.E.J. (1963) "Elastic Wave Velocities in Granular Soils", *Journal of Soil Mechanics and Foundation*, ASCE, 89(1), pp. 33-65.
- Hoque, E. (1996) *Elastic Deformation of Sands in Triaxial Tests*, Ph.D Thesis, University of Tokyo, Japan.
- Japanese Domestic Committee for TC-29 (2005) *International Parallel Test on the Measurement of G_{max} Using Bender Elements Organized by TC-29*, Japan.
- Kiyota, T. (2008) "Small Strain Measurement on Toyoura Sand using Triaxial and Torsional Apparatus in IIS" (personal communication).
- Lee, J.S. and Santamarina, J. (2005) "Bender Elements: Performance and Signal Interpretation", *Journal of Geotechnical and Geoenvironmental Engineering*, 131(9), 1063-1070.
- Maqbool, S. (2005) *Effects of Compaction on Strength and Deformation Properties of Gravel in Triaxial and Plane Strain Compression Tests*, Ph.D Thesis, Dept. of Civil Engineering, The University of Tokyo, Japan.
- Mohsin, A. and Airey, D. (2003) "Automating G_{max} Measurement in Triaxial Tests", *Proceedings of 3rd International Symposium on Deformation Characteristics of Geomaterials*, Lyon, Di Benedetto H, Doanh T, Geoffroy H, Sauzeat C, eds., Vol. 1, Balkema, Lisse, 73-80.
- Mulmi, S., Koseki, J., and Kuwano, R. (2008a) "Sample Size and Shape Effects in Bender Element Tests", *Proceedings of 10th IS Symposium*, JSCE, Japan, pp. 85-88.
- Mulmi, S., Sato, T., and Kuwano, R. (2008b) "Performance of Plate Type Piezoceramic Transducers for Elastic Wave Measurements in Laboratory Soil Specimens", *Seisan Kenkyu*, Vol. 60 No. 6, Japan, pp. 43-47.
- Santamarina, J.C., in collaboration with Klein, K. and Fam, M. (2001) *Soils and Waves*, J. Wiley and Sons, Chichester, UK, 488 pages.
- Stokoe, K.H. II. and Hoar, R.J. (1978) "Field Measurement of Shear Wave Velocity by Cross Hole and Down Hole Seismic Methods," *Proceedings of the Conference on Dynamic Methods in Soil and Rock Mechanics*, Karlsruhe, Germany, 3, 115-137.
- Tanaka, Y., Kudo, K., Nishi, K., Okamoto, T., Kataoka, T., and Ueshima, T. (2000) "Small Strain Characteristics of Soils in Hualien, Taiwan," *Soils and Foundations*, Vol. 40 (3), pp. 111-125.
- Tatsuoka, F. and Shibuya, S. (1991) "Deformation Characteristics of Soils and Rocks from Field and Laboratory Tests", Keynote Lecture for Session No.1, *Proceedings of the 9th Asian Regional Conference on SMFE*, Bangkok, Thailand, 2, pp.101-170.
- Tatsuoka, F. and Shibuya, S. (1992) "Deformation Characteristics of Soils and Rocks from Field and

- Laboratory Tests,” *Proceedings of 9th Asian Regional Conf. of SMFE*, Bangkok, Vol. 2, pp. 101-170.
- Tatsuoka, F. and Kohata, Y. (1995) “Stiffness of Hard Soils and Soft Rocks in Engineering Applications”, Keynote Lecture, *Proceedings of International Symposium Pre-Failure Deformation of Geomaterials* (Shibuya et al., eds.), Balkema, 2, pp. 947-1063.
- Tsutsumi, Y., Builes, M., Sato, T., and Koseki, J. (2006) “Dynamic and Static Measurements of Small Strain Moduli of Toyoura Sand”, *Bulletin of Earthquake Resistant Structure Research Center*, University of Tokyo, 39, pp.91-103.
- Wicaksono, R.I. (2007a) *Small Strain Stiffness of Sand and Gravel Based on Dynamic and Static Measurements*, Master Thesis, Dept. of Civil Engineering, The University of Tokyo, Japan.
- Wicaksono, R.I., Tsutsumi, Y., Sato, T., Koseki, J., and Kuwano, R. (2007b) “Small Strain Stiffness of Clean Sand and Gravel Based on Dynamic and Static Measurements”, *Proceedings of 9th IS Symposium*, JSCE, Japan, pp. 171-174.
- Wicaksono, R.I., Tsutsumi, Y., Sato, T., and Koseki, J., Kuwano, R. (2008) “Laboratory Wave Measurement on Toyoura Sand and Hime Gravel”, *Bulletin of Earthquake Resistant Structure Research Center*, University of Tokyo, Japan 41, pp.35-44.
- Woods, R.D. (1991) “Field and Laboratory Determination of Soil Properties at Low and High Strains,” *Proceedings of Second International Conference on Recent Advances in Geotechnical Earthquake Engineering and Soil Dynamics*, pp. 1727-1741

FORMULATION OF A SIMPLE METHOD TO DESIGN PP-BAND MESH RETROFITTING FOR ADOBE/MASONRY HOUSES

Paola MAYORCA¹ and Kimiro MEGURO²

ABSTRACT: Past earthquakes have shown that the collapse of seismically weak adobe/masonry structures is responsible for most of the fatalities in developing countries. It is, thus, urgent to improve their seismic performance in order to reduce future casualties and to protect the existing housing stock. To encourage seismic retrofitting, inexpensive and easy to implement technical solutions are desirable. Retrofitting by polypropylene band (PP-band) meshes satisfies these requirements. These bands, commonly used for packing, are resistant, inexpensive, durable and worldwide available.

Experiments and advanced numerical simulations have shown that PP-band meshes can dramatically increase the seismic capacity of adobe/masonry houses. Nevertheless, a simple yet accurate design method is still needed to optimize the mesh arrangement and assess its performance. PP-band meshes increase the structure ductility and energy dissipation capacity through controlled cracking. However, large deformations during seismic events are expected and therefore, the design method must take this into account. In this paper, a methodology to design PP-band mesh retrofitted structures is outlined and discussed.

Key Words: Non-engineered structure, adobe house, design method, PP-band mesh, seismic retrofitting, masonry

INTRODUCTION

Collapse of weak adobe/masonry houses is responsible for most of the fatalities due to earthquakes in developing countries. Furthermore, the consequent property losses are a threat to the sustainable development of these regions. The only way to change this situation is to increase the seismic resistance of the existing housing stock. Because people living in this type of structures have limited resources, inexpensive and easy to implement solutions are necessary. Retrofitting by polypropylene band (PP-band) meshes satisfies these requirements. These bands commonly used for packing are resistant, inexpensive, durable and worldwide available.

PP-band meshes (see Figure 1) are wrapped on both sides of the walls and attached with wire connectors. After meshes are installed the wall is plastered with either mud, in case of adobe houses, or mortar, in case of brick structures. This cover protects the meshes from the ultraviolet radiation and other external agents, fills any gaps that may be left between the mesh and the wall after its installation, improves the bond between mesh, mortar, and wall, and gives a good appearance to the retrofitted structure.

¹ Project Research Associate

² Professor, Director of International Center for Urban Safety Engineering (ICUS)

Experiments and numerical simulations have shown that PP-band meshes improve the seismic performance of otherwise poor earthquake resistant adobe/masonry houses. This is mainly achieved by increasing the structure ductility and energy dissipation capacities. Under moderate ground motions, PP-band meshes provide enough seismic resistance to guaranty limited and controlled cracking of the retrofitted structures. Under extremely strong ground motions, they are expected to prevent or delay the collapse, thus, increasing the survival ratio.



Figure 1. PP-band mesh



Figure 2. PP-band retrofitted house before mortar laying

Although there is plenty of evidence showing the good seismic performance of PP-band retrofitted structures, a simple methodology to design PP-band mesh retrofitting and to assess its seismic response for a particular seismic demand is yet to be developed. In the following sections, such methodology will be outlined and discussed.

PROPOSED DESIGN METHODOLOGY

The scope of the design methodology proposed hereinafter is 1-story adobe/masonry houses with flat roofs. Structures with vault/dome roofs are not considered. Figure 3 shows the flowchart of the proposed retrofitting design. The process can be summarized as follows:

1. Determine the original structure strength, V_c , and natural period, T .
2. Calculate the elastic base shear, V , according to the regional seismic code.
3. From the relation between V and V_c , estimate the strength reduction factor, R_d .
4. Choose a certain PP-band mesh density, D , and determine the ductility demand, μ_{dem} , from the μ_{dem} versus R_d graph and also the maximum displacement, $\Delta_{max} = \mu_{dem} \times$ first cracking displacement.
5. Assess Δ_{max} .
If Δ_{max} is acceptable, proceed with out-of-plane verification.
If Δ_{max} is unacceptable, reduce the μ_{dem} . Repeat the calculation.
6. Verify that out-of-plane deformations do not cause instability

Determining the properties of existing structures is not easy especially for adobe/masonry houses due to their low quality and great variability. Because these structures are stiff compared to the PP-band stiffness, their initial natural period does not change after retrofitting. Furthermore, experiments have shown that PP-band meshes do not increase the structure strength before cracking. Therefore, it can be assumed that the retrofitted structure will have the same V_c and T as the original, unreinforced, house.

The expected R_d will be fairly high due to the relatively low resistance of the adobe/masonry houses. The higher the reduction factor, the larger the ductility demand will be as shown schematically in Figure 3. Intuitively the larger the PP-band mesh density, the less μ_{dem} for the same R_d . The nature of this relation will be discussed in detail in the following sections.

Large deformations and controlled damage are anticipated in PP-band mesh retrofitted structures. Therefore, the most important points to check in the design are maximum displacements at the corners (maximum acceptable displacement associated with in-plane actions) and the wall body (out-of-plane verification). Secondary order effects should be avoided. Excessive out-of-plane wall deformations will reduce their in-plane resistance capacity. Maximum acceptable displacements and out-of-plane verification will be discussed in subsequent sections.

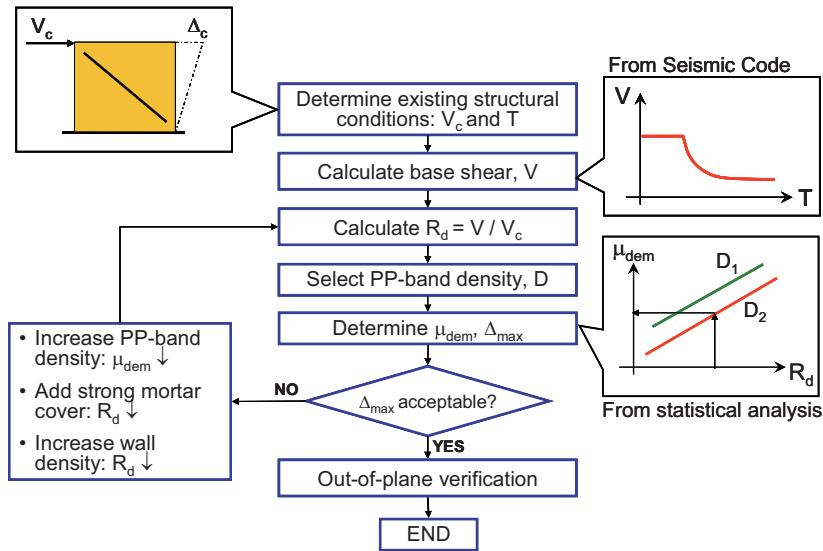


Figure 3. Flowchart of the proposed methodology

If displacements due to in-plane actions are unacceptable, μ_{dem} should be reduced. This can be achieved by increasing the PP-band density. Another solution is to reduce R_d by adding a strong mortar cover or providing additional walls so that the demand on each of them is lower. In the latter case, there will be an increase in mass and as a result V needs to be recalculated. It is also possible to increase the wall density by adding more walls. However, this will change the original floor arrangement and therefore would be more expensive and probably difficult to accept by the house owner.

STRENGTH REDUCTION VERSUS DUCTILITY DEMAND

As mentioned in the previous section, the relation between R_d and μ_{dem} for different PP-band mesh densities is needed to estimate the maximum displacement that the structure will experience. In order to develop a simple relation between these two parameters, non-linear time history analyses of several structures subjected to various strong ground motions were carried out.

Material model

Static monotonic tests have shown that the shear force – lateral deformation curve of a PP-band retrofitted walls can be roughly idealized as shown in the left curve of Figure 4. V_c and Δ_c correspond to the shear strength and cracking deformation of the original wall whereas V_r and K_r correspond to the residual strength and stiffness after the wall cracking. The first two parameters are mainly dependent on the masonry itself, V_r depends on both masonry and PP-band mesh and K_r depends

mostly on PP-band. Under cyclic loading, the skeleton curve resembles the monotonic one with a gradually decreasing unloading stiffness.

To model the retrofitted adobe/masonry structures, the skeleton curve was further idealized as shown on the right side graph of Figure 4. This simplification is assumed to be conservative as a fraction of the wall strength is not considered. In the graph:

$$\Delta'_c = \frac{V_r - K_r \Delta_o}{K_o - K_r} \quad (3.1)$$

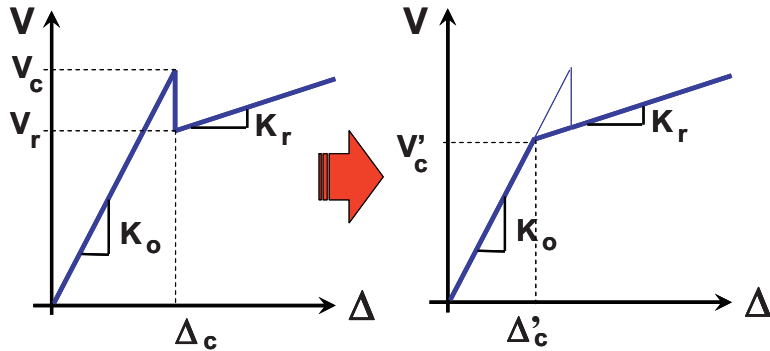


Figure 4. Idealization of shear force versus lateral deformation for a wall retrofitted with PP- band mesh

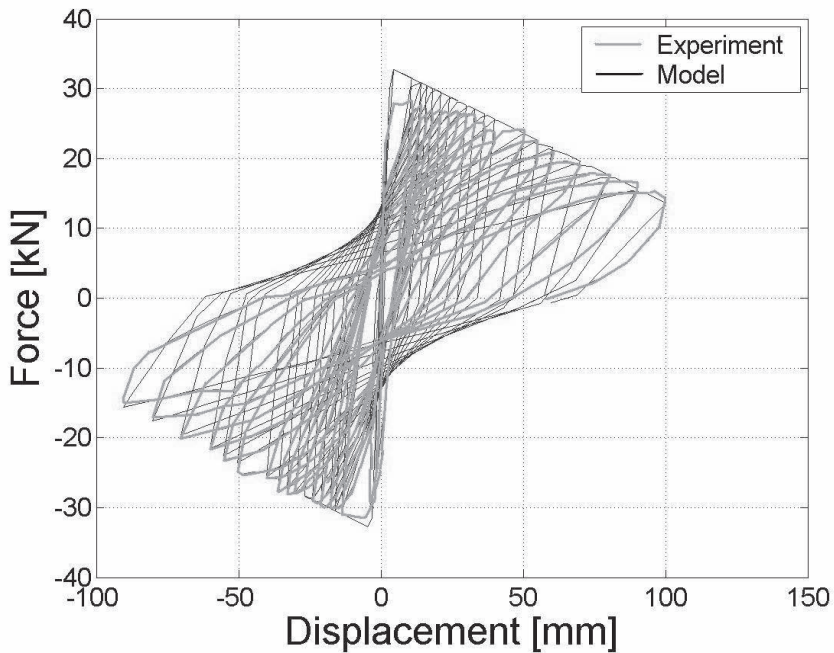


Figure 5. Comparison of experimental results and proposed model

$$V'_c = \frac{K_o}{K_o - K_r} (V_r - K_r \Delta_o) \quad (3.2)$$

Additionally, the hysteresis was represented with a Modified Clough model with unloading degrading stiffness. Two additional parameters to control the later decay are necessary. In total, the model is completely defined with five parameters. Figure 5 shows the comparison between the force deformation curve obtained with experiments and the proposed model. A fairly good agreement is observed.

Strong ground motion database

A total of 144 strong ground motion records were considered for the present study as shown in Table 3.1. All of them were recorded at sites with average shear wave velocities higher than 180 m/s in the upper 30 m of the soil profile. In all the cases, the peak ground acceleration (PGA) was larger than 0.1g and they were recorded on free field or the first floor of low-rise buildings. Figures 6 and 7 show the distribution of PGAs and normalized acceleration response spectra for 5% damping. All the records have high frequency contents below 0.4s. The natural period of 1-story adobe/masonry structures fall in this range.

Analyzed structures

Four structures with mechanical properties representing single story adobe/masonry houses and three different weight roofs as detailed in Table 2 were considered for the present study. The parameters were chosen so as to represent one of the two main walls of a 3-m high, 3-m long, 1-story adobe/brick house. In all the cases, V_r/V_o was considered equal to 0.75, a value which experiments have shown is relatively easy to achieve by tightly attaching an adequate volume of PP-band mesh.

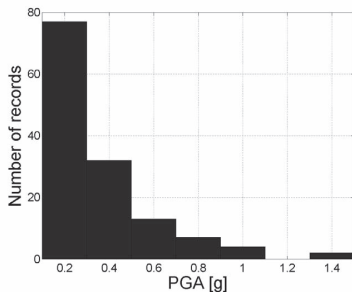


Figure 6. Distribution of the Peak Ground Acceleration of the records used in the study

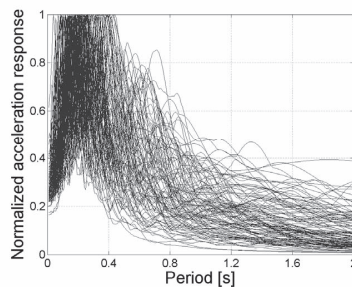


Figure 7. Normalized acceleration response for 5% damping

Table 1 Strong ground motion records used for this study

Date	Earthquake	Station
02/07/1987	Baja California (Mw=5.50)	UNAMUCSD 6604
04/25/1992	Cape Mendocino (Mw=7.01)	CDMG 89005, CDMG 89324, CDMG 89509
07/22/1983	Coalinga (Mw=6.36)	CDMG 47T03, USGS 1604, USGS 1606, USGS 1605, USGS 1607, USGS 1608, USGS 1609, USGS 1651
10/15/1979	Imperial Valley (Mw=6.53)	CDMG 5158, USGS 286, USGS 5051, USGS 5053, USGS 5054, USGS 5055, USGS 5056, USGS 5057, USGS 5058, USGS 5059, USGS 5060, USGS 5165, USGS 931, USGS 952, USGS 955
06/28/1992	Landers (Mw=7.28)	CDMG 24577, SCE 24
10/17/1989	Loma Prieta (Mw=6.93)	CDMG 47006, CDMG 47379, CDMG 47380, CDMG 47381, CDMG 57007, CDMG 57064, CDMG 57066, CDMG 57383, CDMG 57425, CDMG 57504, CDMG 58065, CDMG 58130, CDMG 58135, CDMG 58393, UCSC 13, UCSC 14
04/24/1984	Morgan Hill (Mw=6.19)	CDMG 47006, CDMG 47380, CDMG 47381, CDMG 57383, CDMG 57425
01/17/1994	Northridge (Mw=6.69)	CDMG 24087, CDMG 24278, CDMG 24303, CDMG 24399, CDMG 24401, CDMG 24514, CDMG 24592, CDMG 24611, USC 90014, USC 90055, USGS 5080, USGS 655, USGSVA 637
02/09/1971	San Fernando (Mw=6.61)	CDMG 126, CDMG 127, USGS 128, USGS 266
06/28/1991	Sierra Madre (Mw=5.61)	CDMG 24399
10/01/1987	Whittier Narrows (Mw=5.99)	CDMG 14196, CDMG 14368, CDMG 24303, CDMG 24399, CDMG 24401, CDMG 24461, USGS 289, USGS 709
10/04/1987	Whittier Narrows Aftershock (Mw=5.27)	CDMG 24399

Table 2 Material properties considered for the study

Structure type	V_c [kN]	K_o [kN/mm]	K_r/K_o	Mass [$\times 10^3$ kg]
Adobe	35	10	0.00, -0.02	8.70, 12.75, 17.25
Brick	100	50	0.00, -0.02	8.70, 12.75, 17.25

Results and discussion

Figure 8 and 9 show the force-deformation curves of two groups of structures subjected to the same strong ground motion record. Because the adobe structure has lower strength, the ductility demand is larger. Structures with larger masses experience larger inertial forces and therefore larger ductility demands.

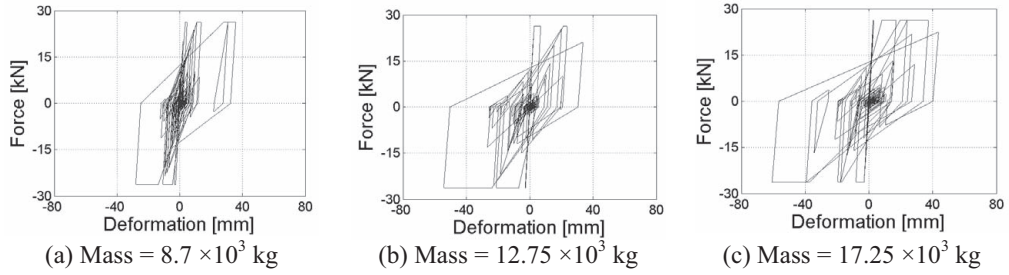


Figure 8. Results for adobe structure with $K_r/K_o = 0.0$, input motion: Northridge Eq., Sation USGSVA 637

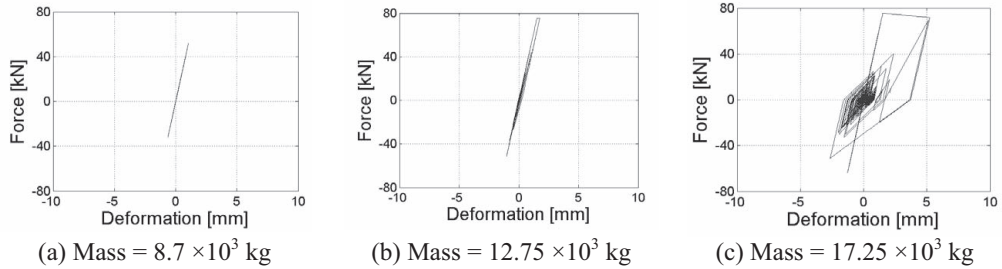


Figure 9. Results for brick structure with $K_r/K_o = -0.2$, input motion: Northridge Eq., Sation USGSVA 637

For all the records and structures analyzed, μ_{dem} and R_d were determined and plotted as shown in Figures 10 and 11. Maximum R_d for adobe and masonry structures were 10.9 and 3.4, respectively. The values of μ_{dem} were 41.5 and 23.6 in the same cases. Regression functions were determined for each group as shown in Table 3 and are shown in thick lines in Figures 10 and 11. In general, the results are scattered, especially for adobe structures. For instance, for R_d equal to 3, μ_{dem} ranges from 2 to 35, if $K_r/K_o=0$, and from 2 to 20, if $K_r/K_o= -0.2$.

The large scatter does not seem to be caused by the post-peak softening behavior of the structure. Groups with different values of K_r/K_o give similar scattered results. Nor seems it to be caused by the used strong ground motion records, which have similar characteristics as shown in Figure 7. Additional evaluation of the model used is necessary to grasp the causes of the dispersed results.

Table 3 Regression functions obtained for each of the group structures considered in the study

Structure type	K_r/K_o	Regression function	R^2
Adobe	0.00	$\mu_{dem} = 1.0018 \times R_d^{1.4539}$	0.620
	-0.02	$\mu_{dem} = 1.0121 \times R_d^{1.4873}$	0.630
Brick	0.00	$\mu_{dem} = 1.0247 \times R_d^{1.5359}$	0.66
	-0.02	$\mu_{dem} = 0.9905 \times R_d^{1.6512}$	0.71

Even though the results require further evaluation, a few conclusions may be drawn. For instance, it seems that the factor K_r/K_o does not affect considerably the maximum displacements experienced by the structure. Initial and residual strengths (V_o , V_r) are more important as suggested in previous studies. Also, for R_d values lower than 9, μ_{dem} may be considered at most 9 for adobe structures. For masonry, a μ_{dem} of 5, at most, may be expected for R_d up to 4.

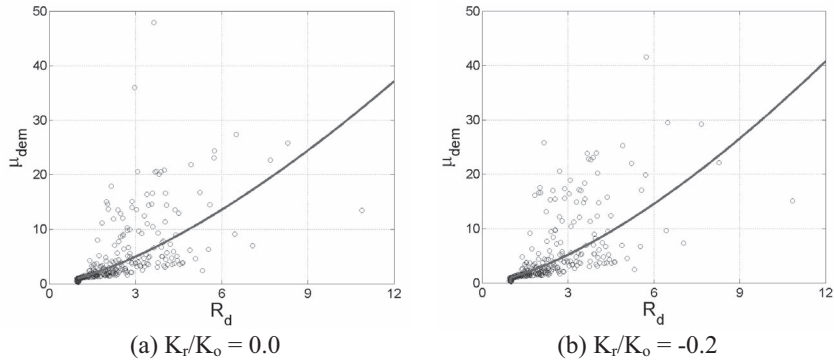


Figure 10. Strength reduction versus ductility demand for adobe structures

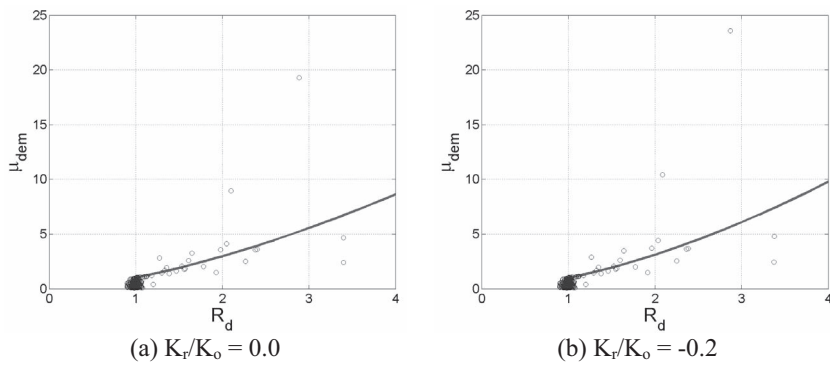


Figure 11. Strength reduction versus ductility demand for masonry structure

A more comprehensive statistical analysis, considering more strong ground motion records and structures with larger R_d is required to reach to a final expression of μ_{dem} as a function of R_d .

MAXIMUM ACCEPTABLE DISPLACEMENT

A maximum acceptable displacement or drift should be defined to guaranty the structure stability. Material tests have shown that PP-band retrofitted walls under in-plane loads can tolerate very large drifts, in the order of 10% or more, without losing their in-plane resistance capacity. However, such large deformations along the plane of certain walls will cause excessive out-of-plane deformations on the walls perpendicular to them. If a structural wall is excessively damaged by out-of-plane actions and consequent displacements, its ability to resist in-plane forces will be reduced.

There are two ways to take into account the interaction of the in-plane and out-of-plane actions on the wall in the design. One is to reduce the in-plane resistance with a penalty factor which should be a function of the maximum out-of-plane displacement. Although presently this point is under study, so far there is no model to determine what factor would be appropriate. Another way is to limit the maximum acceptable displacement to a conservative low value. Although more analyses and calculations are required to determine the most appropriate value, at this point, it is recommended to set it as a half of the wall thickness so that the resultant of vertical loads on the wall (under out-of-plane actions) will always fall within the limits of the wall base. Furthermore, out-of-plane deformations in the wall, not only its sides, need to be controlled as explained in the next section.

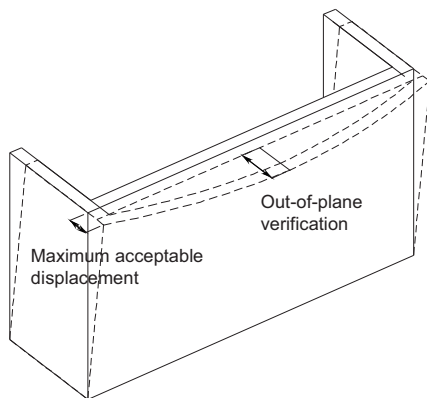


Figure 12. Difference between maximum acceptable displacement and out-of-plane verification



Figure 13. PP-band meshes connecting wall and roof restrain out-of-plane wall displacements

OUT-OF-PLANE VERIFICATION

The maximum acceptable displacement discussed in the previous section corresponds to the drift of the walls under in-plane actions or in other words, to the displacement of the walls subjected to out-of-plane actions at their sides. If the unsupported length of the walls under out-of-plane actions is too long, the center of the walls may be subjected to considerable larger displacements perpendicular to their plane. Presently, a model to determine the displacements due to out-of-plane seismic actions for PP-band retrofitted walls is being developed.

Experiments have shown that attaching the PP-band mesh so that it is wrapped around the roof frame as shown in Figure 13 can greatly contribute to control out-of-plane displacements. Whenever possible, it is recommended to install the mesh in this way. Another solution to limit out-of-plane displacements in walls with large length/height ratio is to provide intermediate supports by means of pilasters well attached to the wall with PP-band meshes.

CONCLUSIONS

A methodology to design 1-story, flat roof, adobe/masonry houses with PP-band meshes was proposed. Although there are still some issues to be addressed to complete the design procedure, the general process was outlined. It is important to keep in mind that this procedure is just one step towards the development of a simple set of rules of thumb than can be used in the field for determining the most appropriate PP-band mesh arrangement for each particular situation.

Permanent displacements are expected when PP-band mesh retrofitted structures are subjected to strong ground motions. If these displacements are too large, the remaining structure may be either unusable or too expensive to repair. This information is very important to assess the suitability of PP-band mesh retrofitting for different type of structures, taking into account initial investment and eventual reparation costs. A procedure to evaluate permanent displacements of PP-band mesh retrofitted structures will be investigated in the future.

ACKNOWLEDGEMENTS

The authors are grateful to Prof. Y. Nakano, Institute of Industrial Science, The University of Tokyo, for his valuable comments and suggestions regarding this research.

REFERENCES

- Coburn A. and Spence R. (1992) Earthquake Protection, John Wiley & Sons Ltd, West Sussex.
- Miranda, E. (2000). Inelastic displacement ratios for structures on firm sites. *Journal of Structural Engineering*, Vol. 126, No. 10.
- Sathiparan, N., Mayorca, P., Nesheli, N., Guragain, R., and Meguro, K. (2005). In-plane and out-of-plane behavior of PP-band retrofitted masonry wallties. *Proc. of the 4th International Symposium on New Technologies for Urban Safety of Megacities in Asia*, Singapore.
- Meguro, K., Mayorca, P., Sathiparan, N., Guragain, R., and Nesheli, N. (2005). Shaking table tests of small scaled masonry models retrofitted with PP-band meshes. *Proceeding of the 4th International Symposium on New Technologies for Urban Safety of Megacities in Asia*, Singapore.
- Nesheli, K., Sathiparan, N., Guragain, R., Mayorca, P., Ito, F., Kagawa, H., Tsugawa, T., and Meguro, K. (2006). Full-Scale Shaking Table Tests On Masonry Buildings Retrofitted By PP-Band Meshes, *Proc. of the 5th International Symposium on New Technologies for Urban Safety of Megacities in Asia*, Thailand.
- Mayorca, P. and Meguro, K. (2007). Proposal of a methodology to design PP-band meshes to retrofit low earthquake resistant houses, *Proc. of the 6th International Symposium on New Technologies for Urban Safety of Megacities in Asia*, Bangladesh.
- Pacific Earthquake Engineering Research (PEER) Center Strong Ground Motion Database.



DYNAMIC BEHAVIOR OF TIMBER ROOF MASONRY HOUSE MODELS RETROFITTED BY PP-BAND MESHES

Navaratnarajah SATHIPARAN¹, Paola MAYORCA²,
and Kimiro MEGURO³

ABSTRACT: Unreinforced masonry is one of the most popular construction materials in the world. It is also unfortunately, the most vulnerable against earthquakes. Damage to unreinforced masonry buildings has caused huge number of human casualties historically and during recent earthquakes in developing countries. Therefore, retrofitting of low earthquake-resistant masonry structures is the key issue for earthquake disaster mitigation in developing countries to reduce the casualties significantly. When we propose the retrofitting in developing countries, retrofitting method should respond to the structural demand on strength and/or deformability as well as to availability of material with low cost including manufacturing and delivery, practicability of construction method and durability in each region. Considering these issues of developing appropriate seismic retrofitting techniques for masonry buildings to reduce the possible number of casualties due to future earthquakes in developing countries, a technically feasible and economically affordable PP-band (polypropylene bands) retrofitting technique has been developed and many different aspects have been studied by Meguro Laboratory, Institute of Industrial Science, The University of Tokyo. PP-band is commonly used for packing.

In order to understand the dynamic response of masonry houses with and without PP-band mesh retrofitting, crack patterns, failure behavior, and overall effectiveness of the retrofitting technique, shaking table tests were carried out. In this experimental program, $\frac{1}{4}$ scale single box shape room structure with wooden roof models were used. Addition to that, effect of surface plaster on PP-band retrofitted house model also studied.

From the experimental results, it was found that a scaled dwelling model with PP-band mesh retrofitting was able to withstand larger and more repeatable shaking than that without PP band retrofitting, which all verified to reconfirm high earthquake resistant performance. When surface finishing applied above house model, due to improve bond connection between PP-band and brick wall, surface plaster kept well with wall.

Key Words: unreinforced masonry, polypropylene band, shaking table test, surface finishing, arias intensity

INTRODUCTION

A real scale model test makes possible to obtain data similar to real structures. However, it requires large size testing facilities and large amount research funds, so it is difficult to execute parametric tests by using full scaled models. Recently, structural tests of scaled models become larger and larger as the overall behavior of the system can be understood from scaled model also.

¹ Post Doctoral Research Fellow

² Project Research Associate

³ Professor, Director of International Center for Urban Safety Engineering (ICUS)

In this experimental program $\frac{1}{4}$ scale models were used to investigate the seismic behavior of masonry houses and effectiveness of PP-band retrofitting technique.

EXPERIMENTAL PROGRAM

Description of the specimens

For shaking table experiment, four models were built in the reduced scale of 1:4 using the unburnt bricks as masonry units and cement, lime and sand (1:2.8:8.5) mixture as mortar with cement/water ratio of 33%. Attention was paid to make the models as true replica of adobe masonry buildings in developing countries in terms of masonry strength even though the construction materials used were those available in Japan.

All the building models dimensions were 933mmx933mmx720mm with 50mm thick walls. The sizes of door and window in opposite walls were 243x485mm² and 325x245mm² respectively.

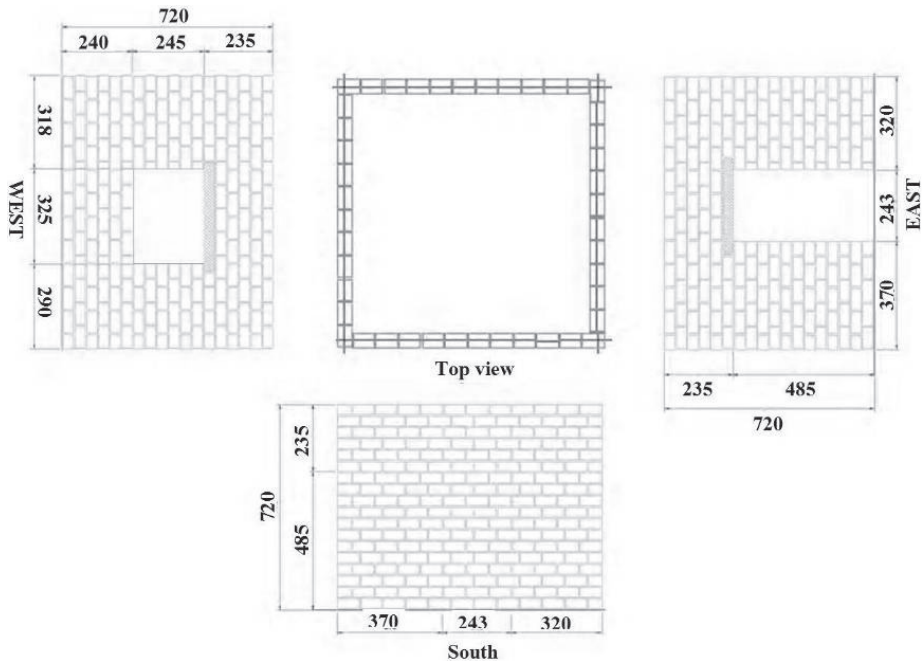


Figure 1. Model dimension (mm)

All specimens consisted of 18 rows of 44 bricks in each layer except openings. Construction process takes place in two days, first 11 rows in first day and remaining rows construct in following day. The geometry, construction materials and mix proportion, construction process and technique and other conditions that may affect the strength of the building models were kept identical for better comparison. The cross-section of the band used was 6mm×0.32mm and the pitch of the mesh was 40mm.

All four models were represented one-storey box-like building including two models without surface finishing and other two models with surface finishing. This simple geometry and boundary conditions were considered as the data generated will be used for numerical modeling in future.

The specimens were named according to the following convention: **B-R-P-S** in which;

B is masonry unit,

A: unburned brick;

R is roof connection type,

4: roof connected to all four walls;

P is retrofitted condition,

NR: non retrofitted

RE: retrofitted;

S is condition of surface finishing applied above masonry house,

X: no surface finishing applied

P: 7.5 mm surface finishing applied;

For surface finishing material mixing ratio as follows; Water: Cement: Sand: Lime = 1.00: 0.14: 2.80:

1.11. Totally two models were retrofitted with PP-band mesh after construction.

Table 1. Mechanical property of masonry specimens

Specimen	Diagonal shear strength (MPa)	Compression strength (MPa)	Shear strength (MPa)	Bond Strength (MPa)
A-4-NR-X	0.041	4.28	0.0057	0.0046
A-4-RE-X	0.045	4.36	0.0068	0.0046
A-4-NR-P	0.048	4.29	0.0061	0.0050
A-4-RE-P	0.050	4.35	0.0056	0.0048

Retrofitting Procedure

The procedure presented below is illustrated with photos taken during the experimental program.

- PP-bands arranged in mesh fashion was prepared (because of original purpose of the PP-bands is to serve as packing material, so far PP-band meshes are not produced. we would like to gratefully acknowledge SEKISUI JUSHI CORPORATION for providing the PP-band meshes used in the reported experimental program).
- PP-band mesh was cut in convenient size according to the dimension of the house.
- Straw, which placed in holes are removed (in this experiment, during construction of model house, we placed the straw in where we required a holes. Straw are placed at approximately 200mm pitch. In real case holes can be prepared by drilling through the wall) and the model house walls are cleaned.
- The meshes are installed on both sides of the wall and wrapped around the corner wall edges. An overlapping length of approximately 300mm is recommendable.
- Wire is passed through the holes and used to connect the meshes on the both wall sides. In order to prevent the wires cutting the PP-bands, aluminum plates (20mm×20mm) were placed between the band and the wire. Initially, fixing the meshes with connectors along the wall and at the foundation is recommendable.
- Connecting inner and outer meshes by wires and aluminum plates except around the openings.
- Fixed connectors around the openings after the mesh was cut and overlapped on the other side.

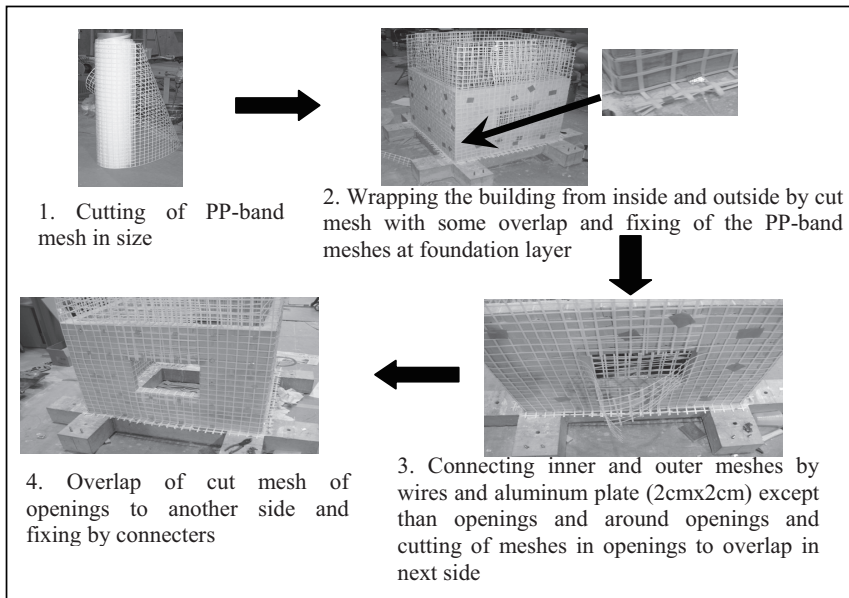


Figure 2. Retrofitting process by PP-band

Input motion

Simple easy-to-use sinusoidal motions of frequencies ranging from 2Hz to 35 Hz and amplitudes ranging from 0.05g to 1.4g were applied to obtain the dynamic response of both retrofitted and non-retrofitted structures. This simple input motion was applied because of its adequacy for later use in the numerical modeling. Figure 3 shows the typical shape of the applied sinusoidal wave.

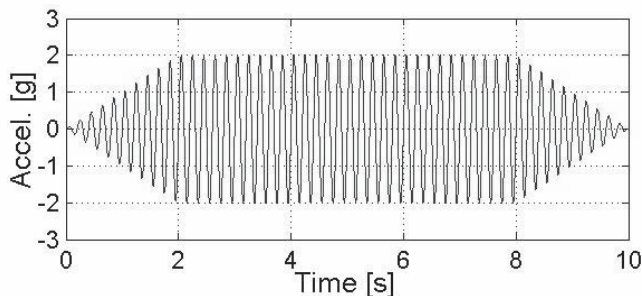


Figure 3. Typical Shape of Input Sinusoidal Motion

Loading was started with a sweep motion of amplitude 0.05g with all frequencies of 2Hz to 35Hz for identifying the dynamic properties of the models. The numbers in table 2 indicate the run numbers. General trend of loading was from high frequency to low frequency and from lower amplitude to higher amplitude. Higher frequencies motions were skipped towards the end of the runs.

Table 2. Loading Sequence

Amplitude	Frequency							
	2Hz	5Hz	10Hz	15Hz	20Hz	25Hz	30Hz	35Hz
1.4g		50						
1.2g	54	49						
1.0g		48						
0.8g	53	47	43	40	37	34	31	28
0.6g	52	45	42	39	36	33	30	27
0.4g	51	44	41	38	35	32	29	26
0.2g	46	25	24	23	22	21	20	19
0.1g	18	17	16	15	14	13	12	11
0.05g	10	09	08	07	06	05	04	03
sweep	01,02							

CRACK PATTERN AND FAILURE BEHAVIOR

Models A-4-NR-X & A-4-RE-X

In both specimens, due to shrinkage, some minor cracks were observed before the test. These cracks mainly appear closer to opening in horizontal direction. For non-retrofitted specimen (A-4-NR-X) up to Run 21, no major crack was observed. Major cracks were observed closer to openings from Run 23. At run 28, crack was observed at one of the top corner of the door opening and it propagates up to top layer of the wall. After that, cracks widened with each successive run. At run 44, there were large amount cracks observed in walls in the direction of shaking. Exciting cracks widened and connection between adjacent walls was become weak. In case of walls perpendicular to shaking direction, top part of the east wall (part, above the door opening) was totally separated from the specimen. It was removed from specimen before next test run proceed. At run 45, all top part of the wall with opening was totally separated from the specimen. It was fallen from specimen. Now the roof only supported by two walls, which were in the direction of shaking. Therefore, due to walls subjected to out-of-plane load; they were bursts outwards in shaking direction. This finally led to the structure collapse.

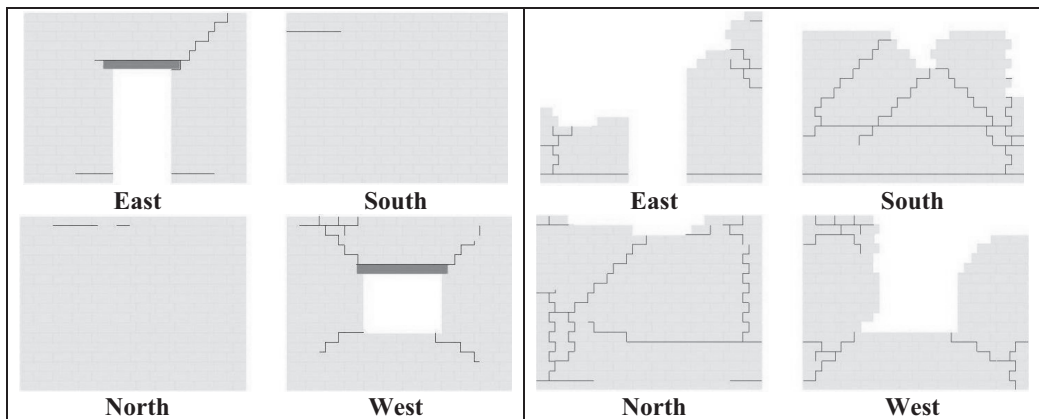


Figure 4. Crack pattern after Run 28 (left) and after run 45(right) for specimen A-4-NR-X

For retrofitted specimen (A-4-RE-X) up to run 21, no major crack was observed in this model. Major cracks were observed closer to openings from Run 25. After those new cracks appear in each run and cracks widened with each successive run, thus, extensive cracking was observed. Although the PP-band mesh kept the structure integral during the shaking, it allowed the sliding of the bricks along these cracks to some extent. In later stages, there was significant permanent deformation of the structure. At the final stage of the test, run 52, with 37.3mm base displacement, 6 times more than the input displacement applied in run 45 and 2.5 times more velocity, virtually all the brick joints were cracked and the building had substantial permanent deformations. However, building did not lose the overall integrity as well as stability and collapse was prevented in such a high intensity of shaking.

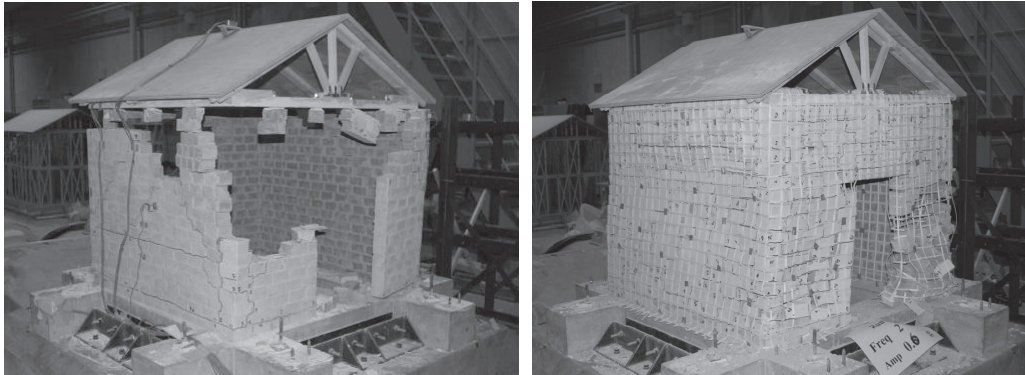


Figure 5. Specimen A-4-NR-X after run 45 (left) & Specimen A-4-RE-X after run 52 (right)

Models A-4-NR-X & A-4-RE-X

For specimen A-4-NR-P, at run 26, major cracks were observed close to connection between roof and south wall. At run 43, lot of damage observed in the modal. Separation between east wall and its adjacent walls was observed. Also lot of surface finishing separated from the walls. At run 44, Top corner of the east wall and its adjacent walls was totally separated from specimen. At run 45, all the top part of the north and south walls was totally separated form specimen. Now roof only supported by two walls, which are in the perpendicular direction of shaking. This finally led to the structure collapse at run 47 (Figure 6).



Figure 6. Specimen A-4-NR-P after run47

In case of the retrofitted model A-4-RE-P, similar cracks as non-retrofitted building started from top corner of the south wall in the run 33. After that, the process of widening of the cracks occurred and propagation of new cracks continues until the run 50. Although at the end of 50th run almost cracks observed in entire walls, the specimen did not lose stability. Some bricks from bottom part of east wall were spilled out from PP-band mesh. Therefore some looseness was observed in bottom part of the wall. Even this very high input motion, most of the surface finishing still attached with walls. At the final stage of the test, run 54, with 74.6 mm base displacement, 9 times more than the input displacement applied in run 47 and 3.7 times more velocity, virtually all the brick joints were cracked and the building had substantial permanent deformations. However, building did not loose the overall integrity as well as stability and collapse was prevented in such a high intensity of shaking. Thus, PP-band retrofitting technique maintained the integrity of the structural elements. Further, the retrofitted model showed the better energy dissipation mechanism as many new cracks were propagated without loosing the overall integrity and stability of the structure.

When we applied the surface finishing to house model, due to improve bond connection between PP-band and brick wall, surface plaster kept well with wall. This is not observed in non-retrofitted model. Because of this, brick unit confined effect inside the PP-band mesh is improved and it improves the overall earthquake resistant performance.



Figure 7. Specimen A-4-NR-P after run 43 (left) & Specimen A-4-RE-P after run 48 (right)

PERFORMANCE EVALUATION

The performances of the models were assessed based on the damage level of the buildings at different levels of shaking. Performances were evaluated in reference to five levels of performances: light structural damage, moderate structural damage, heavy structural damage, partially collapse, and collapse.

Table 3. Damage categories

Category	Damage extension
D0: No damage	No damage to structure
D1: Light structural damage	Hair line cracks in very few walls. The structure resistance capacity has not been reduce noticeably.
D2: Moderate structural damage	Small cracks in masonry walls, falling of plaster block. The structure resistance capacity is partially reduced.
D3: Heavy structural damage	Large and deep cracks in masonry walls. Some bricks are fall down. Failure in connection between two walls.
D4: Partially collapse	Serious failure of walls. Partial structural failure of roofs. The building is in dangerous condition
D5: Collapse	Total or near collapse

The Japan Meteorological Agency seismic intensity scale (JMA) is a measure used in Japan to indicate the strength of earthquakes. Unlike the Richter magnitude scale (which measures the total magnitude of the earthquake, and represents the size of the earthquake with a single number) the JMA scale describes the degree of shaking at a point on the Earth's surface.

The JMA scale was colored according to the following convention:

Index	JMA ~4	JMA 5-	JMA 5+	JMA 6-	JMA 6+	JMA 7
-------	--------	--------	--------	--------	--------	-------

Table 4 shows the performances of non retrofitted model A-4-NR-X and retrofitted model A-4-RE-X with different JMA intensities. Partial collapse of the non-retrofitted building was occurred at the 44th run at intensity JMA 5-. The retrofitted building performed moderate structural damage level at 45th run at which the non-retrofitted building was partially collapsed. Moreover, moderate structural damage level of performance was maintained until 50th run, leading to intensity JMA 6-. As the model was already considerably deformed beyond the limit of measurement system, test was stopped after the 52nd run. It should be noted again that this model survived 7 more shakings in which many runs were with higher intensities than JMA 5- at which the non-retrofitted building was collapsed before reaching to the final stage at the 52nd run.

Table 4. Performance of A-4-NR-X and A-4-RE-X

Performance of A-4-NR-X model									Performance of A-4-RE-X model								
Acceleration (g)	Frequency (Hz)								Acceleration (g)	Frequency (Hz)							
	2	5	10	15	20	25	30	35		2	5	10	15	20	25	30	35
1.4									1.4	D2							
1.2									1.2	D2							
1.0									1.0	D2							
0.8				D3	D2	D2	D2	D2	0.8	D2	D2	D2	D2	D2	D1	D1	
0.6			D4	D3	D2	D2	D2	D1	0.6	D4	D2	D2	D2	D2	D1	D1	
0.4			D4	D3	D2	D2	D2	D1	0.4	D3	D2	D2	D2	D2	D1	D1	
0.2			D3	D1	D1	D1	D1	D0	0.2	D2	D1	D1	D1	D1	D1	D1	
0.1	D0	D0	D0	D0	D0	D0	D0	D0	0.1	D1	D1	D1	D1	D0	D0	D0	
0.05	D0	D0	D0	D0	D0	D0	D0	D0	0.05	D0	D0	D0	D0	D0	D0	D0	

Table 5 shows the performances of non retrofitted model A-4-NR-P and retrofitted model A-4-RE-P with different JMA intensities. Total collapse of the non-retrofitted building was occurred at the 47th run at intensity JMA 5+. The retrofitted building performed moderate structural damage level at 47th run at which the non-retrofitted building was partially collapsed. Moreover, moderate structural damage level of performance was maintained until 48th run, leading to intensity JMA 6-. It should be noted again that this model survived 7 more shakings in which many runs were with higher intensities

than JMA 5+ at which the non-retrofitted building was collapsed before reaching to the final stage at the 54th run.

Table 5. Performance of A-4-NR-P and A-4-RE-P

Performance of A-4-NR-P model									Performance of A-4-RE-P model								
Acceleration (g)	Frequency (Hz)								Acceleration (g)	Frequency (Hz)							
	2	5	10	15	20	25	30	35		2	5	10	15	20	25	30	35
1.4	D5	D5							1.4	D3	D3						
1.2	D5	D5							1.2	D4	D3						
1.0	D5	D5							1.0	D2	D2						
0.8	D5	D5	D3	D3	D2	D2	D1	D1	0.8	D4	D2	D2	D2	D1	D1	D0	D0
0.6	D5	D5	D3	D2	D2	D2	D1	D1	0.6	D3	D2	D2	D1	D1	D0	D0	D0
0.4	D5	D5	D3	D2	D2	D1	D1	D1	0.4	D3	D2	D2	D1	D1	D0	D0	D0
0.2	D0	D0	D0	D0	D0	D0	D0	D0	0.2	D2	D0						
0.1	D0	D0	D0	D0	D0	D0	D0	D0	0.1	D0	D0	D0	D0	D0	D0	D0	D0
0.05	D0	D0	D0	D0	D0	D0	D0	D0	0.05	D0	D0	D0	D0	D0	D0	D0	D0

Performance evaluation based on Arias intensity scale

The Arias intensity was initially defined (Arias, 1970) as

$$I_a = \frac{\pi}{2g} \int_0^t a^2(t) dt$$

and was called scalar intensity. It is directly quantifiable through the acceleration record a(t), integrating it over the total duration of the earthquake. The arias intensity is claimed to be measure of the total seismic energy absorbed by the ground. Figure 8 & Figure 9 shows the performance level of each specimen against dynamic motion.

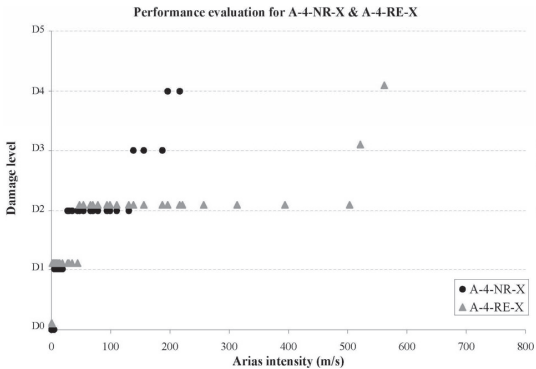


Figure 8. Performance evaluation for A-4-NR-X & A-4-RE-X

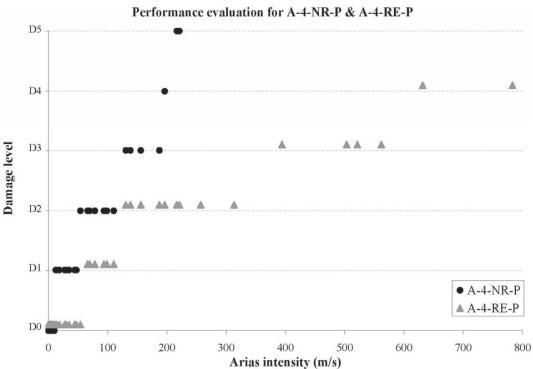


Figure 9. Performance evaluation for A-4-NR-P & A-4-RE-P

CONCLUSION

Four adobe masonry building models, identical in terms of masonry strength and geometry were constructed and two models were retrofitted with an easy-to-install and economic retrofitting technique. Models were tested on shaking table by applying similar input motions. Dynamic behaviors

of the models were studied. Cracks patterns were analyzed and failure behavior and performances were evaluated.

- Shaking table test showed that; a scaled dwelling model with PP-band mesh retrofitting is able to withstand larger and more repeatable shaking than that without PP band retrofitting, which all verified to reconfirm high earthquake resistant performance.
- When we applied the surface finishing to house model, due to improve bond connection between PP-band and brick wall, surface plaster kept well with wall. This is not observed in non-retrofitted model. Because of this, brick unit confined effect inside the PP-band mesh is improved and it improves the overall earthquake resistant performance.

From the experimental results, it was found that this retrofitting technique can enhance safety of both existing and new masonry buildings even in worst case scenario of earthquake ground motion like JMA 7 intensity. Therefore proposed method can be one of the optimum solutions for promoting safer building construction in developing countries and can contribute earthquake disaster in future.

REFERENCE

- Sathiparan, N., 2008. *Experimental Study on PP-Band Mesh Seismic Retrofitting for Low Earthquake Resistant Masonry Houses*, Ph.D. Dissertation, The University of Tokyo, Japan.
- Mayorca, P., 2003. *Strengthening of Unreinforced Masonry Structures in Earthquake Prone Regions*, Ph.D. Dissertation, The University of Tokyo, Japan.
- T. Okada, F. Kumazawa, S. Horiuchi, M. Yamamoto, A. Fujioka, K. Shinozaki, Y. Nakano, *Shaking Table Tests of Reinforced Concrete Small Scaled Model Structures*, Bull. ERS, No.22 (1989).
- Roko Zarnic, Samo Gostic, Adam J. Crewe and Colin A. Taylorm, *Shaking Table Tests of 1:4 Reduced Scale Models of Masonry Infilled Reinforced Concrete Frame Buildings*, Earthquake Engineering and Structural Dynamics. 2001, Vol.30, 819-834.
- Alidad Hahemi and Khalid M.Mosalam, *Shake-table Experiment on Reinforced Concrete Structure Containing Masonry Infill Wall*, Earthquake Engineering and Structural Dynamics. 2006, Vol. 35, 1827-1852.



DAMAGE TO NON-STRUCTURAL COMPONENTS IN LARGE ROOF BUILDINGS BY TWO MAJOR EARTHQUAKES OCCURRED IN THE NORTHEASTERN REGION OF JAPAN IN 2008

Ken'ichi KAWAGUCHI¹, Yoshiro OGI², Shunji OHYA³
Shin'ichiro KATAYAMA⁴, Shogo KUMAGAI⁵ and Shigeyoshi SAKURAI⁶

ABSTRACT: Damage to non-structural components such as suspended ceilings in large roof buildings, failed during the Iwate-Miyagi Nairiku Earthquake and the Iwateken Engan-Hokubu Earthquake in 2008, is reported. The northeastern region of Japan had been hit by major earthquakes frequently in recent years. Nevertheless, the similar damage had been repeated, since the failed parts had been fixed and recovered always with no essential improvements.

Key Words: *Earthquake, Non-structural component, Suspended ceiling*

INTRODUCTION

This paper reports investigations on damage to non-structural components of large roof buildings caused by two major earthquakes, occurred in 2008, in the northeastern region of Japan. One of them is the "Iwate-Miyagi Nairiku Earthquake" which occurred in the morning of June 14, 2008. The other is the "Iwateken Engan-Hokubu Earthquake" which occurred in the early hours of June 24, 2008.

While very little damage to building skeletons was reported, a number of reports about failure of non-structural components, especially suspended ceilings, came out. The northeastern region of Japan had been hit by major earthquakes frequently in recent years. Nevertheless, the similar damage had been repeated, since the failed parts had been fixed and recovered always with no essential improvements. Moreover, as is described in this report, it was found that different damage may occur due to the difference of seismic input.

IWATE-MIYAGI NAIRIKU EARTHQUAKE

Overview of the Earthquake

The Iwate-Miyagi Nairiku Earthquake occurred at 8:43 a.m., June 14, 2008 (39.0N, 140.5E, focal depth = 8 km) [1], as illustrated in Fig. 1. The magnitude of the main shock was 7.2 on Japan

¹ Professor, Institute of Industrial Science, The University of Tokyo

² Research associate, Institute of Industrial Science, The University of Tokyo

³ Technical support specialist, Institute of Industrial Science, The University of Tokyo

⁴ Graduate student, Department of Architecture, The University of Tokyo

⁵ Graduate student, Department of Architecture, Waseda University

⁶ Undergraduate student, Department of Architecture, Waseda University

Meteorological Agency (JMA) scale. The largest aftershock occurred at 9:20 a.m. on the same day registering the magnitude of 5.7 (38.5N, 140.4E, focal depth = 6 km). As for the main shock, the maximum intensity of 6-Upper on the JMA scale was observed in Oshu city of Iwate prefecture and Kurihara city of Miyagi prefecture, both of which are approximately 20-45 km away from the focus. The reported buildings in the successive section are located in the two cities and Yokote city of Akita prefecture, which is approximately 35-50 km away from the focus, and the intensity was 5-Lower. The time histories of acceleration recorded in the three cities are shown in Figs. 2 to 4. The details of buildings described in this section are summarized in Table 1.

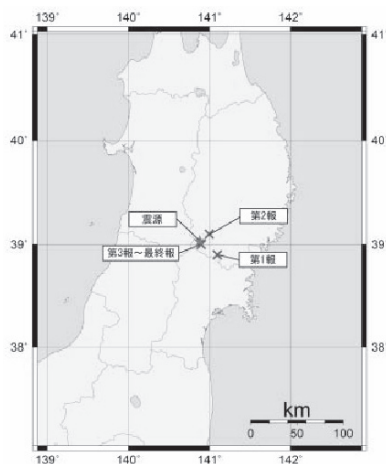


Figure 1. Location of the focus (“震源” in Japanese) of the Iwate-Miyagi Nairiku Earthquake[1]

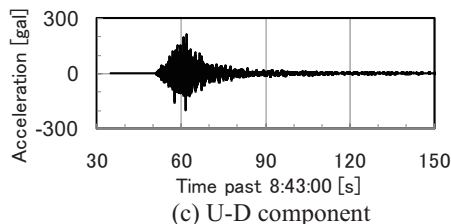
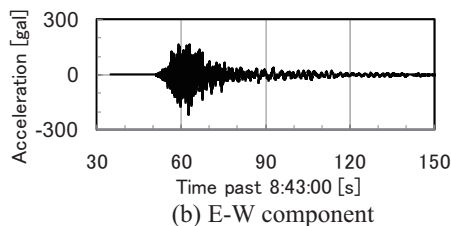
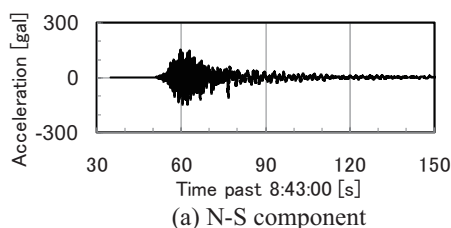


Figure 2. Acceleration of the Iwate-Miyagi Nairiku Earthquake recorded at Oshu city (39.1N, 141.2E)

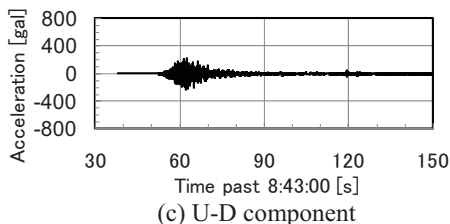
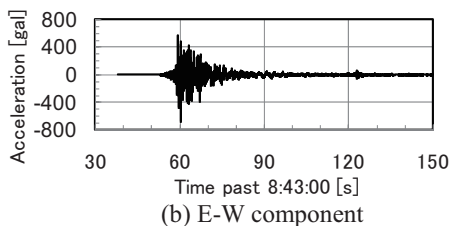
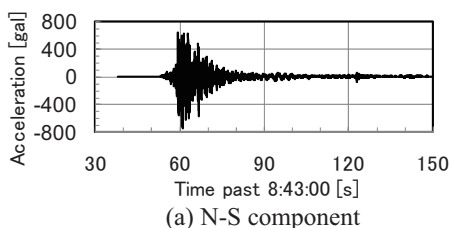
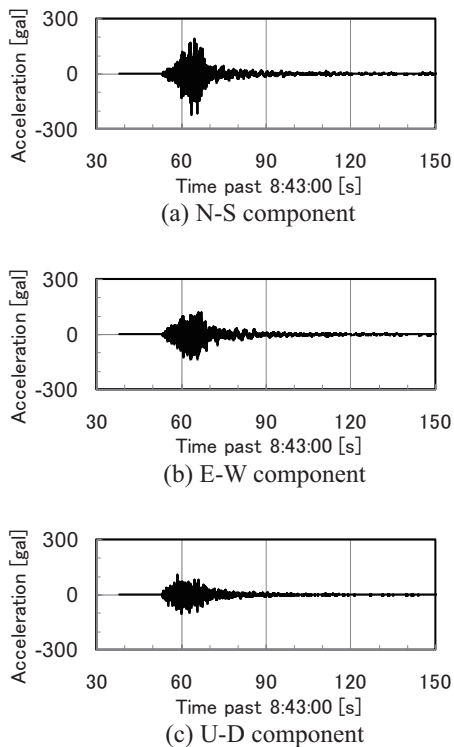


Figure 3. Acceleration of the Iwate-Miyagi Nairiku Earthquake recorded at Kurihara city (38.7N, 141.0E)

Table 1. Details of buildings investigated after the Iwate-Miyagi Nairiku Earthquake

Name	Building	Completion year	Structure	Investigated space
Gymnasium-1	Public gymnasium	1984	RC, Steel	Arena, 36 x 28 m Hight to ceiling: 10-12.9 m
Hall-1	Public hall	1974	RC	Assembly room, 18 x 6 m Hight to ceiling: 2.6 m
Gymnasium-2	Public gymnasium	1997	RC, Steel	Arena, 45 x 42 m Hight to ceiling: 13-16 m
Gymnasium-3	Public gymnasium	—	RC, Steel	Eaves
Gymnasium-4	Elementary school gymnasium	1991	RC, Steel	Arena, 32 x 23 m Hight to ceiling: 8.5-10.5 m

**Figure 4.** Acceleration of the Iwate-Miyagi Nairiku Earthquake recorded at Yokote city (39.3N, 140.6E)

around. Local deformation of M-bars showed the locations where the clips had failed off (Fig. 2(f)). M-bars had prints of scratch showing that M-bars and the runners had relatively moved each other at the joints.

Gymnasium-1

At a public gymnasium (Fig. 5), ceiling panels and lightings inside the arena, and ceiling panels under exterior eaves had fallen off (Fig. 6).

Inside the arena, while cracks could be seen in concrete surrounding the base of some columns, permanent deformations were not observed. Mortar exfoliations were also seen at bearings of the steel roof.

Ceiling panels were located above a gallery and were continuously placed horizontally and vertically. Some of the bracing members at the corner connecting horizontal and vertical surfaces seemed to push off the panels at their ends. Several welds of bracing members seemed to have failed. These indicate that damage shown in Figs. 6(a) and 6(b) had occurred by relative deformation between these finishing surfaces.

Lightings were equipped with safety wires against falling. But the end cramps of wires dislocated, and lightings had fallen off together with their safety wires (Fig. 2(c)).

Most of the suspended ceiling panels (1380 x 900 x 12 mm) under exterior eaves had fallen off bounded in a belt along a span-direction with furring bars, so-called M-bars (Figs. 2(d) and 2(e)). A lot of deformed clips were observed scattering



(a) External view



(b) Internal view

Figure 5. External and internal view of Gymnasium-1



(a) Failure of horizontal ceiling panel



(b) Failure of vertical ceiling panel



(c) Fallen lighting



(d) Fallen ceiling panel under exterior eave



(e) Fallen ceiling panel under exterior eave



(f) Local deformation of M-bar

Figure 6. Damage to Gymnasium-1

Hall-1

A small public hall (Fig. 7) had structural problems due to cold joints in its RC skeletons, and had been suffered from structurally fundamental damage (Figs. 8(a) to 8(c)). In the gathering room on the second floor, many metal ceiling panels (2920 x 460 x 10 mm) had fallen off (Fig. 8(e)). As shown in Fig. 9, the ceiling panels constituted a symmetric bilge shape on one wooden center frame. Each ceiling panel was suspended at mid 2 points through M-bars (2 meters from above), and both ends mounted on the wooden center frame and a wall. The ceiling panels might have fallen off due to curving deformation of the wooden center frame, since most of the panels put on one side had fallen.

It is important that they repeated similar damage again even though they had experienced several times in past major earthquakes. Recoveries had been done without fundamental improvements.



(a) External view



(b) Internal view of gathering room

Figure 7. External and internal view of Hall-1



(a) Failure of cold joint



(b) Failure of cold joint



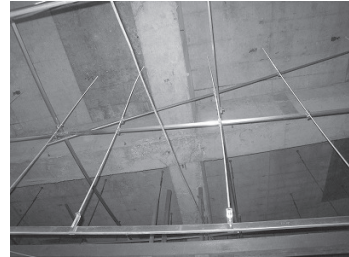
(c) Failure of cold joint



(d) Failure of glass

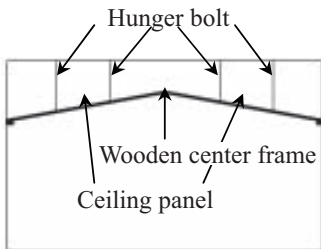


(e) Failure of ceiling panel in gathering room



(f) Deformation of runner in gathering room

Figure 8. Damage to Hall-1



(a) Cross section of gathering room



(b) Situation of failed ceiling panels and curving deformation of wooden center frame in gathering room

Figure 9. Schematic diagram of Hall-1

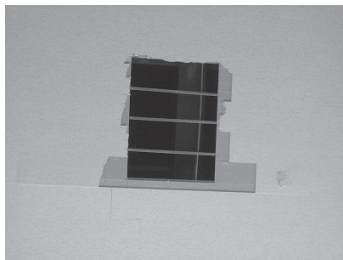


(a) External view



(b) Internal view

Figure 10. External and internal view of Gymnasium-2



(a) Failure of ceiling panel



(b) Failure of ceiling panel



(c) Hanged blind of top light

Figure 11. Damage to Gymnasium-2

Gymnasium-2

At a public gymnasium (Fig. 10), ceiling panels failed (Figs. 11(a) and 11(b)), blinds of top lights hanged down (Fig. 11(c)), and ducts in roof-space and covers of lightings dislocated. They had experienced similar damage during previous earthquakes in 2003 and 2005, and this is the third time that they were suffered from same damage.

Ceiling panels had failed mainly at four places in the arena. The ceiling panel had a 9-mm-thick plaster board as a base layer and a 9-mm-thick rock-wool board, set below of the base layer, as a finishing layer. As the ceiling is following the domical shape with positive double curvature of the roof structure, there might have been geometric incompatibility to cover the ceiling with flat panels. Falling of narrow strip panels near the top light, that adjusted the gap between rectangular plane panels and curved surfaces, indicates such geometric difficulties of three dimensional curved surfaces.

Gymnasium-3

At a public gymnasium (Fig. 12), while buckling of braces set in vertical plane and roof plane was observed, permanent deformations were not observed in its building skeletons. Sixteen suspended ceiling panels (slate board, 910 x 910 x 5 mm) under exterior eaves surrounding the building had fallen off (Fig. 13).



(a) External view



(b) Internal view

Figure 12. External and internal view of Gymnasium-3



(a) Failure of ceiling panel under exterior eave



(b) Deformation of runner under exterior eave



(c) Fallen ceiling panel under exterior eave

Figure 13. Damage to Gymnasium-3

Gymnasium-4

There was damage at an elementary school gymnasium (Fig. 14). Inside the arena as shown in Fig. 15, 18 ceiling panels (glass-wool board, 1760 x 860 x 30 mm) had fallen off, and 7 panels had nearly fallen off. There were several failed frames of ceiling panels, which might have leads to sliding and falling of the panels. Viewing from the floor level, we could not observe any braces in ceiling frame systems. A glass-wool board is light and its falling won't be harmful for people, but falling of a frame may injure people.



(a) External view



(b) Internal view

Figure 14. External and internal view of Gymnasium-4

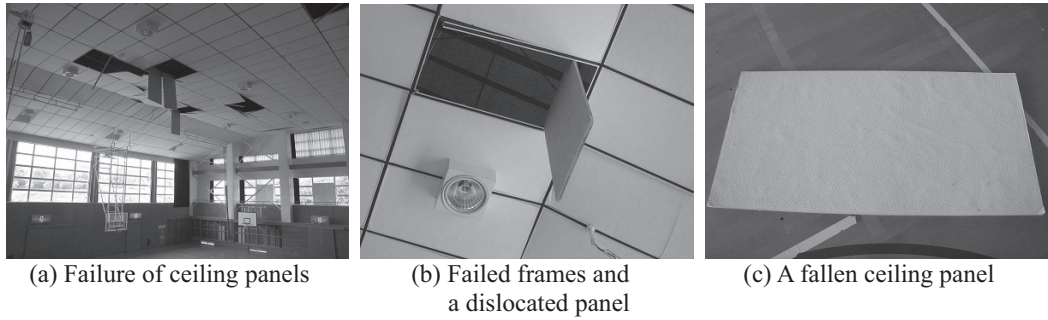


Figure 15. Damage to Gymnasium-4

IWATEKEN ENGAN-HOKUBU EARTHQUAKE

Overview of the Earthquake

The Iwateken Engan-Hokubu Earthquake occurred at 0:26 a.m., July 24, 2008 (39.4N, 141.4E, focal depth = 108 km) [2], as illustrated in Fig. 16. The magnitude of the main shock was 6.8. The maximum intensity was 6-Lower. The reported buildings in the successive section are located in Hachinohe city of Aomori prefecture, which is approximately 70-90 km away from the focus, and the intensity was 6-Lower. The time histories of acceleration recorded in Hachinohe city are shown in Fig. 17. The details of buildings described in this section are summarized in Table 2.

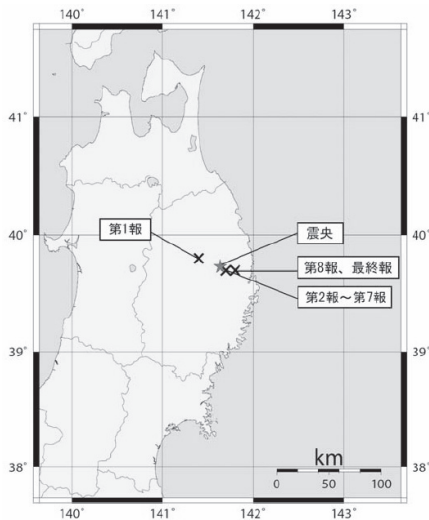
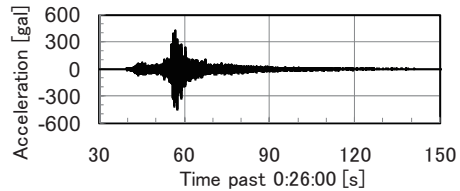
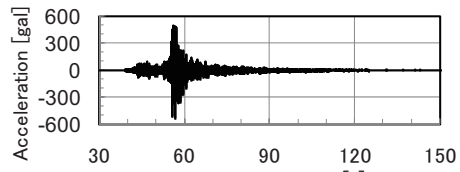


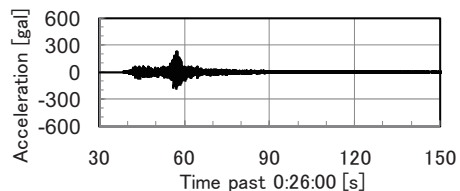
Figure 16. Location of the focus (“震央” in Japanese) of the Iwateken Engan-Hokubu Earthquake[2]



(a) N-S component



(b) E-W component



(c) U-D component

Figure 17. Acceleration of the Iwateken Engan-Hokubu Earthquake recorded at Hachinohe city (40.5N, 141.5E)

Table 2. Details of buildings investigated after the Iwateken Engan-Hokubu Earthquake

Name	Building	Completion year	Structure	Investigated space
Gymnasium-5	Elementary school gymnasium	2003	Steel	Arena, 26 x 30 m Hight to ceiling: 7-9.8 m
Auditorium-1	Public auditorium	1975	RC	Hight to ceiling: 9-12.5 m

Gymnasium-5

An elementary school gymnasium build in 2003 was damaged (Figs. 18 and 19). The ceiling had a slope of 10/66.5 parallel to its gable roof. As shown in Fig. 20, hunger bolts of ceiling panels were arranged normal to the slope, which caused constant thrust to both edge-lines of the ceiling. Therefore, tension force at the center and compression force at the edge-lines had been always acting in the ceiling. A plan view of the ceiling is illustrated in Fig. 21. Ceiling panels (rock-wool board, 300 x 600 x 9 mm) attached to M-bars had been torn apart in the center and were pushed onto the edge-lines (Figs. 19(a), 19(b), and 21). Moreover, as shown in Figs. 19(c) and 21, shear failures at specific regions, where ceiling panels were attached to the gable wall, could be observed. From the overall situation of the failure shown in Fig. 21, we can see the possibility of the relative rotation of the gymnasium skeleton and ceiling panels during the earthquake.

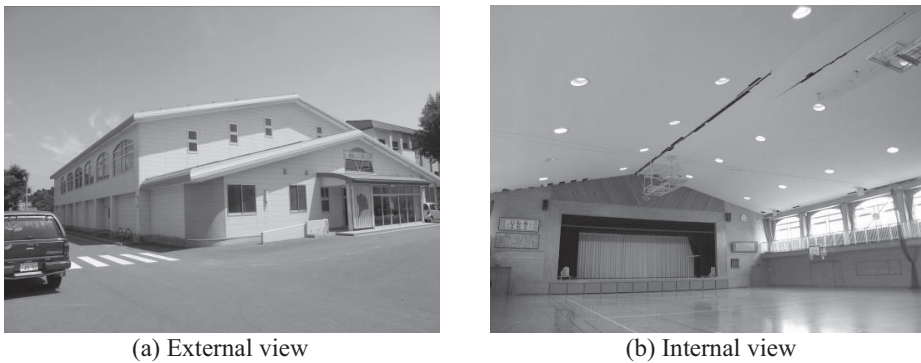


Figure 18. External and internal view of Gymnasium-5

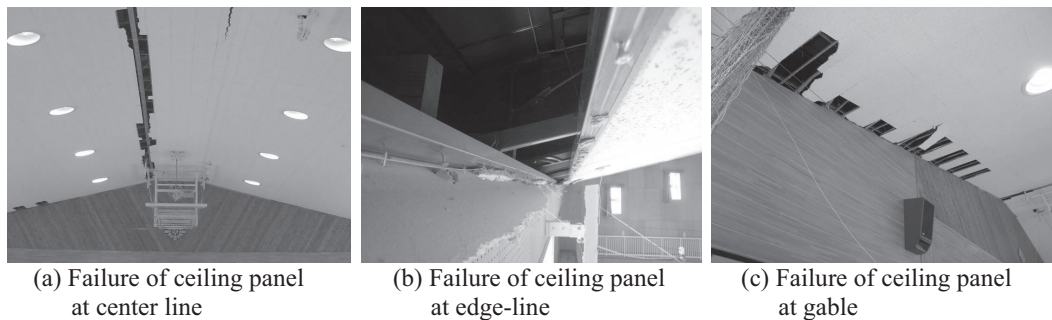


Figure 19. Damage to Gymnasium-5



Figure 20. Hunger bolts normal to the slope near edge-line of ceiling at Gymnasium-5

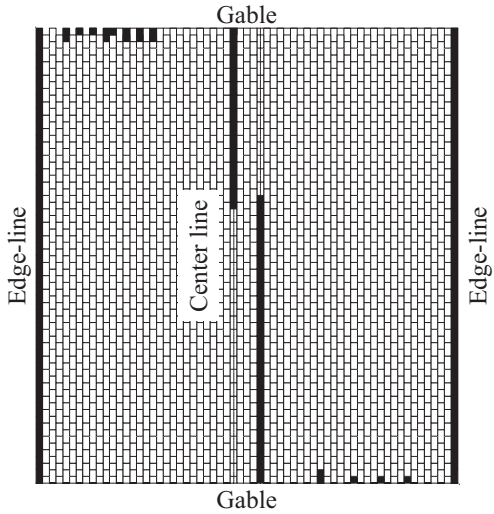


Figure 21. Plan view of failed ceiling panel of Gymnasium-5

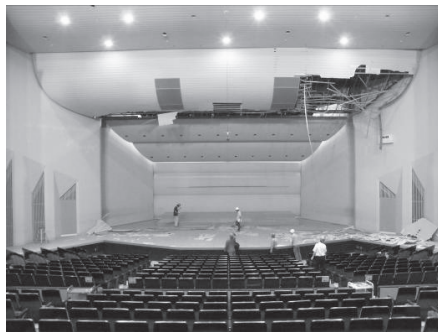
Auditorium-1

At a public auditorium (Fig. 22), ceiling panels, which were placed above its orchestra pit had fallen off (Fig. 23). The ceiling had the function as a movable acoustic reflector, balanced with a set of counter weights at the back of the stage. While there were no prints of collision of the ceiling to the wall placed very loosely to the panel, the heavy counter weight had been derailed from a guiding rail as shown in Fig. 23(e). It can be said that, during the earthquake, the ceiling and the counter weights, connected each other through hanging cables, jumped up and down heavily. As shown in Fig. 24, the ceiling had a free edge like a cantilever stuck out horizontally. It can be said that the damage had begun at the free edge while the ceiling were heavily moved.

The auditorium had experienced damage during the 1994 Sanriku-Haruka-Oki Earthquake[3]. However, the failure of ceiling during the previous earthquake occurred not above orchestra pit but above audience seats. After that, ceiling above audience seats equipped braced, but damage during the Iwateken Engan-Hokubu Earthquake indicated that different damage may occur due to the difference of seismic input.

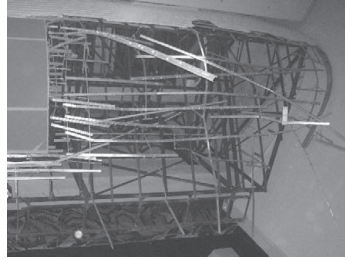


(a) External view

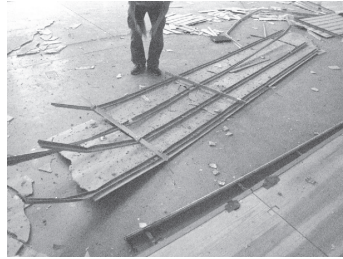


(b) Internal view

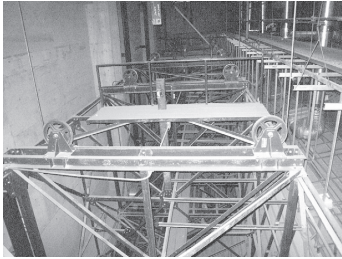
Figure 22. External and internal view of Auditorium-1



(a) Failure of ceiling



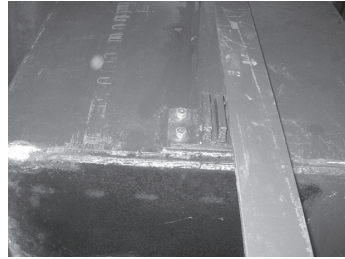
(b) Fallen ceiling panel



(c) Movable frame of ceiling



(d) Counter weight



(e) Counter weight and guide rail

Figure 23. Damage to Auditorium-1

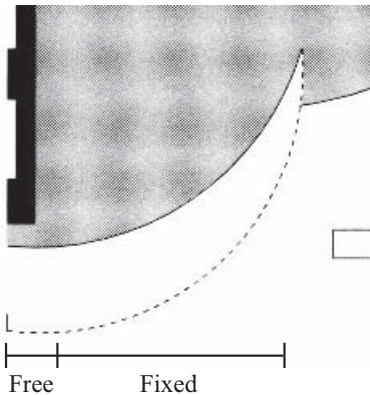


Figure 24. Cross section of ceiling

CONCLUSIONS

From the field investigations after the two major earthquakes, it can be concluded that:

- 1) Damage to ceiling panels under exterior eaves was significant.
- 2) The northeastern region of Japan had been hit by major earthquakes frequently in recent years. Nevertheless, the similar damage had been repeated, since the failed parts have been fixed and recovered always with no essential improvements.

The vicious fact is that past damages were not used to prevent possible large damage in future, including injury to people. Especially, large roof buildings such as gymnasiums are used as shelters during disasters, and may harm people by themselves if their non-structural components are not improved suitably. Immediate improvements are necessary with support of the administration.

ACKNOWLEDGMENT

We are grateful to the National Research Institute for Earth Science and Disaster Prevention, Japan

for opening motion data of strong earthquakes to the public.

REFERENCES

- [1] Japan Meteorological Agency: Iwate-Miyagi Nairiku Earthquake in 2008 (in Japanese), Report of natural phenomenon in disaster,
“http://www.jma.go.jp/jma/kishou/books/saigaiji/saigaiji_200801.pdf”, 2008.
- [2] Japan Meteorological Agency: Earthquake in Iwateken Engan-Hokubu on July 24, 2008 (in Japanese), Report of natural phenomenon in disaster,
“http://www.jma.go.jp/jma/kishou/books/saigaiji/saigaiji_200802.pdf”, 2008.
- [3] Architectural Institute of Japan: Report on the Damage Investigation of the 1994 Hokkaido-Toho-Oki Earthquake and the 1994 Sanriku-Haruka-Oki Earthquake (in Japanese), Tokyo, 1996.

**LIST OF PAPERS BY MEMBERS OF
EARTHQUAKE RESISTANT STRUCTURE RESEARCH CENTER**

SEISAN-KENKYU : Monthly Journal of the Institute of Industrial Science,
The University of Tokyo

JSCE : The Japan Society of Civil Engineers

JSME : The Japan Society of Mechanical Engineers

AIJ : The Architectural Institute of Japan

JCI : Japan Concrete Institute

JSSC : The Japan Society of Steel Construction

JGS : The Japanese Geotechnical Society

JAEE : The Japan Association for Earthquake Engineering

* : Written in Japanese

K. Konagai, T. Fujita, T. Ikeda and S. Takatsu, Tectonic deformation buildup in folded mountain terrains in the October 23, 2004, Mid-Niigata Earthquake, *Soil dynamics and earthquake engineering*, 29(2), 261-267, 2009.

K. Konagai, T. Fujita, T. Ikeda and S. Takatsu, Kizawa tunnel cracked on 23 October 2004 Mid-Niigata earthquake: An example of earthquake-induced damage to tunnels in active-folding zones, *Soil dynamics and earthquake engineering*, 29(2), 394-403, 2009.

K. Konagai, Huge landslides caused by massive earthquakes and long-lasting geotechnical risks, Landslides – Disaster risk reduction –, Kyoji Sassa/ Paolo Canuti eds., Springer, ISBN 978-3-540-69966-8, 159-176, 2009.

K. Konagai, T. Fujita, T. Ikeda and S. Takatsu, Landform changes in an active folding zone induced by the October 23, 2004, Mid Niigata Earthquake, Japan, 14th World Conference on Earthquake Engineering, Beijing, China, Paper-ID: 01-1001, Oct. 12-17, 2008.

K. Konagai, J. Johansson, T. Ikeda, S. Takatsu, F. Nomura and Y. Tomiyasu, Geological conditions and soil deformations in the July 17, 2007, Chuetsu Off-shore Earthquake, 14th World Conference on Earthquake Engineering, Beijing, China, Paper-ID: 01-1002, Oct. 12-17, 2008.

T. Ikeda, K. Konagai and S. Takatsu, The Construction of earthquake damage data archives for

earthquake disaster mitigation, 14th World Conference on Earthquake Engineering, Beijing, China, Paper-ID: 01-1066, Oct. 12-17, 2008.

K. Konagai, T. Fujita, T. Ikeda and S. Takatsu, Deformation Buildup in Tertiary Rocks in the October 23, 2004 Mid-Niigata Earthquake, Geotechnical Earthquake Engineering and Soil Dynamics, Sacramento, CA, May 18-22, 2008.

K. Konagai, S. Tsuchiya, Y. Ishikawa and F. Wang, Provisional report of landslides, debris mass flows in the May 12th 2008, Wenchuan Earthquake, SEISANKENKYU, 60(6), 3-8, 2008

K. Konagai, J. Johansson, Y. Tajima, Y. Tomiyasu, F. Nomura, M. Date, and T. Katagiri, Provisional report of damage caused by the June 14th 2008, Iwate/Miyagi Prefectures Earthquake, SEISANKENKYU, 60(6), 9-14, 2008.

Y. Nakano, Design Load Evaluation for Tsunami Shelters Based on Damage Observations after Indian Ocean Tsunami Disaster Due to the 2004 Sumatra Earthquake, Proceedings of the 14th World Conference on Earthquake Engineering, Paper ID 15-0008, October 12-17, 2008, Beijing, China.

N. Takahashi and Y. Nakano, Impact of R/C Building Components on Its Seismic Reparability Due to the Life Cycle Economic Loss, Proceedings of the 14th World Conference on Earthquake Engineering, Paper ID 10-0022, October 12-17, 2008, Beijing, China.

Y. Sanada, N. Yamauchi, E. Takahashi, Y. Nakano, and Y. Nakamura, Interlocking Block Infill Capable of Resisting Out-of-Plane Loads, Proceedings of the 14th World Conference on Earthquake Engineering, Paper ID 05-04-0018, October 12-17, 2008, Beijing, China.

H. Choi and Y. Nakano, Residual Seismic Performance of RC Frames with Unreinforced Masonry Infill, Proceedings of the 14th World Conference on Earthquake Engineering, Paper ID 05-04-0005, October 12-17, 2008, Beijing, China.

Y. Nakano and W.J. Yang, Substructure Online Test Using Parallel Hysteresis Modeling by Neural Network, Proceedings of the 14th World Conference on Earthquake Engineering, Paper ID 12-01-0185, October 12-17, 2008, Beijing, China.

Y. Nakano, Damage to Buildings due to 2008 May 12 Wenchuan Earthquake and Cooperative

Activities for Damage Restoration by Japanese Experts, Proceedings of the 7th International Symposium on New Technologies for Urban Safety of Mega Cities in Asia (7USMCA), pp. 89-98, Tsinghua University, Beijing, China, October 21-22, 2008.

Y. Nakano, Building Damage due to 2008 Sichuan (Wenchuan) Earthquake and Cooperative Activities on Damage Restoration by Japanese Experts, Proceedings of the 34th National Convention, CD-ROM, Philippine Institute of Civil Engineers, Cagayan de Oro City, Philippines, November 27-29, 2008.

*S. Yamada, Y. Takei and T. Fujita, Feasibility Study on Structure-Born Noise Control of Steel Railway Bridge Utilizing Piezoelectric Actuators, Transactions of AIJ, Vol. 73, No. 626, pp. 527-533, 2008.4

T. Kamada and T. Fujita, State of the Art of Development and Application of Antiseismic Systems in Japan, 2008 Seismic Engineering International Conference commemorating 1908 Messina and Reggio Calabria Earthquake, Reggio Calabria, Italy, 2008.7

E. Sato and T. Fujita, Study on Application of Controllable Dampers Using Smart Materials to Full-Scale Base-Isolated Buildings, 14th World Conference on Earthquake Engineering, Paper No. 11-0094, Beijing, China, 2008.10

H. Hora, M. Yasuda, T. Osako, Y. Noguchi, H. Kato, T. Fujita and M. Shimazaki, Feasibility Study of Active Micro-Vibration Control System Using Piezoelectric Actuators for Floor Structure of Precision Manufacturing Facilities, 14th World Conference on Earthquake Engineering, Paper No. 05-06-0027, Beijing, China, 2008.10

T. Atsumi, H. Kitamura, T. Fujita, M. Miyazaki, K. Sasaki, M. Ishii and K. Yoshie, Shaking Table Tests for a 10-Story Frame using Combinations of Hysteretic and Viscous Dampers, 14th World Conference on Earthquake Engineering, Paper No. 05-06-0046, Beijing, China, 2008.10

O. Takahashi, H. Hasegawa, Y. Kunimatsu, H. Aida, J. Suhara, R. Matsumoto, H. Torita, S. Okamoto, Y. Tsuyuki, T. Kamei, and T. Fujita, Construction of Civil Building Using Three Dimensional Seismic Isolation System (Part 1, Design of Building Using Three Dimensional Seismic Isolation System), 14th World Conference on Earthquake Engineering, Paper No. 05-06-0107, Beijing, China, 2008.10

J. Suhara, R. Matsumoto, H. Torita, S. Okamoto, Y. Tsuyuki, T. Kamei, and T. Fujita, Construction of Civil Building Using Three Dimensional Seismic Isolation System (Part 2, Tests for Three Dimensional Seismic Isolation System), 14th World Conference on Earthquake Engineering, Paper No. 05-06-0086, Beijing, China, 2008.10

M. Shimazaki and T. Fujita, Experimental Study of Piezoelectric Actuators and Magnetostrictive Actuators for Large-Scale Smart Structures, 14th World Conference on Earthquake Engineering, Paper No. 05-06-0117, Beijing, China, 2008.10

H. Furukawa, T. Fujita, T. Kamada and H. Misoka, Active-Passive Seismic Isolation System for Monocrystal Pullers, 14th World Conference on Earthquake Engineering, Paper No. 12-01-0212, Beijing, China, 2008.10

H. Tanaka, Y. Toi, K. Maeda and T. Sakai, Damage and fracture analysis of brittle structural elements reinforced with carbon fiber sheets, Journal of Environment and Engineering, 3(1), 111-122, 2008.

M. Takagaki, Y. Toi and T. Asayama, Analysis of thermal fatigue crack propagation based on local approach to fracture, Journal of Solid Mechanics and Materials Engineering, 2(5), 675-684, 2008.

Y. Toi and W.-S. Jung, Finite element modeling of electrochemical-poroelastic behaviors of conducting polymer films, Journal of Solid Mechanics and Materials Engineering, 2(7), 865-876, 2008.

Y. Toi and D.-G. Choi, Constitutive modeling of porous shape memory alloys considering strain rate effect, Journal of Computational Science and Technology, 2(4), 511-522, 2008.

Y. Toi and W.-S. Jung, Computational modeling of electrochemical-poroelastic bending behaviors of conducting polymer (PPy) membranes, Journal of Computational Science and Technology, 2(4), 523-534, 2008.

Y. Toi and D.-G. Choi, Computational modeling of superelastic behaviors of shape memory alloy devices under combined stresses, Journal of Computational Science and Technology, 2(4), 535-546, 2008.

J. Koseki, M. Tateyama, K. Watanabe and S. Nakajima, Geosynthetic-reinforced soils in Japan and their seismic behavior, Keynote Lecture, Proc. of International Workshop on Contributions of Geotechnical Engineering to Sustainable Civil Constructions, Indonesian Society for Geotechnical Engineering, Bandung, pp.1-12, 2008.

N. HongNam, J. Koseki and T. Sato, Effect of specimen size on quasi-elastic properties of Toyoura sand in hollow cylinder triaxial and torsional shear tests Geotechnical Testing Journal, ASTM, Vol.31 No.2, 2008.

T. Kiyota, T. Sato, J. Koseki and M.M. Abadi, Behavior of liquefied sands under extremely large strain levels in cyclic torsional shear tests, Soils and Foundations, Vol.48, No.5, pp.727-739, 2008.

J. Koseki, Y. Tsutsumi, T. Namikawa, S. Mihira, R. Salas-Monge, Y. Sano and S. Nakajima, Shear and tensile properties of cement-treated sands and their application to liquefaction mitigation, Keynote Lecture, Proc. of 4th International Symposium on Deformation Characteristics of Geomaterials (IS-Atlanta 2008), Vol. 1, pp. 27-50, 2008.

Y. Tsutsumi, T. Sato and J. Koseki, Strain localization characteristics of dense Toyoura sand in plane strain compression tests under different confining pressures, Proc. of 4th International Symposium on Deformation Characteristics of Geomaterials (IS-Atlanta 2008), Vol. 1, pp. 365-370, 2008.

L.I.N. DeSilva, J. Koseki, T. Sato, T. Kiyota and T. Honda, Quasi-elastic bulk modulus of sand based on volume change and local deformation measurement of hollow cylindrical specimen, Proc. of 4th International Symposium on Deformation Characteristics of Geomaterials (IS-Atlanta 2008), Vol. 2, pp. 775-781, 2008.

T. Namikawa, and J. Koseki, Fracture zone formation of cement-treated sand in plane strain compression tests, Proc. of 4th International Symposium on Deformation Characteristics of Geomaterials (IS-Atlanta 2008), Vol. 1, pp. 371-376, 2008.

T. Kiyota, J. Koseki and T. Sato, Interpreting natural aging effects on liquefaction properties of sands based on small strain characteristics, Proc. of 4th International Symposium on Deformation Characteristics of Geomaterials (IS-Atlanta 2008), Vol. 1, pp. 489-494, 2008.

S. Maqbool and J. Koseki, Development of an S-wave measurement system for laboratory specimens, Proc. of 4th International Symposium on Deformation Characteristics of Geomaterials (IS-Atlanta 2008), Vol. 2, pp. 711-715, 2008.

N. HongNam and J. Koseki, Behavior of dry Toyoura sand in large cyclic torsional loading with local strain measurement, Proc. of 4th International Symposium on Deformation Characteristics of Geomaterials (IS-Atlanta 2008), Vol. 2, pp. 801-807, 2008.

J. Lee, T. Mikami, T. Sato and J. Koseki, Effects of bedding error in cyclic triaxial tests on a granular material made from recycled glass, Proc. of 10th International Summer Symposium, International Activities Committee, JSCE, pp.89-92, 2008.9

J. Deng, Y. Tsutsumi, H. Kameya, T. Sato and J. Koseki, Triaxial tests on undisturbed samples retrieved from a failed slope at Higashi-Takezawa due to 2004 Niigata-ken Chuetsu Earthquake, Proc. of 10th International Summer Symposium, International Activities Committee, JSCE, pp.69-72, 2008.9

L.I.N. DeSilva, T. Sato and J. Koseki, Modelling of cyclic shear behavior of sand, Proc. of 10th International Summer Symposium, International Activities Committee, JSCE, pp.73-76, 2008.9

K. Hong, S. Nakajima and J. Koseki, A method to evaluate seismic earth pressure considering effects of negative pore air pressure in backfill soil, Proc. of 10th International Summer Symposium, International Activities Committee, JSCE, pp.129-132, 2008.9

J. Koseki, K. Hong, S. Nakajima and S. Mulmi, Negative pore air pressure generation in backfill soil of retaining walls during earthquake excitation, Proc. of Second Japan-Korea Geotechnical Engineering Workshop -Geotechnics in Urban Areas-, pp. 109-114, 2008.

Kuwano, R. and Miyashita, T., Model tests on behaviour of flexible buried pipe in sand with different densities, Proc. the International conference "Development of Urban Areas and Geotechnical Engineering", St. Petersburg, 2008.

Kuwano, R., Wicaksono, R.I. and Mulmi, S., Small strain stiffness of coarse granular materials measured by wave propagation, Proc. the 4th international symposium on deformation characteristics of geomaterials, IS-Atlanta 2008, Vol.2, 749-756, 2008.

Wicaksono, R.I., Tsutsumi, Y., Sato, T., Koseki, J., and Kuwano, R., Stiffness measurements by cyclic loading, trigger accelerometer, and bender element on sand and gravel, Proc. the 4th international symposium on deformation characteristics of geomaterials, IS-Atlanta 2008, Vol.2, 733-740, 2008.

*Kuwano, R. and Miyashita, T., Behaviour of flexible pipe under cyclic loading buried in sandy backfill with different densities, Seisan Kenkyu, Vol.60, No.3, 48-52, 2008.

*Miyashita, T. and Kuwano, R., Effects of backfill density and degree of deterioration on the deformation characteristics of double layer pipe under cyclic loading, Seisan Kenkyu, Vol.60, No.3, 53-56, 2008.

*Kuwano, R. and Miyashita, T., Effects of diameter and height of triaxial cylindrical specimen on bender element test, Seisan Kenkyu, Vol.60, No.3, 57-59, 2008.

R.I. Wicaksono and R. Kuwano, Study on Deformation Characteristic of Lightly Cemented Sand, Proc. of 10th International Summer Symposium, International Activities Committee, JSCE, 81-84, 2008.

Mulmi, S., Koseki, J. and Kuwano, R., Sample Size and Shape Effects in Bender Element Tests, Proc. of 10th International Summer Symposium, International Activities Committee, JSCE, 85-88, 2008.

Beltrán Galvis, A.L. and Kuwano, R., Small Strain Stiffness of Edosaki-Sand in Dry, Saturated and Partially Saturated Condition, Proc. of 10th International Summer Symposium, International Activities Committee, JSCE, 77-80, 2008.

Bagus, C., Ko, D.-H., Sato, T. and Kuwano R., Modified Model Test of Flexible Buried Pipe in Loose Backfill Sand Under Cyclic Loading, Proc. of 10th International Summer Symposium, International Activities Committee, JSCE, 125-128, 2008

Sato, M. and Kuwano, R., Experimental Study on the Evaluation of Loose Ground Surrounding a Cavity in Soil, Proc. the 7th International symposium on new technologies for urban safety of mega cities in Asia, USMCA, Beijing, October 2008, 751-758, 2008.

Kuwano, R., Ko, D.-H. and Bagus, C., Model Tests on the Behavior of Flexible Buried Pipe in

sandy backfill with insufficient compaction, Proc. the 7th International symposium on new technologies for urban safety of mega cities in Asia, USMCA, Beijing, October 2008, 741-750, 2008.

Ko, D.-H., Cokorda, B.P.D. and Kuwano, R., Deformation and stresses acting on Flexible Buried Pipe in sandy backfill under repeated loading, Proc. the 2nd Japan-Korea Geotechnical Engineering Workshop, Geotechnics in Urban Areas, 41-46, 2008.

Wicaksono, R.I., Kuwano, R., De Silva, L.I.N., Mulmi, S., Enomoto, T., Kiyota and Tsutsumi, Y., Small Strain Stiffness of Toyoura Sand Obtained from Various Techniques in the IIS, Seisan Kenkyu, Vol.60, No.6, 561-564, 2008.

Mulmi, S., Sato, T. and Kuwano, R., Performance of Plate Type Piezo-ceramic Transducers for Elastic Wave Measurements in Laboratory Soil Specimens, Seisan Kenkyu, Vol.60, No.6, 565-569, 2008.

Kohiyama Masayuki, Kiremidjian Anne S., Meguro Kimiro, Ohara Miho Yoshimura, Incentives and Disincentives Analysis for Improving Policy for Seismic Risk Management of Homeowners in Japan, Natural Hazards Review, American Society of Civil Engineers, V.9/No.4/P.170-178, 2008.11.

Kondo Shinya, Meguro Kimiro, An analysis of a local government's Disaster response activity records from the viewpoint of information management, Journal of Disaster Research, Vol.3, No.6, pp.457-466, 2008.12.

Meguro Kimiro, Promotion of Seismic Retrofitting for Existing Low Earthquake Resistant Structures: The Most Important Issue for earthquake Disaster Reduction, pp.29-74, Vulnerable Cities: Realities, Innovations and Strategies, Edited by T. Kidokoro, J. Okata, S. Matsumura, N. Shima, 330p, Springer, 2008.

Mariko Abe, Kimiro Meguro, A Study for Improving the Total Disaster Reduction Ability of Little Children's Guardians, Proceedings on 14th World Conference on Earthquake Engineering, CD-Rom, 2008.10.

Kondo Shinya, Meguro Kimiro, Proposal of a New Disaster Manual for Implementation of Efficient Disaster Management Measures, Proceedings on 14th World Conference on

Earthquake Engineering, CD-Rom, 2008.10.

Meguro Kimiro, Strategy for Taking Full Advantage of Earthquake Early Warning System for Earthquake Disaster Reduction, Proceedings on 14th World Conference on Earthquake Engineering, CD-Rom, 2008.10.

Meguro Kimiro, Ito Daisuke, Sato Yoshihito, Efficiency of Furniture Overturning Protection Devices During Earthquakes - A Experimental and Numerical Study, Proceedings on 14th World Conference on Earthquake Engineering, CD-Rom, 2008.10.

Meguro Kimiro, Technological and Social Approaches to Achieve Earthquake Safer Non-Engineered Houses, Proceedings on 14th World Conference on Earthquake Engineering, CD-Rom, 2008.10.

Mayorca Paola, Meguro Kimiro, A Step Towards the Formulation of a Simple Method to Design PP-Band Mesh Retrofitting for Adobe/Masonry Houses, Proceedings on 14th World Conference on Earthquake Engineering, CD-Rom, 2008.10.

Worakanchana Kawin, Mayorca Paola, Guragain, Ramesh; Navaratnaraj, Sathiparan; Meguro, Kimiro: 3-D Applied Element Method for PP-Band Retrofitted Masonry, Proceedings on 14th World Conference on Earthquake Engineering, CD-Rom, 2008.10.

Worakanchana Kawin, Meguro Kimiro, Voronoi Applied Element Method for Structural Analysis: Theory and Application for Linear and Non-Linear Materials, Proceedings on 14th World Conference on Earthquake Engineering, CD-Rom, 2008.10.

Ohara Miho Yoshimura, Nakashima Naomi, Meguro Kimiro, A Study on the Effect of Land Use Control by Active Fault Zoning in Japan, Proceedings on 14th World Conference on Earthquake Engineering, CD-Rom, 2008.10.

Uehan Fumiaki, Meguro Kimiro, Development of Non-Contact Vibration Measuring System for Inspection of Seismic Damage to Railway Structures, Proceedings on 14th World Conference on Earthquake Engineering, CD-Rom, 2008.10.

Ohara Miho Yoshimura, Kitsuta Yoichi, Yahagi Naoki, Koyama Fujio, Meguro Kimiro, Study on Use of E-learning System for Increasing Emergency Response Capacity of Doctors and

Nurses in Hospitals, Proceedings on 14th World Conference on Earthquake Engineering, CD-Rom, 2008.10.

Sathiparan Navaratnarajah, Paola Mayorca, Meguro Kimiro, Parametric Study on Diagonal Shear and Out of Plane Behavior of Masonry Wallettes Retrofitted by PP-Band Mesh, Proceedings on 14th World Conference on Earthquake Engineering, CD-Rom, 2008.10.

Hada Yasunori, Kodama Noriko, Suzuki Takeyasu, Meguro Kimiro, Road Information Sharing Using Probe Vehicle Data in Disasters, Proceedings on 14th World Conference on Earthquake Engineering, CD-Rom, 2008.10.

Kimiro Meguro, Strategy for Efficient Use of Earthquake Early Warning System for Earthquake Disaster Reduction, Proceedings of the 7th International Symposium on New Technologies for Urban Safety of Mega Cities in Asia, CD-ROM, Beijing, China, 2008.10.

Sathiparan Navaratnarajah, Mayorca Paola, Meguro Kimiro, Shaking Table Test of Timber Masonry House Models Retrofitted by PP-band Meshes, Proceedings of the 7th International Symposium on New Technologies for Urban Safety of Mega Cities in Asia, CD-ROM, Beijing, China, 2008.10.

Mayorca Paola, Meguro Kimiro, Relation between Strength Reduction and Ductility Demand for PP-Band Mesh Retrofitted Houses, Proceedings of the 7th International Symposium on New Technologies for Urban Safety of Mega Cities in Asia, CD-ROM, Beijing, China, 2008.10.

Meguro Kimiro, Kawasaki Akiyuki, Torres Tatiana, Integrated Information System for Landslide Disaster Management, Proceedings of the 7th International Symposium on New Technologies for Urban Safety of Mega Cities in Asia, CD-ROM, Beijing, China, 2008.10.

Kawasaki Akiyuki, Rogers Peter, Herath Srikantha, Meguro Kimiro, Considering the Impact of Climate and Land Cover Change on a Local Hydrological Flow: The Case Study of Srepok River Basin in Viet Nam and Cambodia, Proceedings of the 7th International Symposium on New Technologies for Urban Safety of Mega Cities in Asia, CD-ROM, Beijing, China, 2008.10.

Ohara Miho Y., Kitsuta Yoichi, Yahagi Naoki, Koyama Fujio, Miyazaki Sanae, Meguro Kimiro, Development of E-learning Contents for Increasing Emergency Response Capacity of Doctors and Nurses in Key Disaster Hospitals, Proceedings of the 7th International Symposium on New

Technologies for Urban Safety of Mega Cities in Asia, CD-ROM, Beijing, China, 2008.10.

Mariko Abe, Kimiro Meguro, A Study for Promoting Communication between Research Institutes and General Society, Proceedings of the 7th International Symposium on New Technologies for Urban Safety of Mega Cities in Asia, CD-ROM, Beijing, China, 2008.10.

Worakanchana Kawin, Mayorca, Paola, Guragain Ramesh, Navaratnaraj Sathiparan, Meguro Kimiro, 3-D Applied Element Method for Static Non-linear Simulation of PP-Band Retrofitted Masonry, Bulletin of Earthquake Resistant Structure Research Center, No.41 pp.45-54, 2008.3.

Iritani Satoshi, Mayorca Paola, Meguro Kimiro, Proposal of A system to Promote Retrofitting of Vulnerable Masonry Houses in Developing Countries, Bulletin of Earthquake Resistant Structure Research Center, No.41 pp.55-60, 2008.3.

Ohara Miho Yoshimura, Nakashima Naomi, Meguro Kimiro, A Basic Study on Effect of Land use Controll Plan Along Active Faults in Japan, Bulletin of Earthquake Resistant Structure Research Center, No.41 pp.61-66, 2008.3.

Fujieda Takumi, Mayorca Paola, Navaratnaraj Sathiparan, Meguro Kimiro, Experimental Study of the Behavior of PP-band Mesh Retrofitted Masonry Houses using Miniature Models, Bulletin of Earthquake Resistant Structure Research Center, No.41 pp.67-72, 2008.3.

S. Kumagai, K. Kawaguchi, M. Araya, T. Nagai and H. Hirama, Numerical Simulation of the Suspended Ceiling Failed during 2005 Miyagiken-Oki Earthquake - Dynamics Behavior of the Suspended Ceiling - (in Japanese), Journal of Structural Engineering, Vol. 55B, 2009, pp. 453-458.

T. Nagai, K. Ando, K. Kawaguchi, M. Araya and S. Kumagai, Simple Dynamic Response Analysis of Large Suspended Ceilings - Formulation and Numerical Results Based on Plane Stress Approach - (in Japanese), Journal of Structural Engineering, Vol. 55B, 2009, pp. 447-452.

Y. Ozawa and K. Kawaguchi, A Study of Interaction Between Units in Unit-Based Tension Structures - Elastic Spring Replacement Making Use of Symmetry and Evaluation for the Effect of Interaction - (in Japanese), Journal of Structural Engineering, Vol. 55B, 2009, pp. 41-48.

M. Miki and K. Kawaguchi, Fundamental Study on Shape-Finding of Tension Structures and

Related Functionals (in Japanese), Journal of Structural Engineering, Vol. 55B, 2009, pp. 35-40.

Y. Ozawa and K. Kawaguchi, A Simple Method for Introducing Tensile Force in Unit-Based Tension Structures (in Japanese), Journal of Structural and Construction Engineering, Transactions of AIJ, Vol. 74, No. 637, 2009, pp. 511-518.

R. Takahama and K. Kawaguchi, Fundamental Research for Seismic Response of Roller Bearings and/or Sliding Bearings (in Japanese), Journal of Structural and Construction Engineering, Transactions of AIJ, Vol. 74, No. 635, 2009, pp. 41-45.

M. Miki and K. Kawaguchi, Examples of Form Finding Analysis of Tension Structures Using Functionals (in Japanese), the 24th Symposium on Space Structure and Materials, Sagamihara, Japan, Dec. 2008, pp. 125-128.

S. Yoshinaka and K. Kawaguchi, Vibration Control of Spatial Structures Using Spatially Distributed MTMDs, Memoirs of the Faculty of Engineering, Osaka City University, Vol.49, 2008, pp.19-28.

K. Kawaguchi, Y. Ogi, S. Ohya, S. Katayama, S. Kumagai and S. Sakurai, Damage to Nonstructural Components in Large Roof Buildings Failed during the Iwate-Miyagi Nairiku Earthquake and Iwateken-Engan Hokubu Earthquake in 2008 (in Japanese), Seisan Kenkyu, Vol. 60, No. 6, 2008, pp. 541-554.

K. Kawaguchi, W.-L. Ke and M. Miki, Minimal Surface with Constraint Conditions and Steepest Descent Method (in Japanese), Journal of Structural and Construction Engineering, Transactions of AIJ, Vol. 73, No. 632, 2008, pp. 1773-1777.

K. Kawaguchi and T. Kawata, Group Theory Approach of a Tensegrity Model with Mechanisms (in Japanese), Journal of Structural and Construction Engineering, Transactions of AIJ, Vol. 73, No. 631, 2008, pp. 1569-1576.

S. Yoshinaka and K. Kawaguchi, Vibration Control of Large Span Structures Using Spatially Distributed MTMDs - Division of MTMDs and its Effect of Vibration Control - (in Japanese), Journal of Structural and Construction Engineering, Transactions of AIJ, Vol. 73, No. 631, 2008, pp. 1551-1559.

R. Takahama and K. Kawaguchi, Fundamental Research for Seismic Response of Roller Bearings (in Japanese), Summaries of Technical Papers of Annual Meeting, Architectural Institute of Japan, Higashihiroshima, Japan, Sep. 2008, CD-ROM, No. 21178, pp. 355-356.

T. Kawata, K. Kawaguchi, Group Theory Approach Applied to a Tensegrity Model with Mechanisms (in Japanese), Summaries of Technical Papers of Annual Meeting, Architectural Institute of Japan, Higashihiroshima, Japan, Sep. 2008, CD-ROM, No. 20492, pp. 983-984.

Y. Ozawa and K. Kawaguchi, Group Theory Approach for Finding Equivalent Springs for Unit-Assembled Tension Structures (in Japanese), Summaries of Technical Papers of Annual Meeting, Architectural Institute of Japan, Higashihiroshima, Japan, Sep. 2008, CD-ROM, No. 20491, pp. 981-982.

K. Suzuki, K. Kawaguchi and S. Oya, Fundamental Study of Development of a Reusable Deployable Arch System (in Japanese), Summaries of Technical Papers of Annual Meeting, Architectural Institute of Japan, Higashihiroshima, Japan, Sep. 2008, CD-ROM, No. 20484, pp. 967-968.

S. Yoshinaka and K. Kawaguchi, Vibration Control of Spatial Structures Using Distributed MTMD Method (Division of MTMDs and its Effect of Vibration Control) (in Japanese), Summaries of Technical Papers of Annual Meeting, Architectural Institute of Japan, Higashihiroshima, Japan, Sep. 2008, CD-ROM, No. 20443, pp. 885-886.

Y. Ozawa and K. Kawaguchi, Preliminary Study of Safety Nets for Suspended Ceilings (in Japanese), Summaries of Technical Papers of Annual Meeting, Architectural Institute of Japan, Higashihiroshima, Japan, Sep. 2008, CD-ROM, No. 20409, pp. 817-818.

S. Oya, K. Kawaguchi, S. Yoshinaka, A. Otsuka and S. Katayama, Comparison of Damage to Suspended Ceilings in Wide Roof Buildings by Niigata-Chuetsu and Chuetsu-Oki Earthquakes (in Japanese), Summaries of Technical Papers of Annual Meeting, Architectural Institute of Japan, Higashihiroshima, Japan, Sep. 2008, CD-ROM, No. 20408, pp. 815-816.

K. Ando, K. Kawaguchi, T. Nagai, M. Araya and S. Kumagai, In-Plane Dynamic Analysis of Large Suspended Ceilings Part 2 Dynamic Response of a Suspended Ceiling Under a Gabled Roof (in Japanese), Summaries of Technical Papers of Annual Meeting, Architectural Institute of Japan, Higashihiroshima, Japan, Sep. 2008, CD-ROM, No. 20399, pp. 797-798.

T. Nagai, K. Kawaguchi, K. Ando, M. Araya and S. Kumagai, In-Plane Dynamic Analysis of Large Suspended Ceilings Part 1 In-Plane Formulation of Elastic Behavior of Ceiling Panels (in Japanese), Summaries of Technical Papers of Annual Meeting, Architectural Institute of Japan, Higashihiroshima, Japan, Sep. 2008, CD-ROM, No. 20398, pp. 795-796.

S. Kumagai, K. Kawaguchi, T. Nagai, M. Araya and K. Ando, Dynamics of Suspended Ceilings Hanged by Hangers with Different Length (in Japanese), Summaries of Technical Papers of Annual Meeting, Architectural Institute of Japan, Higashihiroshima, Japan, Sep. 2008, CD-ROM, No. 20397, pp. 793-794.

Y. Chen and K. Kawaguchi, Preliminary Research of Computational Morphogenesis with Inverted Force Density Method (in Japanese), Summaries of Technical Papers of Annual Meeting, Architectural Institute of Japan, Higashihiroshima, Japan, Sep. 2008, CD-ROM, No. 20388, pp. 775-776.

M. Miki, K. Kawaguchi and W.-L. Ke, Minimal Surfaces with Constraints and their Existence on the Solution-Surface (in Japanese), Summaries of Technical Papers of Annual Meeting, Architectural Institute of Japan, Higashihiroshima, Japan, Sep. 2008, CD-ROM, No. 20384, pp. 767-768.

Y. Xu and K. Kawaguchi, A New Method in Deployment Analysis of Membrane Structure, Summaries of Technical Papers of Annual Meeting, Architectural Institute of Japan, Higashihiroshima, Japan, Sep. 2008, CD-ROM, No. 20383, pp. 765-766.

S. Katayama, K. Kawaguchi, S. Yoshinaka, S. Oya and A. Otsuka, Preliminary Study of Safety of Non-Structural Components in Wide Roof Buildings, Part3: Impact Hammer Experiment with a Dummy Head (in Japanese), Summaries of Technical Papers of Annual Meeting, Architectural Institute of Japan, Higashihiroshima, Japan, Sep. 2008, CD-ROM, No. 1107, pp. 213-214.

A. Otsuka, K. Kawaguchi, S. Yoshinaka, S. Oya and S. Katayama, Preliminary Study of Safety of Non-Structural Components in Wide Roof Buildings, Part2: Human Body Tolerance Applied for the Safety Criteria of Non-Structural Components (in Japanese), Summaries of Technical Papers of Annual Meeting, Architectural Institute of Japan, Higashihiroshima, Japan, Sep. 2008, CD-ROM, No. 1106, pp. 211-212.

T. Uchida, K. Kawaguchi, S. Yoshinaka, A. Otsuka and S. Katayama, Preliminary Study of Safety of Non-Structural Components in Wide Roof Buildings, Part1: Floor Area and Suspended height of Ceiling (in Japanese), Summaries of Technical Papers of Annual Meeting, Architectural Institute of Japan, Higashihiroshima, Japan, Sep. 2008, CD-ROM, No. 1105, pp. 209-210.

K. Kawaguchi, S. Yoshinaka, A. Otsuka and S. Katayama, Comparison of Damage to Nonstructural Components (Suspended Ceilings) in Large Enclosures by Niigata-Chuetsu and Chuetsu-Oki Earthquakes (in Japanese), AIJ Journal of Technology and Design, Vol. 14, No. 27, 2008, pp. 73-78.

K. Kawaguchi, K. Abe, J. Abe, T. Taguchi and R. Takahama, Development of New Base-Isolation System for Detached Houses and Full-Scale Shaking Table Test (in Japanese), AIJ Journal of Technology and Design, Vol. 14, No. 27, 2008, pp. 49-54.

K. Kawaguchi, K. Abe, J. Abe, T. Taguchi and R. Takayama, A New Base-Isolation System using Gage-Pendulum Principle for Light Timber Structures for the Safety of Their Structural and Non-Structural Components, Bulletin of Earthquake Resistant Structure Research Center, No. 41, 2008, pp. 73-76.

News

After the 2008 devastating Wenchuan Earthquake in Sichuan Province, international academic societies expressed great deal of condolences and showed great concerns to the related scientific issues. With the Grants-in-Aid for Scientific Research, Ministry of Education, Culture, Sports, Science and Technology, Japan (MEXT hereafter) and the network of Japanese experts in the field of seismology, geology and earthquake engineering organized a team (Leader: K. Konagai, the first author) asking collaboration from Chinese organizations and experts with the China Earthquake Administration (CEA) as its core, with the support from Ministry of Science and Technology of China. Professor Konagai visited Beijing three times to have kick-off meetings with experts from CEA and Dalian University of Technology and Sichuan Province two times to survey mountainous regions affected by the earthquake. He also attended the China-Japan Symposium on Seismic disaster Prevention and Mitigation, Oct. 8-12, 2008, Chendu organized by the Japan Society for Promotion of Science (JSPS), National Institute of Earth Science and Disaster Prevention, Japan (NIED) and Chinese Academy of Science (CAS), and 2nd China-Japan Science Forum, “The 2008 Wenchuan Earthquake and Natural Disaster Mitigation,” March 9-10, 2009, Beijing, organized by JSPS, CEA and National Natural Science Foundation, China (NSFC).

Professor Kazuo Konagai attended the 1st World Landslide Forum (Nov. 18-21, 2008), United Nations University, with the International Consortium on Landslides (ICL) as the key organizer. He provided an invited lecture on the “Huge landslides caused by massive earthquakes and long-lasting geotechnical risks”.

Professor Kazuo Konagai attended a technical seminar at Padang, Indonesia (Aug 25 - 28) as the President of the Engineers without Borders, Japan (EWBJ). The opening of the seminar was a kick-off ceremony of the earthquake observation system project for the West-Sumatra Province with four seismometers provided by EWBJ. Prof. Dr. Ismail Febrin, Dean of Engineering Faculty, Andalas University, will lead the project.

Prof. Kazuo Konagai and his laboratory members made survey trips twice to both Muzaffarabad and Hattian Ballah landslide area, the first and second trips for June 23 to July 1, and Nov. 24 to Dec. 2, respectively. They have measured landforms at these different times to check if the landforms would change. Their papers with some new findings are available in this volume of the ERS Bulletin.

Prof. Kazuo Konagai attended the 14th World Conference on Earthquake Engineering, Oct. 13 – 17, Beijing.

Prof. Kazuo Konagai and his laboratory members made reconnaissance trips, the first one from June 15 to 17, the second from July 12 to 14, and then Sept. 8 to 9, to the areas affected by the Mid Iwate/Miyagi Prefectures Earthquake of June 14th, 2008.

Prof. Jorgen Johansson moved to the Norwegian Geotechnical Institute (NGI) on Dec. 1, 2008.

Professor Y. Nakano was invited to Indonesia-Japan Joint Seminar –Technical Seminar for Earthquake Disaster Mitigation–, held at Andalas University, Padang, Indonesia, on January 28. He made a presentation on "Seismic Evaluation and Rehabilitation of Vulnerable RC Buildings -Experiences and Lessons in Japan-".

Professor Y. Nakano visited Sichuan Province, China and surveyed areas affected by the 2008 May 12 Wenchuan, China Earthquake, during the period of May 28 to June 1. He inspected damaged buildings suffered by the earthquake, and recommended necessary actions including repair, rehabilitation, reconstruction etc. to be taken on the buildings.

Professor Y. Nakano attended the China-Japan Workshop on Rehabilitation Techniques of Damaged Buildings suffered by the 2008 May 12 Wenchuan, China Earthquake, held at Southwest Jiaotong University, Chengdu city, Sichuan Province, China, during the period of June 20 to 25. He made a presentation on "Seismic Rehabilitation of Existing buildings in Japan".

Professor Y. Nakano was invited to the guest lectures held at Southwest Jiaotong University, Chengdu city, Sichuan Province, China, during the period of September 13 to 16. He made presentations on "Seismic Evaluation of Existing buildings in Japan" and "Seismic Rehabilitation of Existing buildings in Japan".

Professor Y. Nakano and Dr. N. Takahashi attended the 14th World Conference on Earthquake Engineering held in Beijing, China, during the period of October 12 to 17. Professor Y. Nakano presented "Design Load Evaluation for Tsunami Shelters Based on Damage Observations after Indian Ocean Tsunami Disaster Due to the 2004 Sumatra Earthquake" and "Substructure Online Test Using Parallel Hysteresis Modeling by Neural Network". Dr. N. Takahashi presented "Impact of R/C Building Components on Its Seismic Reparability Due to the Life Cycle Economic Loss".

Professor Y. Nakano attended the 7th International Symposium on New Technologies for Urban Safety of Mega Cities in Asia held in Beijing, China, during the period of October 21 to 22 and he made a presentation on "Damage to Buildings due to 2008 May 12 Wenchuan Earthquake and Cooperative Activities for Damage Restoration by Japanese Experts".

Dr. H. Choi attended the 28th Annual Conference in Architectural Institute of Korea held in Kwangju city, Korea, during the period of October 24 to 25 and he made a presentation on "The Relationship between Residual Crack Width and Residual Deformation of Reinforced Concrete Column".

Professor Y. Nakano was invited to the 34th National Convention of Philippine Institute of Civil Engineers, held in Cagayan de Oro city, Philippines, on November 29. He made a presentation on "Building Damage Due to 2008 Sichuan (Wenchuan) Earthquake and Cooperative Activities on Damage Restoration by Japanese Experts". He was also invited to the guest lectures held at University of The Philippines, Manila, Philippines, on December 2. He made a presentation on "Recovery and Reconstruction after the Wenchuan, China Earthquake of 2008".

Professor J. Koseki made a keynote lecture at the conference on Geosynthetics for Soil Reinforcement held in Perugia, Italy, 12 February 2008.

Professor J. Koseki attended the US-Japan Workshop on Ground Improvement II held in Sacramento, USA, 16 - 17 May 2008.

Professor J. Koseki made a keynote lecture at the 4th International Symposium on Deformation Characteristics of Geomaterials, held in Atlanta, USA, 22 - 24 September 2008.

Professor J. Koseki visited China from 16 to 25 October 2008 to conduct geotechnical survey in Sichuan areas.

Professor J. Koseki attended the Second Japan-Korea Geotechnical Engineering Workshop held in Tokyo, Japan, 10 - 11 November 2008.

Professor J. Koseki made a keynote lecture at the International Workshop on Contributions of Geotechnical Engineering to Sustainable Civil Constructions, held in Bandung, Indonesia, 18 - 19 November 2008.

Associate professor R. Kuwano visited Akita and Iwate prefecture for surveying roads damaged by Iwate-Miyagi Nairiku earthquake, on 17 - 18 June and 1 July 2008.

Associate professor R. Kuwano and Mr. R.I. Wicaksono, graduate student, attended the 4th international symposium on deformational characteristics of geomaterials held in Atlanta, USA, 22 - 24 September 2008.

Associate professor R. Kuwano, together with two students of Kuwano laboratory, attended the 7th International Symposium on New Technologies for Urban Safety of Mega Cities in Asia held in Beijing, China, 21 - 22 October 2008.

Associate professor R. Kuwano attended the 2nd Japan-Korea geotechnical engineering workshop held in Tokyo, 10 - 11 November 2008.

Associate professor R. Kuwano, together with two students of Kuwano laboratory visited Aratosawa dam site for the investigation on landslide caused by Iwate-Miyagi Nairiku earthquake, on 29 August and 10 December 2008.

Prof. K. Meguro visited Bangladesh University of Engineering and Technology, BUET, Dhaka, Bangladesh to discuss BNUS (Bangladesh Network Office for Urban Safety) management and research project on earthquake disaster mitigation for major cities in Bangladesh with Prof. Mehedi Ahmed Ansary. This project regarding seismic hazard and vulnerability mapping of Dhaka, Chittagong & Sylhet city corporation area is sponsored by Comprehensive Disaster Management Programme (CDMP) using EC-fund. Dr. Kawin Warakanchana from RNUS, ICUS and Dr. Pennung Warnitchai from AIT are involved in this project.

Prof. K. Meguro visited Beijing, China to attend the 14th World Conference on Earthquake Engineering, and to hold the 7th International Symposium on New Technologies for Urban Safety of Mega Cities in Asia, USMCA2008 from October 12 to 23. At the 14 WCEE, Prof. Meguro gave two invited speeches at two special sessions. From his research group, totally 13 research papers were presented. About the USMCA2008, Prof. Meguro gave one keynote speech and 7 research papers were presented.

Prof. K. Meguro traveled to Bangkok, Thailand from Nov. 18 to 22 to attend the Expert Group Meeting (EGM), and Committee on Information and Communication Technology (ICT) by United Nations Economic and Social Commission for Asia and the Pacific (UNESCAP). Prof

Meguro gave two lectures at the EMG and the opening ceremony of the Committee on ICT. Titles of his lectures were “The most important issue for disaster mitigation and integrated information system for total disaster management” and “Development of a new generation disaster manual -efficient use of information for integrated urban disaster management”. At the opening ceremony of the Committee on ICT, there were many important persons, such as Ms. Noeleen Heyzer, Under-Secretary-General of the United Nations and Executive Secretary of the ESCAP, Thai ICT Minister, Secretary to the Sri Lankan President equivalent to a Cabinet minister in Sri Lanka, and so on. Prof. Meguro introduced them his research outcomes and activities and exchanged the opinions with them.

Prof. K. Meguro attended the meeting of the board of directors of the World Seismic Safety Initiative (WSSI) held in Singapore from Dec. 7 to 9.

Prof. K. Meguro visited 2008 Sichuan earthquake affected areas and Beijing with Dr. N. Sathiparan, post doctoral fellow at Meguro Laboratory. China Development Research Foundation invited them to introduce their newly developed efficient retrofit method to the people in affected areas and local government officials in the other parts of the country. At the affected areas, Prof. Meguro explained local masons and people about PP-band retrofit method and people showed strong interests. In Beijing, Prof. Meguro gave special lecture on how to apply PP-band technique to strengthen constructions to over 400 Chinese local governmental officials from the Sichuan earthquake affected areas and other earthquake prone areas in China.

Dr. P. Mayorca project researcher of Meguro research group, won the best paper award by an young researcher at the 14WCEE for her research paper titled “A Step Towards the Formulation of a Simple Method to Design PP-Band Mesh Retrofitting for Adobe/Masonry Houses”. Prof. Meguro was the co-author of the paper. She received certificate at the closing ceremony of 14 WCEE on October 16.

Dr. N. Sathiparan and Dr. A. Kawasaki, both post doctoral fellows of Meguro Laboratory, won the best presentation award at the USMCA2008.

Mrs. Naoki Sorimachi and Mr. Yoshiki Hiruma, both master course students of Meguro Laboratory, won best presentation award at the annual conference of Japan Society of Civil Engineers on Dec.10

Professor K. Meguro has published 65 technical papers including conference papers in 2008. Among them, 27 papers were written in English and are listed in this volume. Newspapers and

TV have introduced and reported his various research topics and outputs 30 times in 2008. He has given special lectures as an invited lecturer 33 times by Japanese organizations and 7 times by overseas and international organizations.

Dr. M. Ohara visited Beijing, China from October 12 to October 23, 2008 for attending the 14th World Conference on Earthquake Engineering and the Seventh International Symposium on New Technologies for Urban Safety of Mega Cities in Asia.

Dr. Ogi and Mr. Oba visited Kobe on March 16 of 2009, to investigate large roof buildings damaged by the Great Hanshin-Awaji Earthquake.

Dr. Ogi and Mr. Oba visited Amagasaki, Itami, and Takarazuka on January 29 and 30 of 2009, to investigate large roof buildings damaged by the Great Hanshin-Awaji Earthquake.

Dr. Ogi and Mr. Oba visited Amagasaki on November 27 and 28 of 2008, to investigate large roof buildings damaged by the Great Hanshin-Awaji Earthquake.

Prof. Kawaguchi, Dr. Ogi, and Mr. Oba visited Nishinomiya, Kobe, and Ashiya on October 10 and 11 of 2008, to investigate large roof buildings damaged by the Great Hanshin-Awaji Earthquake.

Dr. Ogi and Mr. Oba visited Kobe and Nishinomiya on September 24 to 26 of 2008, to investigate large roof buildings damaged by the Great Hanshin-Awaji Earthquake.

Dr. Ogi and Mr. Oba visited Kobe on September 11 and 12 of 2008, to investigate large roof buildings damaged by the Great Hanshin-Awaji Earthquake.

Dr. Ogi and Mr. Oba visited Kobe from August 20 to 22 of 2008, to investigate large roof buildings damaged by the Great Hanshin-Awaji Earthquake.

Prof. Kawaguchi, Dr. Ogi, Mr. Katayama, and Mr. Kumagai visited Hachinohe on July 26 of 2008, to investigate large roof buildings damaged by the Iwateken Engan- Hokubu Earthquake.

Dr. Ogi, Mr. Katayama, and Mr. Kumagai visited Akita prefecture on June 21 of 2008, to investigate large roof buildings damaged by the Iwate-Miyagi Nairiku Earthquake.

Prof. Kawaguchi, Mr. Oya, and Mr. Sakurai visited Miyagi prefecture on June 21 of 2008, to investigate large roof buildings damaged by the Iwate-Miyagi Nairiku Earthquake.

Prof. Kawaguchi, Dr. Ogi, Mr. Oya, and Mr. Katayama visited Iwate prefecture on June 19 of 2008, to investigate large roof buildings damaged by the Iwate-Miyagi Nairiku Earthquake.

Prof. Kawaguchi, Mr. Oya, Mr. K. Abe, Mr. J. Abe, and Mr. Taguchi received a Technology Award (Special Award) on May 29 of 2008, from the Japan Society of Seismic Isolation, for development of a new base-isolation system.

MEETINGS OF EARTHQUAKE RESISTANT STRUCTURE RESEARCH CENTER

May 9, 2008

Speaker : Dr. Jörgen JOHANSSON (Associate Professor, IIS, The University of Tokyo)

Topic : Geotechnical issues in Kashmir affected by the 2005 Kashmir Earthquake, pakistan

Speaker : Dr. Kazuo KONAGAI (Professor, IIS, The University of Tokyo)

Topic : Earthquake damage in active-folding areas: Creation of a comprehensive data archive and suggestions for its application to remedial measures for civil-infrastructure systems

July 25, 2008

Speaker : Dr. Yoshiaki NAKANO (Professor, IIS, The University of Tokyo)

Topic : Quick report of damage caused by the 2008 Wenchuan Earthquake, China

Speaker : Dr. Kimiro MEGURO (Professor, IIS, The University of Tokyo)

Topic : Strategy for retrofitting low earthquake-resistant structures

Speaker : Dr. Kazuo KONAGAI (Professor, IIS, The University of Tokyo)

Dr. Jörgen JOHANSSON (Associate Professor, IIS, The University of Tokyo)

Topic : Geotechnical issues in the Mid Iwate/Miyagi earthquake

Speaker : Dr. Reiko KUWANO (Associate Professor, IIS, The University of Tokyo)

Topic : Damage to roads on the western side of Mt. Kurikoma

Speaker : Dr. Kenichi KAWAGUCHI (Professor, IIS, The University of Tokyo)

Topic : Damage to non-structural members in large-scale open spaces in buildings

They will be followed by plenary discussion

October 3, 2008

Speaker : Mr. Takafumi KUMAGAI (Master Student, The University of Tokyo)
Dr. Mikio KOSHIHARA (Associate Professor, IIS, The University of Tokyo)

Topic : Comprehensive Strategy for the Disaster Mitigation in Preserved Historic Districts

Speaker : Dr. Miho OHARA (Associate Professor, IIS, The University of Tokyo)

Topic : Development of Learning Tool for Proper Response to Earthquake Early Warning

January 9, 2008

Speaker : Dr. Masakazu TAKAGAKI (Research Associate, IIS, The University of Tokyo)

Topic : Finite Element Analysis of TypeIV Creep Damage Behaviors of High Cr Steel Welded Pipes

Speaker : Dr. Osamu TAKAHASHI (Kozo Keikaku Engineering Inc.)
Mr. Junji Suhara (Shimizu Corporation)

Topic : Development and Application of Three-Dimensional Seismic Isolation for Buildings

February 26, 2008

Speaker : Prof. Kazue WAKAMATSU (Kanto Gakuin University)

Topic : "Why the liquefaction did occur there !
-analysis of liquefaction case histories-"